Tectonic evolution and growth of the Zagros Mountain Belt (Fars, Iran): constraints from magnetostratigraphy, sedimentology and low- temperature thermochronometry

Shokofeh Khadivi

THESE DE DOCTORAT DE
L'UNIVERSITE PIERRE ET MARIE CURIE

Spécialité
Sciences de la Terre
(Géosciences et ressources naturelles, 2- ED 398)

Présentée par

Mme. Shokofeh KHADIVI DONBOLI

Pour obtenir le grade de

DOCTEUR de l'UNIVERSITÉ PIERRE ET MARIE CURIE

Sujet de la thèse :

Evolution tectonique et croissance de la chaîne du Zagros (Fars, Iran): contraintes magnétostratigraphiques, sédimentologiques et thermochronométriques basse-température

Tectonic evolution and growth of the Zagros Mountain Belt (Fars, Iran): constraints from magnetostratigraphy, sedimentology and low-temperature thermochronometry

Soutenue le : 26.11. 2010

Devant le jury composé de :

M. Frederic MOUTHEREAU	Directeur de Thèse
M. Olivier LACOMBE	Co-directeur de Thèse
M. Mark ALLEN	Rapporteur
M. Olivier BELLIER	Rapporteur
M. Bertrand MEYER	Examinateur
M. Jaume VERGES MASIP	Examinateur
M. Jocelyn BARBARAND	Examinateur

Université Pierre & Marie Curie - Paris 6
Bureau d'accueil, inscription des doctorants
Esc G, 2ème étage
15 rue de l'école de médecine
75270-PARIS CEDEX 06

Tél. Secrétariat : 01 44 27 28 10
Fax : 01 44 27 23 95
Tél. pour les étudiants de A à EL : 01 44 27 28 07
Tél. pour les étudiants de EM à MON : 01 44 27 28 05
Tél. pour les étudiants de MOO à Z : 01 44 27 28 02
E-mail : scolarite.doctorat@upmc.fr

Acknowledgments

I would like to express my appreciation to who have accepted to be members of the jury for this thesis.

I attribute the level of my Ph.D degree by endless effort and encouragement of my advisor Dr. Frederic Mouthereau has done his best to learn and motivate me during different stages of this undertaking. I would like to thank my Co- adviser Professor Olivier Lacombe who help and support me over the years. I learn a lot through his comments and his office door always was open to me.

Special thanks are likewise expressed to Dr. Abdolah Saidi for his enthusiasm and his role in getting the thesis underway during his responsibility in National Geoscinec Database of Iran.

I wish to acknowledge to Dr. Jucelyn Barbarand, for his tireless effort during my Fission track analysis which always being there and offering his valuable advice and help.

My thanks go especially to Dr. Juan-Cruz Larrasoaña who providing tremendous support in Magnetochronology laboratory, fast return reading the manuscript and his familial support during my residence in Barcelona.

In particular, my thanks go to the Geology Survey of Iran (Tehran and Shiraz) for visa and logistic supports during the extensive field works in Iran.

As remembrance the great geologist, Dr. Mohammad Sepehr from National Iranian Oil Company who has passed away in field campaign in the Zagros; I will never forget you.

I would like to thank most of the people in the University of Pierre and Marie curie and the University of Orsay (Paris-France), the Institute of Earth Sciences Jaume Almera (Barcelona-Spain) and National Geoscience Database of Iran (Tehran-Iran) for their friendship, help and encouragement.

Number of people generously gave up their time in order to help me to learn the French language, especially those, who offered their course services; Soizic Merle responsible of French as a Foreign Language office in UPMC and Professor Sabine Grandlin from the Sorbonne University.

I shall not forget to thank the library of university (JUBIL) for being the vast and boundless source of my research.

Acknowledgments

My parents have been forbearing during the course of my education through my life. My father, Fathollah Khadivi, who is constant to support me with the value that he place on educations. My mother, Iran Ghanbarzadeh, as long as I remember she provide the best condition of life and education to me with an unconditional love.

I appreciate all the sacrifices my spouse has made when I have been in abroad. None of this extraordinary work would have been possible without the help and love of him, Dr. Jalal Abbaspour whom continues to encourage and support me in any endeavor.

Financial support was provided mostly by my family through 40 months stay and study in Paris. My thanks go to the cultural department of French Embassy in Iran for its 8 months grant.

Paris (France), November 2010
Shokofeh KHADIVI

Résumé

La distribution et la datation précise du raccourcissement cénozoïque ainsi que les modalités du soulèvement et de l'exhumation dans la zone de collision du Zagros en Iran sont des paramètres-clés pour mieux comprendre comment le mouvement de la plaque Arabie (AR) a été accommodé pendant la collision avec la plaque Eurasie (EUR). Il s'agit d'un point particulièrement important si l'on utilise les reconstructions cinématiques pour déduire la connectivité entre l'océan Indo-Pacifique, la Méditerranée et la mer para-Téthysienne, pour comprendre l'impact de la convergence Arabie-Eurasie sur l'aridification de l'Asie Centrale et sur les changements climatiques globaux au Cénozoïque, ou encore pour comprendre les mécanismes de soulèvement du plateau Iranien.

Afin de reconstruire l'évolution temporelle du soulèvement et de l'exhumation associés à la formation de la chaîne du Zagros dans le Fars entre l'Eocène et la phase miocène de raccourcissement et de soulèvement régional, nous avons effectué de nouvelles datations magnétostratigraphiques des dépôts terrigènes miocènes. Ces nouvelles datations sont combinées avec (1) une étude de provenance des dépôts du Miocène moyen dans la partie nord de l'avant-pays du Zagros fondée sur l'analyse des assemblages minéralogiques et de la composition des argiles, et (2) de nouvelles datations par traces de fission sur apatite détritique. Les implications de ces résultats sont discutées en termes de géodynamique, d'évolution des paysages et de paléogéographie régionale.

L'ensemble des résultats conduit à proposer un scénario original pour la construction de la chaîne du Zagros. Après une période d'accrétion et d'exhumation dans le « bloc iranien » pendant le Jurassique et le Crétacé, l'obduction se produit vers 70Ma tandis qu'un événement thermique extensif affecte à l'Eocène la zone de Sanandaj-Sirjan. La collision s'initie probablement vers 35 Ma, plusieurs Ma avant que les premiers dépôts clastiques ne se déposent dans le bassin d'avant-pays à 19.7 Ma. Jusqu'à 12.4 Ma, les régions exhumées ont été dominées par la dénudation du domaine de la suture incluant des roches du Haut Zagros (et des clastes ultramafiques et cherts radiolaritiques des ophiolites de Neyriz) et de la zone métamorphique de Sanadaj-Sirjan. Le plissement dans le Zagros externe a commencé entre 15 et 14 Ma, bien que le célèbre système de plis du Zagros ne se soit développé qu'après 12.4 Ma. Depuis cette époque, à la fois la chaîne plissée du Zagros et le plateau iranien ont été soulevés comme en témoignent la stratigraphie des sédiments marins les plus vieux. La phase d'accrétion dans le Zagros s'est produite probablement en moins de 5 Ma et avec un contrôle « érosionnel » faible dont témoignent les conditions climatiques arides qui ont prévalu pendant le Miocène.

Abstract

The distribution and precise timing of Cenozoic shortening as well as the degree of uplift and exhumation in the Zagros collision zone in Iran are keys to better understanding how the Arabia (AR) plate motion was accommodated during the collision with the overriding Eurasia (EUR) plate. This is particularly important if plate reconstructions are used to infer the connectivity between the Indo-Pacific Ocean, the Mediterranean Sea and the Para-Tethyan sea, to interpret the impact of the Arabia-Eurasia convergence on the regional aridification of Central Asia and on the Cenozoic global climate changes or to deduce the mechanisms of Iranian plateau uplift.

In order to unravel the temporal evolution of uplift and exhumation patterns associated with the building of the Zagros in the Fars area from the Eocene period and the Miocene phase of shortening to the final regional uplift, we provide new magnetostratigraphic dating of Miocene detrital sediments. These new dating are combined with the provenance study of middle Miocene (19.7-14.8 Ma) detrital sediments in the northern Zagros foreland based on the analysis of petrological assemblages and clay mineralogy combined with new detrital apatite fission-track ages. The implications of the results are discussed in terms of plate geodynamics, landscape evolution and regional paleogeography.

Combining all informations allowed proposing an original scenario for the building of the Zagros Mountains. After a protracted history of accretion and exhumation during the Jurassic and the Cretaceous on the Iranian plate, obduction occurred at ~70 Ma and a widespread thermal and extensional event affected the SSZ during the Eocene. Collision initiated ca. 35 Ma, several Myrs before first siliciclastic deposits were deposited in the foreland at 19.7 Ma. Until 12.4 Ma, exhumed source areas were dominated by the denudation of the suture domain including rocks from the High Zagros including the Neyriz ophiolites (ultramafic clasts and radiolarian cherts) and the adjacent Sanandaj-Sirjan metamorphic belt. Folding in the outer Zagros Folded Belt started between 15 and 14 Ma. However, the remarkable regional train of folds did not develop before 12.4 Ma. Since this time onwards both the Zagros Folded Belt and the Iranian plateau were uplifted as argued by the stratigraphy of the oldest marine sediments. This very fast accretion in the Zagros occurred probably in less than 5 Myrs and in association with weak erosion feedbacks as revealed by the arid climatic conditions that prevailed during the Miocene.

Contents

Acknowledgments I

Résumé III

Abstract IV

Contents V

Introduction: Tectonics and climate in the Zagros region

I. Motivation 2

II. The Zagros Mountains in the framework of Peri-Himalayan geodynamics 3

II-1.Constraints on Paleogene-Neogene climate evolution in the Zagros region 3

II-2.Timing and mountain building processes in the Zagros and the Iranian plateau 6

III. Objectives, strategy and methodology 11

Chapter I: Geodynamics, tectonics and stratigraphy of the Zagros

I. Plate tectonics 14

II. Geodynamic of the Arabia-Eurasia convergence 16

III. Current Arabia/Eurasia plate motions and the Zagros collision 17

VI. Geology of the Zagros 18

VI-1. Sanandaj-Sirjan Zone (SSZ) 19

VI-2. Urumieh-Dokhtar magmatic arc (UDMA) 22

VII. Zagros Folded Belt (ZFB) 23

VII-1. Zagros main structural subdivisions 23

VII-1-a. The High Zagros Thrust Belt (or Zagros Imbricate Zone) 26

VII-1-b. The Zagros Simply Folded Belt (ZSFB) 26

VII-1-c. The Zagros Foredeep (ZFF) 30

VII-2. Stratigraphy and sedimentology 31

VII-2-a. Paleozoic 31

VII-2-b. Mesozoic 33

VII-2-c. Cenozoic 33

VII-3. Stracture 34

VIII. Reconstruction of the Zagros evolution 37

VIII-1. Overview 37

VIII-1-a. Paleozoic plate tectonics in the Zagros 38

VIII-1-b. Mesozoic main tectonic events in the Zagros 38

Contents

VIII-1-c. Cenozoic plate tectonics in the Zagros 39
VIII-2. Timing of Zagros collision onset and Iranian plateau uplift 41

Chapter II: Magnetostratigraphic dating of the Zagros foreland Neogene synorogenic sediments

I. Concepts and methodology 46
I-1. Nature and Origin of Earth's magnetic field 46
I-2. Principles of remanent magnetization 46
I-3. Demagnetization 47
I-4. Magnetostratigraphy 49
I-5. Biostratigraphic calibrations 49
II. Magnetochronology of synorogenic Miocene foreland sediments in the Fars arc of the Zagros Folded Belt (SW Iran); Published in Basin Research, (2010) 51
II-1. Introduction 53
II-2. Geological setting 56
II-2-a. Main structural features of the Zagros Folded Belt 56
II-2-b.Tectonic constraints on the development of the Zagros foreland basin in the Fars Arc 57
II-3. The studied area 58
II-3-a.Main structural features 58
II-3-b.The studied sections 61
II-4. Magnetostratigraphy 65
II-4-a. Sampling strategy 65
II-4-b. Paleomagnetic results 66
II-4-c. Correlation with the geomagnetic polarity time scale (GPTS) 71
II-5. Discussion 73
II-5-a. Age of the proximal Zagros foreland basin: implications for the development of the Zagros collision 73
II-5-b. Constraints on the timing of folding in the northern Fars 74
II-5-c. Early-Middle Miocene sedimentation rates and unroofing of the internal Zagros 75
II-6. Conclusions 77

Contents

Chapter III: Exhumation rate and sediment provenance study in the Zagros foreland

I. Concepts and methodology 80

I-1. Apatite Fission track analysis (low-temperature thermochronology) 80

I-2. Fission track dating approach 81

I-3. Detrital populations 82

I-4. Sediment provenance study 82

II. Provenance of Miocene Zagros foreland sediments from detrital petrography and apatite fission-track thermochronometry: implications for tectonic evolution of the High Zagros (Fars, Iran); Submitted to Geological Society of America Bulletin 84

II-1. Introduction 86

II-2. Geological background 88

II-2-a. The Zagros Folded Belt (ZFB) 90

II-2-b. The Neyriz Ophiolitic Complex 92

II-2-c. The Sanandaj-Sirjan metamorphic belt or Sanandaj-Sirjan Zone (SSZ) 93

II-2-d. The Urumieh-Dokhtar magmatic Arc(UDMA) 95

II-3. Study area: main tectonic, morphologic and stratigraphic features 95

II-4. Bulk petrography, provenance and clay mineralogy of Miocene sediments 100

II-4-a. Sampling, experimental and analytical procedure 100

II-4-b. Detrital petrological composition of Miocene sediments 102

II-4-c. Bulk rock compositions and clay mineral assemblages 106

II-5. Detrital apatite fission-track thermochronology 108

II-5-a. Experimental and analytical procedure 109

II-5-b. AFT Results 110

II-6. Constraints on paleogeothermal gradient and Miocene PAZ 112

II-7. Origin tectonics and detrital AFT ages 113

II-7-a. Jurassic to Early Mesozoic ages: mixed SSZ and HZ exhumed source areas? 114

II-7-b.Early-Middle Eocene cooling/denudational event: magmatic and/or exhumational event? 115

II-7-c. Late Oligocene-Early Miocene exhumational event: the Zagros collision 117

II-8. Discussion 117

II-8-a. Tectonic-morphologic evolution of the High Zagros revealed by AFT dating and petrography 117

II-8-b. Constraints on climate and paleogeography of the Zagros region 121

II-9. Conclusions 121

Contents

Conclusion 123

References 127

Annexes

I. Concepts and methodology of Magnetostratigraphy 149

II.Compliment Biostratigraphic calibrations 183

III. Concepts and methodology of Provenance study and Low-temperature thermochronology 184

References 219

Introduction

Tectonics and climate in the Zagros region

I. Motivation

The interplay between tectonics and climate on the growth of mountains belts have long been recognized in region of going tectonic activity where crustal thickening, by isostasy, leads to surface uplift (Fig.1) (Willett, 1999). Using the critical wedge approach of topographic evolution coupled with longitudinal river profiles, several studies have attempted to quantify the differential effects of precipitation (a proxy for climate) and tectonics; 1) the steady-state width of the orogenic wedge and 2) the response time of the tectonic wedge to perturbation in climate and tectonics (Hilley and Strecker, 2004; Whipple and Meade, 2004). These studies showed that 1) the width of the orogeny is controlled by the balance between erosion flux and accretion flux and 2) that erosion and accretion rates have different time responses to climatic and tectonic perturbations. These retroactions are of particular interest to understand the causes and consequences of long-term climate changes during the Cenozoic. Indeed, the transition from Paleocene-Eocene "greenhouse" to the present-day "icehouse" world has been interpreted as being the cause of Cenozoic rejuvenation of reliefs (Molnar and England, 1990) or the consequence of the tectonics (Himalayas and Tibetan plateau) which promoted global cooling by chemical weathering of silicate in mountain ranges reducing the atmospheric pCO_2 (Raymo and Ruddiman, 1992).

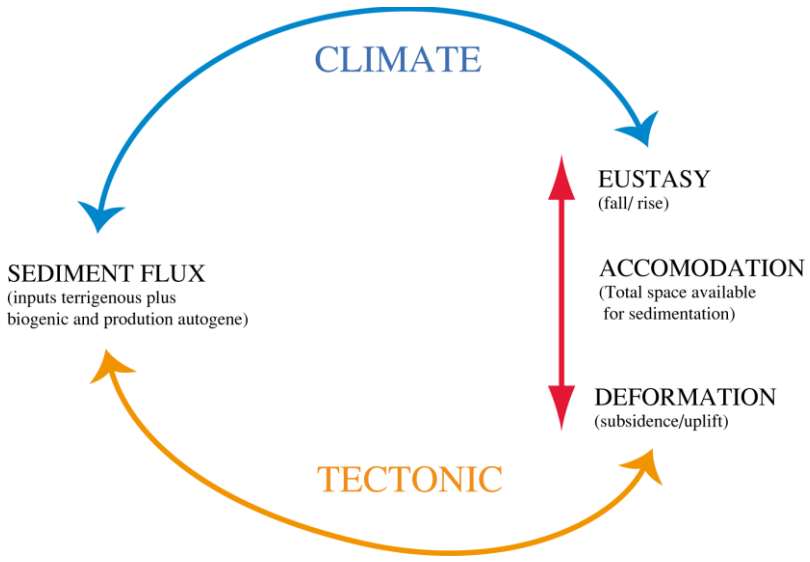

Figure 1: A dynamic system schedule between tectonic, climate and erosion in surface of Earth.

The position of the Zagros mountains at the crossroad between Tibet, Africa and Mediterranean region which have been places of well-established major climatic changes makes it an exceptional natural laboratory for studying both global climate changes together with the interactions between climate and tectonics over the past 20 Myr.

II. The Zagros Mountains in the framework of Peri-Himalayan geodynamics

II-1. Constraints on Paleogene-Neogene climate evolution in the Zagros region

The Zagros orogen in Iran is part of the larger Alpine-Himalayan collision and occupies a peculiar central position between two important tectonic features which resulting from the closure of the Tethys Ocean: the Tibetan plateau and the Mediterranean Sea (Fig. 2).

Equally important is the fact that the Zagros likely developed during the Oligocene-Miocene which is a period characterized by major tectonic and climatic changes that have virtually affected the climate at the global scale.

The Tibetan plateau uplift occurred 35 Ma (Rowley and Currie, 2006) and resulted in the summer ascent of air masses inducing the onset of the summer Monsoon between 30 and 7 Ma in the southern Asia which have strongly impacted the global climate. Together with the closure of the Para-Tethys, the plateau uplift induced a strong regional aridification (Fig. 3) in Central Asia including the Zagros (Ramstein et al., 1997). Over eastern Africa and western India, C_3 tropical vegetation disappeared during the Miocene and was progressively replaced by C_4 plants characteristic of more arid regions (e.g. Segalen et al., 2007) which is also supported by $\delta^{18}O$ of fossil record in teeth enamels and aragonitic shells in the Himalayas (Dettman et al., 2001).

It has been also argued that the Zagros collision had significantly impacted the Eocene-Oligocene cooling event (Zachos et al., 2001). Allen and Armstrong (2008) suggested that the Arabia-Eurasia plate collision following the closure of the Tethys Ocean provides four complementary mechanisms for reducing atmospheric CO_2 and global cooling: waning of pre-collision arc magmatism, storage of organic carbon in the Paratethyan basins, increase in silicate weathering, re-organisation of ocean currents, and hence CO_2 drawdown (Fig. 4).

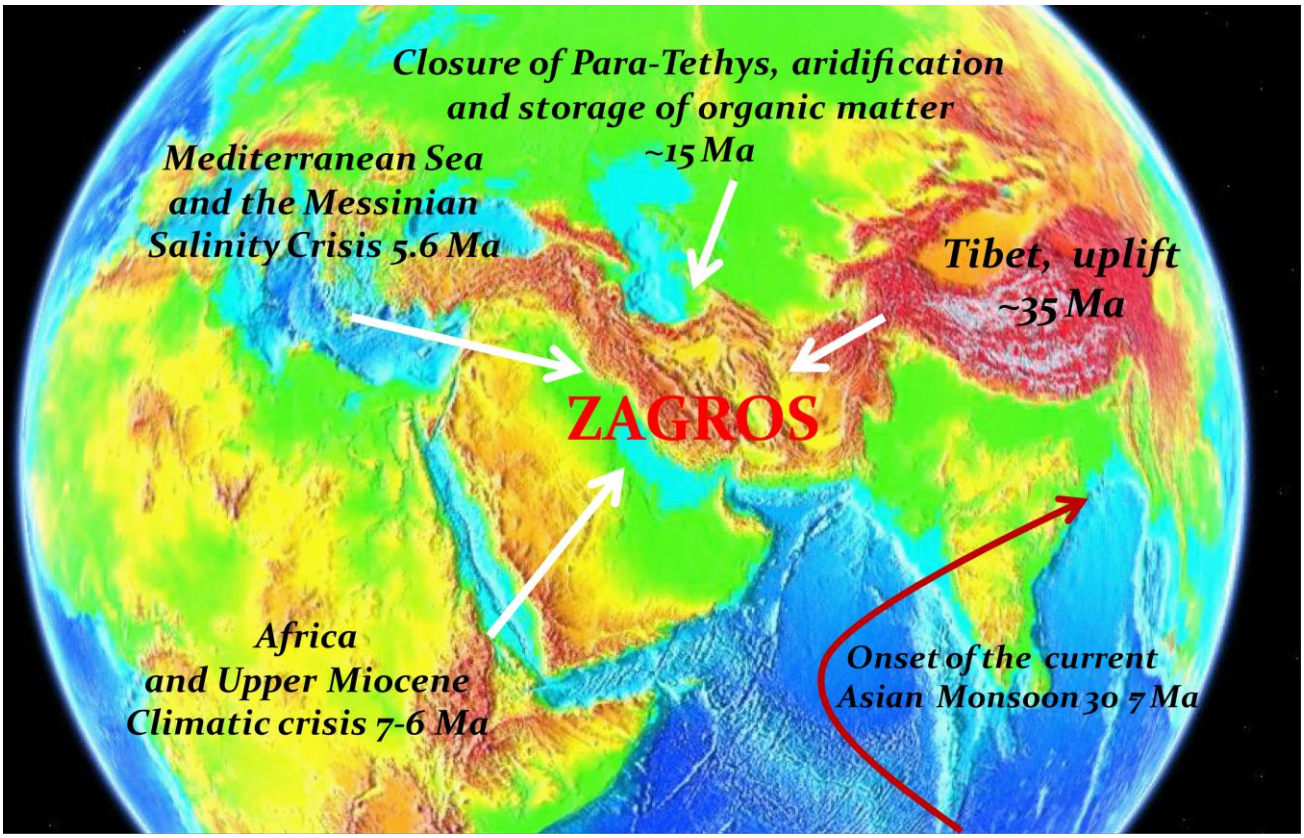

Figure 2: Main tectonic and climate events in Miocene.

The question of climatic versus tectonic control on elevation of mountain ranges can be addressed through the study of changes in erosion dynamics and landscape evolution. Although several low-temperature thermochronological studies have been recently published such as dealing with the timing of mountain building; it is still not clear how these ages can be related to the sediment routing system and paleoclimatic conditions.

For instance, the accumulation of 2-5 km of synorogenic deposits with marine evaporitic successions in the Miocene in the Zagros foreland (James and Wynd, 1965) suggests an episodic arid conditions (Bahroudi and Koyi, 2004; Motiei, 1995). This is coincident with the evolution towards higher temperatures observed in the ocean record at the Mid-Miocene climate optimum (Zachos et al., 2001). In contrast, the onset in the Middle Miocene of a well-identified cooling period (Zachos et al., 2001) seems to be well supported onland in the northern Zagros with the increase of sedimentation rates (Mouthereau et al., 2007b). These synorogenic deposits can thus be interpreted either due to the intensification of erosion-related tectonics or to a shift towards more seasonal climate conditions thus

enhancing erosion. But to date, available constraints do not allow us to definitely support the one or the other hypothesis.

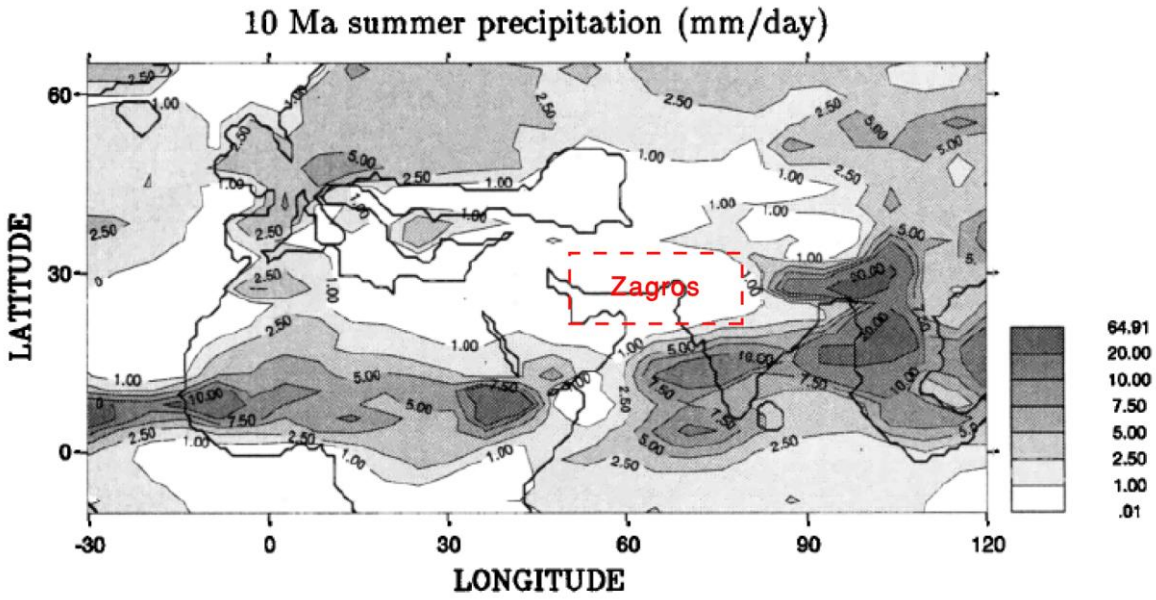

Figure 3: Numerical model of average precipitation (mm/day) in Eurasia 10 Myr ago. The aridification (White) of the areas like the Zagros is related to the closure of the Para-Tethys, the uplift of the Tibetan plateau and the onset of the Asian monsoon (Gray)(Fluteau et al., 1999).

The Zagros thus appears as a key area for testing models of climatic-tectonic interrelationships. Its study provides information on how plate forces drove the convergence and how climate and tectonics interacted over the past 20 Myr.

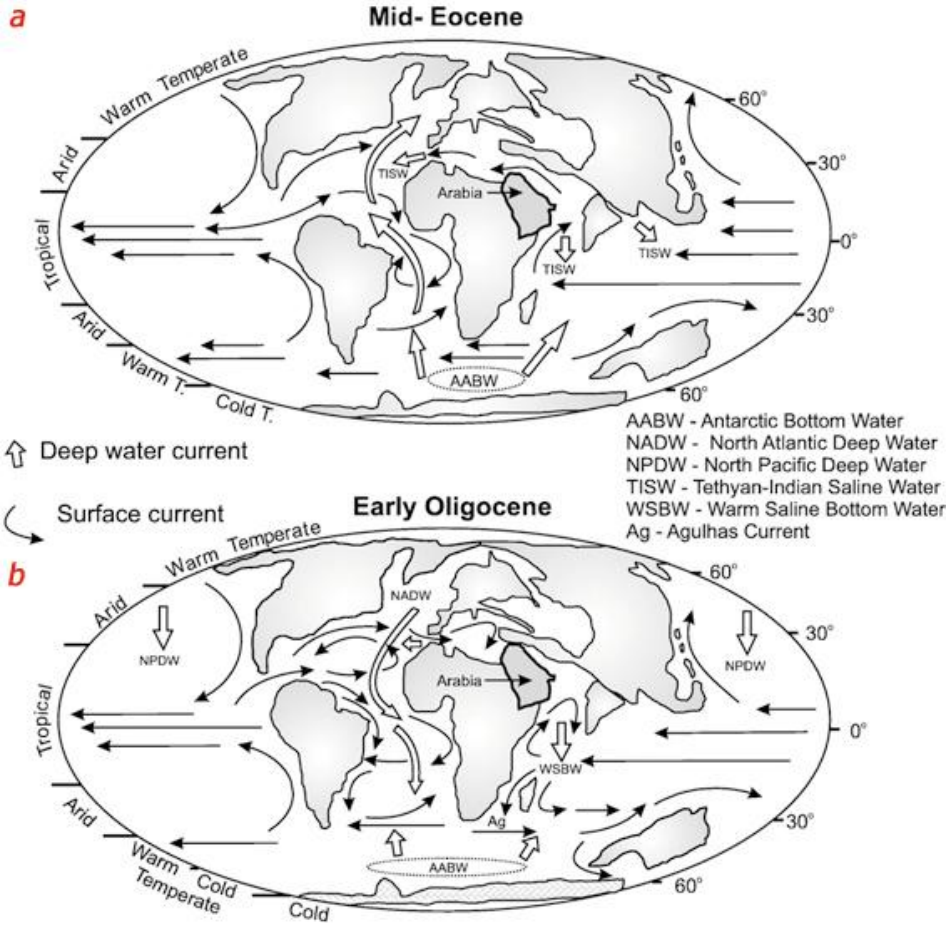

Figure 4: Paleogeographic and oceanographic reconstructions before and after the demise of the Tethys Ocean gateway. a) Eocene period, with westerly transport of warm Indian Oceanwater into the Atlantic via Tethys; b) Oligocene, with connection between the Indian and Atlantic oceans impeded by the Arabia–Eurasia collision zone (Allen and Armstrong, 2008).

II-2. Timing and mountain building processes in the Zagros and the Iranian plateau

From a morphologic and topographic point of view, the Zagros appears positioned on the southern flank of a high-elevation low-relief surface of the High Zagros and Iranian plateau. Mechanisms responsible for this plateau uplift are still debated.

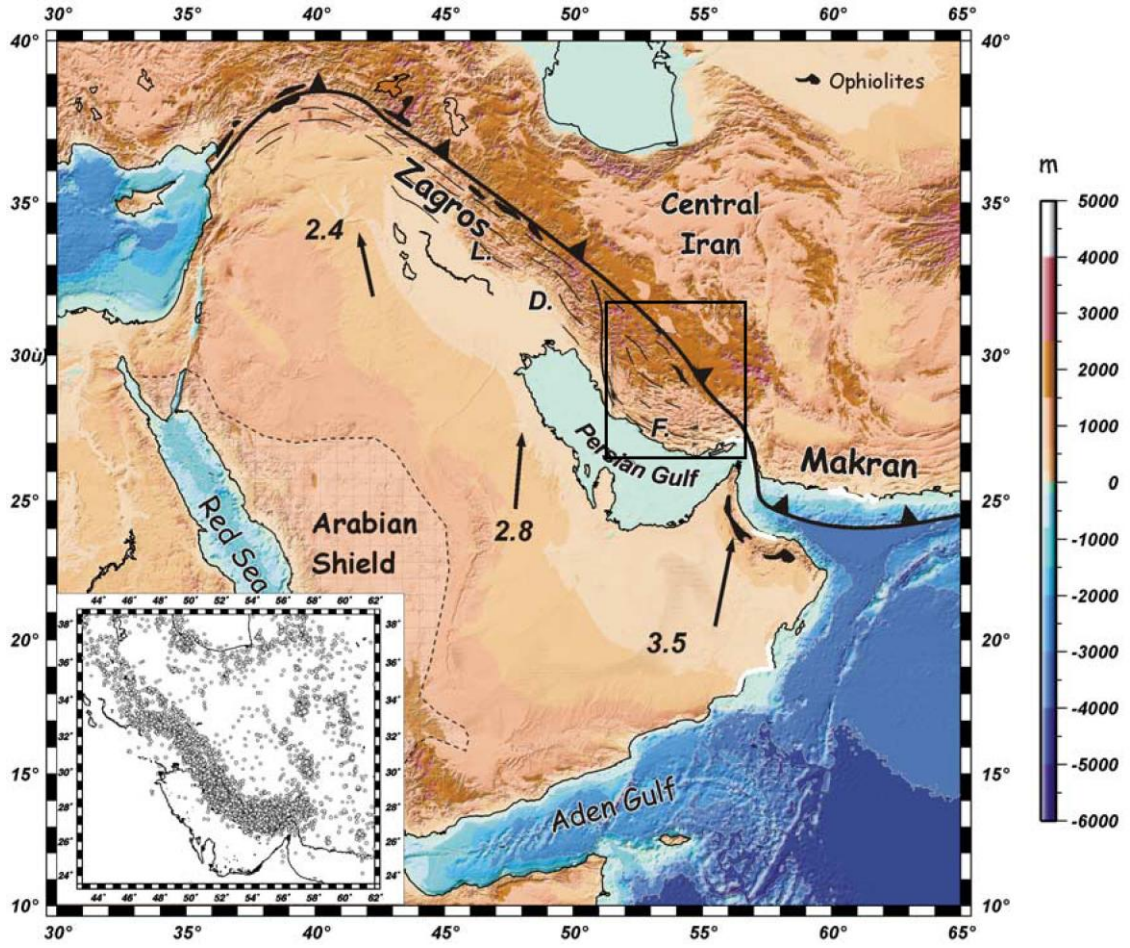

Figure 5: The Zagros Folded Belt (ZFB) in the framework of the active Arabia-Eurasia plate convergence. The present-day convergence between Arabia and Eurasia is 2-3 cm/yr in a N-S direction and is assume to be unchanged since 10 Ma. The Main Zagros Thrust (MZT) which is believed to be the plate boundary is currently inactive in the Fars. The suture zone is formed by remnants of deep-water radiolarites and eruptive volcanic rocks forming the Neyriz ophiolites near Shiraz. Northward, the Sanandaj-Sirjan Zone (SSZ) is a metamorphic belt, which represents the former active margin in front of the Urumieh-Doktar arc. The inset in the lower left shows seismicity in the Zagros for earthquakes with focal depths shallower than 35 km and magnitudes 2.4 < mb < 7.4 (Mouthereau et al., 2007b).

From space, the Zagros topography is outlined by a remarkably large (~200 km) fold train with a constant fold wavelength of ~16 km (Fig. 6).

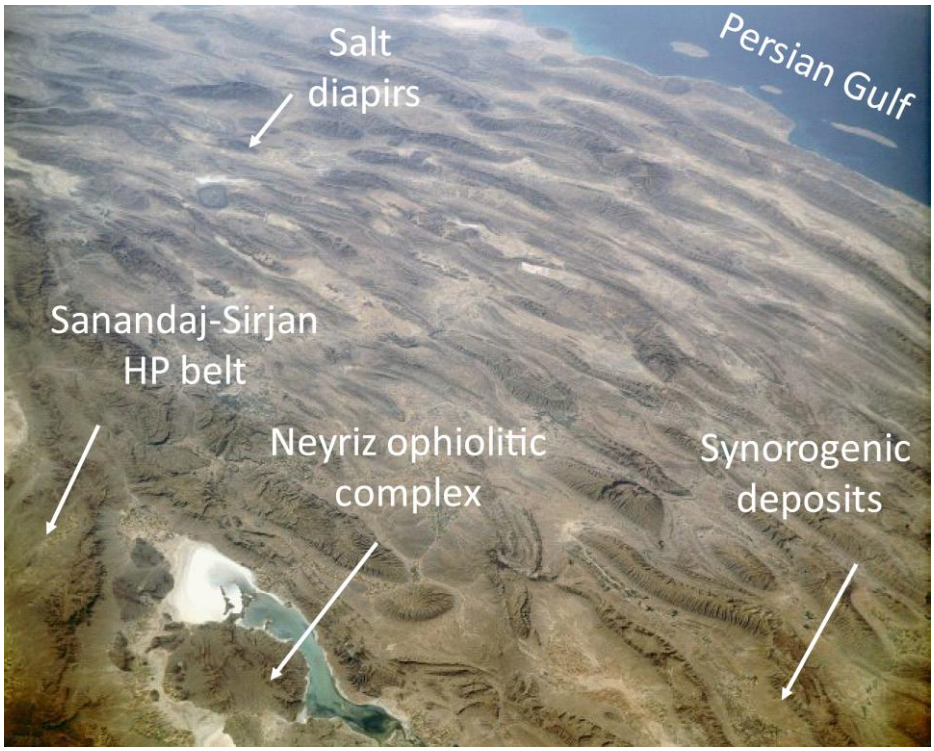

Figure 6: The Zagros Mountains from space (NASA, 1992). The present-day shortening rates of ~7 mm/yr across the Zagros. The Cover folding appears superimposed on a larger wavelength of ~200 km, which outlined the Zagros wedge topography.

The current cross-sectional shape of the Zagros Mountains has been interpreted as a crustal critical wedge, defined by low topographic slopes <0.5° and a low-dipping basal décollement located in the middle-lower crust (Mouthereau et al., 2006; Mouthereau et al., 2007b). Because of the low regional slope and current arid climate, one of the major characteristics of the Zagros is the very good preservation of synorogenic sediments in wedge-top basins from rear to toe (Fig. 7). This potentially allows us to carefully constrain the timing of folding and regional exhumation.

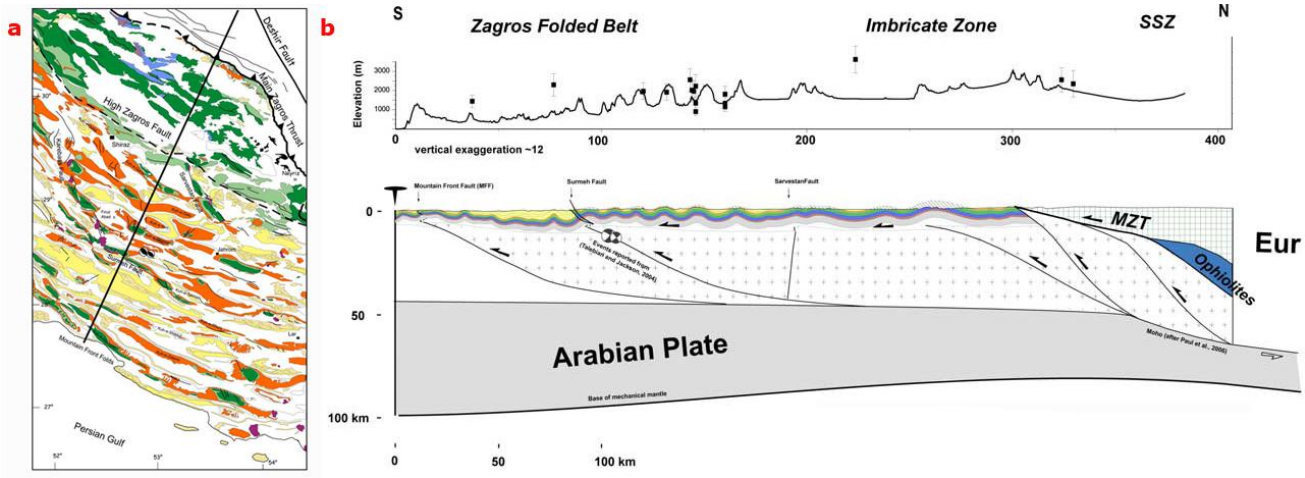

Figure 7: a) Geological map of the Fars. The thick black solid line corresponds to the location of the crustal-scale section; b) A crustal-scale section of the Zagros Folded Belt. Subsurface constraints in the ZFB were provided by the thickness distribution of Paleozoic, Mesozoic (~12km) and Cenozoic strata (~3km) from isopachs and basement depth derived from aeromagnetic surveys. The Sanandaj-Sirjan Zone (SSZ) is shown as a single tectono-metamorphic unit belonging to the upper Iranian plate. The currently inactive suture zone is represented by the ophiolites of Neyriz. Underthrusting beneath the SSZ area is suggested by the geometry of the Moho provided by recent geophysical studies and receiver functions. The yellow layer are shown the syn-orogenic sediments that fill in the vallys (Mouthereau et al., 2007b).

The timing of collision onset is still a matter of debate and currently vary between 65 Ma (Berberian and Berberian, 1981; Berberian and King, 1981), at 35 Ma (Allen and Armstrong, 2008), between 35 and 20 Ma (Agard et al., 2005; Mouthereau et al., 2007a), 10 or 5 Ma (James and Wynd, 1965). This has much importance on the distribution of shortening in the Arabian margin and hence on plate convergence reconstruction between Eurasia and Arabia (McQuarrie et al., 2003). Taking units account a present-day convergence rates of 7 mm/Myr (Vernant et al., 2004), a minimum age of 10 Ma for collision allows to predict ~70 km of total shortening. However, less than the half (i.e. 17-45 km) can be reconstructed from balanced cross-sections (e.g. Molinaro et al., 2005; Mouthereau et al., 2007a; Sherkati and Letouzey, 2004). This has been tentatively explained by assuming that shortening was accommodated, for instance, by underplating beneath the Sanandaj-Sirjan domain (Mouthereau et al., 2007a) or the Iranian plateau (Allen et al., 2004).

Mantle delamination is suggested by tomography data (Fig. 8); alternativly, slab break-off has also been suggested by the recent discovery of adakitic magma (Fig. 9; Omrani et al., 2008).

Importantly, the mechanism proposed for the plateau of Iranian should also apply to the High Zagros which presents the same morphology. Both the Iranian Plateau and Zagros appear coupled in

the Fars region. The timing of the Zagros uplift hence appears a major unknown for the Zagros itself but also for the Iranian plateau. Despite of the numerous study in the region, the exact timing of shortening is still challenged, it is no doubt that a marine gateway connecting the Mediterranean Sea and the Indo-Pacific Ocean existed at least until the early Miocene in the Central Iran (Harzhauser et al., 2007; Schuster and Wielandt, 1999). As a result both the Zagros and plateau uplift occurred after the Early-Middle Miocene. A major plate reorganization seems to have occurred 5 Myr ago (Allen et al., 2004). Hence, several questions still hold: when did exactly the Zagros and Iranian plateau uplift? Did this uplift occur coincidently with the plate reorganization or independently?

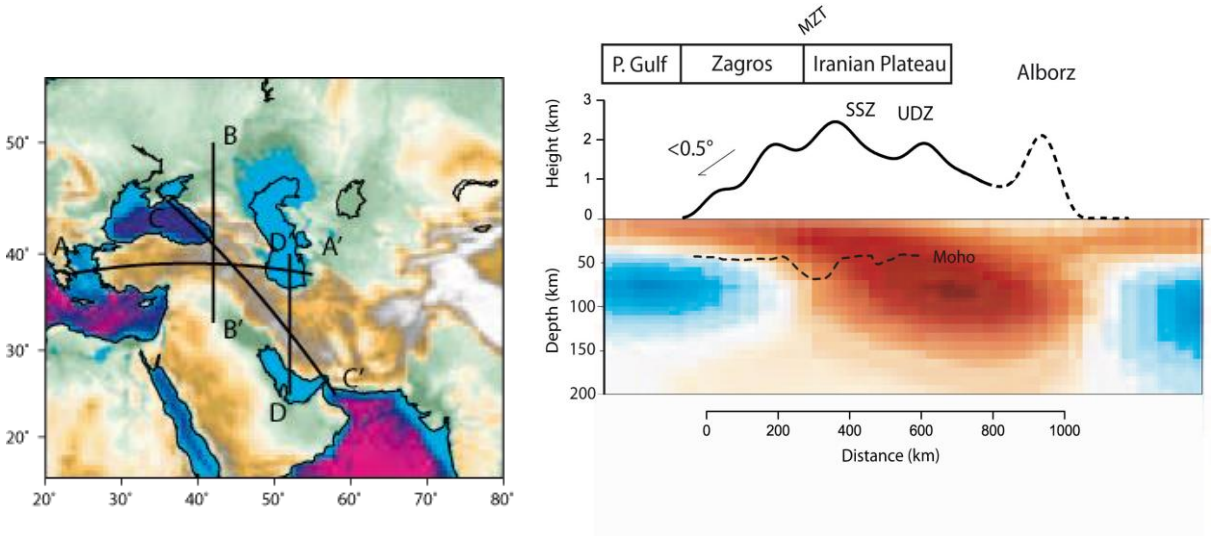

Figure 8: Vertical cross-sections both along and across the Turkish plateau and the Zagros mountains of southern Iran. Depths and distances along the profiles are given in km. Elevations, shown in black above the plots, are exaggerated by a factor of 10 .

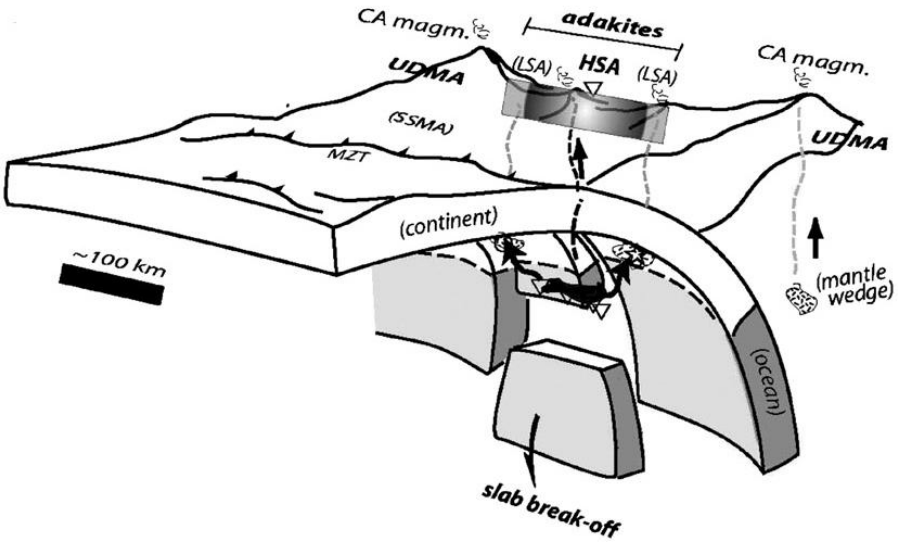

Figure 9: Model of adakite generation through the melting of mafic slab material at the upper lip of a ~500 km long slab break-off below the Anar region. Slab melts generate HSA in the central region (triangles), whereas fluids and melts released from these regions contaminate the mantle wedge (small black arrows) near the two tips of the slab window, thus producing LSA (circle and star, respectively). Abbreviations: CA magm.: calc-alkaline magmatism; MZT: Main Zagros thrust; SSMA: Sanandaj–Sirjan magmatic arc; UDMA: Urumieh–Dokhtar magmatic (Omrani et al., 2008).

III. Objectives, Strategy and methodology

Understanding the timing and rates of shortening in the Zagros and uplift of the Iranian plateau is of main importance to unravel how the Eurasia-Arabia convergence was consumed. Moreover, in order to address the question of the incidence of tectonics or climate on mountain building and plateau growth it appears essential to gain new dating constraints on synorogenic sediments complemented by thermochronological dating and provenance analysis of detrital materials.

Because the Zagros have preserved sufficient synorogenic materials from high to low elevations, an approach focused on these sediments appears particularly useful.

Any attempts to unravel this issue depend on our ability to study independent constraints on the temporal and spatial distribution in rock exhumation-denudation and surface uplift during mountain building.

To this aim we have used a multidisciplinary approach including:

Structural field work and imagery

Extensive field works were combined with a close and detailed analysis of existing geological maps and satellite images. The results allow proposing new mapping of the study area complemented by regional cross sections.

Magnetostratigraphy and biostratigraphy

The magnetostratigraphy dating combined with biostratigraphy has been applied to syntectonic detrital sediments. Comparing the results of this study with the results obtained at other locations allowed to constrain the sequence of the folding associated to growth strata across the study area.

The paleomagnetic analyses used in this study have been performed at the Laboratory of Paleomagnetism of the CSIC-University of Barcelona at the Institute of Earth Sciences "Jaume Almera" in Barcelona (Spain). Biostratigraphic dating of calcareous nannoplankton used in this work were realized in National Institute of Marine Geology and Geo-ecology in Bucharest (Romania) and Laboratoire PaléoEnvironnements & PaléobioSphère; Université Lyon 1 (France).

Low-Temperature Thermochronology

Apatite fission track analysis on detrital grains constrained the exhumation history of the basin and the long-term source-to-sink evolution. Sample preparation and analyses were performed in the fission-track laboratory at University of Paris Sud-Orsay (France).

Sediment Petrography

A petrographic study of the synorogenic sediments was performed on thin-sections and analysis of heavy minerals by optical method and scanning electron microscopy (SEM). We also carried out X-ray diffraction on clay minerals to capture the bulk mineralogy and the clay mineral assemblage that help to determine the type of source rocks and weathering conditions. Coupled with AFT dating this petrographic study provided new insights on the provenance of exhumed source rocks. The X-ray diffraction has been performed at University of Lausanne (Switzerland).

Chapter I

Geodynamics, tectonics and stratigraphy of the Zagros

I. Plate Tectonics

The Zagros forms a collision belt extending over about 2000 km from Turkey to the Strait of Hormuz (Fig. I- 1) (James and Wynd, 1965). This orogenic belt results from the closure of the Neo- Tethys ocean between the Arabia margin and the Eurasia continent (Koop and Stoneley, 1982; Stocklin, 1968). It is bounded to the north by the Main Zagros Thrust (MZT), a major tectonic boundary interpreted as the suture zone of the Neo-Tethys Ocean (Ricou, 1971) outlined by a complex of ophiolitic rocks, deep-water radiolarites and eruptive rocks interpreted as remnants of the obducted Neo-Tethys ocean or one of its derivative (e.g., back-arc or fore-arc crust) (Stoneley, 1990; Ziegler, 2001). To the SE it is connected to the Minab Fault, an intercontinental transform fault, separating the Makran subduction domain from the Zagros collision. To the NE the MZT merges in Turkey with the East Anatolian Fault.

On base on a number of supporting evidence the collision of Arabian plate with Iranian plate did not happen sooner than the Late Eocene (Fig. I- 2) (Berberian and King, 1981; James and Wynd, 1965).

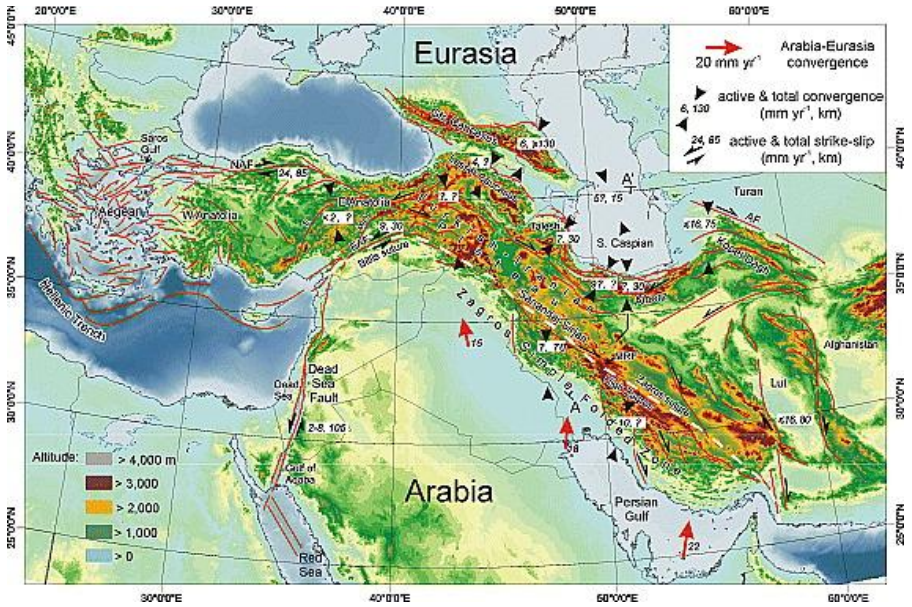

Figure I- 1: Topography, structure, current deformation rates and finite strain of the Arabia-Eurasia collision. Numbers in italics are present shortening or slip rate in mm yr^{-1}, followed by finite shortening or strike-slip in kilometers. Abbreviations are as follows: AF, Ashgabat Fault; E, Ecemiş Fault; EAF, East Anatolian Fault; M-O, Malatya-Ovacik Fault; MRF, Main Recent Fault; NAF, North Anatolian Fault. Red lines indicate main active faults, with thrusts marked by barbs. Present Arabia-Eurasia convergence rates from (Allen et al., 2004a; Sella et al., 2002).

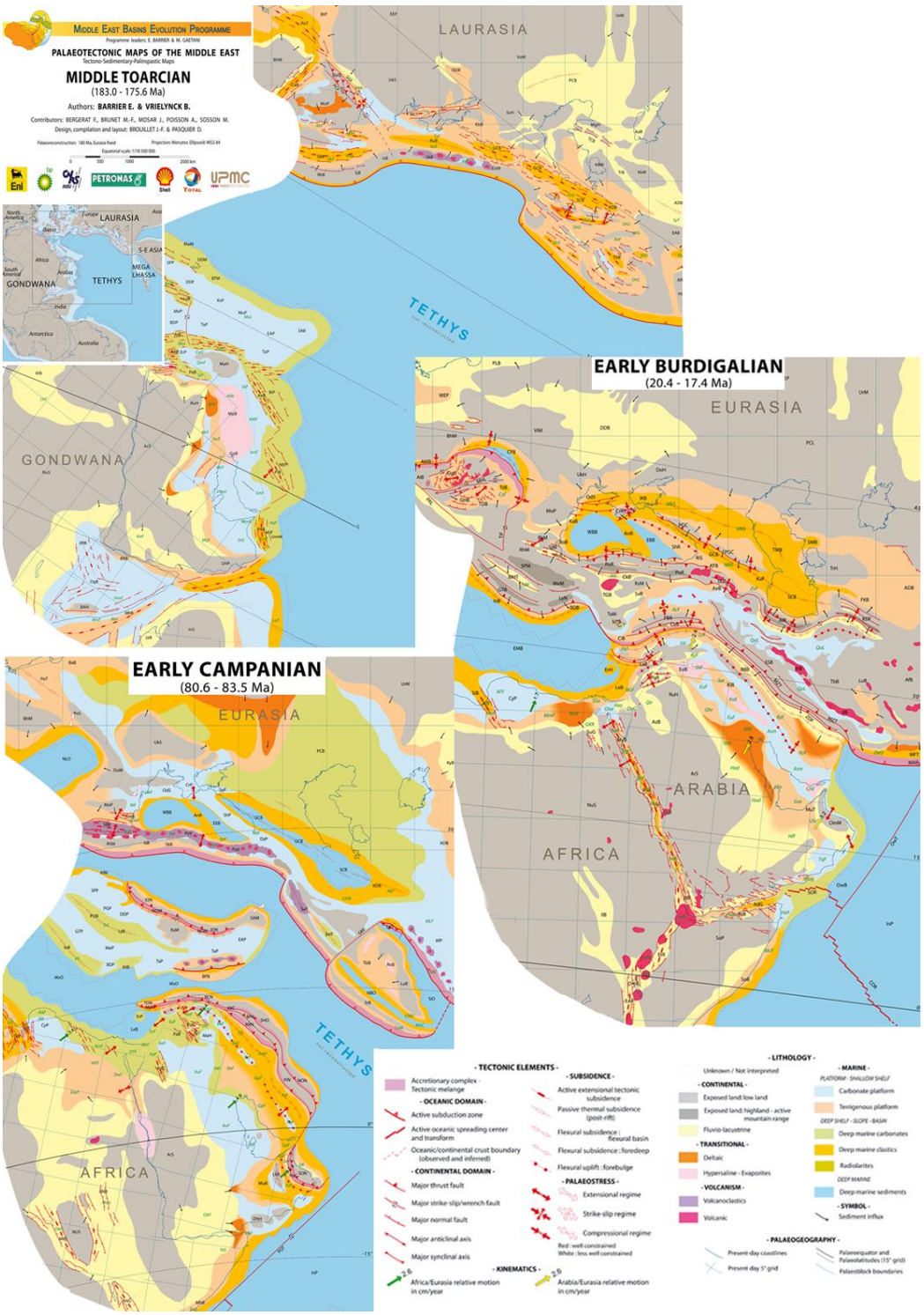

Figure I- 2: Paleogeography and plates position of the Middle East. Note that Arabia was a promontory of the African plate before the opening of the Red sea in the Mid-Cenozoic. The Paleotectonic Maps of the Middle East, 1: 18500000 scale maps from Middle East Basins Evolution Programs (2008).

II. Geodynamic of the Arabia-Eurasia convergence

The Paleo-Tethys which separated Laurasia from Gondwana, has existed since late Palaeozoic times and the Arabian and Iranian crusts, as parts of NE Gondwana (Berberian and King, 1981; Stocklin, 1974), acquired a N-S tectonicfabric during the protracted Pan-African collisional orogeny. During the opening of pull-apart basins, the thick salt deposits of Hormuz Fm were deposited in Late Precambrian-Early Cambrian (Berberian and King, 1981). During the Paleozoic shallow marine deposits covered the Zagros, central Iran, Alborz and Turkey. On basis of paleomagnetic data (Ricou, 1994), geology and paleogeography (Berberian and King, 1981) the closure of the Paleo-Tethys ocean started in Carboniferous time with the initiation of a northward subduction beneath Eurasia. This successive events finally resulted in the development of several micro-continents and the formation of the Neo-Tethys ocean (Stampfli and Borel, 2002) but the Paleo-Tethys was not completely closed at this time. During the earliest Triassic, the Neo-Tethys Ocean opened between the Afro-Arabian. The final closure of the Paleotethys, corresponding to the accretion of Cimmerian terranes to Eurasia took place at the end of the Mid-Triassic (Besse et al., 1998). The suture zone is located along the Alborz and Kopeh Dagh Mountain belts (Berberian and King, 1981; Alavi, 1991, 1996). The subsequent onset of the progressive closure of the Neotethys ocean may have taken place as early as Mid-Jurassic time, when a new northward subduction beneath the Sanandaj-Sirjan block was formed (Berberian and King, 1981). Through this subduction, some part of SSZ metamorphism occurred in the UDMA. During Mesozoic the type of sedimentation was more complex (Berberian and King, 1981; Stocklin, 1968). Subsequent rifting in the Sanandaj-Sirjan Zone and Anatolian blocks occurred in Late Triassic coevally with the Paleotethys closure. The Sanandaj-Sirjan belt and Anatolian blocks were drifted northward through the Neotethys until the collided with Eurasia at the end of the Cretaceous. Throughout the middle Cretaceous the Afro-Arabian and Eurasian plates converged and the Neo-Tethys Ocean began to close. During the Late Cretaceous, the NE passive margin of the Arabian plate started to be subducted under Central Iran. The closure of the Neo-Tethys was marked by obduction of ophiolites onto the continental crust (89.3±1.0 – 83.5±0.7) (Berberian, 1995; Berberian and King, 1981; Falcon, 1974).

The evolution of the Zagros was continued after the closing of the Tethys and continent-continent collision. The separation of the Arabian Plate from Africa (Nubia) along the Red Sea,

at a rate of ~1.2 cm/year in a NNE direction, together with the pull forces acting on the Neo-Tethys slab was probably the engine driven the Arabian plate towards Iran blocks that triggered the Zagros collision in the upper Oligocene and lower Miocene (Agard et al., 2005).

III. Current Arabia/Eurasia plate motions and the Zagros collision

The present-day convergence between Arabia and Eurasia is 19-23 mm/yr (Fig. I- 1) along the Zagros folded belt (McClusky et al., 2003) with about the half (i.e. 7-10 mm/yr) accommodated across the Zagros Simply Folded Belt (Tatar et al., 2002; Nilforoushan et al., 2003; Vernant et al., 2004). Comparison between recent synthesis of GPS data (ArRajehi et al., 2010) and geologic constraints on plate circuit (McQuarrie et al., 2003) suggest that the convergence occurred at a rate of ~20 km/Myr (Hatzfeld et al., 2003; Nilfroushan, 2003; Tatar, 2002; Vernant et al., 2004) since at least 22 Ma, following the separation of Arabia with Africa (Nubia) (Fig. I- 3).

As seen by decreasing GPS velocity northwards, the remainder is currently accommodated, at the longitude of Tehran, in the Alborz Mountains (~6 mm/yr; e.g. Masson et al., 2007), on right-lateral strike-slip faults (MRF ~3 mm/yr or Deshir fault ~2 mm/yr e.g. Meyer et al., 2005) and subduction beneath the central Caspian Sea (Aspheron-Balkan sill) (up to ~6 mm/yr according to Vernant et al., 2004).

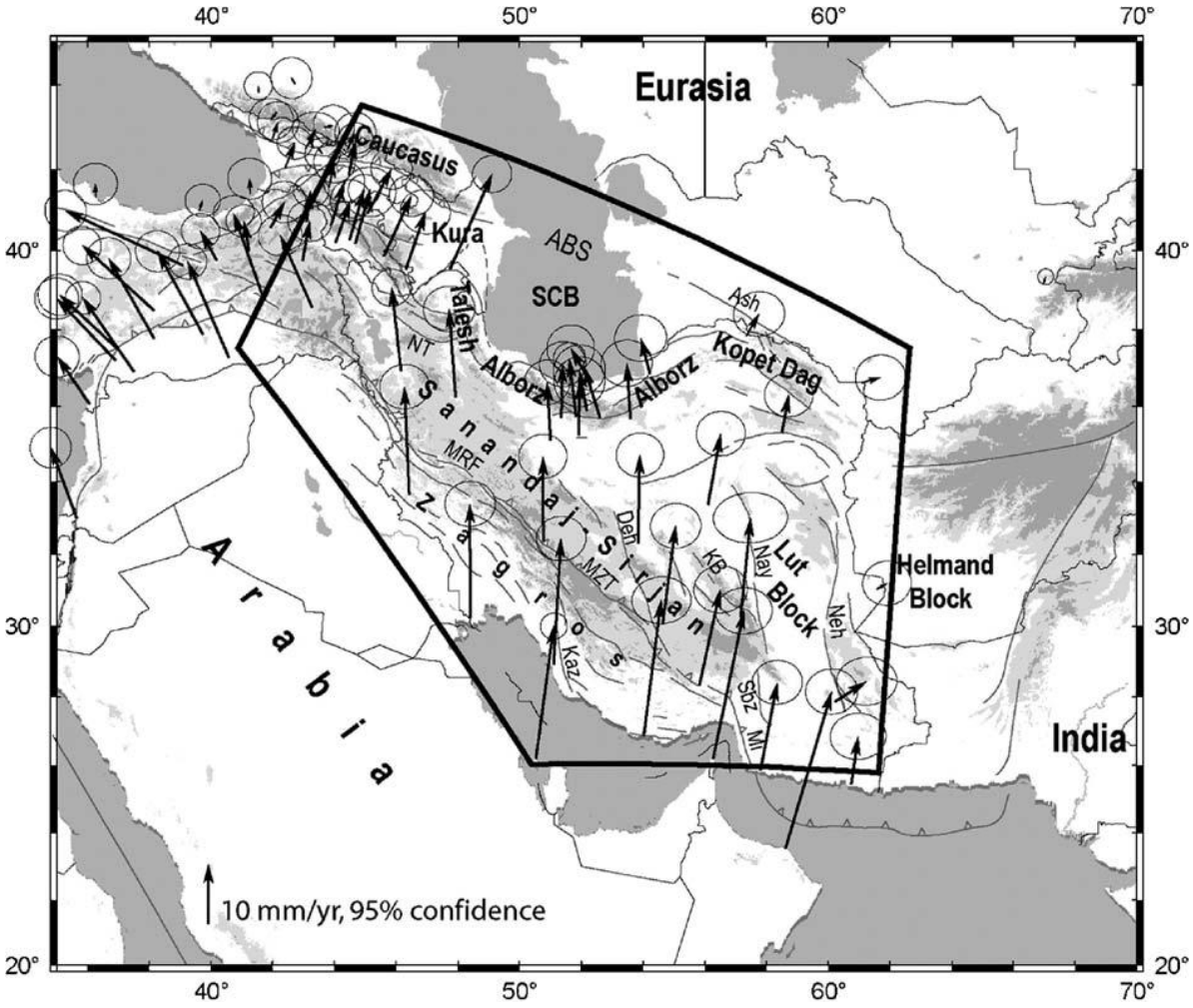

Figure I- 3: Simplified tectonic map and GPS velocity field. The GPS horizontal velocities and their 95% confidence ellipses are in Eurasia-fixed reference frame (Vernant and Chéry, 2006)

VI. Geology of the Zagros

The Zagros collision followed a series of tectono-metamorphic and magmatic events on the Eurasian plate recorded in the Late Mesozoic Sahneh-Neyriz ophiolitic complex, the Mesozoic volcanic arc, fore-arc and tectono-metamorphic belt of the Sanandaj-Sirjan Zone and the Tertiary Andean-type Urumieh-Dokhtar volcanic arc (Berberian and Berberian, 1981; Berberian et al., 1982; Berberian and King, 1981), from south to north, respectively (Fig. I- 4). The formation of the Zagros belt is the result of a complex and long-lived orogeny spanning over the latest Cretaceous and the whole Cenozoic period. Because of this long duration and complexity,

geodynamic events of the Zagros orogen, in particular collision-related tectonics, are difficult to identify and to date. Hereafter, we introduce the main geological characteristics of the Zagros belt as well as the Sanandaj-Sirjan belt and Urumieh-Dokhtar volcanic arc that are relevant to this study.

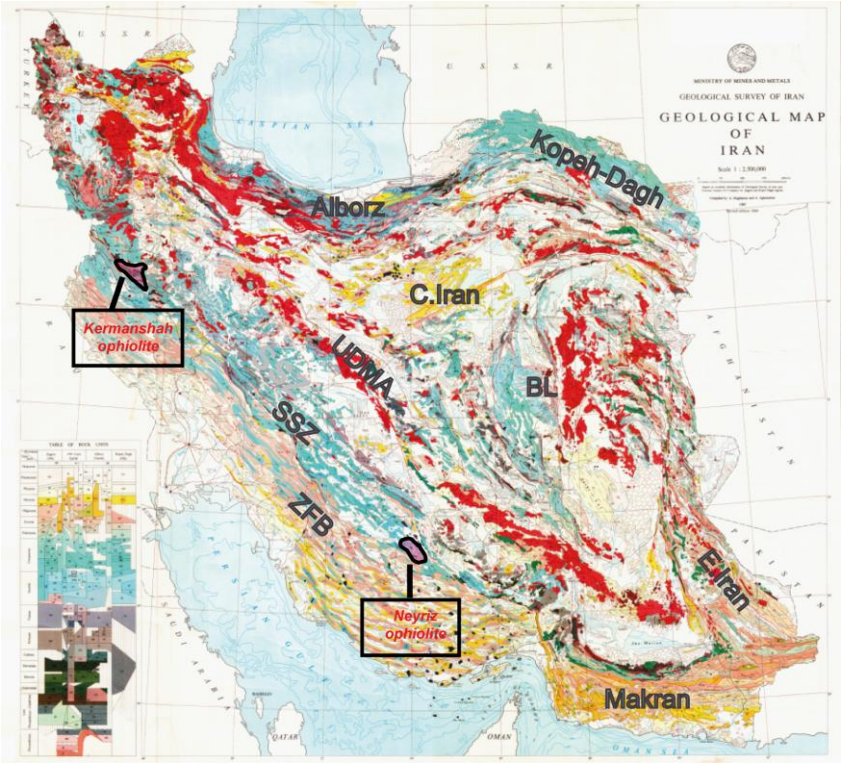

Figure I- 4: Geological map with structural divition of Iran. Abbreviations are UDMA, Urumieh-Dokhtar Magmatic Arc; SSZ, Sanandaj-Sirjan Zone; C.Iran, Central Iran; E.Iran, East Iran; BL, Block Lut; ZFB, Zagros Folded Belt.

VI-1. Sanandaj-Sirjan Zone (SSZ)

The Sanandaj-Sirjan Zone (SSZ), located to the north of the MZT, represents the tectono-magmatic and metamorphic part of the Zagros belt (Figs. I- 5 and 6). It is made of sedimentary and metamorphic Paleozoic to Cretaceous rocks formed in the former active margin of an Iranian microcontinent drifted during the Late Jurassic (Berberian and Berberian, 1981; Golonka, 2004). But alternative interpretations consider it as the metamorphic core of a larger Zagros

accretionary complex built by the thickening of distal crustal portions of the Arabian margin (Alavi, 2004; Shafaii Moghadam et al., 2010).

The Miocene emplacement of the MZT is revealed by the thrusting of the Cretaceous limestones onto Eocene and Miocene sediments south of Eghlid (Fig. I- 5). During the second half of Mesozoic times (Middle Jurassic-Lower Cretaceous), part of the SSZ was an active Andean-like margin characterized by calc-alkaline magmatic activity in which mainly andesitic and gabbroic intrusions were emplaced (Berberian and Berberian, 1981). The metamorphic part of the Sanandaj-Sirjan Zone can be subdivided into HP/LT and HT/LP metamorphic belts that developed at a transpressional plate boundary between Iran and Arabia (Sarkarinejad and Azizi, 2008). For instance, the Tutak Gneiss dome (Fig. I- 5) within the HP/LT belt is cored by gneiss and granite for which $^{40}Ar/^{39}Ar$ dating yielded ages of 180 Ma and 77 Ma (Sarkarinejad and Alizadeh, 2009). In the Cheh-Galatoun (Quri) metamorphic mélange (Fig. I- 6), few tens kilometers to the east of the Neyriz obducted complex, amphibolites, garnet-bearing amphibolites and some eclogites or kyanite schists are exposed (Sarkarinejad et al., 2009). $^{40}Ar/^{39}Ar$ dating of the Quri amphibolites yielded an age of ~91 Ma and 112-119 Ma in biotite gneiss (Fig. I- 6). This cooling event is related to burial and final exhumation of these rocks in an accretionary wedge during the Cretaceous. The good agreement between the cooling ages of the Neyriz Ophiolitic complex and SSZ suggest exhumation during the same tectonic episode. Although critical, the tectonic position of the HP metamorphic rocks with respect to the Neyriz ophiolites is still debated and it is still not clear whether the metamorphic mélange of SSZ should be positioned in the upper Eurasian or the lower Arabian plate (Alavi, 2004; Agard et al., 2006; Shafaii Moghadam et al., 2010) mostly because of the obliteration of original structural relationships by subsequent deformation events. By contrast, the HT/LP belt to the north (Figs. I- 5 and 6) is presumably older and related to regional metamorphism related to magmatism (Sarkarinejad and Azizi, 2008). These latter metamorphic rocks are unconformably overlain by the Lower Cretaceous Orbitolina limestones (Figs. I- 5 and 6), typical of the Central Iran sedimentation (Stocklin, 1974). There are several evidences that magmatism resumed in the Paleocene-Eocene in the SSZ, for instance, when gabbroic intrusions (Gaveh-Rud pluton; see Leterrier, 1985) or granitic intrusions (Gaiduh granite) occurred (Rachidnejad-Omran et al., 2002).

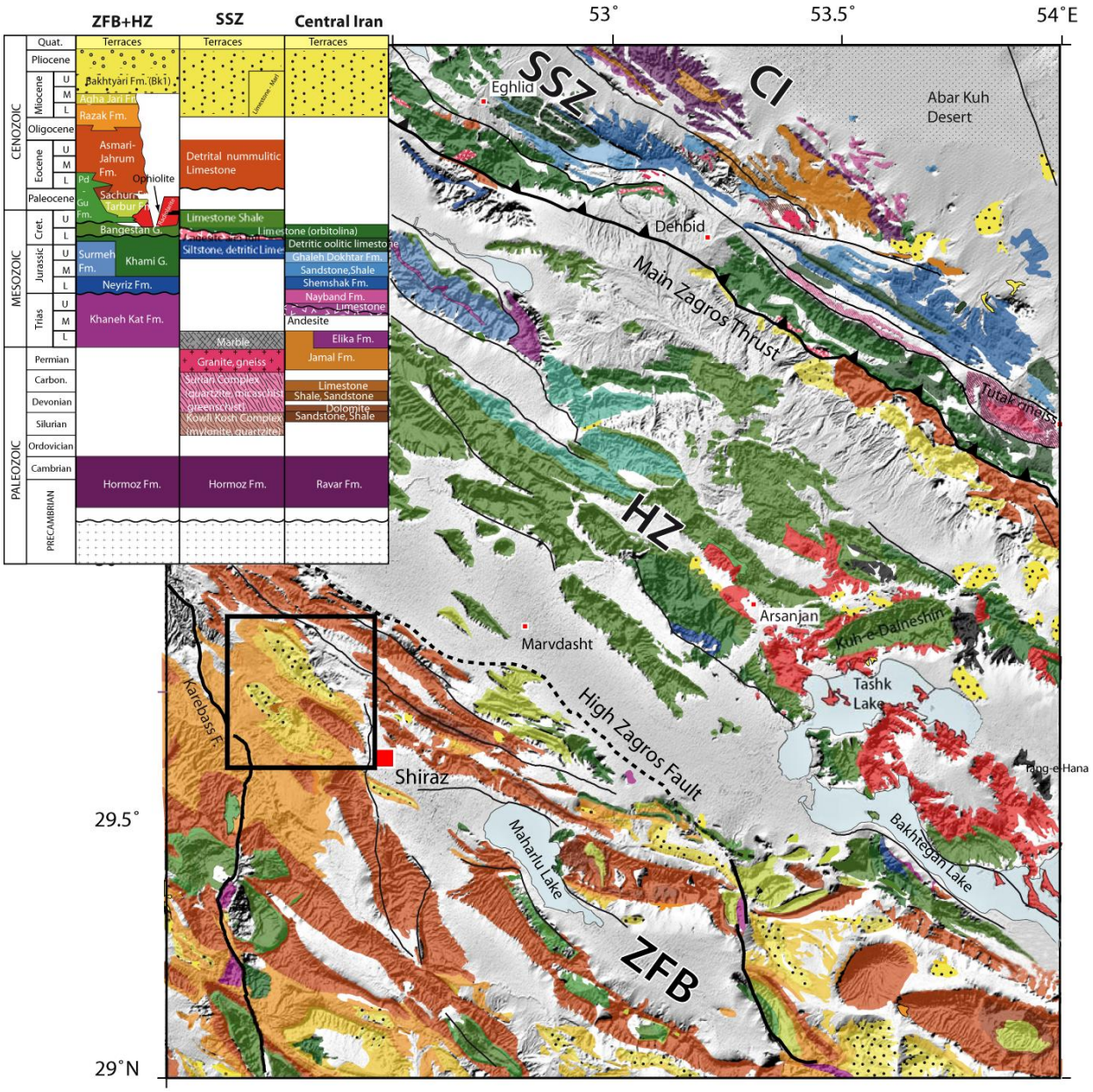

Figure I- 5: Regional scale geology map of High Zagros region (Scale 1:250,000). CI, Central Iran; SSZ, Sanandaj-Sirjan Zone; HZ, High Zagros; ZFB, Zagros Folded Belt. The map is based on a compilation of geological maps of Eghlid and Shiraz by 1:250,000 scale, Kalestan and Shurab by 1:100,000 from GSI. The stratigraphic ages of Agha-Jari and Bakhtyari Fm. in the Zagros is from Khadivi et al (2010) and Tutak Gneiss Dome in SSZ from Sarkarinejad and Alizadeh (2009) (cf. chapter III).

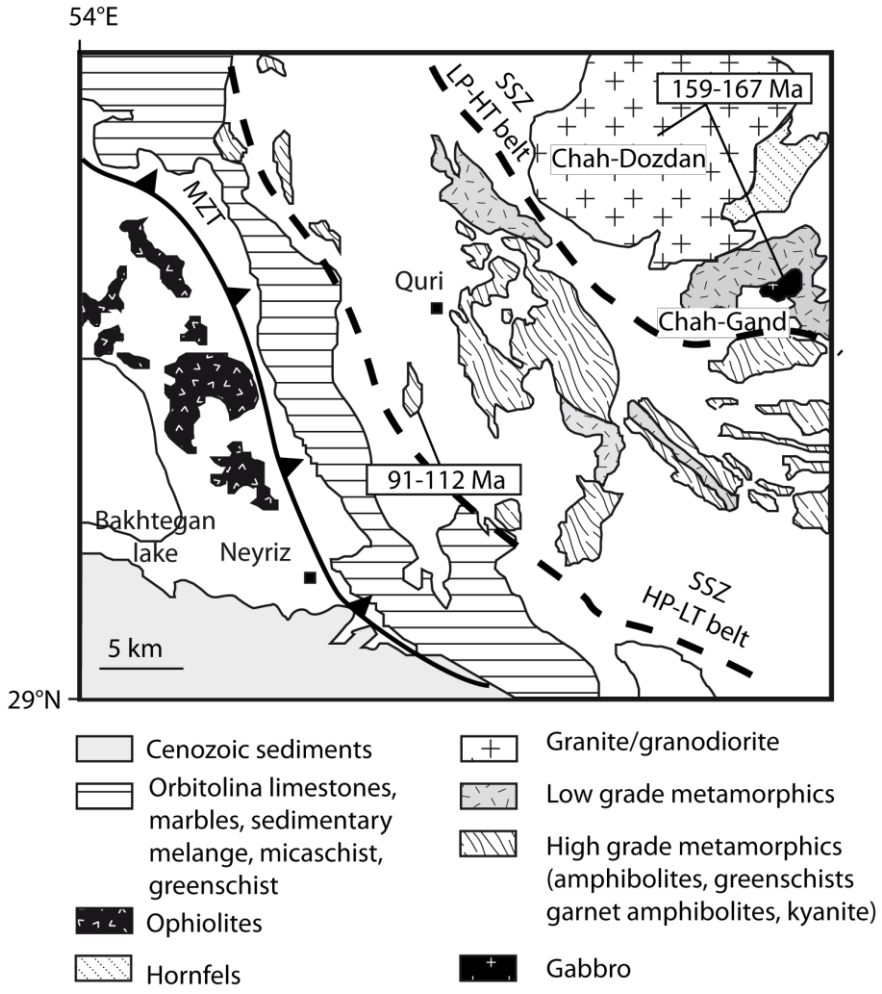

Figure I- 6: Geological map of the northern Fars area, modified after Sheikholeslami et al. (2008), including the Neyriz ophiolitic complex and the low and high grade metamorphic belts of the Sanandaj-Sirjan Zone. $^{40}Ar/^{39}Ar$ radiometric datings of the Quri metamorphic mélange is from Sarkarinejad et al. (2009) and Haynes and Reynolds (1980). Ages of the Chah-Gozdan and Chah-Ghand plutonic massifs are from Sheikholeslami et al. (2008).

VI-2. Urumieh-Doktar magmatic arc (UDMA)

The Urumieh-Dokhtar magmatic assemblage (UDMA; Fig. I- 4) (Alavi, 2004) has been active from the Late Jurassic to the present (Berberian and King, 1981; Berberian et al., 1982). Extrusive volcanism began in the Eocene and continued for the rest of that period with a climax in Middle Eocene (Berberian and King, 1981). The UDMA is composed of voluminous tholeiitic, calc-alkaline, and K-rich alkaline magmatic rocks (with associated pyroclastic and volcanoclastic successions) along the active margin of the Iranian plate (Fig. I- 5). The oldest

rocks in the UDMA are calc-alkaline magmatic rocks, which cut across Upper Jurassic formations and are overlain unconformably by Lower Cretaceous fossiliferous limestone. The youngest rocks in the UDMA consist of lava flows and pyroclastics that belong to Pliocene to Quaternary volcanic cones of alkaline and calc-alkaline nature (Berberian and Berberian, 1981).

The Plio-Quaternary volcanism was suggested to result from the modification of geothermal gradients due to uplift (Berberian and King, 1981) that was further tentatively related to lithosphere delamination beneath the overthickened Iranian plateau (Hatzfeld and Molnar, 2010) and is supported to some extent by surface waveform tomography data (Maggi and Priestley, 2005).

VII. Zagros Folded Belt

Before full presentation of the structure and stratigraphy of the Zagros folded belt we introduce hereinafter the main tectonic boundaries of the Zagros Folded Belt.

VII-1. Zagros main structural subdivisions

To the South, the Imbricate Zone and the Zagros Simply Folded Belt form a large external folded domain within the rifted Arabian continental margin. From a morpho-tectonic point of view five zones can be distinguished along the length of the orogen (Berberian, 1995; Falcon, 1974; Sten, 1985; Stocklin, 1968).

The Zagros Folded Thrust Belt (ZFTB) is divided into:

The High Zagros Thrust Belt (Zagros Imbricate Zone); the Zagros Simply Folded Belt; the Zagros Foredeep; the Zagros Coastal Plain; and the Mesopotamian-Persian Gulf foreland basin (James and Wynd, 1965). The boundaries between these units are defined based on the apparent transitions in topography, deformation style, subsurface data, and seismic characteristics. These boundaries are interpreted as reflecting deep major thrust fault.

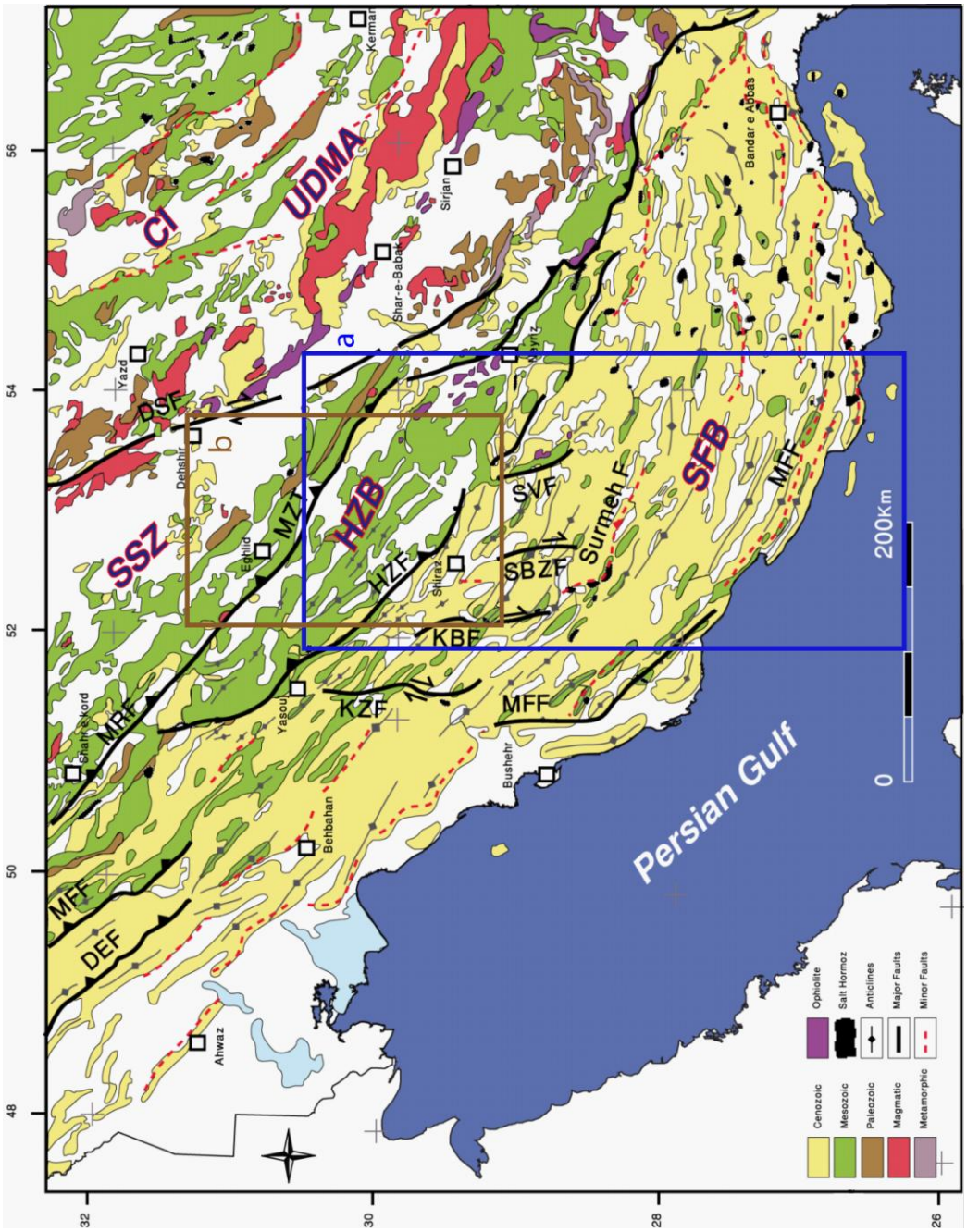

Figure I- 7: Simplified geological map of the SW of Iran on based of geological 1:2,000,000 from Geological Survey of Iran (GSI). The positions of main active faults are shown. Large volumes of Cambrian Hormuz salt extrude through diapirs in the Zagros basin east of the Kazerun fault. Location of Figure I-5 is shown by b and Figure I -8 is shown by a. Abbreviations are UDMA, Urumieh-Dokhtar Magmatic Arc; SSZ, Sanandaj-Sirjan Zone; C.I, Central Iran; HZB, High Zagros Belt; SFB, Simply Folded Belt; DSF, Dehshir Fault; KZF, Kazerun Fault; KBF, Karebas Fault. SBZF, Sabz Pushan Fault; SVF, Sarvestan Fault; MFF, Main Frontal Fault; MRF, Main Recent Fault; MZT, Main Zagros Thrust; HZF, High Zagros Fault; DEF; Dezful Fault.

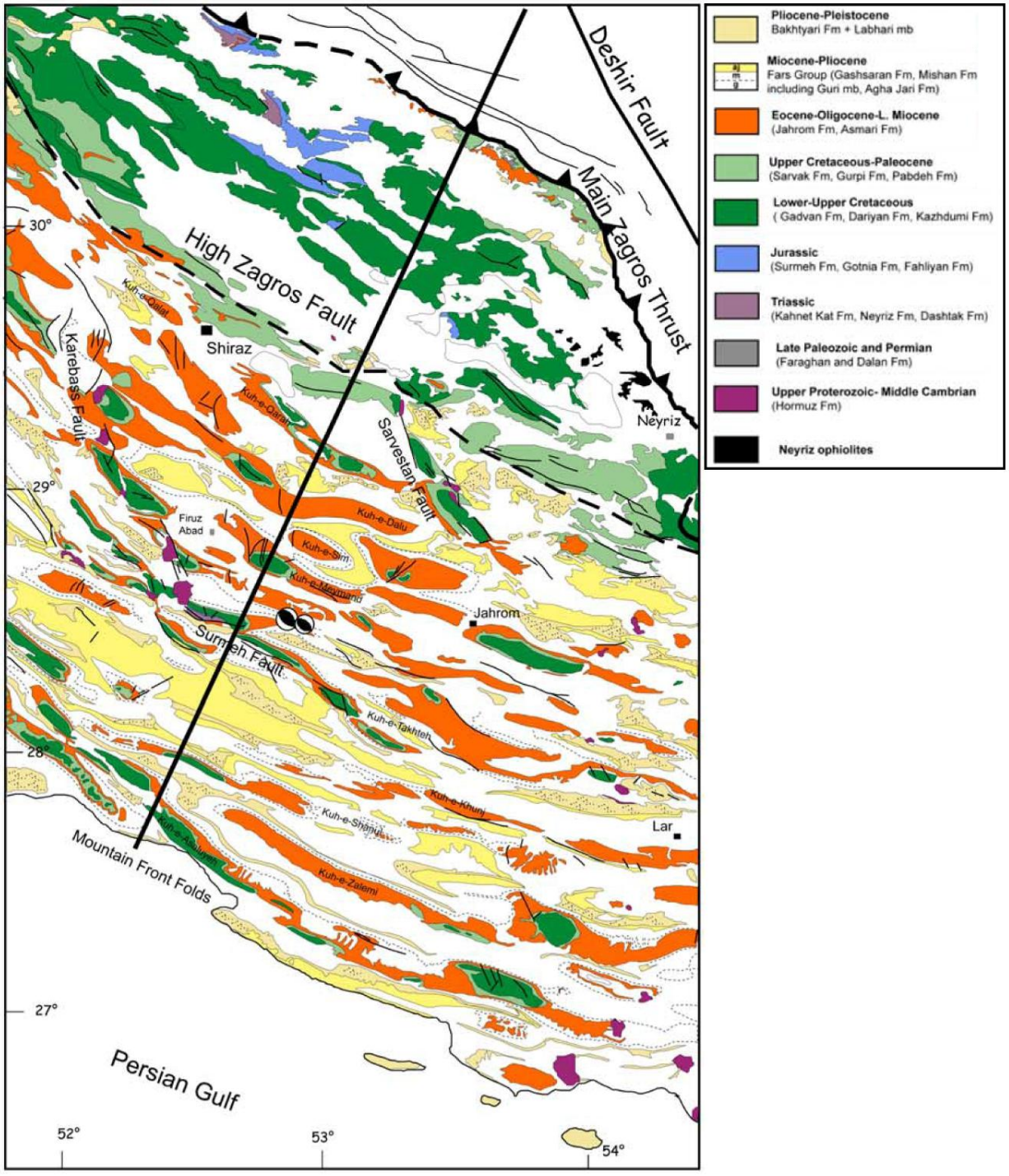

Figure I- 8: Geological map of the Fars based on a compilation of geological 1:250,000 and 1:100,000 scale maps from the National Iranian Oil Company. The Imbricate Zone (High Zagros) north of the High Zagros Fault is characterized by the lack of Oligo-Miocene deposits which contrast with the Zagros Folded Belt to the south. The anticlines and the major transverse strike-slip faults are depicted. Two compressive focal mechanisms located to the north of the Surmeh Fault have been used to constrain the geometry at depth of the Surmeh basement thrust (Mouthereau et al., 2007b).

The Zagros can be divided to two different regions: Hormuz basin in South East and Ahvas basin in North West, the border of these basins is the Qatar-Kazerun line.

In addition, along the strike of the belt, from SE to NW, one can distinguish several tectono-stratigraphic domains: the Fars province (eastern Zagros), the Izeh zone, Dezful Embayment (Central Zagros) and the Lurestan province (Western Zagros) (Motiei, 1993, 1995; Talbot and Alavi, 1996). This classification is actually based on the subdivision proposed by Agard et al (2005) and James and Wynd (1965).

VII-1-a. The High Zagros Thrust Belt (or Zagros Imbricate Zone)

The High Zagros Thrust Belt (HZTB) has a width of more than 80 km and is located between the Main Zagros Thrust (MZT) or the Main Recent Fault (MRF) to and the High Zagros Fault (HZF) in the southeastern part of the HZTB. The High Zagros Thrust Belt is an intensely deformed zone, characterized by high mountains, with maximum elevation reaching about 3000 meters in NW Zagros, and overthrust anticlines that expose deep sedimentary formations. The HZTB was formed as a result of the Late Cretaceous subduction and Pliocene continent-continent collision and represents the inner-most part of the Arabian deformed margin, featuring radiolaritic-ophiolitic thrust sheets over the NE Arabian margin (Fig. I- 3) (Agard et al., 2005; Alavi, 1994; Berberian, 1995).

VII-1-b. The Zagros Simply Folded Belt (ZSFB)

The Zagros Simply Folded Belt is located to the south of the High Zagros Fault (Berberian, 1995). To the south, the Simply Folded Belt is separated from the Persian Gulf- Mesopotamian foreland basin by the Mountain Front Flexure (Falcon, 1961). This belt is 1375 km long, 250 km wide along the southern part, and 120 km wide along the northwestern edge. The main Zagros faults which took place in this region are the following.

The Main Recent Fault (MRF)

The MRF is a NW-SE trending, active, right-lateral strike-slip fault that generally follows the trend of the MZT (Berberian, 1995; Tchalenko and Baraud 1974). This fault is ~640 km

long, bounding the Zagros to the northeast, and separated from the ZFTB by Central Iran (Berberian and Yeats, 2001). This fault is clearly recognized morphologically and structurally along its entire length. The component of right-lateral strike-slip motion between Arabia and central Iran takes place preferentially along different segments of the MRF in western Iran (Jackson, 1992). Strike-slip movement from the MRF appears to be transmitted to the NS-trending right-lateral Kazerun and Karebass faults (Authemayou et al., 2006). The average slip along this fault is 40 mm/yr, and the fault is characterized by high-magnitude seismicity. Geodetic measurement in the Fars arc/Central Zagros indicate that the MZT in the SE is inactive there (Tatar, 2002). Talebian and Jackson (2004) on the basis of earthquake focal mechanisms analysis proposed that oblique convergence is partitioned into right-lateral strike-slip faulting on the MRF and shortening perpendicular belts. A right-lateral strike-slip offset of ~50 km on the Main Recent Fault is compatible with the restoration of the drainage, geological markers and the length of the pull-apart basins (Talebian and Jackson, 2004); the offset may be as much as ~70 km. The configuration of active faulting and earthquake slip vectors today shows that this offset is geometrically linked to a shortening of ~50 km across the NW Zagros and to a total N-S convergence of ~70 km, which is a substantial fraction of the 85-140 km total Arabia-Eurasia convergence over the last 3-5 Myr (Talebian and Jackson, 2002).

The High Zagros Fault (HZF)

The active HZF separates the High Zagros Thrust Belt (HZTB) from the Simply Folded belt. Along this segmented reverse fault, Paleozoic rocks were vertically displaced by 6 km (Berberian, 1995). The result of this displacement is obvious in the level of the exposure of the sedimentary cover strata in both sides of the HZF. At various places along this fault, the Hormuz salt intrudes and reaches the surface, confirming that the HZF is a deep fault that cuts the Lower Cambrian Hormuz Salt horizon, and extends through the entire Phanerozoic sedimentary cover. There is some seismic activity in the southeastern part of the HZF with strike-slip focal mechanism solutions. A long this fault there is a gap in seismicity of about 440 km (Berberian, 1995). By wedging of the post-Asmari deposits (Miocene Gachsaran evaporites together with the Lower Miocene to Pleistocene Agha Jari-Bakhtyari synorogenic molasse) towards the High Zagros, Falcon (1974) and James and Wynd (1965) suggest that uplift of the High Zagros along

the HZF since the Early Miocene, was contemporaneous with subsidence of the Zagros Foredeep, deformation and outward migration of the Zagros basin (Berberian, 1995).

The Mountain Frontal Fault (MFF)

The MFF delineates the south-southwestern boundary of the ZSFB. This fault marks a clear major topographic step and can be viewed as a segmented major blind thrust fault with a clear structural, topographic, geomorphic and seismotectonic expression (Berberian, 1995). It is composed of discrete segments of fault blocks with length ranging from 15 to 115 km. It is believed that since the early Tertiary, the MFF had controlled sedimentation of the Zagros foreland basin (Sepehr and Cosgrove, 2004; Sherkati and Letouzey, 2004). The subsidence of the Zagros Foredeep in the Dezful Embayment area is suggested by the thickening of sediments formed after the deposition of the Asmari Fm. This is argued by the relative motion along the MFF and the Dezful Embayment Fault (DEF) from the Early Miocene. Stratigraphic, seismic, and drilling investigations show that more than 6 km cumulated vertical displacement have occurred along the MFF thrust fault (Berberian, 1986; Falcon, 1974). Due to this vertical movement, the southwestern margin of the ZSFB was uplifted.

The Kazerun fault (KF)

The KF is a right-lateral fault with a N-S trend that cuts across the SFB causing bending, dragging and offsetting of the fold axes in a right-lateral sense (Berberian, 1995) (Fig. I- 9). Cumulative right-lateral displacement of 140 and 150 km of the Zagros Mountain Front (MFF) and the Zagros Foredeep faults (ZFF) can be measured, respectively, along the Kazerun fault (Berberian, 1995; Lacombe et al., 2006). It has the role of transferring differential displacement between tectonic blocks rather than simple strike-slip fault (Lacombe et al., 2006). If slip began after deposition of the Lower Miocene Gachsaran Formation (~10 Ma), an average slip rate of 14.5 mm/yr can be proposed (Berberian, 1995). Movement along the Kazerun Fault can be traced back to the Cambrian, when it controlled the distribution of the Hormuz salt (Talbot and Alavi, 1996). The KF, as a system of active right-lateral strike-slip faults, has propagated southwestward from the MRF toward the main Arabian indenter due to anticlockwise rotation of Arabia; it likely helps transmitting and distributing strike-slip motion of oblique plate

convergence in the ZSFB (Authemayou et al., 2005). Toward the east , numerous Hormuz salt emerging at the surface (Lacombe et al., 2006; Sherkati and Letouzey, 2004).

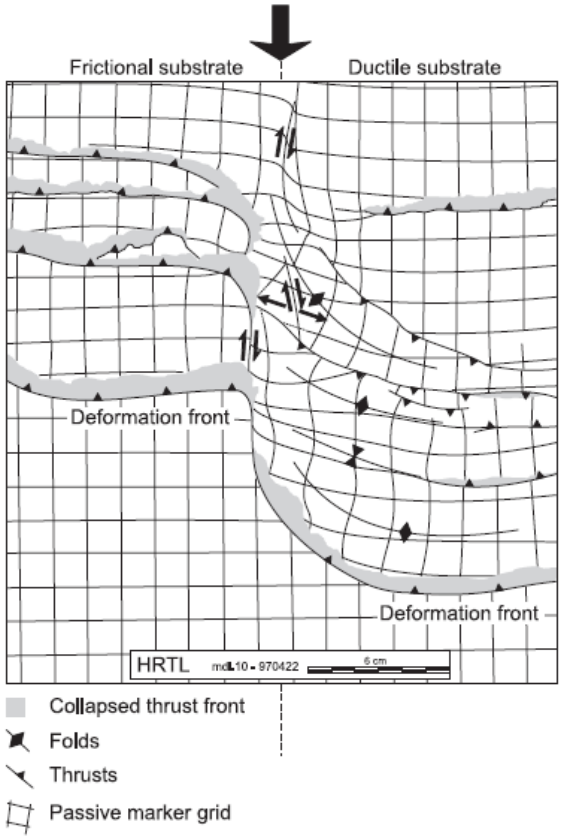

Figure I- 9: This figure show the result of sandbox experiment (Cotton and Koyi, 2000). It could be compare with the situation of Kazerun fault and propagading further fault over the viscous basement.

The Karebass fault (KBF)

The KBF, with a total length of 160 km is situated about 65 km east of the Kazerun fault and 35 km west of the city of Shiraz. It is a nearly N-S-trending fault characterized by right-lateral strike-slip faulting, which like the Kazerun fault, has dragged and displaced anticline axes for at least 10 km (Berberian and Tchalenko, 1976). There is no report about large earthquake evidence along its trend. The Karebass plain is a small pull-apart depression ~90 km formed along the Karebass fault. The southern segment of the Karebass fault turns toward the east to form the Surmeh thrust fault, characterized by the only exposed lower Paleozoic anticlinal in the Zagros Simply Folded Belt. The Sabz-Pushan fault zone marks the limit between the Asmari

Formation facies to the west and the Asmari-Jahrom Formation facies to the east (Berberian, 1995).

Local balanced cross sections east and across the fault zone indicate that the same amount of shortening is accommodated by two folds to the west and distributed on three folds to the east. This means that the Sabz-Pushan fault zone did not behave as a simple strike-slip fault cutting through and offsetting previously formed folds, but rather behaved as a primary tear fault, nearly parallel to local transport direction, and accommodating local kinematic incompatibilities in the cover (Lacombe et al., 2006).

VII-1-c. The Zagros Foredeep (ZFF)

The Zagros Foredeep is limited by the Mountain Front Fault (MFF) from northeast and to the Zagros Foredeep Fault (ZFF) from southwest. This fault is characterized by symmetrical and elongated folds (Berberian, 1995). The ZFF separates the Zagros Foredeep (to the north and northeast) from the Zagros Coastal Plain (in the south and southwest). It forms the northeastern edge of the alluvial Coastal Plain of the Persian Gulf and is principally a reverse-slip system (Berberian, 1995). There are two regional embayments in the Zagros Foredeep: The Dezful Embayment, a depressed area within the Zagros Folded Belt, which is characterized by a thick sequence of post-Miocene sediments. The Dezful Embayment is surrounded by the Mountain Front Fault (MFF) and the Dezful Embayment Fault (DEF) to the north, the N-S trending Kazerun fault zone to the east and southeast, parts of MFF and the E-W trending Bala Rud fault zone to the west and northwest, and Zagros Foredeep Fault (ZFF) to the south and southwest. The anticlines associated with the Zagros Foredeep are actively growing, and the evidence of continuous unconformities in the Pliocene freshwater sediments and folded recent gravels shows that they have been active since the beginning of the Pliocene (Falcon, 1961).

Structural transect shows a shortening of approximately 6% in the Dezful Embayment. Sherkati and Letouzey (2004) suggested that a Middle to Post-Miocene shift of sedimentary depocenter to the southwest allowed rapid subsidence and thick accumulation of the Fars group in the Dezful Embayment. Meanwhile, the inner part of the belt was subjected to folding, uplift and erosion. The fold wavelengths are controlled by thickness between the lower and upper detachments in Dezful Embayment (Sherkati et al., 2005).

Pronounced subsidence of the Zagros Foredeep and the Dezful Embayment with thickening of the post-Asmari deposits (Neogene Gachsaran Evaporites and the Agha Jari-Bakhtyari synorogenic molasse) provides further evidence of relative motion along the MFF and the Dezful Embayment fault since Early Miocene times (Sherkati and Letouzey, 2004).

On the basis of the historical evidence, an uplift rate of l mm/yr in the Shaur anticline in the Dezful Embayment (Zagros Foredeep) has been estimated since the Late Pliocene (Ahmadhadi et al., 2008). Holocene uplift rates of 1.8-6.6 mm/yr derived from the fossil shorelines in the Zagros coastal plain southwest of Bandar Abbas prove that the Zagros front is still very active.

VII-2. Stratigraphy and sedimentology

VII-2-a. Paleozoic

During the Palaeozoic, Iran, Turkey and the Arabian plate together with Afghanistan and India formed the wide passive margin of Gondwanaland bordering the Paleo-Tethys Ocean to the north. The Early Palaeozoic deposits, which extend from the Zagros to central and northern Iran, were deposited during the stage of rifting (Berberian and King, 1981; Beydoun, 1991; Stocklin, 1968).

The Precambrian basement of the Zagros is known just based on the available air-magnetic data and fragments of the metamorphic basement, which brought to the surface by the Hormuz salt diapirs (Gansser, 1992; Kent, 1979). The base of the Zagros sedimentary sequence starts with1-2 km thick of Infra-Cambrian to early Cambrian Hormuz Salt formation which was probably deposited on the northern continuation of the Panafrican basement exposed in Arabia (Talbot and Alavi, 1996). Large volumes of Cambrian Hormuz salt that formerly lay at the base of the cover sequence now extrude through >200 diapirs in the Zagros basin east of the Kazerun fault (Fig. I- 10) (Kent, 1979).

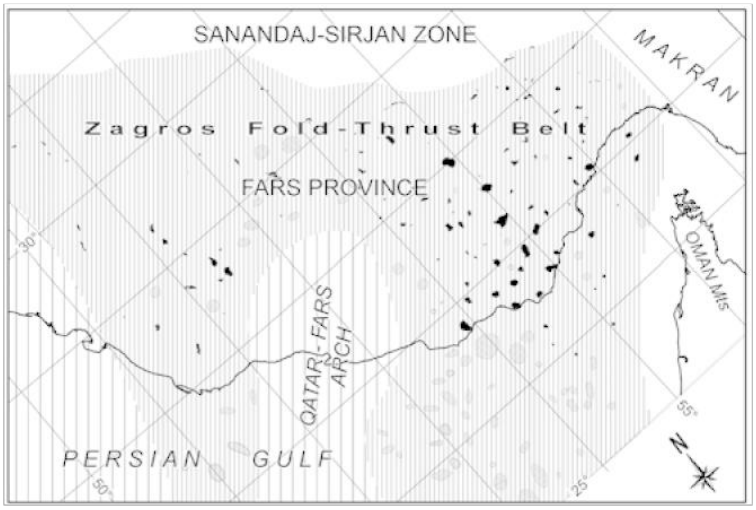

Figure I- 10: Distribution of Hormuz salt diapirs in the Fars region of the Zagros Folded Belt. Dark surfaces denote emergent Hormuz salt diapirs; light gray surfaces denote buried Hormuz salt diapirs (Jahani et al., 2009).

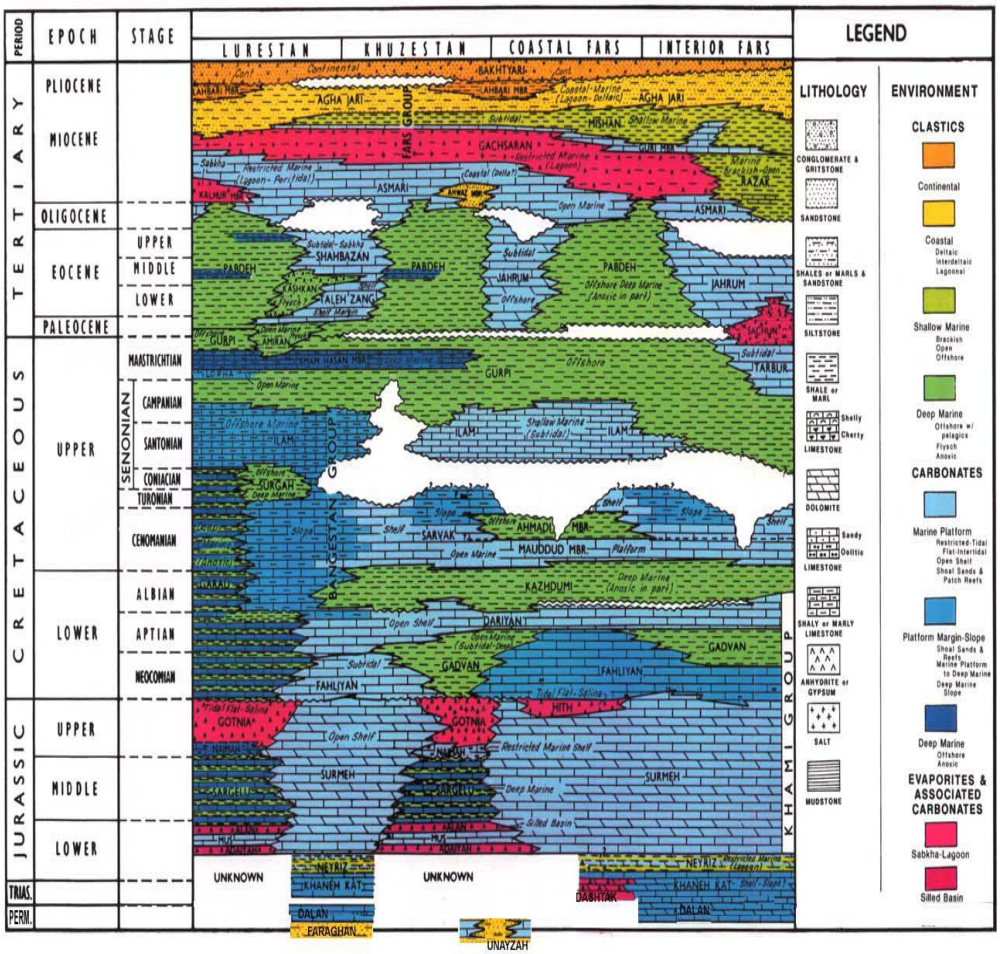

Figure I - 11: Schematic chronostratigraphic chart and lithologies encountered in the Zagros Folded Belt domain from NW to SE; after James and Wynd, 1965., (Bordenave, 2003).

VII-2-b. Mesozoic

By the Late Triassic, the Neo-Tethys Ocean opened between Arabia and Iran (Koop and Stoneley, 1982). Throughout the Late Triassic to Early Cretaceous, the Arabian platform was a stable shallow shelf dominated by carbonate and some evaporitic deposition. Numerous transgression and regression during the Mesozoic explain the lateral facies changes of carbonates from southeastern Zagros to the Lurestan Province in the northwest of the Zagros belt (Setudehnia, 1978).

Hormuz salt unit was overlain by 6-10 km of platform deposits that are predominantly sandstone, shale, and dolomite (Cambrian through Triassic) and limestone with subordinate shales and evaporates (Jurassic through Lower Miocene) (McQuarrie, 2004).

VII-2-c. Cenozoic

In Late Oligocene-Early Miocene, turbidites were deposited in the northeast part of the High Zagros area whereas the limestones of the Asmari Formation were deposited to the south (Fig. I-11). This reveals the presence of a second flexural basin associated with the onset of continental collision during the Late Oligocene-Early Miocene. The mid-Miocene and younger rocks include gypsum, limestones, sandstones, shales, and conglomerates (McQuarrie, 2004).

In the Zagros Basin, foreland sequences of Miocene ages are represented by a thick regressive siliciclastic sequence (up to 3000 m), namely, the Fars group lying above the well-developed carbonate platform of the Asmari Formation. The initiation of foreland siliclastic deposition is delayed toward the foreland: the onset of clastics deposition is Chattian (~28 Ma) in the northern Fars whereas it is Burdigalian (~20-16 Ma) near the Persian Gulf (Fig. I- 11). The Miocene Gachsaran formation generally covers the anticlines and is composed of marls, anhydrite, thin limestone and locally large quantities of salt (Colman-Sadd, 1978). The Agha Jari Formation usually displays an increasing upward abundance of red weathered shales and sandstones and the complete disappearance of carbonates. The subsidence also increases significantly northward in agreement with the flexure of the Arabian margin undergoing tectonic loading (Mouthereau et al., 2007b). The major angular unconformity between the Agha Jari and

Bakhtyari formations is considered as Late Pliocene climax orogeny in the Zagros fold and thrust belt (Haynes and McQuillan, 1974). Growth strata within Agha Jari Formation indicate early movements before this major unconformity (Homke et al., 2004; Sherkati et al., 2005). Khadivi et al (2010) have dated the base of the Agha Jari Formation to 16.6 Ma (cf. chapter II) which is slightly older than the Agha Jari Formation at a similar structural position in the Izeh zone where its base was dated magnetostratigraphically at ca. 15.5 Ma This transition appears also significantly older than at the mountain front in the Lorestan area, where the base of the Agha Jari Fm is dated to 12.8-12.3 Ma (Emami, 2008; Homke et al., 2004).

VII- 3. Structure

The contractional Zagros orogeny formed a variety of asymmetric, NW-SE trending, double-and multiple-hinged, en-echelon folds, and NE-dipping thrusts on the southwestern limbs of the folds. The length and width of these folds along the Zagros are in the order of tens of kilometers. Their wavelengths range is about 16 km in the Fars (Mouthereau et al., 2007a). The low taper angle, the great width and the accurate shape in map view of the Zagros fold belt in the Fars region are commonly considered as reflecting thin-skinned deformation (Lacombe et al., 2006; Mouthereau and Lacombe, 2006; Mouthereau et al., 2006).

Different geological cross-sections have been proposed for the Zagros Folded Belt, which led to different interpretations of the sequence of folding. The base of the sedimentary cover, in the Lower Cambrian incompetent Hormuz series directly overlies the crystalline basement (Berberian, 1995) as a basal detachment level and play an important role in guiding the deformation. This lower décollement level comprises about 1000 m of salt, beneath the thick sedimentary layers 8-10 km. The stratigraphic succession of rock series with highly variable mechanical properties strongly controls deformation in the ZFB (Fig. I- 12 b) (Sherkati and Letouzey, 2004). Bahroudi and Talbot (2003) proposed a model for the structural configuration of the basement of the Zagros Basin. By geophysical and isopach maps of the Zagros Basin they demonstrated the reactivation of the main basement structures. The model confirms that the basement of the Arabian Plate has exhibited heterogeneous tectonic activity since the opening of Tethys in Permian. Since then it has been divided into two mega-blocks an active East Arabian-Zagros Block, and a passive block. The East Arabian-Zagros Block is characterized by a

sedimentary and tectonic history complicated by repeated reactivation of old basement structures. Some authors attribute the arcuate shape of the Zagros belt east of the Kazerun fault to the reactivation of basement blocks beneath a cover decoupled in a patchwork pattern by the ductile décollement of Hormuz salt.

Basement deformation studied through numerous seismotectonic data (modern or historical earthquakes), focal mechanisms and depths of earthquakes show that that the main part of the seismogenic deformation occurred along active reverse faulting within the Precambrian basement (Berberian, 1995; Ni and Barzangi, 1986; Talebian and Jackson, 2004; Tatar, 2004). Dips of nodal planes that are typically in the range of 30-60° suggesting today's reverse faulting earthquakes occur on reactivated normal faults derived from the Paleozoic-Mesozoic extension of the Arabian margin (Jackson, 1980). But the precision of hypocenters determination have casted doubt on whether the earthquakes are located in the cover or the basement. Hatzfeld et al (2003) using the arrival times of local events recorded on a dense seismological network inferred the upper-crust velocity structure for the central Zagros. They proposed 8 km thickness for the upper crystalline crust and 11 km for sedimentary layer. This estimation, although obtained with a small amount of data, was the first quantitative seismological estimates in the central Zagros. They suggest that the total thickness ~35 km of the crystalline crust therefore looks similar to the thickness of the stretched margin of the Arabian Platform. Therefore, according to their interpretations, the shortening of the Zagros basement may be small and has only started recently, whereas the shortening recorded by the folded sediments is due to the long-term scraping of the sediments above the basement (Hatzfeld et al., 2003). Microseismicity represents the response of a prefractured crust to the shortening rather than the motion on large faults (Tatar, 2004).

The broad Fars arc of the Zagros, commonly cited as classic examples of a fold-thrust belt with salt controlled morphology, would have more to do with the extensional basin geometry regardless of the actual distribution of salt within that basin (Fig. I- 12 c) (McQuarrie, 2004).

The ZFB topographic slope is <0.5°. This low slope was initially attributed to the development of a salt-based wedge but the thickness of weak salt cannot mechanically sustain the load of the overlying units over geological timescales as the salt would be rapidly squeezed out (Mouthereau et al., 2006). A possible alternative mechanism at the origin of the topography in the Fars is the shortening and thickening of the Precambrian basement. In this case, the

deformation in the cover have only a local effect on the topography at the origin of the folding (Fig. I- 12 d)(Mouthereau et al., 2006).

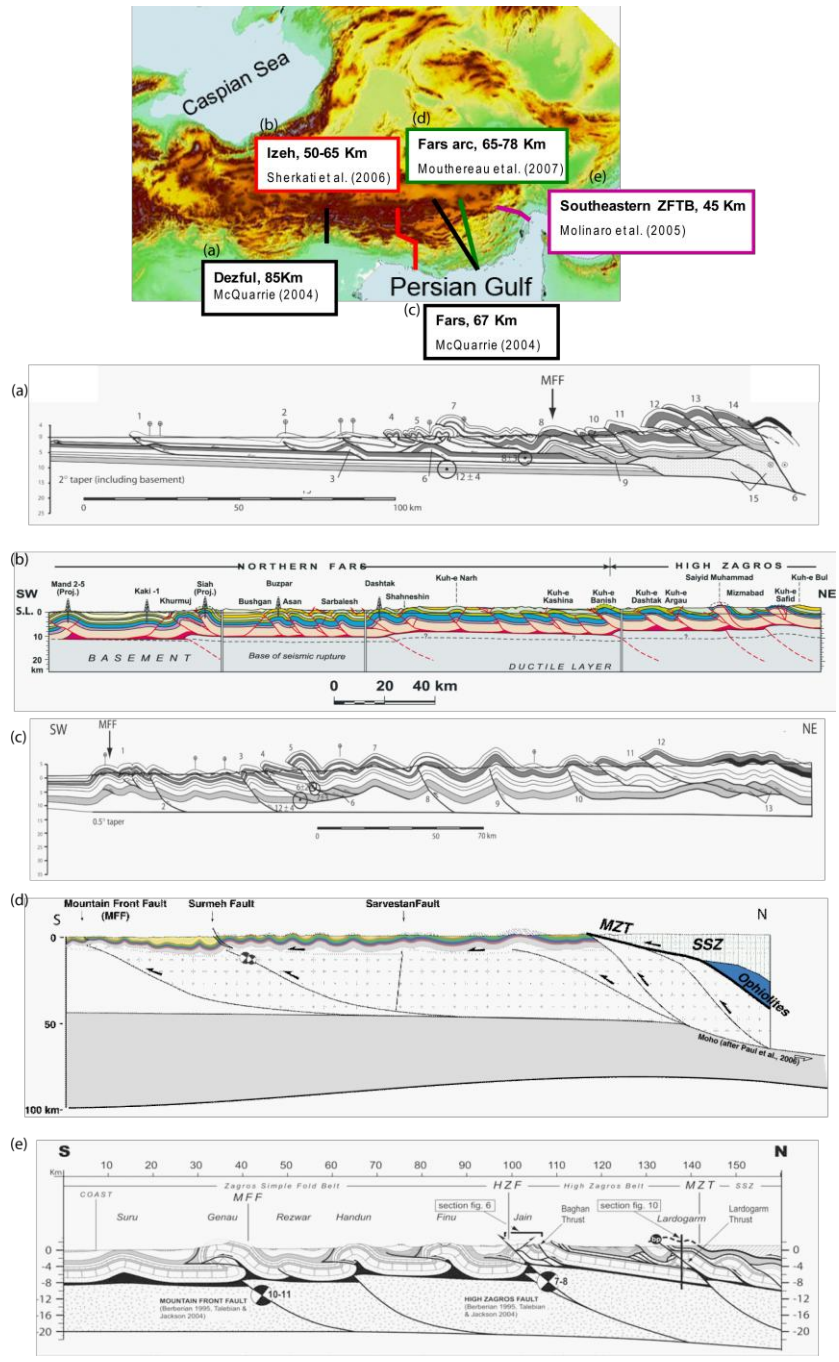

Figure I- 12: Balanced cross-sections proposed across the Zagros Folded Belt. a) Structural transect and regional balanced cross section thin skin style through the Dezful (McQuarrie, 2004); b) Structural transect and regional balanced cross section by involving the basement through the Izeh (Sherkati et al., 2006); c) Regional balanced cross section through the Zagros fold and thrust belt of the Fars domain (McQuarrie, 2004); d) A crustal-scale section across by involving the basement in the Central Fars area of the Zagros Folded Belt (Mouthereau et al., 2007); e) Regional balanced and restored section through the Southestern Zagros fold and thrust belt (Molinaro et al., 2005).

They concluded that basement-involved thickening and shortening is mechanically required to produce the shape of the Zagros Folded Belt since at least 10 Ma. The involvement of the basement provides important mechanical and kinematic constraints that should be accounted for by cross-sections balancing and further studies assessing the evolution of the Zagros at crustal or lithospheric scales (Mouthereau et al., 2007b).

It is also interesting to notice that the nearly aseismic High Zagros shows present-day mean elevations similar to the Iranian plateau. This means that the growth of the plateau is closely coupled with the growth of the High Zagros. This result is consistent with the observation that only 10% of the convergence is accounted for by deformation released during earthquakes (Jackson et al., 1995) which is roughly equivalent to the long-term shortening in the ZFB.

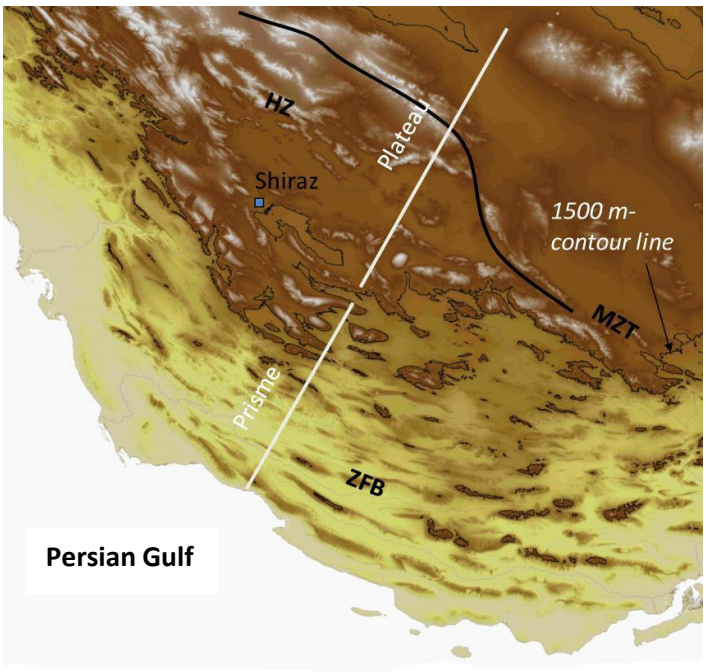

Figure 13: SRTM topography. High Zagros is now part of the Iranian plateau while outer ZFB has a low topographic slope dipping toward the Persian Gulf.

VIII. Reconstruction of the Zagros evolution

VIII-1. Overview

Here in after we attempt at briefly presenting the evolution framework of the Arabian-Eurasia plate boundary from the Paleozoic to the present.

VIII-1-a. Paleozoic plate tectonics in the Zagros

The Persian platform was extended from the latest Precambrian to Early Permian. It is generally agreed that the Persian platform was initiated by a cratonization event during the latest Precambrian when these microcontinents were accreted to Africa. It is possible that some of the N-S trending structural elements of this region formed during the Late Precambrian tectonic activities.

An extensional period either due to continental rifting or due to a back-arc basin affected the platform during the latest Precambrian resulting in the formation of intraplate depressions where major evaporites of this time interval were deposited (Berberian and King, 1981; Husseini, 1989; Ramezani and Tucker, 2003; Sharland et al., 2001). Extensive carbonate deposition suggests the presence of a passive margin setting during the Cambrian but detailed investigations have concluded that the platform was an active margin during this time interval (Golonka, 2000). Subsequently, the platform became a passive margin from Ordovician to Middle Devonian and from Mississippian to Permian whereas an active margin was established during Late Devonian (Golonka, 2000). The similarity in sedimentological characteristics of the uppermost Precambrian to Permian strata suggests that all microplates of the Persian platform remained together during this time interval (Berberian and King, 1981; Beydoun, 1991; Davoudzadeh et al., 1986; Davoudzadeh and Schmidt, 1984; Davoudzadeh and Weber-Dierenbach, 1987; Stocklin, 1968)

VIII-1-b. Mesozoic main tectonic events in the Zagros

Several microplates collectively referred to as the Cimmerian continent were subsequently separated from the Persian Platform by the Neotethys Ocean (Dercourt et al., 1986; Golonka and Ford, 2000; Kazmin et al., 1986; Stampfli et al., 1991). This event could have also produced a horst and graben system close to northeastern edge of the Zagros region (Sharland et al., 2001; Weidlich and Bernecker, 2003; Ziegler, 2001). This passive margin phase continued until the latest Cretaceous. The Sanandaj-Sirjan microplate separated from the Arabian Platform during the latest Triassic to the earliest Jurassic. The tectonic regime between the Sanandaj-Sirjan

microplate and the Arabian Platform changed during the latest Cretaceous and the platform changed from passive to a convergent margin setting (Golonka, 2000).

VIII-1-c. Cenozoic plate tectonics in the Zagros

The Arabian platform phase was ended when the oceanic domain of the Neo-tethys was obducted onto the margin during the upper Cretaceous. In addition, the Neo-Tethys ocean became progressively narrower during this time due to subduction below northern margin (Golonka, 2000). Active margin processes took place in the Zagros region. These events initiated the Zagros Foreland Basin phase which still continues to the present time (Sharland et al., 2001; Sepehr and Cosgrove, 2004; Sherkati and Letouzey, 2004; Sherkati et al., 2006). This phase was characterized by the formation of a narrow, northwest-southeast foreland basin in which Tertiary strata were deposited. The Arabian Plate eventually collided with Iran microcontinent during the Zagros orogeny, closing the Neotethys ocean and forming the fold-and-thrust belt of the Zagros Mountains (Fig. I- 15) (Alavi, 1980; Alavi, 1994; Berberian and King, 1981; Golonka, 2000).

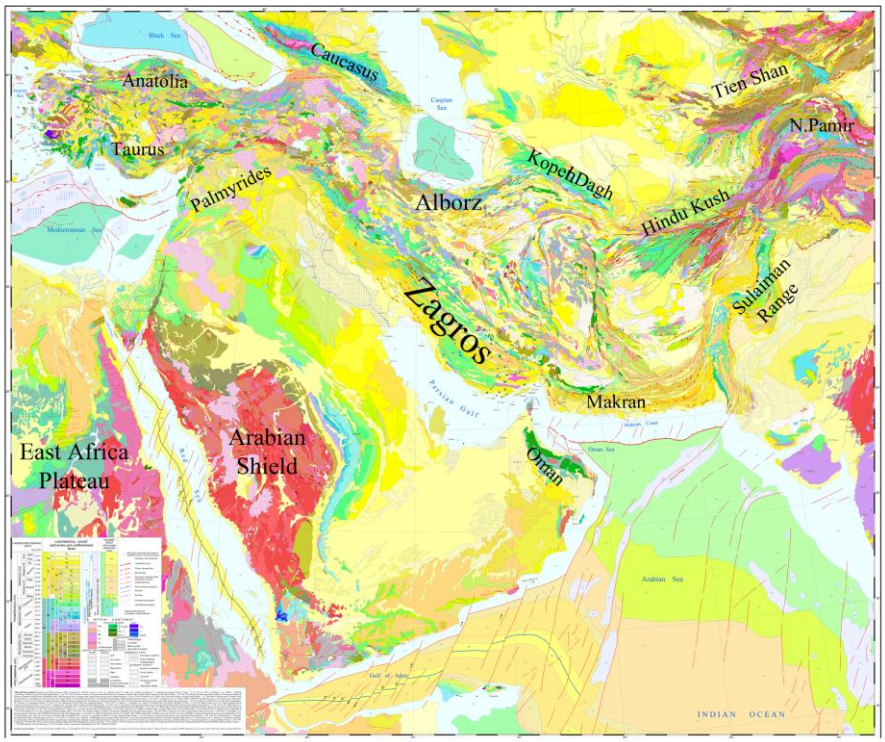

Figure I- 13: a) Geology map of Middle-East and the location of the Zagros (Haghipour, 2009).

Tilting of the upper-Pliocene Bakhtyari conglomerates throughout the Zagros (Hessami et al., 2001) suggests a recent folding. This is consistent with a series of deep, narrow, parallel gorges incised into mountain fronts and the accumulation of more than 250 m of alluvial deposits.

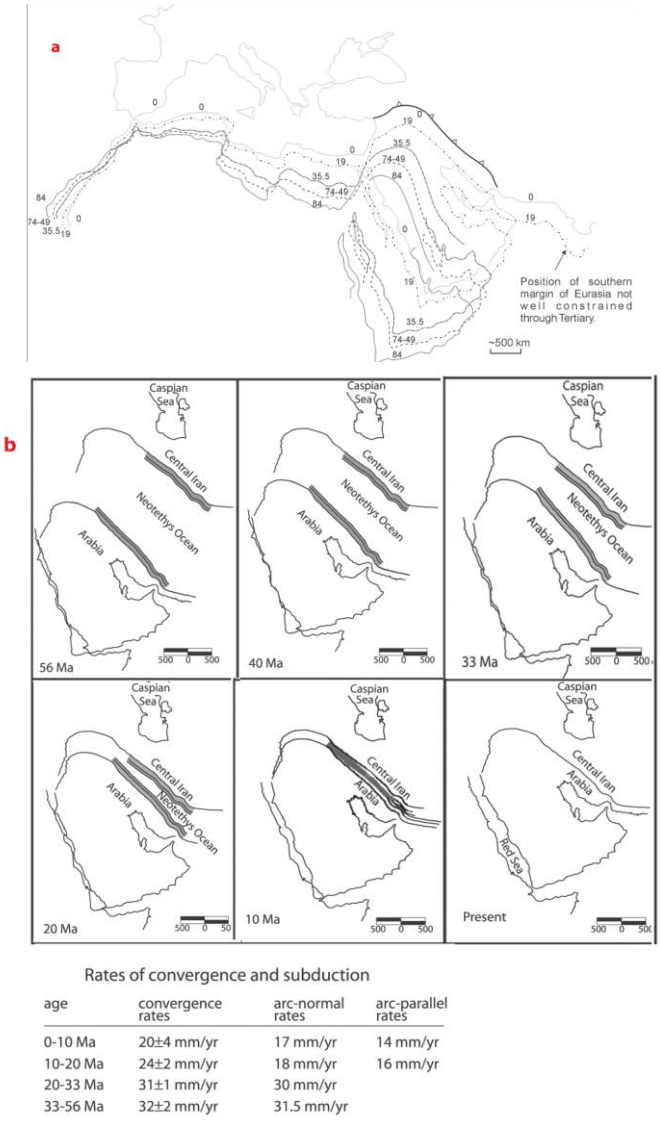

Rates of convergence and subduction

age	convergence rates	arc-normal rates	arc-parallel rates
0-10 Ma	20±4 mm/yr	17 mm/yr	14 mm/yr
10-20 Ma	24±2 mm/yr	18 mm/yr	16 mm/yr
20-33 Ma	31±1 mm/yr	30 mm/yr	
33-56 Ma	32±2 mm/yr	31.5 mm/yr	

Figure I- 15: a) Plate reconstructions for the convergence of Africa-Arabia and Eurasia. Numbers are ages in Ma. Adapted from the Africa-Europe reconstructions of Dewey et al (1989) by extending the continental margin to include Arabia, and allowing for ~100 km relative motion between Arabia and Africa post 20 Ma. There has been roughly 300-500 km of Arabia-Eurasia convergence since initial collision at 20-30 Ma. This is comparable with the convergence recognized within the collision zone (Allen et al., 2004b); b) Maps showing the reconstruction of Neo-tethys, and the relationship between opening of the Red Sea and collision of Arabia and Eurasia (as show by the overlap of the shaded region). The wide gray-shaded bands represent the amount of shortened crust (70 km) on the Arabian plate and in Eurasia (80 km). Narrower (inside) bands represent passive margins (50 km) on both the north and south side of the Neotethyan ocean basin. Rates of convergence are for a point located at 32.70°N, 50.38°E (McQuarrie et al., 2003).

VIII-2. Timing of Zagros collision onset and Iranian plateau uplift

Comparison between recent synthesis of GPS data and geologic constraints on plate circuit suggest that the convergence occurred at a rate of ~20 km/Myr (Tatar et al., 2002; Hatzfeld et al., 2003a; Nilforoushan et al., 2003; Vernant et al., 2004) since at least 22 Ma, following the separation of Arabia with Africa (Nubia). This timing is consistent with stratigraphic/structural constraints in the Zagros near plate suture arguing for a minimum age of 23-25 Ma for the final closure of the Neo-tethyan ocean. In the Zagros, this observation is consistent with the replacement of the Oligocene carbonates by siliciclastic sedimentation in the Lower Miocene (Beydoun et al., 1992) and with the 19.7 Ma synorogenic sandstones of the Razak Formation precisely dated by magnetostratigraphy (Khadivi et al., 2010). Published seismic lines from the Persian Gulf provide further evidence for a flexural unconformity in the Middle Miocene or slightly earlier supporting the above conclusions (Soleimany and Sabat, 2010). These concurrent data taken together confirm that uplift, erosion and contraction in the northern Zagros was underway, and that final suturing, occurred in the early Miocene.

Complementary data are brought by a number of evidence supporting, instead, a contractional episode on the Arabian margin before the Early Miocene. For instance, a middle Eocene-late Oligocene or Late Eocene-Lower Miocene unconformity has long been recognized in the carbonates succession of the Zagros (Berberian and King, 1981; James and Wynd, 1965). This adds to the erosional or non-depositional hiatus described to the NW, in the Lorestan area, that lasted 15 Ma in the middle-late Eocene interval (Homke et al., 2009).

The recent re-evaluation of the stratigraphy of the coarse-grained facies shows that the onset of coarsening upward sedimentation in the foreland basin occurred during late Oligocene in the vicinity of the suture zone (Fakhari et al., 2008). This result strongly suggests that this major unconformity resulted from the tectonic loading in the northern Zagros likely between the middle Eocene and the late Oligocene. This event predated the Miocene overfilled stage in the Zagros foreland basin (Khadivi et al., 2010; Mouthereau et al., 2007b) and hence likely signs the initiation of the current Zagros collision, which should hence be dated to the Late Eocene-Early Oligocene transition at ~35 Ma. A recent review of timing of deformation to the north of the suture zone argues for collisional shortening started in the Late Eocene-Oligocene (e.g. Allen

and Armstrong, 2008). This is further supported by the occurrence of detrital zircons with U/Pb ages of 45-50 Ma, derived from the overriding Iranian microplate, in the late Oligocene conglomerates deposited in the northern Zagros (Horton et al., 2008). Detrital apatite fission-track ages in Miocene sediments indicate a rapid cooling at ~38 Ma in the NW Zagros belt (Homke et al., 2009). We conclude that the initial episode of contraction occurred, north of the current Zagros suture zone, in the paleo-fore arc domain, during the middle-late Eocene and the late Oligocene (~35 Ma).

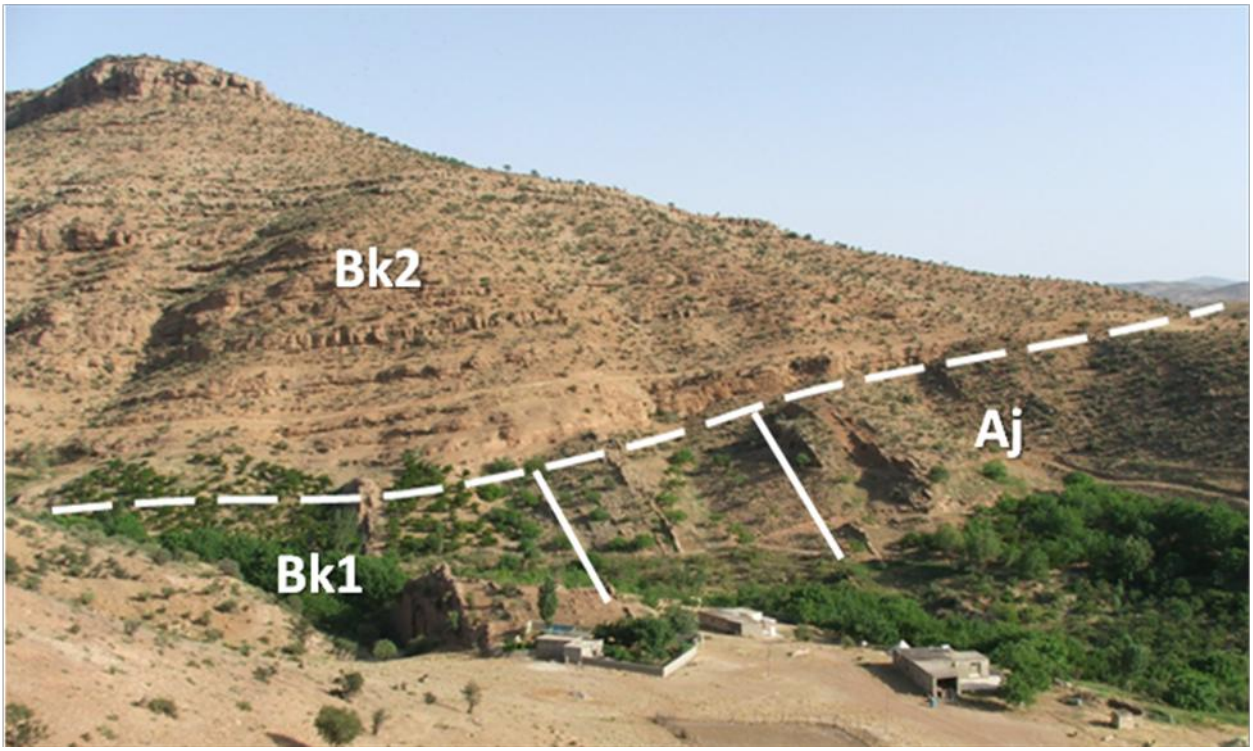

Figure I- 16: The great angular unconformity study between the Agha Jari and Bakhtyari 2 Formations in NW Shiraz in ZFB (see Khadivi et al. 2010 or the submitted paper to GSA bulletin for more explanations).

Gavillot et al (2010) using helium dating on detrital zircon and apatite in the Dezful area of the northern Zagros has established that rapid cooling and sedimentation occurred between 19-15 Ma and 12-8 Ma in the High Zagros. The youngest grain-age population of ~22 Ma together with AHe ages indicate that the Arabian margin exhumed rapidly between 20 and 10 Ma ago. Uplift and exhumation in both the Zagros and the Iranian plateau was consequently also delayed by ~20 Ma with respect to the initiation of the collision ca. 35 Ma. Despite these studies the

exact sequential timing of collision events is still a matter of debate, there is no doubt that a marine gateway connecting the Mediterranean Sea and the Indo-Pacific Ocean existed at least until the early Miocene in the Central Iran and until ca. 15 Ma on the Arabian margin in the Zagros ~20 Ma after the initial collision.

Continent-continent collision starting in Tertiary has led to the formation of the Zagros fold-and-thrust belt (ZFTB), continued shortening of the mountain range, and creation of the Zagros foreland basin. The SW-NE oriented contraction, led to the development of NW-SE trending, SW-verging folds and NE dipping thrusts in the Phanerozoic sedimentary cover. This basement is above a detachment zone of the Infracambrian-Cambrian Hormuz evaporites (Alavi, 1994; Kadinsky-Cade and Barzangi, 1982).

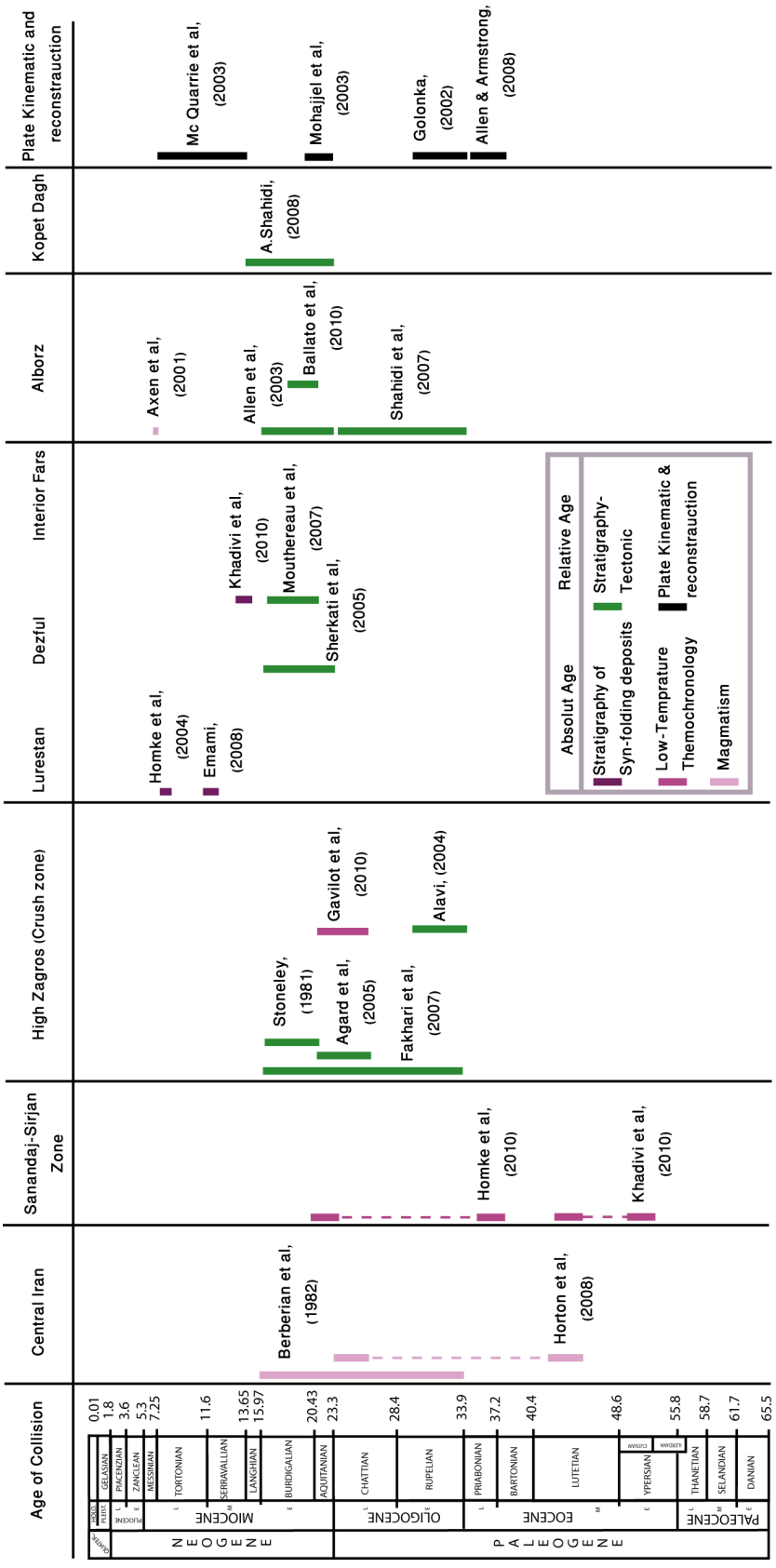

Figure I- 17: Compilation of ages of continent-continent collision between Arabia-Eurasia plates reported from evidence in different structural division of Iran and based on different techniques for obtaining the absolute or relative ages for these studies.

Agard, P., Omrani, J., Jolivet, L., and Mouthereau, F., 2005, Convergence history across Zagros (Iran): constraints from collisional and earlier deformation: International Journal of Earth Sciences, v. 94, p. 401-419.

Ahmadhadi, F., Daniel, J.-M., Azzizadeh, M., and Lacombe, O., 2008, Evidence for pre-folding vein development in the Oligo-Miocene Asmari Formation in the Central Zagros Fold Belt, Iran: Tectonics, v. 27, no. 1, p. TC1016.

Alavi, M., 1980, Tectonostratigraphy evolution of the Zagrosides of Iran: Geology, v. 8, p. 144-149.

-, 1994, Tectonics of the zagros orogenic belt of iran: new data and interpretations: Tectonophysics, v. 229, no. 3-4, p. 211-238.

Allen, M., Jackson, J. A., and Walker, R., 2004a, Late Cenozoic reorganization of the Arabia-Eurasia collision and the comparison of short-term and long-term deformation rates: Tectonophysics, v. 23.

Allen, M. B., Jackson, J., and Walker, R., 2004b, Late Cenozoic reorganization of the Arabia-Eurasia collision and the comparison of short-term and long term deformation rates: Tectonics, v. 32, p. 659-672.

ArRajehi, A., McClusky, S., Reilinger, R., Daoud, M., Alchalbi, A., Ergintav, S., Gomez, F., Sholan, J., Bou-Rabee, F., Ogubazghi, G., Haileab, B., Fisseha, S., Asfaw, L., Mahmoud, S., Rayan, A., Bendik, R., and Kogan, L., 2010, Geodetic constraints on present-day motion of the Arabian Plate: Implications for Red Sea and Gulf of Aden rifting: Tectonics, v. 29, no. TC3011.

Authemayou, C., Bellier, O., Chardon, D., Malekzade, Z., and Abassi, M., 2005, Role of the Kazerun fault system in active deformation of the Zagros fold-and-thrust belt (Iran): Comptes Rendus Geosciences, v. 337, no. 5, p. 539-545.

Authemayou, C., Chardon, D., Bellier, O., Malekzadeh, Z., Shabanian, E., and Abbassi, M. R., 2006, Late Cenozoic partitioning of oblique plate convergence in the Zagros fold-and-thrust belt (Iran): Tectonics, v. 25, no. doi:10.1029/2005TC001860.

Berberian, F., and Berberian, M., 1981, Tectono-Plutonic episodes in Iran, *in* Gupta, H. K., and Delany, F.M., ed., Zagroz-Hindu Kush-Himalaya Geodynamic Evolution: Washington, American Geophysical Union & Geological Society of America, p. 5-32.

Berberian, F., Muir, I. D., Pankhurst, R. J., and Berberian, M., 1982, Late Cretaceous and early Miocene Andean-type plotunic activity in northern Makran and Central Iran: Journal of Geological Society of London, v. 139, p. 605-614.

Berberian, M., 1986, Seismotectonics and earthquake-fault hazard study of the Karkheh river project: Jahad-e-Sazandegi.

-, 1995, Master "blind" thrust faults hidden under the Zagros folds: active basement tectonics and surface morphotectonics: Tectonophysics, v. 241, no. 3-4, p. 193-195.

Berberian, M., and King, G. C. P., 1981, Towards a paleogeography and tectonic evolution of Iran: Canadian Journal of Earth Sciences, v. 18, p. 210-265.

Berberian, M., and Tchalenko, J., 1976, Earthquake of southern Zagros (Iran) : Bushehr region, in Contribution to the Seismotectonics of Iran: Geological survay of Iran.

Berberian, M., and Yeats, R. S., 2001, Contribution of archaeological data to studies of earthquake history in the Iranian Plateau: Journal of Structural Geology, v. 23, no. 2-3, p. 563-584.

Besse, J., Torcq, F., Gallet, Y., Ricou, L. E., Krystyn, L., and Saidi, A., 1998, Late Permian to Late Triassic palaeomagnetic data from Iran: constraints on the migration of the Iranian block through the Tethyan Ocean and initial destruction of Pangaea: Geophysical Journal International, v. 135, p. 77-92.

Beydoun, Z. R., 1991, Arabian plate hydrocarbon geology and potential – a plate tectonic approach, American Association of Petroleum Geologists, 77 p.

Beydoun, Z. R., Clarke, M. W. H., and Stoneley, R., 1992, Petroleum in the Zagros Basin: A late Tertiary foreland basin overprinted onto the outer edge of a vast hydrocarbon-rich Paleozoic-Mesozoic passivemargin shelf: Foreland Basins and Fold Belts, AAPG Mem, v. 55, p. 309 – 339.

Bordenave, M. L., 2003, Gas prospective area in the Zagros domain of Iran and in the Gulf Iranian waters, *in* AAPG, Houston, Texas.

Colman-Sadd, S. P., 1978, Fold Development in Zagros Simply Folded Belt, Southwest, Iran: American Association of Petroleum Geologists Bulletin, v. 62, p. 984-1003.

Cotton, J. T., and Koyi, H. A., 2000, Modeling of thrust fronts above ductile and frictional detachments: Application to structures in the Salt Range and Potwar Plateau, Pakistan 10.1130/0016-7606(2000)112<351:MOTFAD>2.0.CO;2: Geological Society of America Bulletin, v. 112, no. 3, p. 351-363.

Davoudzadeh, M., Lensch, G., and Weber-Dierenbach, K., 1986, Contribution to the paleogeography, stratigraphy and tectonics of the Infracambrian and Lower Paleozoic of Iran: Neues Jahrbuch für Geologie und Paläontologie Abhandlungen, v. 172, p. 245 – 269.

Davoudzadeh, M., and Schmidt, K., 1984, A review of the Mesozoic Paleogeography and Paleotectonic evolution of Iran: N. Jb. Geol. Palaont. Abh., v. 168, no. 2/3, p. 182-207.

Davoudzadeh, M., and Weber-Dierenbach, K., 1987, Contribution to the paleogeography,stratigraphy and tectonics of the Upper Paleozoic of Iran: Neues Jahrbuch für Geologie und Paläontologie Abhandlungen, v. 175, p. 121 – 146.

Dercourt, J., Zonenshain, L. P., Ricou, L.-E., Kazmin, V. G., Le Pichon, X., Knipper, A. L., Grandjacquet, C., Sbortshikov, I. M., Geyssant, J., Lepvrier, C., Pechersky, D. H., Boulin, J., Sibuet, J.-C., Savostin, L. A., Sorokhtin, O., Westphal, M., Bazhenov, M. L., Lauer, J. P., and Biju-Duval, B., 1986, Geological evolution of the tethys belt from the atlantic to the pamirs since the LIAS: Tectonophysics, v. 123, no. 1-4, p. 241-315.

Emami, H., 2008, Foreland propagation folding structure of the mountain front flexure in the Pusht-e-Kuh arc (NW Zagros, Iran): University of Barcelona, 199 p.

Fakhari, M. D., Axen, G. J., Horton, B. K., Hassanzadeh, J., and Amini, A., 2008, Revised age of proximal deposits in the Zagros foreland basin and implications for Cenozoic evolution of the High Zagros: Tectonophysics ,Asia out of Tethys: Geochronologic, Tectonic and Sedimentary Records, v. 451, no. 1-4, p. 170-185.

Falcon, N. L., 1961, Major earth-flexuring in the Zagros Mountains of south-west Iran: Quarterly Journal of the Geological Society of London,, v. 117, p. 367-376.

-, 1974, Southern Iran: Zagros Mountains, *in* Spencer, A. M., ed., Mesozoic-Cenozoic orogenic belts-Data for orogenic studies: London, Special Publication of Geological Society of London, p. 199-211.

Gansser, A., 1992, The enigma of the Persian dome inclusions: Eclogae Geologica Helveticae, v. 85, p. 825-846.

Golonka, J., 2000, Cambrian-Neogen Plate Tectonic Maps: Wydawnictwo Uniwersytetu Jagiellonskiego.

Golonka, J., and Ford, D., 2000, Pangean (Late Carboniferous-Middle Jurassic) paleoenvironment and lithofacies: Palaeogeography, Palaeoclimatology, Palaeoecology, v. 161, no. 1-2, p. 1-34.

Haghipour, A., 2009, International Geological Map of Middle East: CGMW.

Hatzfeld, D., Tatar, M., Priestley, K., and Ghafory-Ashtiany, M., 2003, Seismological constraints on the crustal structure beneath the Zagros Mountain belt (Iran): Geophysical Journal International, v. 155, no. 2, p. 403-410.

Haynes, S. J., and McQuillan, H., 1974, Evolution of the Zagros suture zone, southern Iran: Geological Society of America Bulletin, v. 85, p. 739-744.

Hessami, K., Koyi, H. A., Talbot, C. J., Tabasi, H., and Shabanian, E., 2001, Progressive unconformities within an evolving foreland fold-thrust belt, Zagros Mountains: Journal of the Geological Society of London, v. 158, p. 969-981.

Homke, S., Vergés, J., Beek, P. v. d., Fernàndez, M., Saura, E., Barbero, L., Badics, B., and Labrin, E., 2009, Insights in the exhumation history of the NW Zagros from bedrock and detrital apatite fission-track analysis: evidence for a long-lived orogeny: Basin Research, v. 9999, no. 9999.

Homke, S., Verges, J., Garces, M., Emami, H., and Karpuz, R., 2004, Magnetostratigraphy of Miocene-Pliocene Zagros foreland deposits in the front of the Push-e Kush Arc (Lurestan Province, Iran): Earth and Planetary Science Letters, v. 225, no. 3-4, p. 397-410.

Horton, B. K., Hassanzadeh, J., Stockli, D. F., Axen, G. J., Gillis, R. J., Guest, B., Amini, A., Fakhari, M. D., Zamanzadeh, S. M., and Grove, M., 2008, Detrital zircon provenance of Neoproterozoic to Cenozoic deposits in Iran: Implications for chronostratigraphy and collisional tectonics: Tectonophysics, v. 451, no. 1-4, p. 97-122.

Husseini, M. I., 1989, Tectonic and deposition model of Late Precambrian-Cambrian Arabian and adjoining plates: The American Association of Petroleum Geologists Bulletin, v. 73, no. 9, p. 1117-1131.

Jackson, J., 1980, Reactivation of basement faults and crustal shortening in orogenic belts.: Nature, v. 283, p. 343-346.

-, 1992, Partitioning of strike-slip and convergent motion between Eurasia and Arabia in Eastern Turkey and the Caucasus: J. Geophys. Res., v. 97, p. 12471-12479.

Jackson, J., Hains, J., and Holt, W., 1995, The accomodation of Arabia-Eurasia plate: Journal of Geophysical Research, v. 100, no. B8, p. 15,205-15,219.

Jahani, S., Callot, J.-P., Letouzey, J., and Frizon de Lamotte, D., 2009, The eastern termination of the Zagros Fold-and-Thrust Belt, Iran: Structures, evolution, and relationships between salt plugs, folding, and faulting: Tectonics, v. 28, no. 6, p. TC6004.

James, G. A., and Wynd, J. G., 1965, Stratigraphic nomenclature of Iranian Oil Consortium Agreement Area: AAPG Bulletin, v. 49, no. 12, p. 2182-2245.

Kadinsky-Cade, K., and Barzangi, M., 1982, Seismotectonics of Southern Iran: The Oman line.: Tectonics, v. 1, p. 389-412.

Kazmin, V., Ricou, L.-E., and Sbortshikov, I. M., 1986, Structure and evolution of the passive margin of the eastern tethys: Tectonophysics, v. 123, no. 1-4, p. 153-179.

Kent, P. E., 1979, The emergent Hormuz salt plugs of southern Iran: Journal of Petroleum Geology, v. 2, no. 2, p. 117-144.

Khadivi, S., Mouthereau, F., Larrasoaña, J.-C., Vergés, J., Lacombe, O., Khademi, E., Beamud, E., Melinte-Dobrinescu, M., and Suc, J.-P., 2010, Magnetochronology of synorogenic Miocene foreland sediments in the Fars arc of the Zagros Folded Belt (SW Iran): Basin Research, v. 9999, no. 9999.

Koop, W., and Stoneley, R., 1982, Subsidence history of the Middle East Zagros basin, Permian to recent: Philosophical Transactions of the Royal Society of London, v. 305, p. 149-168.

Lacombe, O., Mouthereau, F., Kargar, S., and Meyer, B., 2006, Late Cenozoic and modern stress fields in the western Fars (Iran): Implications for the tectonic and kinematic evolution of central Zagros: Tectonics, v. 25, no. doi:10.1029/2005TC001831.

McClusky, S., Reilinger, R., Mahmoud, S., Ben Sari, D., and Tealeb, A., 2003, GPS constraints on Africa (Nubia) and Arabia plate motions: Geophysical Journal International, v. 155, p. 126-138.

McQuarrie, N., 2004, Crustal scale geometry of the Zagros fold-thrust belt, Iran: Journal of Structural Geology, v. 26, no. 3, p. 519-535.

McQuarrie, N., Stock, J. M., Verdel, C., and Wernicke, B. P., 2003, Cenozoic evolution of Neotethys and implications for the causes of plate motions: Geophysical Resarch Letters, v. 30, p. doi:10.1029/2003GL017992.

Molinaro, M., Leturmy, P., Guezou, J. C., Frizon de Lamotte, D., and Eshraghi, S. A., 2005, The structure and kinematics of the southeastern Zagros fold-thrust belt, Iran: from thin-skinned to thick-skinned tectonics: Tectonics, v. 24, p. doi:10.1029/2004TC001633.

Motiei, H., 1993, Stratigraphy of Zagros: Tehran, Geological Survey of Iran, 536 p.

-, 1995, Petroleum Geology of Zagros: Tehran, Geological Survey of Iran, 589 p.

Mouthereau, F., and Lacombe, O., 2006, Inversion of the Paleogene Chinese continental margin and thick-skinned deformation in the Western Foreland of Taiwan: Journal of Structural Geology ,Tectonic inversion and structural inheritance in mountain belts, v. 28, no. 11, p. 1977-1993.

Mouthereau, F., Lacombe, O., and Meyer, B., 2006, The Zagros folded belt (Fars, Iran): constraints from topography and critical wedge modelling: Geophysical Journal International, v. 165, no. 1, p. 336-356.

Mouthereau, F., Lacombe, O., Tensi, J., Bellahsen, N., Kargar, S., and Amrouch, K., 2007a, Mechanical Constraints on the Development of the Zagros Folded Belt (Fars), Thrust Belts and Foreland Basins: Fold Kinematics to Hydrocarbon Systems.Series: Frontiers in Earth Sciences, Springer, p. 247-266.

Mouthereau, F., Tensi, J., Bellahsen, N., Lacombe, O., De Boisgrollier, T., and Kargar, S., 2007b, Tertiary sequence of deformation in a thin-skinned/thick-skinned collision belt: The Zagros Folded Belt (Fars, Iran): Tectonics, v. 26, no. doi: 10.1029/2007TC002098.

Ni, J., and Barzangi, M., 1986, Seismotectonics of the Zagros Continental Collision Zone and a Comparison With the Himalayas: J. Geophys. Res., v. 91, p. 8205-8218.

Nilfroushan, F., Masson, F., Vernant, P., Vigny, C., Martinod, J., Abbasi, M., Nankali, H., Hatzfeld, D., Bayer, R., Tavakoli, F., Ashtiani, A., Doerflinger, E., Daigniéres, M., Collard, P., and Chéry, J., 2003, GPS network monitors the Arabia-Eurasia collision deformation in Iran: Journal of Geodesy, v. 77, p. 411-422.

Ramezani, J., and Tucker, R. D., 2003, Convergence history across Zagros (Iran): constraints from collisional and earlier deformation: International Journal of Earth Sciences, v. 94, p. 401-419.

Ricou, L. E., 1971, Le croissant ophiolitique péri-arabe, une ceinture de nappes mise en place au crétacé supérieur: Revue de géographie physique et de géologie dynamique, v. 13, p. 327-350.

-, 1994, Tethys reconstructed: plates, continental fragments and their boundaris since 260 Ma from Central America to South-eastern Asia: Geodinamica Acta, v. 7, p. 169-218.

Sella, G. F., Dixon, T. H., and Mao, A., 2002, REVEL: A model for Recent plate velocities from space geodesy: J. Geophys. Res., v. 107.

Sepehr, M., and Cosgrove, J. W., 2004, Structural framework of the Zagros Fold-Thrust Belt, Iran: Marine and Petroleum Geology ,Oil and Gas in Compressional Belts, v. 21, no. 7, p. 829-843.

Setudehnia, A., 1978, The Mesozoic sequence in South_West Iran: Journal of Petroleum Geology, v. 1, no. 1, p. 3-42.

Sharland, P. R., Archer, R., Casey, D. M., Davies, R. B., Hall, S. H., Heward, A. P., Horbury, A. D., and Simmon, M. D., 2001, Arabian Plate sequence stratigraphy, GeoArabia Special Publication: Manama Bahrain, Oriental Press, 371 p.

Sherkati, S., and Letouzey, J., 2004, Variation of structural style and basin evolution in the central Zagros (Izeh zone and Dezful Embayment), Iran: Marine and Petroleum Geology, v. 21, no. 5, p. 535-554.

Sherkati, S., Letouzey, J., and Frizone de Lamotte, D., 2006, Central Zagros fold-thrust belt (Iran): New insights from seismic data, field observation and sandbox modeling: Tectonics, v. 25, p. 1-27.

Sherkati, S., Molinaro, M., Frizon de Lamotte, D., and Letouzey, J., 2005, Detachment folding in the Central and Eastern Zagros fold-belt (Iran): salt mobility, multiple detachments and late basement control: Journal of Structural Geology, v. 27, no. 9, p. 1680-1696.

Soleimany, B., and Sabat, F., 2010, Style and age of deformation in the NW Persian Gulf: Petroleum Geoscience, v. 16, no. 1, p. 31-39.

Stampfli, G., Marcoux, J., and Baud, A., 1991, Tethyan margins in space and time: Palaeogeography, Palaeoclimatology, Palaeoecology

Palaeogeography and Paleoceanography of Tethys, v. 87, no. 1-4, p. 373-409.

Stampfli, G. M., and Borel, G. D., 2002, A plate tectonic model for the Paleozoic and Mesozoic constrained by dynamic plate boundaries and restored synthetic oceanic isochrons: Earth and Planetary Science Letters, v. 196, no. 1-2, p. 17-33.

Sten, R. J., 1985, The Najd fault system, Saudi Arabia and Egypt: a Late Precambrian rift-related transform system: Tectonics, v. 4, p. 497-511.

Stocklin, J., 1968, Structural history and tectonics of Iran: a review: The American Association of Petroleum Geologists Bulletin, v. 52, p. 1229-1258.

-, 1974, Possible ancient continental margins in Iran, *in* Burk, C. A., and Drake, C.L., ed., The Geology of Continental Margins: Berlin, Springer, p. 873-887.

Talbot, C. J., and Alavi, M., 1996, The past of a future syntaxis across the Zagros, *in* Alsop, G. I., Blundell, D. J., and Davison, I., eds., Salt Tectonics, Geological Society Special Publication, p. 89-109.

Talebian, M., and Jackson, J., 2002, Offset on the Main Recent Fault of NW Iran and implications for the late Cenozoic tectonics of the Arabia-Eurasia collision zone: Geophysical Journal International, v. 150, p. 422-439.

-, 2004, Reappraisal of earthquake focal mechanisms and active shortening in the Zagros mountains of Iran: Geophysical Journal International, v. 156, p. 506-526.

Tatar, M., Hatzfeld, D., and Ghafori-Ashtiany, M., 2004, Tectonics of the Central Zagros (Iran) deduced from microearthquake seismicity: Geophysical Journal International, v. 156, p. 255-266.

Tatar, M., Hatzfeld, D., Martinod, J., Walpersdorf, A., Ghafori-Ashtiany, M., and Chéry, J., 2002, The presend-day deformation of the cnetral Zagros from GPS measurements: Tectonics, v. 29.

Tchalenko, J. S., and Baraud , J., 1974, Seismicity and structure of the Zagros (Iran)—the main recent fault between 33 and 35_N: Royal Sosiety of Londen, v. 277, p. 1-25.

Vernant, P., and Chéry, J., 2006, Low fault friction in Iran implies localized deformation for the Arabia-Eurasia collision zone: Earth and Planetary Science Letters, v. 246, no. 3-4, p. 197-206.

Vernant, P., Nilforoushan, F., Chéry, J., Bayer, R., Djamour, Y., Masson, F., Nankali, H., Ritz, J.-F., Sedighi, M., and Tavakoli, F., 2004, Deciphering oblique shortening of central Alborz in Iran using geodetic data: Earth and Planetary Science Letters, v. 223, no. 1-2, p. 177-185.

Weidlich, O., and Bernecker, M., 2003, Supersequence and composite sequence carbonate platform growth: Permian and Triassic outcrop data of the Arabian platform and Neo-Tethys: Sedimentary Geology, v. 158, no. 1-2, p. 87-116.

Ziegler, M. A., 2001, Late Permian to Holocene paleofacies evolution of the Arabian Plate and its hydrocarbon occurrences: GeoArabia, v. 6, p. 445 – 504.

Chapter II

Magnetostratigraphic dating of the Zagros foreland Neogene synorogenic sediments

I. Concepts and methodology

This part contains a briefly discussion about the concepts and methodology, more details are presented in Annex I and II.

I-1. Nature and Origin of Earth's magnetic field

Earth's magnetic field is a magnetic dipole, with the magnetic field N pole near the Earth's geographic North Pole and the other magnetic field S pole near the Earth's geographic South Pole.

Paleomagnetism is the record study of the Earth's magnetic field which preserved in various magnetic minerals through the time.

Normal and Reversal polarity

When the past magnetic field is oriented similar to present-day field (North Magnetic Pole near the North Rotational Pole) the strata retain a Normal Polarity. Inversely, when the data indicate that the North Magnetic Pole was near the South Rotational Pole, the strata show Reversed Polarity. Inclination (I) angle with respect to vertical is between 90° and -90° and the declination (D) angle with respect to horizontal is near to 0° in case of normal polarity and 180° in case of reverse polarity.

I-2. Principles of remanent magnetisation

Natural Remanent Magnetisation (NRM); is the permanent magnetism of a rock. The most important paleomagnetic laboratory work is the isolating the characteristic component of NRM by selective removal of secondary NRM. The NRM is stripped away in a stepwise manner using thermal or alternating field demagnetisation techniques to reveal the stable magnetic component.

NRM analysis is the method which measures the intensity and direction of residual magnetism in rocks to determine their age and history. Detrital Remanent Magnetisation (DRM) show the polarity of Earth's magnetic field at the time a stratum was deposited (Fig. II- 1).

Detrital remanent magnetisation (DRM): is acquired during deposition and lithification of sedimentary rocks. In most sedimentary environments, the dominant detrital ferromagnetic mineral is magnetite. In a completely different process, magnetic grains in sediments may align with the magnetic field during or soon after deposition; this is known as detrital remnant magnetisation (DRM) (Fig. II- 1). If the magnetisation is acquired as the grains are deposited, the result is a depositional detrital remanent magnetisation (dDRM); if it is acquired soon after deposition, it is a post-depositional detrital remanent magnetisation (pDRM). pDRM processes can operate in the upper 10-20 cm of the accumulating sediment, where water contents are high.

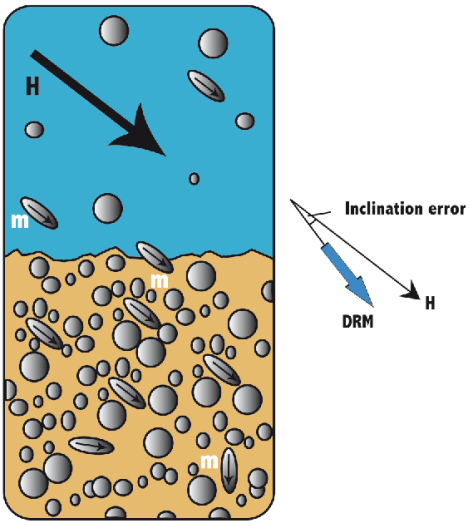

Figure II- 1: Acquisition of the Detrital Remanent Magnetism (DRM) by sediments due to the physical orientation of ferromagnetic grains with magnetic moments m, setting along the ambient geomagnetic field (H) during the sediment deposition and compaction, after (Butler, 2004; Lowrie, 2007).

I-3. Demagnetisation

Thermal Demagnetisation (Relaxation Time and Blocking Temperature). In order to discuss the theory behind thermal demagnetisation of a specimen, it is necessary to understand the principles of relaxation time and blocking temperature for a SD grain. Relaxation time, the time over which

remanent magnetisation of an assemblage of SD grains decays, may vary over many orders of magnitude. Relaxation time for SD grains of a given material at a constant temperature depends on grain volume (v) and microscopic coercive force (hc). Grains with low product (v·hc) have short relaxation time, whereas grains with high product (v·hc) have long relaxation time. Ultimately, these properties help to define the range over which an SD grain will remain stable.

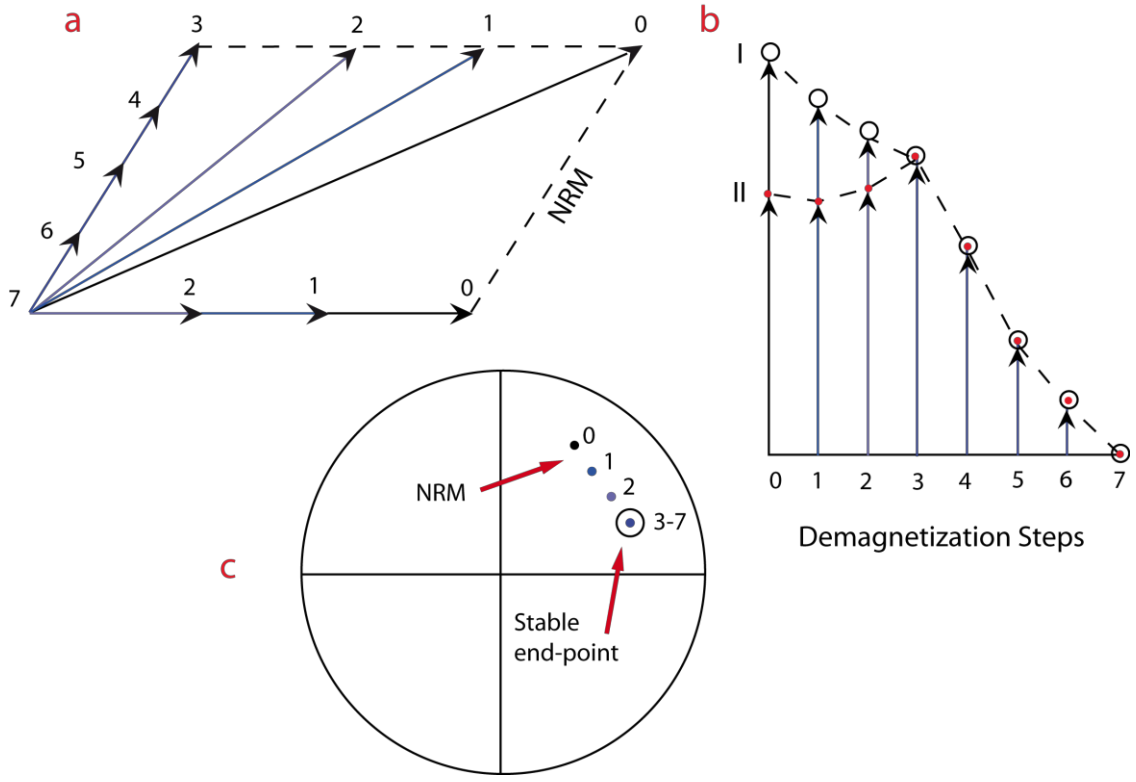

Figure II- 2: a) Stepwise demagnetisation of a NRM (Natural Remanent Magnetisation) consisting of two components with different blocking temperature or coactivity spectra; b) variation of intensity between I and II; c) directional changes of NRM on a stereogram. Numbers on points indicate successive demagnetisation temperatures in C, after (Lanza and Meloni, 2006; Lowrie, 2007).

I-4. Magnetostratigraphy

Magnetostratigraphy is a chronostratigraphic technique which is classically used to date sedimentary and volcanic sequences. The method works by collecting oriented samples at measured intervals throughout the section. The most important geomagnetic property for stratigraphy purposes is a periodic polarity reversal of the geomagnetic field. The direction of the magnetisation of a rock is by definition its north, so magnetisation can be designated either normal or reverse polarity (Opdyke and Channell, 1996).

The direction of the remnant magnetic polarity (ChRM direction for each sample after corrected for tectonic effects) is used to compute the virtual geomagnetic pole (VGP) latitude for each stratigraphic horizon. Because VGP latitude is computed from both inclination and declination of ChRM, it is a convenient parameter for displaying results of a magnetostratigraphy investigation. A positive VGP latitude indicates normal polarity of the geomagnetic field at the time of ChRM acquisition, while a negative VGP latitude indicates reversed polarity.

The VGP latitudes allow determination of magnetic polarity zones in the stratigraphic succession, the term "zone" being used to refer to a particular rock stratigraphic interval.

I-5. Biostratigraphic calibrations

When the GPTS was developed, ages of polarity chrons were predicted, testing the predicted ages of polarity chrons was a major objective of the Magnetostratigraphist. So magnetostratigraphic investigations of marine sedimentary sequences have provided detailed biostratigraphic calibrations.

The result of the magnetostratigraphic investigations can allow by biostratigraphic calibration of the geomagnetic polarity time scale. Development of geologic time scales involves association of isotopically dated horizons with the biostratigraphic zones. There are numerous geologic time scales because evaluating these absolute age calibrations is complex. The process of developing a geomagnetic polarity time scale invariably requires the choice of a geologic time scale.

New magnetochronology constraints for the SE Zagros

The study area is located in the Fars province of Iran, in the northern part of the Zagros Folded Belt, 20 km to the NW of Shiraz. It is characterized by the occurrence of a trend of folds just westwards of the active Sabz-Pushan strike-slip fault. We have done an absolute chronology of the syntectonic sedimentary sequences on base of magnetostratigraphy method. The result of this method was compared by suggested ages for Nanoplankton dating. This study reveals that tectonic deformation was already ongoing in the Middle-Upper Miocene in the northern part of the Zagros folded belt.

In study area, the authors distinguished two different units of Bakhtyari Fm. which the lowest one called Bakthyari 1 (Bk1) as a pre-folding in northern flank of syncline. The upper flat succession of conglomerates, named Bakthyari 2 (Bk2), appears to be mainly post-folding as it unconformably overlies the Bk1 conglomerates. In this study the age of BK1 is constrained and the age of BK2 is not study yet.

This research is published 2010 in Basin Research Journal as ‘Magnetochronology of synorogenic Miocene foreland sediments in the Fars arc of the Zagros Folded Belt (SW Iran)’.

II. Magnetochronology of synorogenic Miocene foreland sediments in the Fars arc of the Zagros Folded Belt (SW Iran)

Basin Research (2009) doi: 10.1111/j.1365-2117.2009.00446.x

Sh. Khadivi [a,b,*], F. Mouthereau [a,c], J.-C. Larrasoaña [d], J. Vergés [d], O. Lacombe [a], E. Khademi [e], E. Beamud [f], M. Melinte-Dobrinescu [g], J.-P. Suc [h]

[a] Institut des Sciences de la Terre et de l'Environnement de Paris, UMR 7193, Université Pierre et Marie Curie, T. 45,-46, E2, P.O. Box 129, 75252 Paris Cedex 05, France

[b] National Geoscience Database of Iran, Tehran, Iran

[c] Also at : Centre de Recherches Pétrographiques et Géochimiques, Vandœuvre-lès-Nancy, France

[d] Institute of Earth Sciences Jaume Almera, CSIC, Lluís Solé Sabaris s/n, 0828, Barcelona, Spain

Now at : Instituto Geológico y Minero de España, c/ Manuel Lasala 44, 9B, 50006 Zaragoza, Spain

[e] Geological Survey of Iran, Shiraz, Iran

[f] Paleomagnetic Laboratory, Institute of Earth Sciences Jaume Almera, UB-CSIC, Lluís Solé Sabaris s/n, 0828, Barcelona, Spain

[g] National Institute of Marine Geology and Geo-ecology (GEOECOMAR), 23-25 Dimitrie Onciul Street, RO-024053, Bucharest, Romania

[h] Laboratoire PaléoEnvironnements & PaléobioSphère, UMR 5125, Université Lyon 1, Campus de La Doua, Bâtiment Géode, 69622 Villeurbanne Cedex, France

[*] *Corresponding author*. Now at: Institut des Sciences de la Terre et de l'Environnement de Paris, Université Pierre et Marie Curie, T. 45-46, E2, Box 129, 75252 Paris Cedex 05, France, Phone +33(0)144275256, Fax +33(0)144275085, shokofeh.khadivi@upmc.fr

Abstract

The timing of deformation in the northern Zagros Folded Belt is poorly constrained because of the lack of an accurate absolute chronology of the syntectonic sedimentary sequences. The foreland basin infill in the northern part of the Fars arc is composed of supratidal sabkha deposits (Razak Fm), medium-grained deltaic deposits (Agha Jari Fm) and coarse conglomerates of nearshore fan deltas deposits at the base (Bakhtyari Fm, Bk1) and continental alluvial deposits at the top of the section (Bakhtyari Fm, Bk2). A magnetostratigraphic study was carried out in a composite section spanning about 1300 m on the northern flank of the Chahar-Makan syncline. Magnetostratigraphic correlation of the Razak Fm with chron C6n yields an age of 19.7 Ma at the base of the composite section. The transition to Agha Jari Fm is correlated with chron C5Cn yielding an age of 16.6 Ma. The transition to the conglomerates of the Bakhtyari Fm (Bk1) correlates with the chron C5AD at approximately 14.8 Ma, which is considerably older than previously thought. The base of the Bakhtyari Fm growth strata, and thus the beginning of the deformation in northern Fars, is dated at 14-15 Ma. The topmost preserved Bakhtyari Fm (Bk1) is folded and unconformably overlain by Bakhtyari Fm (Bk2) conglomerates. This indicates that the tectonic deformation in the northern Zagros was already underway in the Middle Miocene.

Key words: Zagros, magnetostratigraphy, foreland basin, mountain building, vertical-axis rotation

II-1. Introduction

Chronostratigraphic constraints within foreland sequences are critical for understanding the growth of orogenic systems. They are commonly used to assess the timing and rates of shortening and deposition. Along with provenance studies in the foreland and thermochronological constraints in the hinterland, the stratigraphic ages account for the evolution of tectonic accretion and sediment fluxes and thus help distinguishing between tectonic and climatic forcing on the foreland stratigraphy.

Magnetostratigraphy is an appropriate technique for dating non marine deposits, which is particularly important when other methods are not feasible. Successful examples of dating foreland basin deposits through magnetostratigraphy include fold-thrust belts such as the Himalaya , Andes , Alps , Pyrenees , Tien Shan and Zagros .

The Zagros Folded Belt (ZFB), in southwest Iran, results from the closure of the Neo-Tethys ocean between the Arabia margin and the Eurasia continent . The collision belt extends over 2000 km in a NW-SE direction from eastern Turkey to the strait of Hormoz in southern Iran (Fig. II -3). Based on the reconstruction of plate circuits, suggested that plate convergence rates of 2-3 cm/yr between Arabia and Eurasia have held since ~56 Ma. According to the same authors, the true continental collision started no later than 10 Ma. The present-day convergence is oriented N-S at a rate of 2.2-1.5 mm/yr and decreasing westwards, as suggested by recent geodetic surveys .

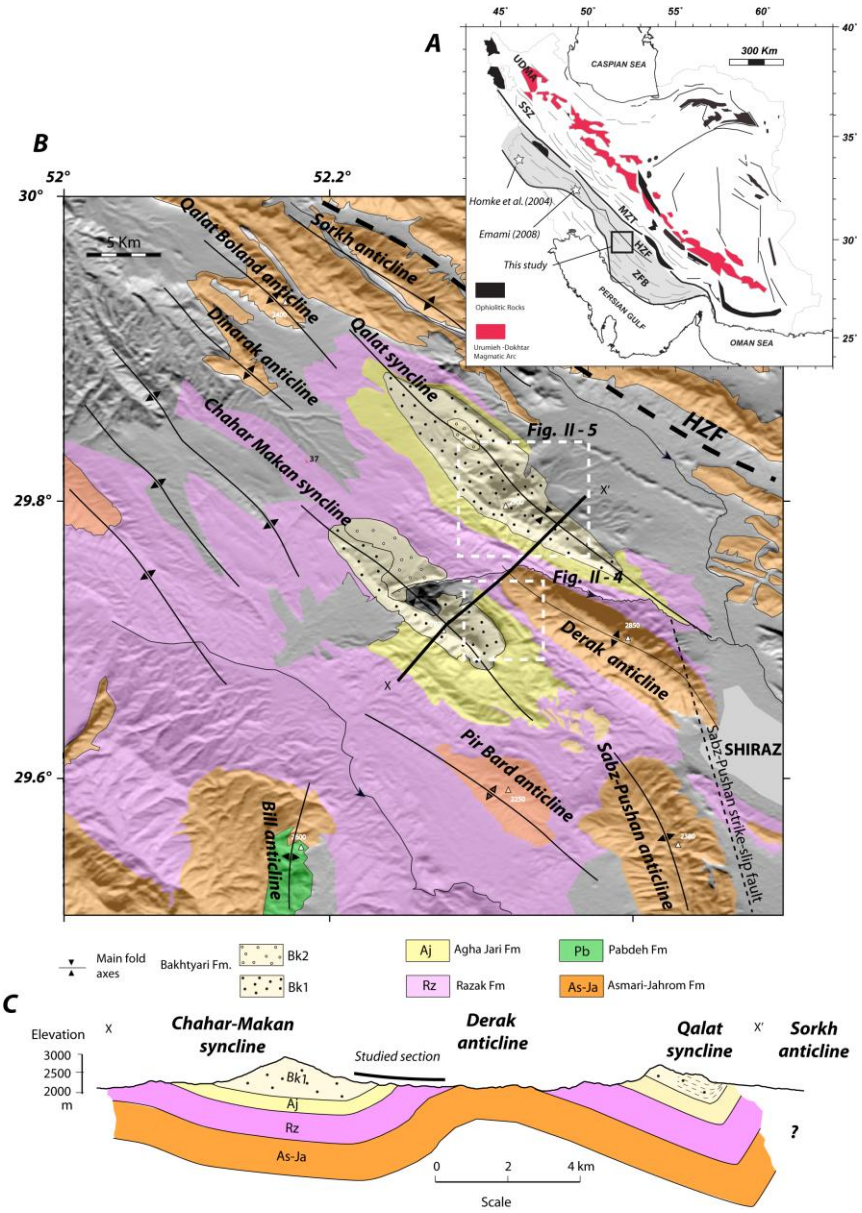

Figure II - 3: a) Location of the studied area, with indication of main structural divisions, in the framework of the Arabia-Eurasia plate convergence. UDMA (Urumieh-Doktar Magmatic Arc); SSZ (Sanandaj-Sirjan Zone); MZT (Main Zagros Thrust); HZF (High Zagros Thrust); ZFB (Zagros Folded Belt). Black-filled areas correspond to ophiolites; b) Geological map of the studied area, with indications of major structural and geological units, superimposed on the shaded topography (SRTM data); c) Geological section across the main studied structural features e.g. Chahar-Makan, Qalat synclines and Derak anticline. Surface constraints are based on bedding dip measurements at samples sites and formation thickness (see Fig. II- 4 for location of sample sites) with additional mapping based on SPOT (5x5 m resolution) images and DEM.

Our understanding of Zagros foreland continental sequences have greatly suffered from the lack of accurate stratigraphic dating. Based on biostratigraphic dating available in the Fars region, the onset of deposition of siliciclastic sediments in the foreland succession is thought to have started roughly 28 Ma ago (Chattian-Late Oligocene) in the proximal Zagros foreland basin, and between 20-16 Ma (Burdigalian-Langhian-Early Miocene) in its distal part, consistent with the migration of foreland sequences forelandwards (e.g., The increasing flux of siliciclastic deposits represented by the Razak Formation, Mishan Formation and Agha Jari Formation of the Fars group points to the start of the overfilled stage in the Zagros foreland basin. The Miocene foreland basin development is confirmed by the noticeable increase in thickness of the Fars group sediments northwards. The lack of chronostratigraphic constraints in the upper continental successions has been partially solved, thanks to recent magnetostratigraphic studies carried out in the distal part of the foreland. In the Lorestan area, magnetostratigraphy has dated the initiation of folding at about 7.6 Ma ago . A similar study suggests older ages of 11 Ma for initiation of folding in the inner part of the Zagros belt (see Fig. II- 3a). The conglomerates of the Bakhtyari Formation unconformably overlie the older foreland strata. However, the age of these conglomerates is still a matter of debate. Biostratigraphic control on underlying successions led to propose a Late Pliocene or younger age. In the distal part of the Zagros foreland, ages of 3 Ma have also been proposed for the base of the Bakhtyari conglomerates. In the southern Fars, a recent study argued for a minimum depositional age of 0.8-0.5 Ma based on cosmogenic dating combined with local paleomagnetic constraints on Bakhtyari conglomerates. However, such alluvial deposits are expected to be largely diachronous throughout the foreland. It is thus not surprising that recent micropaleontological dating and pollen stratigraphy within marine beds of the Bakhtyari Formation found in the High Zagros point to an Early Miocene and even Late Oligocene age.

In spite of these earlier works two major questions remain to be solved. The ages of synorogenic foreland deposits are still not reliably constrained in the northern proximal portions of the Zagros foreland. The recent stratigraphic constraints on the Bakhtyari Formation in the High Zagros are far from the Fars area and may be related to the development of a basin restricted to the northern Zagros. The purpose of this study is to bring new chronostratigraphic constraints on synorogenic deposits of

the proximal Zagros foreland. These results are then used to assess the timing of folding in the northern Zagros folded belt.

II-2. Geological setting

II-2-a. Main structural features of the Zagros Folded Belt

The collision suture zone is marked along the Main Zagros Thrust (MZT) by ophiolitic rocks associated with deep-water radiolarites and eruptive rocks interpreted as remnants of the obducted Neo-Tethyan ocean or associated back-arc or fore-arc crust (Fig. II-3a). The metamorphic Sanandaj-Sirjan belt, north of the MZT represents the former active margin of the Iranian microplate (Fig. II-3a). To the South, the High Zagros and the Zagros Folded Belt (ZFB) are made up of folded and thrusted Paleozoic, Mesozoic and Tertiary sediments. The orogenic wedge sensu-stricto is represented by the ZFB, which is being built above two major décollement levels localized in the Cambrian salt and in the ductile mid-lower crust (Colman-Sadd, 1978; Berberian, 1995; McQuarrie, 2004; Molinaro et al., 2004; Sherkati & Letouzey, 2004; Molinaro et al., 2005; Mouthereau et al., 2006; Mouthereau et al., 2007). In contrast, the High Zagros and the Sanandaj-Sirjan domain form a highly-elevated low-relief domain on the southern edge of the Iranian plateau.

The tectonic and magmatic history of the Zagros collision can be summarized as follows. Following the obduction in the upper Cretaceous and arc magmatism in the Sanandaj-Sirjan belt during the Mesozoic, the Eurasian side of the collision experienced arc magmatism in the Urumieh-Doktar belt in the Eocene. The timing of this last magmatic arc event is confirmed by U/Pb ages of zircon grains from magmatic plutons and by Eocene cooling ages reported in the Zagros foreland basin from the fission-track analysis on detrital apatites. This Eocene volcanic event is likely related to northward subduction of the Tethys although its tectonic setting can be attributed to either Andean-type volcanism or back-arc spreading. On the Arabian margin a period of subsidence is recorded by the remarkable deposition of turbidites onto previously emplaced ophiolitic units (Berberian & King, 1981; Stoneley, 1981; Hempton, 1987; Beydoun et al., 1992). The two main possible causes for the

observed subsidence could be either loading by the thickened northern Eurasian margin, including the fore-arc domain, or deep-seated loading originating from the Arabian slab pull.

Despite numerous regional evidences from Irak, the Caucasus and the South Caspian basin that the Arabia-Eurasia collision could have started in the Late Eocene , it seems that the beginning of contraction within the southern Zagros of our studied area did not occur before the Late Oligocene-Early Miocene. This timing is based on the following arguments: 1) the initiation of inversion of the Arabian margin in the Zagros basin occurred at this time (Mouthereau et al., 2006; Ahmadhadi et al., 2007; Mouthereau et al., 2007); 2) the Iranian plateau and the Zagros basin were below sea-level during the Oligocene except the morphological ridge formed by the stacked ophiolitic units; 3) the persistence of early Miocene flyschs in the High Zagros and 4) Miocene marine incursions in the High Zagros found in close relations with the first deposition of alluvial-fan conglomerates of the Bakhtyari Formation as attested by new stratigraphic constraints.

II-2-b. Tectonic constraints on the development of the Zagros foreland basin in the Fars Arc

Few studies have specifically focused on the history of the Zagros foreland basin in the Fars province in part because of a missing robust chronostratigraphy, which is the purpose of this paper. In the following, we summarize the main features of its stratigraphic evolution.

Coevally with the deposition of Eocene turbidites on Arabian and Eurasian margins (Berberian & King, 1981; Stoneley, 1981; Hempton, 1987; Beydoun et al., 1992; Vincent et al., 2005), dolostones of the Jahrom Formation were deposited in the Zagros basin. This formation overlies a former regressive succession that ended up with subaerial deposition of the Sachun Formation , the age of which can be indirectly constrained laterally by the Kashkan Formation dated as Ypresian (~56 Ma; Homke et al., 2009). The Jahrom Formation (Fig. II- 3b) has been deposited during an early phase of the development of the Zagros foreland basin. Although the origin of the flexure can be debated, as presented in the previous section, it occurred prior to the propagation of contraction into the Arabian margin.

Available stratigraphic correlations and well data also support the presence of a Middle Eocene-Late Oligocene or Late Eocene-Lower Miocene unconformity between the Jahrom Formation and the Asmari Formation in the Fars. Because this episode preceded the overfilled stage in the Zagros basin and is related to a major transgression, the above-mentioned unconformity can be tentatively interpreted as a flexural unconformity. If this is confirmed by further stratigraphic and sedimentological studies, this unconformity could sign the initiation of the foreland basin and the beginning of the current Zagros collision. Since this time onwards, more efficient plate coupling led to the thickening of the Arabian margin and its uplift. The increase of erosion on the orogenic side together with the migration of the flexural wave into the Arabian margin led to the deposition of a characteristic prograding foreland sequence formed by the Fars Group. This sequence is composed, in the Fars, by a synorogenic succession including the Razak Formation that conformably overlies the Asmari Formation. The Razak Formation grades upwards into the Agha Jari Formation and Bakhtyari Formation. The increase of sediment accumulation together with the establishment of current plate velocities likely occurred coevally with the deposition of the shallow-marine siliciclastic deposits of the Agha Jari Formation.

II-3. The studied area

II-3-a. Main structural features

The study area is located in the Fars province of Iran, in the northern part of the Zagros Folded Belt, 20 km to the NW of Shiraz. It is characterized by the occurrence of a trend of folds just westwards of the active Sabz-Pushan strike-slip fault (Fig. II-3b). We have examined the strata within the Qalat and Chahar-Makan synclines which are on the north and south sides of the Derak anticline (also named Qalat anticline), respectively (The Derak anticline is one of the main structural features in the area (Fig. II- 3b). It is oriented NW-SE with an axial length of 20 km and a width of 10 km. The geomorphic expression of the Derak anticline is controlled by the resistant unit corresponding to the Eocene Jahrom and Late Oligocene-Miocene Asmari limestones. These series are overlain by the erodible units of the Fars Group that are well exposed in both synclines. On top of the Fars Group,

the thick succession of Bakhtyari conglomerates forms topographic highs due to the large proportion of limestone pebbles that are more resistant to erosion occurring in these series. Based on field observations and analysis of SPOT 5x5 m resolution images, and in agreement with earlier work, two types of Bakhtyari conglomerates can be distinguished on the basis of their different structural-stratigraphic relationships. The lowest unit, called Bakthyari 1 (Bk1), is pre-folding in the northern flank of the Chahar-Makan syncline (Fig. II- 4) but is clearly syn-folding on the northern flank of the Qalat syncline (Fig. II- 5). In contrast, the upper flat succession of conglomerates, named Bakthyari 2 (Bk2), appears to be mainly post-folding as it unconformably overlies the Bk1 conglomerates in the core of both the Qalat and Chahar-Makan synclines (Figs. II- 4 and 5).

In spite of local evidence for salt-related deformation within the Razak Formation to the SE of the studied area, both the Razak and Agha Jari Formations conformably overlie the Asmari limestones. No major fault has been recognized from field observation or based on SPOT images. The most remarkable active feature is found to the East and corresponds to the N160° right-lateral Sabz-Pushan fault, which is the most likely source of great damage and deaths in the city of Shiraz and Qalat village related to a major historical earthquake (Ms=6.4) in 1824.

Regular measurements of structural dips in the field and calculation of dips based on SPOT images indicate that the northern flank of the Chahar-Makan syncline is dipping roughly 50°S while its southern flank gently dips 30°N (Fig. II- 3b). Such an asymmetry also characterizes the Qalat syncline, the bedding on the northern flank being steeper than on the southern one. The extraordinary preservation of synorogenic deposits together with evidence of local syn-folding unconformities (Bk1) and post-folding unconformities (Bk2) makes this area the perfect target to carry out magnetostratigraphy in the northern Fars.

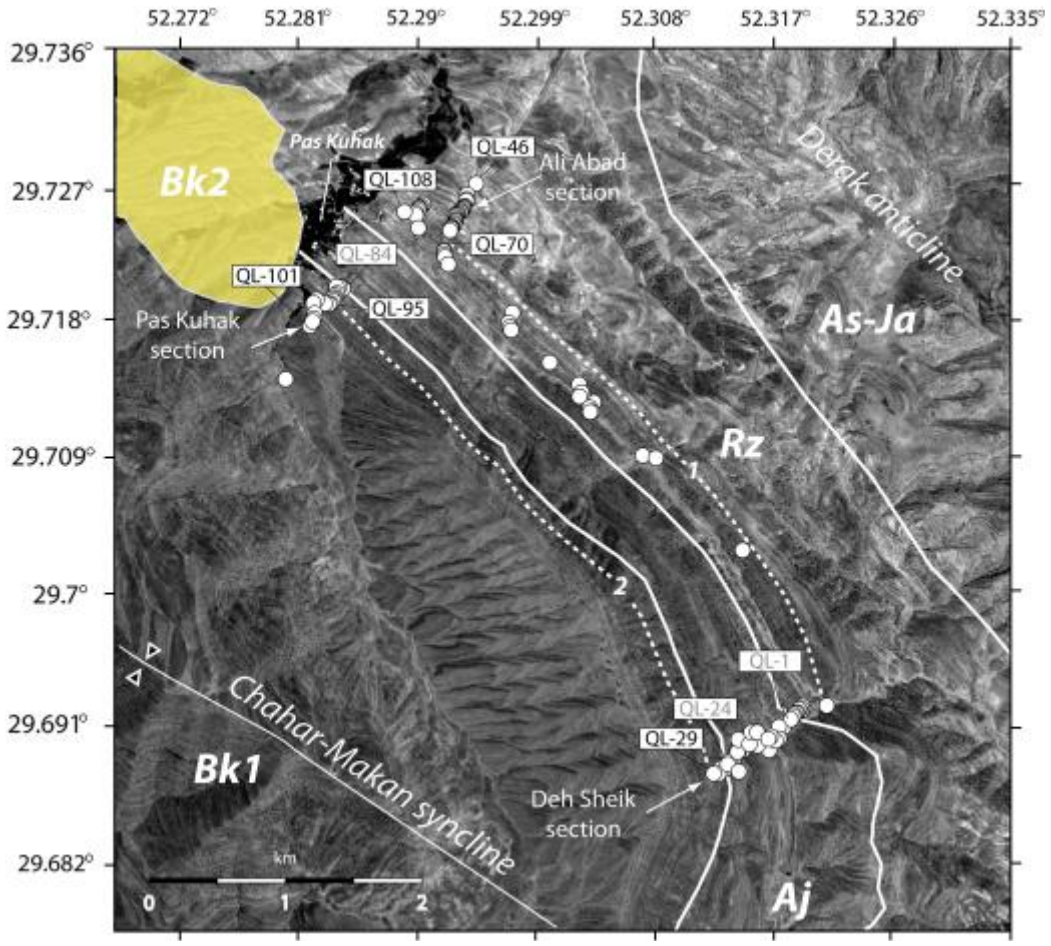

Figure II- 4: SPOT (5x5 m resolution) image of the northern flank of the Charar-Makan syncline showing the location of sections and sample sites. Boundaries between Asmari-Jahrom (As-Ja), Razak Formation (Rz), Agha Jari Formation (Aj) and the Bakhtyari Formation (Bk1), as well as the correlation between each section (thick dashed white lines labeled 1 and 2) are also shown.

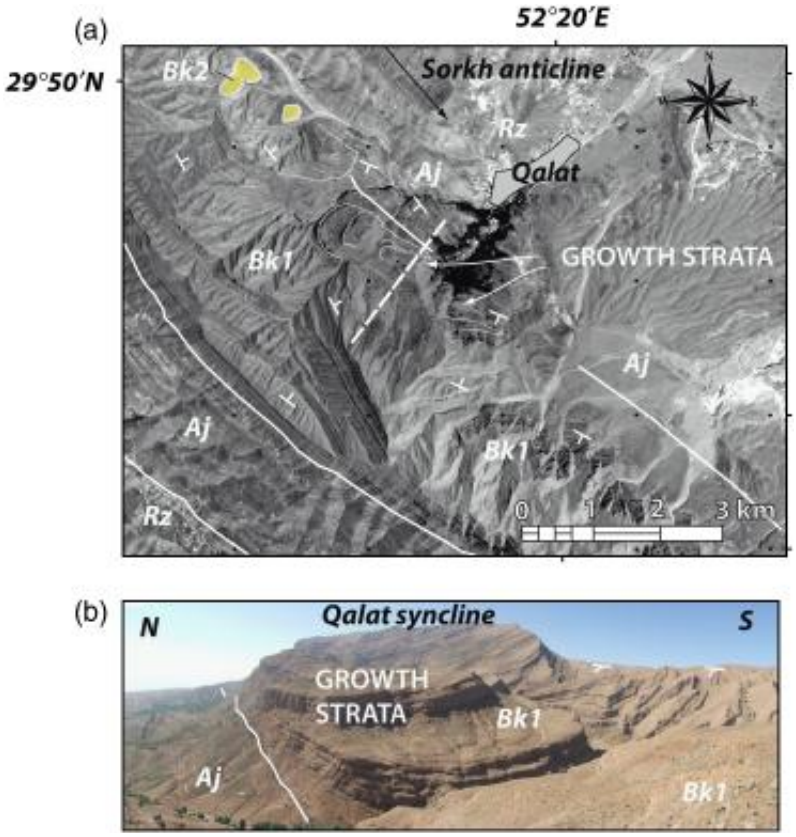

Figure II- 5: a) SPOT (5x5 m resolution) images and b) field photograph of the northern side of the Qalat syncline showing the growth strata located near the base of the Bk1 conglomerates. Abbreviations are Razak Fm (Rz), Agha Jari (Aj) and Bk1 and Bk2 conglomerates correspond to both types of Bakhtyari conglomerates distinguished on the basis on their different structural positions and sediment facies.

II-3-b. The studied sections

On the northern flank of the Chahar-Makan syncline, three main sections have been studied in order to obtain a complete succession from the Razak Formation to the lowermost part of the Bakhtyari Bk1 conglomerates (Fig. II- 6). The first section, named Ali Abad section, includes ~500 m of Razak Formation made up of blue and red clays interbedded with yellow calcareous sandstone sheets (10 cm to 2 m thick) with occasional gypsum beds on top (< 1 m thick) (Fig. II- 7). These sediments are interpreted to be deposited in coastal lagoons and supratidal sabkha environments; their cyclic evolution is related to episodic connection with open marine environments.

The second section, named Deh Shaikh section, was sampled in the same structural domain but 4 km to the SE, where the transition between the uppermost part of the Razak Formation and the Agha Jari Formation was accessible. The Deh Shaikh section includes about 100 m of Razak Formation, which grades progressively upwards into the Agha Jari Formation. The outcropping ~400 m of the Agha Jari Formation are composed of reddish sandstones and meter-scale conglomeratic sheets interbedded with thick (up to 20 m) intervals of red siltstones. Sandstone beds are often thicker than 2-3 m, and conglomerates include limestone cobbles of Paleogene and Cretaceous formations of up to 10 cm (Fig. II- 6). The presence of bidirectional current ripples and frequent cross-bedding laminations in sandstones (Fig. II- 7b) in the lower part suggests a deltaic environment; an open marine connection is confirmed by the presence of nannoplankton (Fig. II- 6). Measurements of current directions suggest local longitudinal currents parallel to the axis of the foreland basin. The upper part of the Deh Shaikh section includes the lowermost ~150 m of the Bakhtyari 1 conglomeratic succession (Figs. II- 6 and 7c).

The third section, named Pas Kuhak, is located south of the Pas Kuhak locality (Figs. II- 6 and 7d). This section includes ~600 m of sandstones and red silts with frequent conglomeratic beds that can be up to 40 m thick. The conglomerates are clast-supported, poorly-sorted, and well-rounded (Fig. II- 7e). They are arranged as thick channel-like conglomeratic beds intercalated with trough cross-bedding in sandstones. This type of facies association suggests the predominance of subaqueous debris flows and migrating barforms. They likely correspond to an alluvial fan deposited in a fluvial-dominated deltaic environment whose facies appears characteristic of the Bakhtyari Formation. In the following, we refer to this formation as Bakhtyari 1 (Bk1) in order to differentiate it from Bakhtyari 2 (Bk2), which corresponds to the upper Bakhtyari conglomerates of alluvial origin lying unconformably above Bk1 conglomerates (Figs. II- 7f and g). Clasts of the Bakhtyari 1 Formation are typically made up of radiolarian cherts (< 10 cm) and well-rounded pebbles of Mesozoic limestones and Nummulitic limestone of the Jahrom Formation, with diameters up to 30 cm (Fig. II- 6). Currents markers show a more pronounced southward flow, oblique to the main structural patterns.

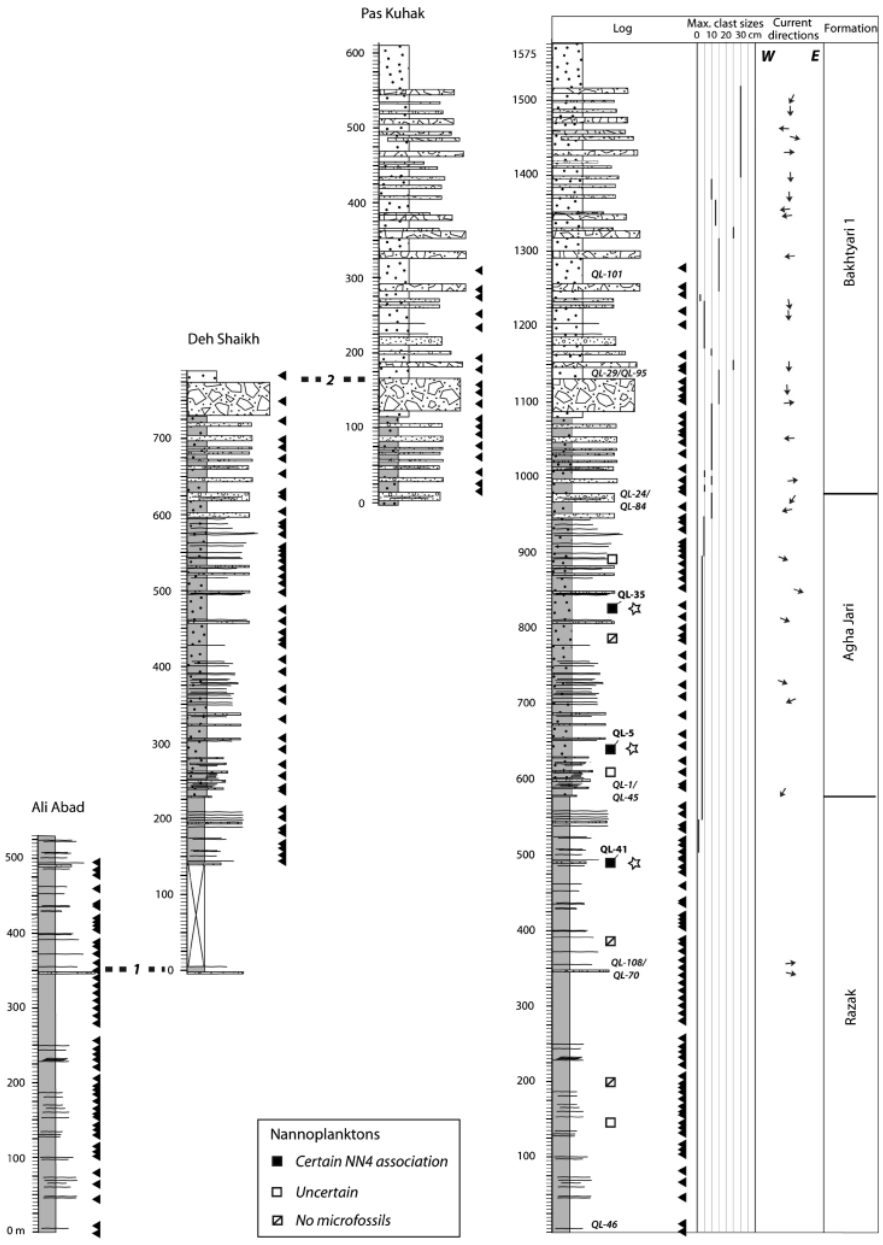

Figure II- 6: Correlation between the studied stratigraphic subsections Pas Kuhak, Ali Abad and Deh Sheik, used to construct the composite magnetostratigraphic Chahar-Makan section shown on Figure II- 9. Positions of samples located on Figure II- 4 are indicated by black triangles. On the right of the composite stratigraphic section, we present the evolution of measured grain sizes and current orientations. The nine studied nannoplankton samples are also presented according to whether they have yielded a certain determination of the NN4 biozone such as QL-5, QL-35 and QL-41 (black-filled boxes; see also Fig. II- 11), uncertain determination (white-filled boxes) or no microfossils (cross white-filled boxes). The position of samples bearing dinokysts is also shown (open stars). Horizontal black dashed lines represent key beds (1, 2) that have been used for correlation between studied subsections (see locations in Fig. II- 4).

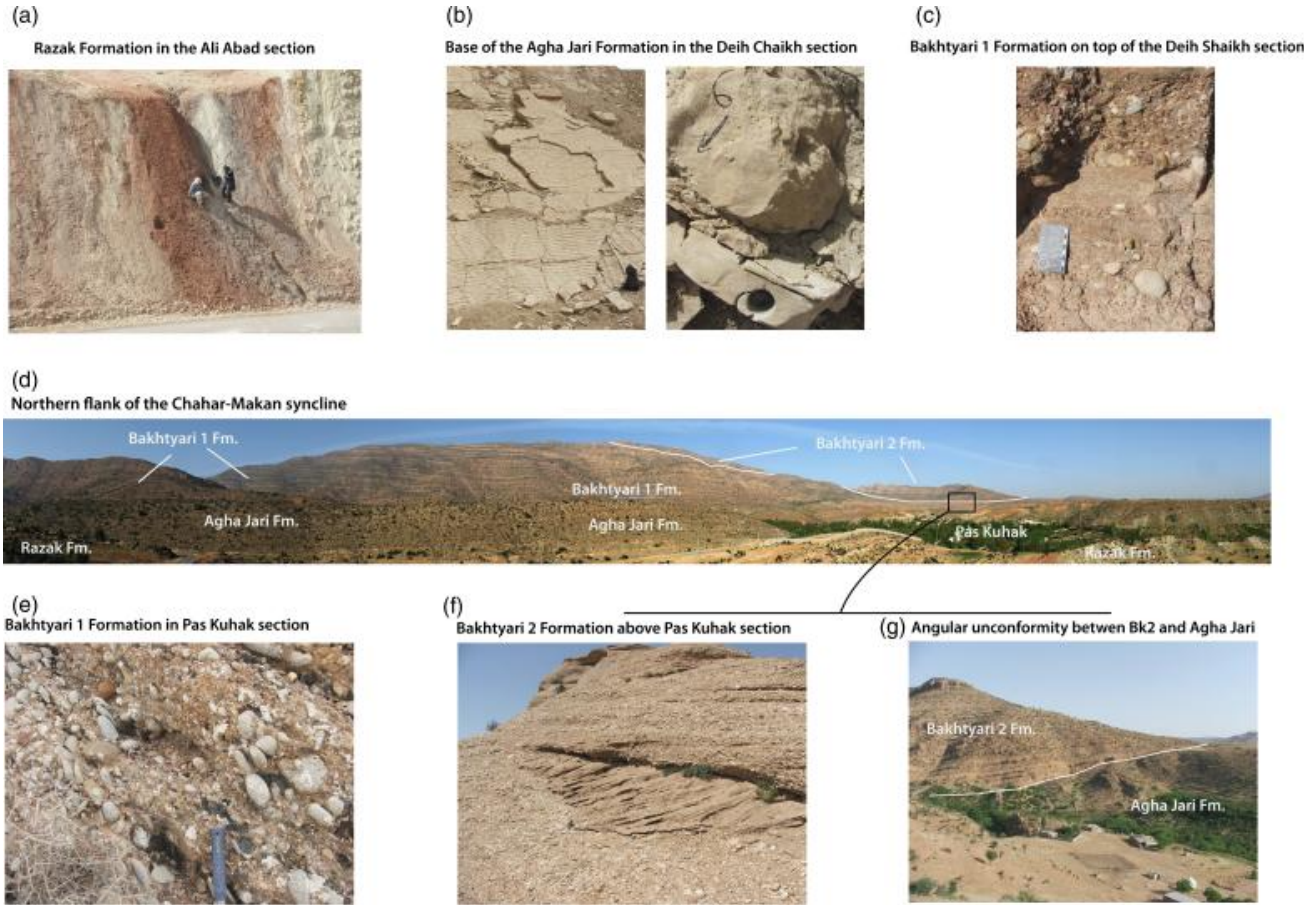

Figure II- 7: Photographs of key outcrops in the sampled formations. a) Alternating blue-to-yellow mudstones with thin beds of limestones, thin sandstones and dolostones typical of the Razak Formation (Ali Abad section); b) Base of the Agha Jari Formation in the Deh Shaikh section. Sedimentary structures such as current ripples confirm the marine origin of the basal Agha Jari Formation; c) Conglomerates of the Bakhtyari 1 Formation in the Deh Shaik section. The red color of the matrix expresses the abundance of radiolarian cherts rather than weathering. The facies correspond to clast-supported, poorly to very poorly-sorted gravels to cobbles interbedded with coarse sandstones showing through cross-stratification. They were deposited in a coastal fan delta; d) Panorama of the studied area striking N-S (right side) to E-W (in the center of the image); e) Clast-supported stratified cobbles and gravels in the Bakhtyari 1 with clast imbrications in Pas Kuhak section; f) Bakhtyari 2 conglomerates. The facies consists of clast-supported poorly to well-sorted planar alignments of 5-10 cm well-rounded massive gravels associated with gravels with planar through cross-bedding. They can be interpreted as sub-aquous sheet flood in alluvial fan related to migrating bar forms; g) The angular unconformity between Bakhtyari 2 conglomerates and the Agha Jari formation, west of the Pas Kuhak village. The unconformable contact between Bk1 and Bk2 can be inferred from panorama view in d) and is in consistent with satellite image presented in Figure II- 4.

Stratigraphic correlations between all sections were constrained by combining field mapping, SPOT images and aerial photographs. Correlation between the Ali Abad and Deh Shaikh sections is based on the presence of a distinctively thick package of calcareous sandstone beds that appears at meter ~350 in the Ali Abad section and is found ~150 m below the lowermost sampled site in the Deh Shaikh section. Correlation between the Deh Shaikh and Pas Kuhak sections is based on the presence of distinctively thick (50 m) package of conglomerates. Correlation between the three sections enables the construction of a composite section, named Chahar-Makan, with a total thickness of 1575 m.

II-4. Magnetostratigraphy

II-4-a. Sampling strategy

A total of 46, 45 and 18 paleomagnetic sites were sampled using a portable gas-powered drill along the Ali Abad, Deh Shaikh and Pas Kuhak sections, respectively. The total number of 109 sites is distributed along 1450 m of sedimentary succession, which corresponds to the lowermost 1275 m of the Chahar-Makan composite section and results in a mean sampling resolution of 12 m. Considering mean accumulation rates of 20 to 30 cm/kyr reported by Homke et al. (2004) for foreland sediments of the Zagros in the Lurestan region, this resolution corresponds to an estimated mean of one sample per 40 to 60 kyr. More than 85% of polarity intervals in the Lower and early Middle Miocene have a duration longer than 120 kyr (Lourens et al., 2004). Therefore, our sampling strategy is likely to resolve most polarity intervals with at least two consecutive samples in spite of difficult logistic and outcrop conditions, which prevented tighter sampling. The presence of thick conglomerate beds and covered mudrock intervals in the upper and lower parts of the section, respectively, has determined the presence of some sampling gaps of up to 30 m. Paleomagnetic sampling was focused on fine grained lithologies such as blue mudstones, red siltstones and fine-grained sandstones. Due to the scarcity of such suitable lithologies in some parts of the section, carbonates and coarse-grained sandstones were also drilled in the middle part of the Razak Formation and in the Bakhtyari 1 conglomerates. Nine samples for nannoplankton dating were collected from

marine sediments located around the transition between Razak and Agha Jari formations, in order to provide independent age constraints.

Paleomagnetic analyses were made using a 2G superconducting rock magnetometer at the Institute of Earth Sciences "Jaume Almera" in Barcelona (Spain). The noise level of the magnetometers is less than 7 x10^{-6} A/m, which is much lower than the magnetisation of the measured samples. Thermal treatment involved between 8 and 16 steps at intervals of 100°, 50°, 30° and 20°C to a maximum temperature of 690°C. Demagnetisation of a set of pilot samples representative for all the lithologies studied allowed optimization of the demagnetisation steps to allow accurate calculation of the Characteristic Remanent Magnetisation (ChRM) directions minimizing heating and formation of new magnetic phases in the oven. ChRM directions were identified through visual inspection of vector endpoint diagrams of demagnetisation data . Based on their demagnetisation pattern, ChRM directions have been divided into three groups. Type 1 magnetisations are those that describe well-defined linear trends directed towards the origin of the demagnetisation plot, which enables very accurate calculation of their directions. Type 2 magnetisations are those that display less-developed linear trends, yet they enable reliable calculation of their directions. Type 3 magnetisations are those that display either poorly-developed directions or incomplete demagnetisations due to growth of new magnetic minerals in the oven, yet they provide reliable polarity determinations by fitting clustered directions to the origin of the demagnetisation plots. Magnetisation directions were calculated by means of Principal Component Analysis .

II-4-b. Paleomagnetic results

In most of the samples, a low temperature magnetic component is unblocked below 250-300°C (Fig. II- 8). This component is parallel to the present-day field in the region (Dec=0°, Inc=46°) in geographic coordinates, and is interpreted as a viscous component with no geological meaning. Above this temperature, a ChRM can be identified in about 65 % of the studied samples. About 10, 33 and 22% of ChRM directions belong to quality types 1, 2, and 3, respectively. Unblocking temperatures range between ~500ºC-690ºC in red siltstones, some grey mudrocks and fine-grained sandstones from the Razak, Agha Jari and Bakhtyari 1 formations (Figs. II- 8d and g), which points

to hematite as the main magnetic carrier. In limestones and most grey mudrocks of the Razak Formation, the ChRM is unblocked below 500ºC (Fig. II- 8e), which points to magnetite as the main carrier. The ChRM shows northerly and southerly directions with shallow inclinations in geographic coordinates, which become similar to the Miocene reference direction for the studied area (Dec=0.7º; Inc=39.8º; α95=5.8º; see Smith et al., 2005) after tilting the beds back to their initial horizontal position (Fig. II- 9). Although no significant results are obtained when performing the fold test due to the similar dip of all studied beds, this strongly suggests that the ChRM was acquired before folding. In paleogeographic coordinates, normal and reversed ChRM directions of quality types 1 and 2 pass the reversal test with class C , which reinforces the interpretation that the ChRM represents a primary magnetisation acquired at, or shortly after, deposition of the studied rocks. Only in some cases, the ChRM seems to show a complex behaviour so that an additional pre-folding component is unblocked below 590ºC (Figs. II- 8c and h). This component, named D, displays a polarity opposite to the higher temperature ChRM, and is interpreted as a delayed magnetisation acquired most probably around polarity transitions. Results described here for the ChRM of the Razak, Agha Jari and Bakhtyari formations are similar to those reported in previous studies (Homke et al., 2004; Smith et al., 2005; Aubourg et al., 2008; Emami, 2008).

Virtual Geomagnetic Pole (VGP) directions have been calculated using ChRM directions of quality type 1, 2 and 3. The obtained VGP latitudes provide a sequence of polarity changes for the Chahar-Makan composite section in which polarity intervals have been determined by at least two consecutive samples (Fig. II- 10). The established sequence includes 8 normal magnetozones, which have been labeled N1 to N8 from bottom to top, and 7 reverse magnetozones, which have been labeled R1 to R7 (Fig. II- 10). The most conspicuous patterns of this polarity sequence are a long normal polarity interval in the upper part of the section (N8), and a cluster of three short normal magnetozones (N4 to N6) separated by two reverse intervals (R4, R5) in its middle part. In the lower part of the section, just above N2 and N1, the presence of samples with alternating normal and reverse polarities allow identification of two intervals with uncertain polarity attribution (Fig. II- 10). In addition, three single-sample intervals appear just above N1 and within the upper part of R6 and N8 (Fig. II- 10).

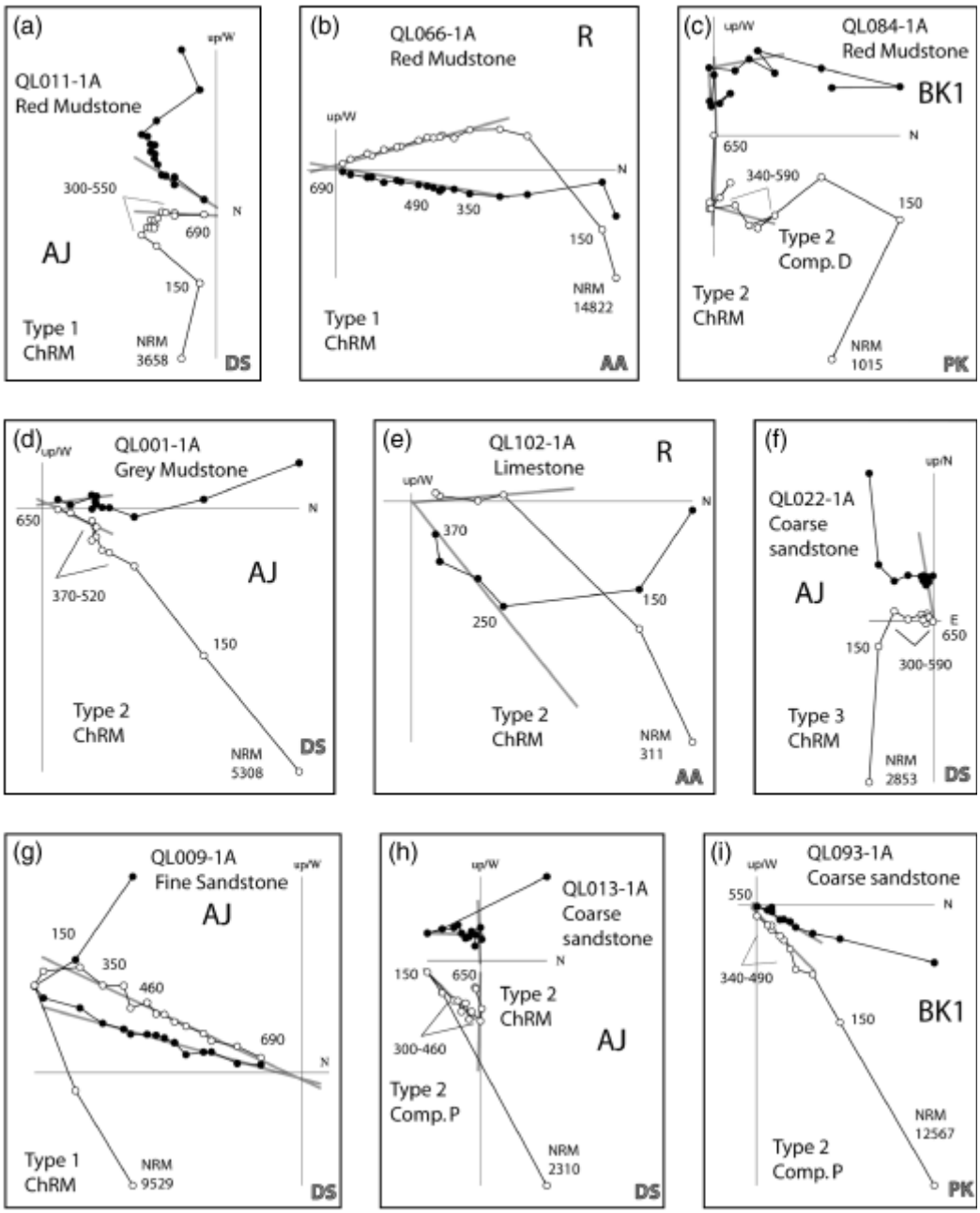

Figure II- 8: Demagnetisation plots representative for the different types of rocks and sedimentary formations studied. Grey lines represent the linear fit to the calculated directions. Demagnetisation plots are in geographic coordinates, the temperature steps in degrees Celsius C, and the intensity of the NRM in 10-6 A/m. The quality of the paleomagnetic directions for the ChRM and components D and P has been indicated. AJ: Agha Jari; R: Razak; BK1: Bakhtyari 1; AA: Ali Abad; DS: Deh Shaikh; PK: Pas Kuhak.

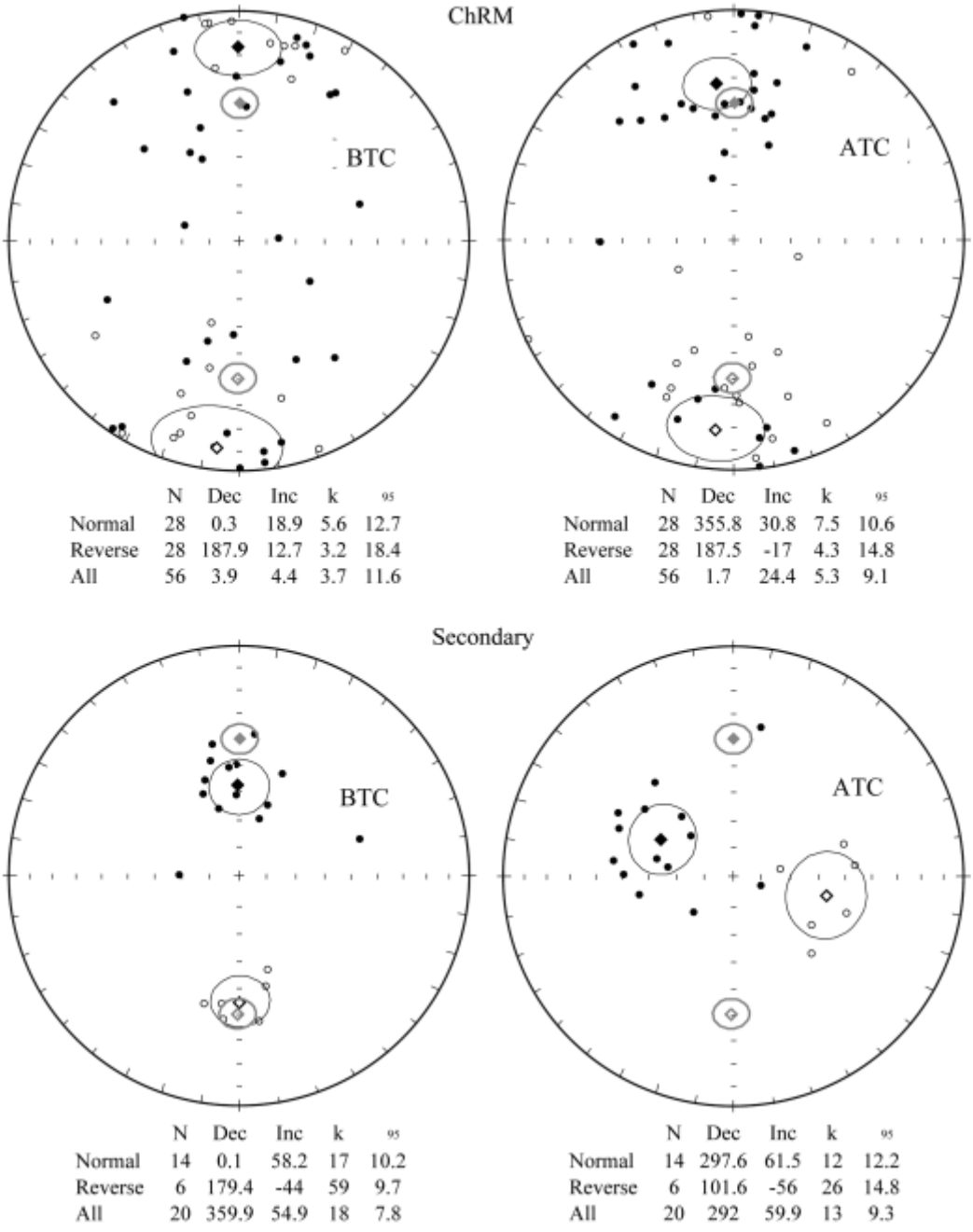

	N	Dec	Inc	k	95
Normal	28	0.3	18.9	5.6	12.7
Reverse	28	187.9	12.7	3.2	18.4
All	56	3.9	4.4	3.7	11.6

	N	Dec	Inc	k	95
Normal	28	355.8	30.8	7.5	10.6
Reverse	28	187.5	-17	4.3	14.8
All	56	1.7	24.4	5.3	9.1

	N	Dec	Inc	k	95
Normal	14	0.1	58.2	17	10.2
Reverse	6	179.4	-44	59	9.7
All	20	359.9	54.9	18	7.8

	N	Dec	Inc	k	95
Normal	14	297.6	61.5	12	12.2
Reverse	6	101.6	-56	26	14.8
All	20	292	59.9	13	9.3

Figure II- 9: Equal-area stereographic projections of the ChRM (upper panel) and component P (lower panel) directions before (BTC) and after (ATC) tectonic correction. Mean directions with the 95 % confidence angle are displayed. N: number of directions; Dec: declination; Inc: inclination; k: precision parameter; α95: confidence angle. Grey symbols indicate the normal and reverse components of the Miocene reference direction in the area.

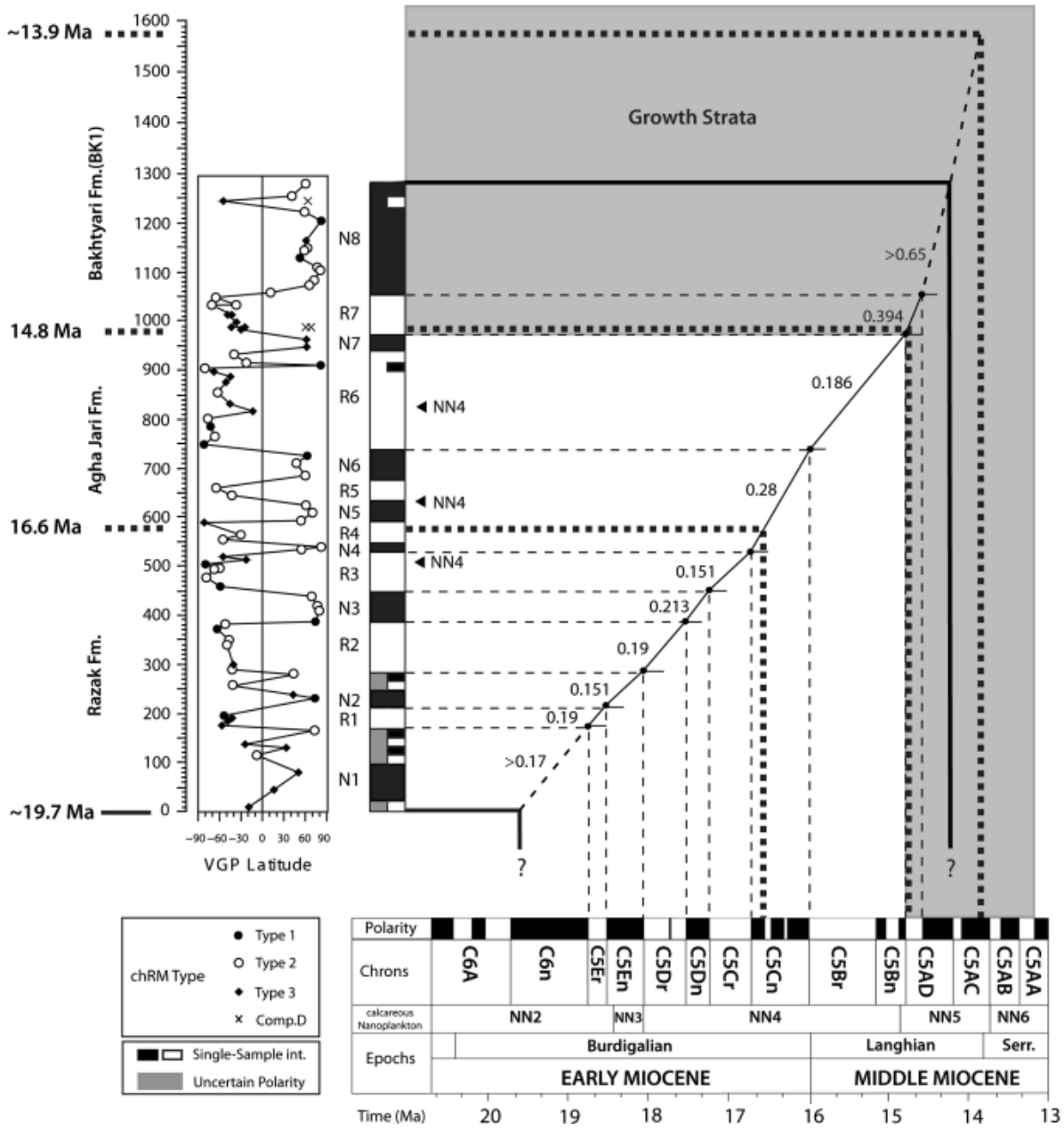

Figure II- 10: Correlation of the magnetic polarity sequences of the studied Chahar-Makan section to the GPTS2004 (Lourens et al., 2004). Sedimentation rates are given in mm/yr. Ages for the base of the Razak, Agha Jari and Bakhtyari 1 formations, are displayed. Black triangles labeled NN4 refer to samples containing characteristic nannoplankton assemblages (see Figure II- 11). Correlation of the NN4 biozone with GPTS2004 is after Raffi et al. (2006). Grey area shows the likely stratigraphic extent of the growth strata related to the development of the Sorkh anticline.

II-4-c. Correlation with the geomagnetic polarity time scale (GPTS)

Correlation between the middle part of the Chahar-Makan composite magnetostratigraphy and the Geomagnetic Polarity Time Scale (GPTS) reported in Lourens et al. (2004) is straightforward based on the distinctive pattern of polarity reversals and the anchor point provided by the calcareous nannofossils. Three nannofossil samples of the Deh Shaikh section, characterized by nannoplankton assemblages with Sphenolithus heteromorphus (first common occurrence at about 17.7 Ma and last occurrence at about 13.6 Ma), Cyclicargolithus foridanus (last occurrence at 12 Ma), Helicosphaera ampliaperta (first occurrence at about 20.4 Ma and last occurrence at about 14.9 Ma) and Discoaster deflandrei (Fig. II- 11) can be ascribed to biozone NN4, which ranges from Burdigalian to Langhian in age (i.e. 18-14.9 Ma) . This constrains the characteristic triplet formed by N4 to N6 to correlate with chron C5Cn, and the underlying magnetozones (R2 to R3) to correlate with chrons C5Dr, C5Dn and C5Cr, respectively. Similarly, the long, overlying reverse magnetozone (R6) must correspond to chron C5Br. Correlation to the GPTS is less straightforward for the lower part of the section due to the intervals of uncertain polarity attribution. Noticeably, the two intervals with alternating normal and reverse polarity directions occur just above N1 and N2. This suggests that both N1 and N2 correspond to genuine normal polarity intervals in which reverse ChRM directions at their tops represent delayed remanences acquired after the shift in polarity was completed (Fig. II- 10). Such behaviour, which is very common in Miocene continental deposits of the Zagros (Homke et al., 2004) and other foreland basins within the Alpine-Himalayan collision belt (e.g. Larrasoaña et al., 2006), is equivalent to that of Component D mentioned above, although in that case part of the ChRM retained the original polarity. Based on our interpretation, and pinning the sequence down from R2 (chron C5Dr), intervals N1, R1 and N2 can be correlated with chrons C6n, C5Er and C5En, respectively. This solution, which is entirely consistent with the thickness pattern of the inferred magnetozones (N1 to N2), implies that the base of the section is slightly younger than the C6A/C6n boundary.

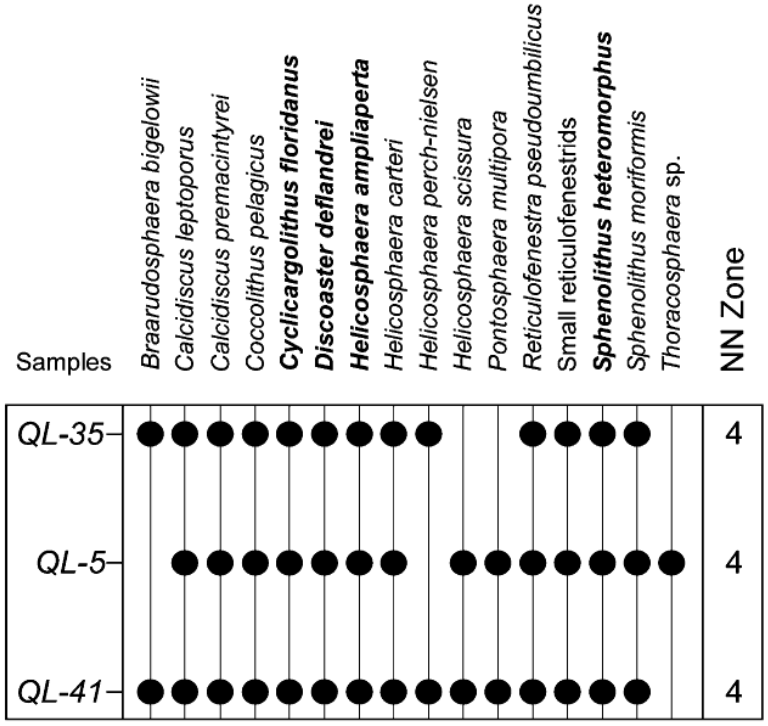

Figure II- 11: Nannofossil record from three samples of the Deh Shaikh section. Biostratigraphic markers are in bold characters.

Correlation of the upper part of the section to the GPTS is somewhat problematic due to the presence of single-sample polarity intervals (Fig. II- 10). Correlating the two normal magnetozones (N7 and N8) above R6 to the two consecutive normal chrons above C5Br (i.e. within C5Bn) results in unrealistically high sedimentation rates for the top of the section. The alternative solution, correlating N8 with C5AD.1n implies that one of the normal events within C5Bn might be missing. Given the presence of the single-sample normal polarity interval below N7, we interpret that it might represent a poorly captured chron C5Bn.2n and that N7 correlates with C5Bn.1n. We consider this second possibility much more likely because it provides a significantly better fit with the GPTS and results in a plausible rise in mean sedimentation rates just at the onset of Bk1 deposition. According to this interpretation, an age of 14.2 Ma (i.e. slightly older than the C5AD/C5AC boundary) can be estimated for the top of the sampled section.

The proposed solution for the Chahar-Makan composite section results in smooth accumulation rates that steadily increase from 0.17 at the base to 0.65 mm/yr at the top of the section. Our results indicate that the composite section spans from chrons C6n to C5AD (ca. 19.7 to 14.2 Ma), and give an age of >19.7, 16.6 and 14.8 Ma for the base of the Razak, Agha Jari and Bakhtyari 1 formations, respectively (Fig. II- 10). Based on a linear sedimentation rate upwards from the uppermost reversal, we infer an age of 13.9 Ma for the upper boundary of the logged Bakhtyari 1 conglomerates.

II-5. Discussion

II-5-a. Age of the proximal Zagros foreland basin: implications for the development of the Zagros collision

The magnetostratigraphy carried out in this study places new constraints on the age of foreland sedimentation in the northern part of the Zagros foreland basin. The present work shows that the base of the Razak Formation is older than 20 Ma, in agreement with ages of 32-18 Ma obtained from strontium isotope stratigraphy within the underlying Asmari Formation . According to , the onset of siliclastic sedimentation in the Zagros basin started between 28 and 16 Ma. This is consistent with the age of the Razak Formation, which further marked the onset of the overfilled stage of the Zagros foreland. As such, we infer that the flexural development associated with the onset of the collision might should have occurred before 20 Ma on the Arabian passive margin, as argued previously (Agard et al., 2005; Mouthereau et al., 2006; Ahmadhadi et al., 2007). This event is consistent with the start of decreased plate convergence rates between Arabia and Eurasia near 25 Ma . We date the base of the Agha Jari Formation at 16.6 Ma, which is slightly older than the Agha Jari Formation at a similar structural position in the Izeh zone (NW of our studied area) where its base was dated magnetostratigraphically at ca. 15.5 Ma . This transition appears to be significantly older than at the mountain front in the Lorestan area, where it is dated at 12.8-12.3 Ma .

Our magnestostratigraphic study indicates that the transition from Agha Jari to the lower Bakhtyari conglomerates (Bk1) is dated to 14.8 Ma (Fig. II- 10). This result contrasts with the long-lived tendency to assume a Pliocene age for the Bakhtyari conglomerates, but is consistent with a slightly older Miocene age recently proposed for a marine interval of the Bakhtyari conglomeratic

succession based on the paleontological and palynological content. By extrapolating the sedimentation rate from the uppermost polarity reversal upwards in the section, the age of the top of the logged section can be roughly estimated to be 13.9 Ma (Fig. II- 10). At the scale of the foreland basin, part of these conglomerates might be the proximal equivalent to the Agha Jari Formation found in the southern coastal Fars. The overall southward migration of the sedimentation and the upward coarsening outline the evolution towards an overfilled foreland basin (e.g. Covey, 1986; Sinclair, 1997). Finally, taking into account that the studied Bakhtyari 1 conglomerates were deposited approximately at sea level, we infer that the uplift of the northern Zagros to its present-day elevation of 2000 m was achieved after 13.9 Ma.

II-5-b. Constraints on the timing of folding in the northern Fars

Two stages of folding have been previously described, but not accurately dated, in the study area. The first stage of folding corresponds to the growth of the Sorkh anticline. It is recorded by the growth strata within the Bk1 conglomerates on the northern flank of the Qalat syncline (Figs. II- 5 and 12). Despite the lack of direct stratigraphic constraints within the Bk1 succession, an age for this folding can be determined assuming a simple correlation between similar depositional sequences, ages and structural position (Fig. II- 3) at the scale of the overall studied area (15 x 15 km). The oldest growth strata are located close to the base of the Bk1 conglomerates. As a result, and if our hypothesis is correct, one can estimate an age of 14-15 Ma for the initiation of the Sorkh anticline and more generally for the folding in the northern Zagros folded belt. This new stratigraphic age indicates that this early folding stage is 3 to 9 Ma older than initially thought .

The second stage of folding is associated with the growth of the Derak anticline and the development of adjacent Chahar-Makan and Qalat synclines (Fig. II- 3). During this second stage of folding, the uppermost Bk1 conglomerates were tilted and sealed by the regional-scale unconformity outlined by the horizontal Bk2 alluvial conglomerates, which are not dated as yet (Figs. II- 5 and 12). Unfortunately, growth strata related to this episode, if any, have not been preserved in the conglomeratic succession. Together with the drastic shift towards more continental conditions, this

observation supports rapid uplift in a subaerial environment and limited coeval sedimentation. Although, Mouthereau et al. (2007) proposed an age of 2-3 Ma for this stage, folding can have started at any time after 14-15 Ma. This calls for the need to gain more complete dating throughout the syn-orogenic deposits of the Zagros foreland basin. With regards to the kinematics of the studied structural units, it is worth noting that neither the ChRM (after tectonic correction), nor the post-folding remagnetisation (before tectonic correction), show a statistically significant deviation from the expected reference direction in the area (Fig II- 9). This demonstrates the absence of significant vertical-axis rotations in the studied area despite its location near the active Sabz-Pushan strike-slip fault (Fig. II- 3b). This result needs to be incorporated with previously published paleomagnetic results in the region in order to determine the pattern of regional scale vertical-axis rotations in the western part of the Fars arc.

II-5-c. Early-Middle Miocene sedimentation rates and unroofing of the internal Zagros

The sedimentation rates derived from magnetostratigraphy shows three main trends that follow the deposition of the Razak, Agha Jari and Bakhtyari formations (Fig. II- 10). The Razak Formation is characterized by mean sedimentation rates of 0.18 mm/yr. Sediments of this formation (bioclastic sediments, dolostones and blue mudstones) are indicative of marine sabkha environments, although interbedded red clays reveal some sporadic subaerial exposure. The Agha Jari Formation is characterized by slightly increasing mean sedimentation rates of 0.23 mm/yr. Larger clasts sizes (up to 10 cm), and a significant fraction of chert and limestone pebbles originating from Mesozoic limestones, Eocene or Miocene limestones, indicate a source located in the High Zagros or close to the MZT. There, the radiolarian red cherts of the Mesozoic ophiolitic units have been eroded, transported and re-deposited into the foreland basin from the Eocene until the Miocene. Such evidence indicates unroofing of the Neyriz ophiolites located in the northeast or much farther ophiolitic units found northwestwards in the Kermanshah area (Fig. II- 3a). This is consistent with paleocurrent orientations revealing south to southeast directed flows (Fig. II- 6). Finally, sedimentation rates increase significantly for the Bakhtyari 1 conglomerates, reaching a mean rate of

0.52 mm/yr. The abundance and the size of limestone clasts increase upwards to reach 30 cm at most. This indicates a more local source of sedimentation and implies the unroofing of more proximal units of the High Zagros where limestones are present. The occurrence of nummulitic pebbles in the Agha Jari and Bakhtyari 1 Formations argues for the erosion of the Jahrom Formation or Asmari Formation currently exposed in the Sorkh anticline (Fig. II- 3b). This is consistent with the intraformational unconformity found within the Bk1 conglomerates and the dominant south-directed flows. The small-scale fan deltas transporting sediments from the Sorkh anticline likely fed the surrounding marine deltas situated at the current position of the Qalat and Chahar-Makan synclines. We consequently infer that the Sorkh anticline located in the footwall of the High Zagros Fault was emerged above sea level by about 14-15 Ma.

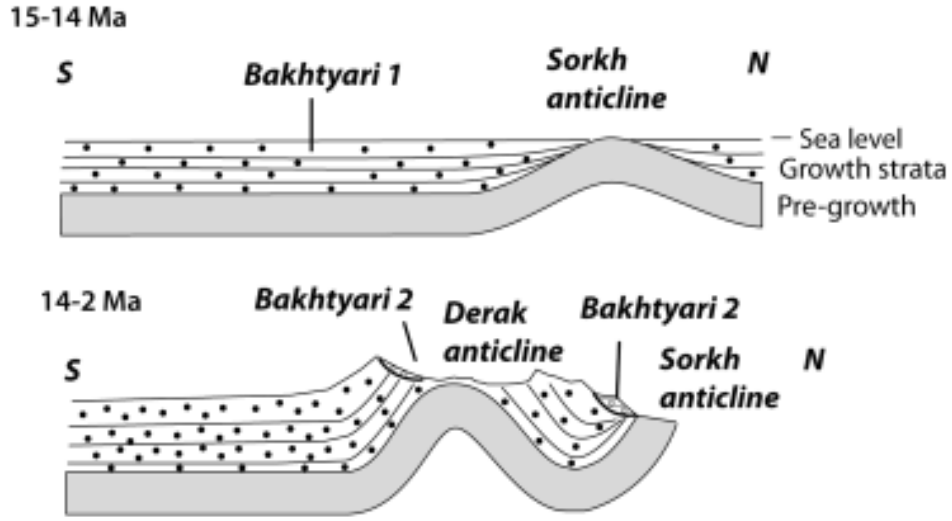

Figure II- 12: Schematic reconstruction of the sequence of folding in the studied area. Magnetostratigraphic dating of the growth strata (Bakhtyari 1 conglomerates) reveals that folding in the Sorkh anticline started ca. 14-15 Ma. At this time the Zagros Folded Belt was close to sea level. A remarkable change occurred after 14-15 Ma and before 2 Ma (assumed base of the Bakhtyari 2 conglomerates) when the Derak anticline developed coeval with the uplift of the whole Zagros Folded Belt.

II-6. Conclusions

Magnetostratigraphy data presented here for the northern flank of the Chahar-Makan syncline provides new time constraints on the onset of foreland sedimentation and the initiation of folding in the northern part of the Zagros folded belt. The correlation of magnetic polarity sequences to the GPTS indicates that deposition of the synorogenic siliciclastic succession started as early as the Early Miocene at least 19.7 Ma ago, and corresponds to the Razak Formation in the Chahar-Makan syncline. The overlying Agha Jari Formation was deposited between 16.6 Ma and 14.8 Ma. The deposition of the Bakhtyari 1 conglomerates started after 14.8 Ma. The sediment accumulation rates increase from 0.18 mm/yr in the Razak Formation to 0.52 mm/yr in the Bakhtyari Formation (Bk1) at the top of the studied section.

The onset of deformation in the northern Zagros likely started around 14-15 Ma and was associated with growth strata at the base of the Bk1 succession found in the northern limb of the Qalat syncline. We suggest that the onset of folding might be related to the rapid (nearly instantaneous) propagation associated with the buckling of the sedimentary cover as previously proposed. A second stage of folding reveals increasing contraction marked by the change towards more continental environmental conditions. This phase is found in association with the growth of the Derak anticline and produced tilting of the Bk1 conglomerates. The Bk1 conglomerates are truncated by an erosional surface on top of which Bk2 conglomerates are deposited unconformably. Though new dating campaigns are necessary to unravel the age of the Bk1/Bk2 unconformity, this study reveals that tectonic deformation was already ongoing in the Middle-Upper Miocene in the northern part of the Zagros folded belt.

Acknowledgements:

This work greatly benefited from the support of the Geological Survey of Iran (Tehran and Shiraz) during the extensive field work in Iran. The authors would like to address special thanks to M.A. Sedaghat manager of Shiraz headquarter. We are grateful to Miguel Garcés who has provided insightful comments during the analysis of the paleomagnetic results. We also thank the ISIS

program, which provided SPOT 5x5m resolution images. This work has been funded by CNRS, UPMC and the Franco-Spanish Picasso PHC program. We also thank Mark Allen and two anonymous reviewers, as well as Editor Peter van der Beek for their helpful comments that helped to improve the manuscript.

Chapter III

Exhumation rate and sediment provenance study in the Zagros foreland

I. Concepts and methodology

This part contains a briefly discussion about the concepts and methodology, more details are presented in Annex III.

I-1. Apatite fission track analysis (low-temperature thermochronology)

The fission-track method, also known as spontaneous fission-track dating, is a radioisotope dating method that depends on the tendency of ^{238}Uranium to undergo spontaneous fission in parallel the usual decay process.

The high relative abundance of ^{238}U and the longer half-life with respect to fission of other naturally fission isotopes (such as ^{235}U and ^{232}Th) infer that all natural tracks in terrestrial minerals are the products of fission of ^{238}U atoms, located within the mineral itself (Fleischer et al., 1975).

Upon heating, tracks are annealed or shortened to a length that is determined by the maximum temperature and the time experienced. For example, at a temperature of 110°-120°C for a period of 10^5-10^6 years, tracks are completely annealed. This characteristic allows construction of time-temperature paths of many different rock types by inverse modelling of observed FT age and confined track length data (Galbraith, 1994; Ketcham et al., 2000).

The major difference between fission track dating and other conventional isotopic dating methods is that the daughter product causes physical damage to the crystal lattice, rather than the production of another isotope (Braun et al., 2006).

Fission track analysis was proposed as a geological dating tool by Price and Walker (1963). Low-temperature thermochronometric dating techniques provide a direct constraint in cooling of exhumed rocks by tectonic processes. In fact, it is even possible to calculate different burial depths and post-depositional uplifts; so this method is ideally suited to record the cooling effects of exhumation processes that operate in the upper crust.

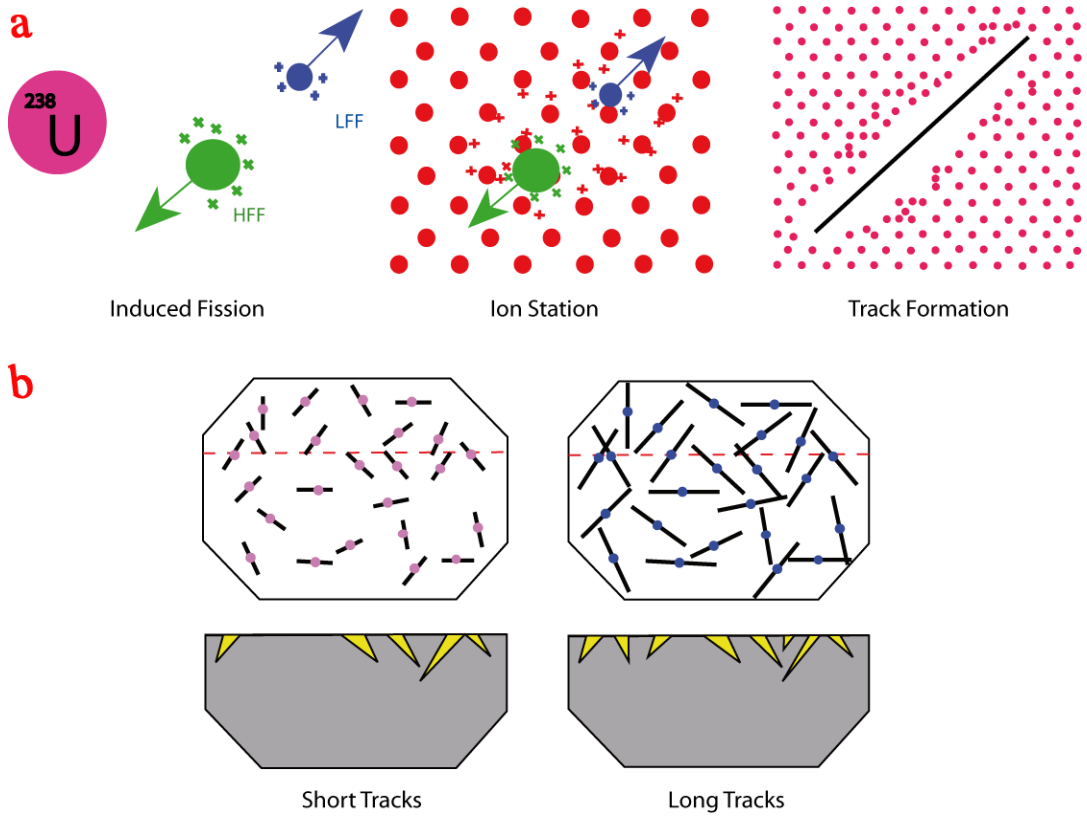

Figure III- 1: a) the three stages of track formation, natural fission of the U nucleus is an explosive event during which two highly charged particles fly in opposite direction from each other at high velocity (Fleischer et al., 1975) producing a single damage trail in the crystal that is identified as a spontaneous fission track; b) different fission track lengths.

I-2. Fission track dating approach

Zeta calibration factor has been determined by using the following age standards; Durango (DUR) from the Cerro de Mercado (iron mountain) Mexico (31.4 ± 0.8 Ma), Fish Canyon Tuff (FCT) from Colorado (27.9 ± 0.7 Ma). Zeta value is expressed relative to the CN5 glass with a U of 12.19 ppm.

There are three common mean age estimation for single grain age method; the mean, pooled, and central ages. The pooled age is simply the sum of the spontaneous counts divided by the sum of the induced counts, while the mean age is the arithmetic mean of the individual ratios of spontaneous to induced tracks. The central age is a more recent development (Galbraith and Laslett, 1993) and is essentially the weighted mean of the log normal distribution of single grain ages. When the variation

in the count population is consistent with a Poisson distribution, then all three age estimates are essentially the same.

I-3. Detrital population

Fission track results for individual detrital grains may be presented in histogram form. However, a more quantitative age estimate is possible if errors are assigned to each individual grain determination, so that the data can be presented as a probability density function (Hurford et al., 1984).

A problem with the probability density plot is that individual data points cannot be distinguished, so that some important but small components in the data distribution can be buried under the other data. To avoid these problem, Galbraith (1988) introduced a kind of isochron diagram for the presentation of fission track data measured on individual grains of a heterogeneous sample (Galbraith, 1988). Radial plots (Galbraith, 1990) were used to graphically display single crystal ages of each sample.

I-4. Sediment Provenance study

The sediment provenance study on base of Gazzi-Dickinson method is a point-counting technique used in geology to statistically measure the components of a sedimentary rock, chiefly sandstone. This method was developed by Dickinson and Suczek (1979) and later modified by Dickinson (1985); Dickinson et al (1983) is potentially a powerful tool for reconstructing palaeo-plate tectonic settings on the basis of the detrital composition. Results from such analyses help in the interpretation of uplift and sediment input from surrounding source terrains. In addition, by integrating petrographic and geochemical techniques from the sediment sorting, recycling and terrain weathering study, we can constrain temporal distribution of distinct sources. This is important for understanding the controls on the depositional systems.

Exhumation and Denudation in Miocene the Zagros foreland

The study area is located located ~100 km to the south of the Main Zagros Thrust and ~100 km to the west of the Neyriz ophiolitic complex. This region is positioned near the NW corner of the Mand river (Rud-e-Mand) catchment (~78000 km^2) that is currently draining the HZ and the ZFB. This Miocene detrital sediments in the Zagros foreland successfully provided new insights on the temporal evolution of uplift and exhumation patterns associated with the building of the Zagros.

Through this research the authors used the results of low-temprature fission track, petrography of detrital sediments and clay mineralogy for providing new constraints on the timing of deformation in the Zagros and exhumation associated with mountain building.

This research is submitted in Geological Society of America Bulletin as "Provenance of Miocene Zagros foreland sediments from detrital petrography and apatite fission-track thermochronometry: implications for tectonic evolution of the High Zagros (Fars, Iran)".

II. Provenance of Miocene Zagros foreland sediments from detrital petrography and apatite fission-track thermochronometry: implications for tectonic evolution of the High Zagros (Fars, Iran)

Submitted to Geological Society of America Bulletin

Sh. Khadivi [1, 2 *], F. Mouthereau [1, 2], J. Barbarand [3], T. Adatte [4], O. Lacombe [1,2]

[1] UPMC Univ Paris 06, UMR 7193, Institut des Sciences de la Terre de Paris, F-75005, Paris, France.

[2] CNRS, UMR 7193, Institut des Sciences de la Terre de Paris, F-75005, Paris, France.

[3] IDES, University of Orsay, Bldg 504, 91405,Orsay, France

[4] IGP, University of Lausanne, Bldg Anthropole, CH-1015, Lausanne, Suisse

[*] *Corresponding author*: Institut des Sciences de la Terre et de l'Environnement de Paris, Université Pierre et Marie Curie, T. 45-46, E2, Box 129, 75252 Paris Cedex 05, France, Phone +33(0)144275256, Fax +33(0)144275085, shokofeh.khadivi@upmc.fr

Abstract

The precise timing of shortening and exhumation in the Zagros during the protracted Meso-Cenozoic plate convergence between Arabia and Eurasia is still poorly understood. In this study we carried out a coupled analysis of petrographic composition, clay mineralogy and low-temperature fission-track dating on well-dated Miocene detrital sediments (19.7-14.8 Ma) of the Zagros foreland.

From AFT grain-age population we identify three main tectonic-magmatic episodes including the Jurassic-early Mesozoic accretion, metamorphism and magmatism in the Sanandaj-Sirjan belt, the obduction of the Neyriz ophiolitic complex and the associated tectonic mélange, the Eocene magmatic period and finally the initiation of rapid exhumation related to the ongoing Zagros collision. The preservation of such a protracted history of cooling limits to 2.5 km the burial of the Miocene series in the Zagros foreland.

Petrographic analysis reveals that the Miocene eroding catchment was essentially eroding ophiolitic and mélange derived rocks and the overlying carbonaceous sediment cover. Second order metamorphic clasts of the HP metamorphic belt were probably recycled from the SSZ and likely originated from clasts of the mélange series outcropping in the suture zone.

A remarkable change in the detrital record occurred after 16.6 Ma when the eroding landscape originally made with local and small-scale catchments eroding the exhumed source rocks of the High Zagros fault hangingwall changed to catchment involving the contribution of more regional source areas like the Zagros suture zone similar to the current drainage basin. With this change, more sediment cover and deeper, more mafic, structural level of the ophiolitic sheets were eroded. This modification of the type of exhumed source areas was coincident with the initiation of folding in the Zagros Folded Belt.

Since 12.4 Ma and the uplift of the Zagros and Folded Belt and the Iranian plateau accretion occurred rapidly in probably less than 5 Myrs and in association with weak erosion feedbacks as revealed by the prevailing arid climatic conditions since the early Miocene.

Key words: Zagros, foreland basin, exhumation, uplift, thermochronology, apatite fission track

II-1. Introduction

The distribution and precise timing of Cenozoic shortening as well as the degree of uplift and exhumation in the Zagros collision zone in Iran are keys to better understanding how the Arabia (AR) plate motion was accommodated during the collision with the overriding Eurasia (EUR) plate. This is particularly important if plate reconstructions are used to infer the connectivity between the Indo-Pacific Ocean, the Mediterranean Sea and the Para-Tethyan (sea e.g. Kocsis et al., 2009; Reuter et al., 2009), to interpret the impact of the Arabia/Eurasia convergence on the regional aridification of Central Asia (Ramstein et al., 1997) and on the Cenozoic global climate changes (Allen and Armstrong, 2008) or to deduce the mechanisms of Iranian plateau uplift (Hatzfeld and Molnar, 2010).

Comparison between recent synthesis of GPS data (ArRajehi et al., 2010) and geological constraints on past plate motions (McQuarrie et al., 2003) suggest that the AR/EUR convergence occurred at a rate of ~20 km/Myr (Tatar et al., 2002; Hatzfeld et al., 2003; Nilforoushan et al., 2003; Vernant et al., 2004) since at least 22 Ma, following the separation of Arabia with Africa (Nubia). This timing is consistent with stratigraphic/structural constraints in the Zagros near plate suture arguing for a minimum age of 23-25 Ma for the final closure of the Neo-Tethyan ocean (Agard et al., 2005). In the Zagros, this observation is consistent with the replacement of the Oligocene carbonates by siliciclastic sedimentation in the Lower Miocene (Beydoun et al., 1992) and with the onset of deposition of synorogenic sandstones of the Razak Formation precisely dated at 19.7 Ma using magnetostratigraphy (Khadivi et al., 2010). Published seismic lines from the Persian Gulf provide further evidence for a flexural unconformity in the Middle Miocene or slightly earlier supporting the above conclusions (Soleimany and Sàbat, 2010). These concurrent data taken together confirm that uplift, erosion and contraction in the northern Zagros was underway, and that final suturing occurred in the early Miocene.

Complementary data supporting, instead, a contractional episode on the Arabian margin before the Early Miocene are brought by tectonic/stratigraphic relationships in the Zagros. For instance, a middle Eocene-late Oligocene or Late Eocene-Lower Miocene unconformity has long been recognized in the carbonates succession of the Zagros (James and Wynd, 1965; Berberian and King, 1981). In the Lorestan area, it has been argued that this erosional or non-depositional hiatus lasted 15 Myrs (Homke et al., 2009). The recent re-evaluation of the stratigraphy of the coarse-grained facies

in the Zagros foreland basin shows that the onset of coarsening upward sedimentation occurred during late Oligocene (Fakhari et al., 2008). This strongly suggests that this major unconformity resulted from tectonic loading and unroofing in the northern Zagros between the middle Eocene and the late Oligocene.

To North of the Zagros, a review of the timing of deformation argues for collisional shortening starting in the Late Eocene-Oligocene (e.g. Allen and Armstrong, 2008) or slightly earlier (Golonka, 2004). This is supported by the occurrence of detrital zircons with U/Pb ages of 45-50 Ma, derived from the overriding Iranian plate, in the late Oligocene conglomerates deposited in the northern Zagros (Horton et al., 2008). A previous analysis of detrital apatite fission-track ages in the Miocene sediments of the NW Zagros belt also reported a rapid cooling at ~38 Ma, in agreement with the proposed timing (Homke et al., 2010).

Despite the exact sequential timing of collisional events is still challenged, it is beyond doubt that a marine gateway connecting the Mediterranean Sea and the Indo-Pacific Ocean existed at least until the early Miocene in the Central Iran (Schuster and Wielandt, 1999; Harzhauser et al., 2007) and until ca. 15 Ma on the Arabian margin (Khadivi et al., 2010). Helium dating on detrital zircon and apatite in the Dezful-Izeh area of the northern Zagros has revealed rapid cooling and sedimentation between 19-15 Ma and 12-8 Ma in the High Zagros (Gavillot et al., 2010) in agreement with the early phase of folding illustrated by growth strata dated at 14-15 Ma in the Fars area of the northern Zagros (Khadivi et al., 2010). Together with the youngest apatite fission-track grain-age population of ~22 Ma (Homke et al., 2010) these data indicate that the Arabian margin was exhumed rapidly between 20 and 10 Ma ago.

From this brief review of available tectonic-stratigraphic constraints, the Arabia-Eurasia convergence appears to have induced an initial episode of contraction at ~35 Ma north of the ophiolitic domain. An obscure stage of shortening then occurred for ~20 Myrs on the southern margin of the SSZ occupied by a NW-trending accretionary complex and the remnant oceanic crust that was closed by the early Miocene. Since this time onwards shortening propagated onto the Arabian margin to build the Zagros Mountains and the Iranian plateau.

With this study, we attempt to resolve the temporal evolution of uplift and exhumation patterns associated with the building of the Zagros in the Fars area from the Eocene period and the Miocene phase of shortening to the final regional uplift. In particular, we seek to provide new constraints on the nature of exhumed source areas and weathering/climatic conditions in the eroding landscape of

the northern Zagros, which is key location to unravel the initial collision stage and late regional uplift. To this aim, we present a provenance study of middle Miocene (19.7-14.8 Ma) detrital sediments in the northern Zagros based on the analysis of petrological assemblages and clay mineralogy combined with new detrital apatite fission-track ages. The implications of the results are discussed in terms of plate geodynamics, landscape evolution and regional paleogeography.

II-2. Geological background

The NW–SE trending Zagros orogeny, which is part of the much larger Alpine-Himalayan orogenic system, extends some 2000 km from the East Anatolian fault in eastern Turkey to the Makran subduction in southern Iran (Fig. III- 2). GPS-derived velocity model shows present-day convergence rates between Arabia and Eurasia of 19-23 mm/yr (McClusky et al., 2003) with about half i.e. 7-10 mm/yr accommodated across the Zagros Folded Belt (Tatar et al., 2002; Nilforoushan et al., 2003; Vernant et al., 2004).

Figure III- 21 shows the in the current plate tectonic framework a series of tectono-metamorphic and magmatic belts that resulted from the protracted Arabia-Eurasia plate convergence. These belts comprise to the north the Zagros, the Sahneh and Neyriz ophiolitic complexes that shape the Zagros suture zone, the volcanic arc and tectono-metamorphic belt of the Sanandaj-Sirjan Zone and the Tertiary Andean-type Urumieh-Dokhtar volcanic arc (Berberian and Berberian, 1981; Berberian and King, 1981; Berberian et al., 1982).

Hereafter, we briefly introduce the main geological features of the Zagros belt, the Sanandaj-Sirjan belt and the Urumieh-Dokhtar volcanic arc that are relevant to this study.

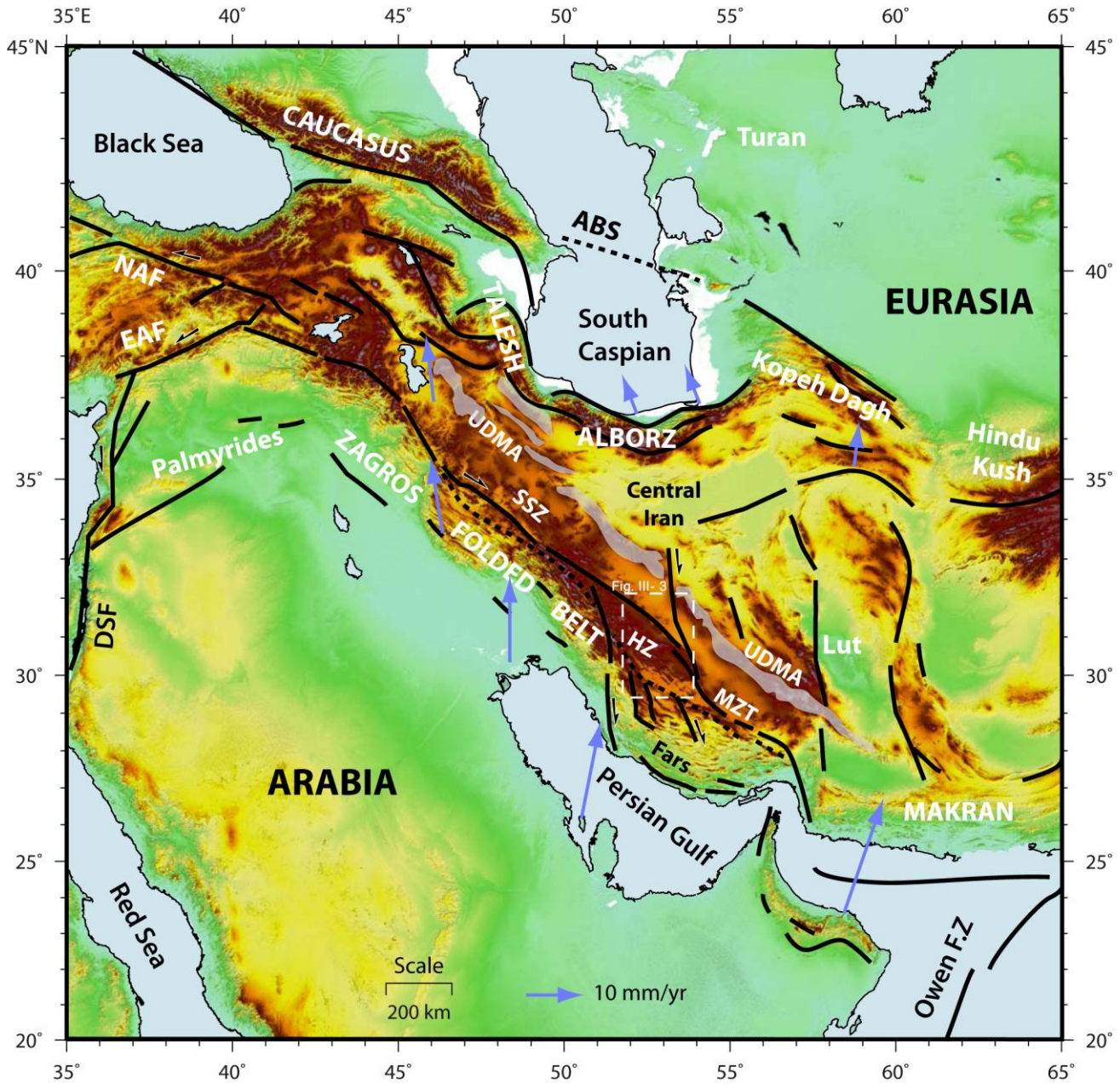

Figure III- 2: Geodynamic setting of the Zagros collision and main topographic and tectonic features of the Arabia/Eurasia convergence. Black lines display major faults. GPS velocities shown as blue arrows are from Vernant et al. (2004) and Masson et al. (2007). Black dashed line are the main active Faults. Abbreviations are Sanandaj-Sirjan Zone (SSZ), Urumieh-Dokhtar Magmatic Arc (UDMA), Apsheron-Balkan Sill (ABS), East Anatolian Fault (EAF), North Anatolian Fault (NAF) and Dead Sea Fault (DSF).

II-2-a. The Zagros Folded Belt (ZFB)

The Zagros Folded Belt makes up the currently active accretionary wedge of the Zagros collision. It is characterized by remarkably regular, long and large-wavelength NW-trending concentric folds (Fig. III- 3) that result from buckling and detachment folding of a 12 km-thick sediment cover detached in the Cambrian Hormuz salt as it is shown by field geology and tectonic analysis in the Fars region (Lacombe et al., 2007; Mouthereau et al., 2007a; Mouthereau et al., 2007b) as well as recent numerical modeling (Schmalholz et al., 2002; Yamato et al., submitted).

The pre-Cambrian basement of the Arabia margin is also actively deforming. Yet controversial, the thick-skinned style of shortening in the ZFB is supported by a number of morphotectonic observations in the Fars (Molinaro et al., 2004; Lacombe et al., 2006; Mouthereau et al., 2007b) and is required to tectonically build the regional topography (e.g. Mouthereau et al., 2006). The recent analysis of the 2006 sequence of Fin earthquakes indicated that deformation beneath the ZFB is currently involving both the cover (5-9 km) and the basement (10-30 km) (Roustaei et al., 2010).

The ZFB can be divided in two sub-structural domains, the High Zagros (HZ) belt characterized, in the Fars region, by dominantly Mesozoic outcropping strata including the radiolaritic series and ultramafic bodies of Neyriz ophiolitic complex and the Zagros Folded Belt (ZFB) sensu stricto, also called the Zagros Simply Folded Belt (ZSFB) with folded Miocene to Pliocene synorogenic strata (Fig. III- 3). They are separated by the High Zagros Fault, a currently inactive fault across which neither significant displacement nor remarkable geomorphic features can be detected in our studied area, thus contrasting with the 6 km offset along the NW segment or associated earthquakes along the SE fault segments (Berberian, 1995).

The High Zagros is bounded to the north by the Main Zagros Thrust (MZT) also called the Main Zagros Reverse Fault (MZRF), a major tectonic feature associated with the ophiolitic suture zone, which therefore approximates the boundary between the Arabian and Eurasian plates (Figs. III- 3 and 4). Most of the larger earthquakes occur in the ZFB (Talebian and Jackson, 2004) leaving the High Zagros relatively aseismic, in agreement with very few evidence for active shortening (Tatar et al., 2002).

The timing of shortening is not well constrained in the HZ due to the lack of syntectonic stratigraphic markers. However, the presence of Eo-Oligocene limestones unconformably overlying the folded Mesozoic carbonaceous series (Fig. III- 3) shows that uplift and erosion initiated slightly

before deformation in the ZFB, following a classical forward-propagating sequence. Such a sequence is supported by the Oligocene-Late Miocene age of the first siliciclastic conglomerates (Fakhari et al., 2008) as well as the oldest synfolding sediments of the northern ZFB dated at 14-15 Ma (Khadivi et al., 2010).

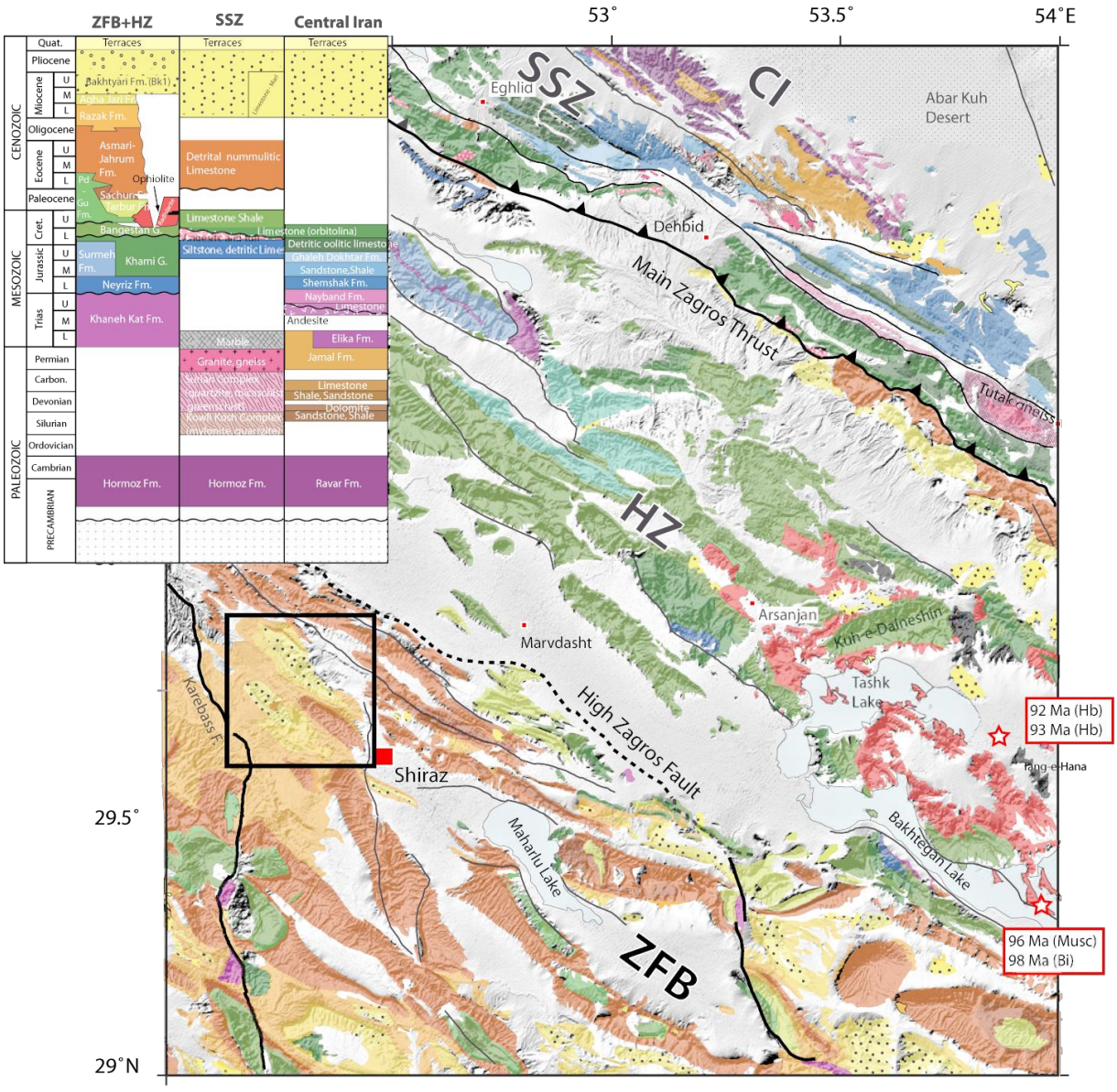

Figure III- 3: Draped geology map of the Zagros (northern Fars area; see location on Fig. III- 2) on SRTM topographic data (http://srtm.csi.cgiar.org/) and main lithostratigraphic units. The map is mainly redrawn and simplified based on the 1/250,000 scale geological maps of Eqlid and Shiraz and 1/100,000 scale geological maps of Kalestan and Shurab. The stratigraphy age of Bakhtyari Fm is from Khadivi et al. (2010) and $^{40}Ar/^{39}Ar$ radiometric datings in the Neyriz ophiolitic complex shown in red boxes are after Haynes and Reynolds (1980) and Babaie et al. (2006). Abbreviations are Central Iran (CI); Sanandaj-Sirjan Zone (SSZ); High Zagros (HZ); Zagros Folded Belt (ZFB).

II-2-b. The Neyriz Ophiolitic Complex

The ophiolitic complex of Neyriz is considered to be an allochthonous fragment of the western branch of the Neo-Tethyan (i.e. Pindos) oceanic lithosphere exposed to the east of our study area (Fig. III- 3) (Stocklin, 1968; Golonka, 2004). These units are currently observed in synclinal valleys indicating the thrust contact was folded during a subsequent phase of Zagros orogeny. The ophiolitic complex contains a sedimentary assemblage of radiolarian cherts, turbidites, middle Jurassic oolitic and micro-brecciated limestones, and Middle Cretaceous limestones (Ricou, 1976) from which thrust sheet units can be distinguished. Mafic and felsic extrusive and associated intrusive rocks (gabbros, diorites and plagiogranites) constitute the crustal sequence of the Neyriz ophiolite which is particularly well exposed in Tang-e Hana (Fig. III- 3). The ophiolites contain peridotites, mainly harzburgites and dunites, with olivine and pyroxene that are variably serpentinized into lizardite (dominant) and antigorite (Babaie et al., 2006). They also include remarkable planar chromite interlayers. East of lake Bakhtegan, the Hajiabad mélange (Fig. III- 3), probably Mesozoic in age, is composed of Permian-Triassic limestones, radiolarian cherts, tuffs, basalts (pillow lavas) and greenschist-to-amphibolite metamorphic rocks lying above the basal detachment shear zone of the allochtonous ophiolite complex (Babaie et al., 2006; Sarkarinejad et al., 2009). This mélange contrasts with that of the Sahneh ophiolite near Kermanshah made with sheets of Eocene turbidites and gabbros thrusted during the Miocene. To the west of Lake Bakhtegan (Fig. III- 3), both the tectonic mélange and the ophiolite are thrusted over the highly folded Pichakun Formation, interpreted as deep-water radiolarian sediments dated from Late Triassic to Middle Cretaceous (Ricou, 1976; Robin et al., 2010). The Neyriz ophiolite complex was tectonically emplaced onto the Cenomanian-Turonian shallow-marine Sarvak Formation (e.g. Hallam, 1976). $^{40}Ar/^{39}Ar$ dating on hornblende in diabase and plagiogranite yielded an age of 92-93 Ma (Babaie et al., 2006) consistent with ages of ~95 Ma obtained in amphibolites and slightly younger ages of ~86 Ma in tholeiitic sheeted dykes (Lanphere and Pamic, 1983). Together with the age of the unconformably overlying limestones of the Tarbur Formation, the ophiolites have therefore been emplaced between 86 Ma and 70 Ma (James and Wynd, 1965; Hallam, 1976; Ricou, 1976). Even though the oceanic origin for the Neyriz ophiolites has become the more popular model (Stocklin, 1974; Hallam, 1976; Haynes and Reynolds, 1980; Lanphere and Pamic, 1983), numerous geochemical studies linking the obducted ophiolites to Ca/K volcanic arc magmatism (e.g. Hassanabad unit) has also been proposed (Babaie et

al., 2001; Babaie et al., 2006). Other authors suggested that they were originated in a Red Sea-type rift in a shallow passive continental margin (Stoneley, 1981; Arvin, 1982) or have resulted from the emplacement of a forearc oceanic basement (Shafaii Moghadam et al., 2010).

II-2-c. The Sanandaj-Sirjan metamorphic belt or Sanandaj-Sirjan Zone (SSZ)

The Sanandaj-Sirjan Zone (SSZ), located to the north of the MZT, represents the tectono-magmatic and metamorphic part of the Zagros belt (Figs. III- 2, 3 and 4). It is made of sedimentary and metamorphic Paleozoic to Cretaceous rocks formed in the former active margin of an Iranian microcontinent drifted during the Late Jurassic (Berberian and Berberian, 1981; Golonka, 2004). But alternative interpretations consider it as the metamorphic core of a larger Zagros accretionary complex built by the thickening of distal crustal portions of the Arabian margin (Alavi, 2004; Shafaii Moghadam et al., 2010).

The Miocene emplacement of the MZT is revealed by the thrusting of the Cretaceous limestones onto Eocene and Miocene sediments south of Eghlid (Fig. III- 3). During the second half of Mesozoic times (Middle Jurassic-Lower Cretaceous), part of the SSZ was an active Andean-like margin characterized by calc-alkaline magmatic activity in which mainly andesitic and gabbroic intrusions were emplaced (Berberian and Berberian, 1981). The metamorphic part of the Sanandaj-Sirjan Zone can be subdivided into HP/LT and HT/LP metamorphic belts that developed at a transpressional plate boundary between Iran and Arabia (Sarkarinejad and Azizi, 2008). For instance, the Tutak Gneiss dome (Fig. III- 3) within the HP/LT belt is cored by gneiss and granite for which $^{40}Ar/^{39}Ar$ dating yielded ages of 180 Ma and 77 Ma (Sarkarinejad and Alizadeh, 2009). In the Cheh-Galatoun (Quri) metamorphic mélange (Fig. III- 4), few tens kilometers to the east of the Neyriz obducted complex, amphibolites, garnet-bearing amphibolites and some eclogites or kyanite schists are exposed (Sarkarinejad et al., 2009). $^{40}Ar/^{39}Ar$ dating of the Quri amphibolites yielded an age of ~91 Ma and 112-119 Ma in biotite gneiss (Fig. III- 4). This cooling event is related to burial and final exhumation of these rocks in an accretionary wedge during the Cretaceous. The good agreement between the cooling ages of the Neyriz Ophiolitic complex and SSZ suggest exhumation during the same tectonic episode. Although critical, the tectonic position of the HP metamorphic rocks with respect to the Neyriz ophiolites is still debated and it is still not clear whether the

metamorphic mélange of SSZ should be positioned in the upper Eurasian or the lower Arabian plate (Alavi, 2004; Agard et al., 2006; Shafaii Moghadam et al., 2010) mostly because of the obliteration of original structural relationships by subsequent deformation events. By contrast, the HT/LP belt to the north (Figs. III- 3 and 4) is presumably older and related to regional metamorphism related to magmatism (Sarkarinejad and Azizi, 2008). These latter metamorphic rocks are unconformably overlain by the Lower Cretaceous Orbitolina limestones (Figs. III- 3 and 4), typical of the Central Iran sedimentation (Stocklin, 1974). There are several evidences that magmatism resumed in the Paleocene-Eocene in the SSZ, for instance, when gabbroic intrusions (Gaveh-Rud pluton; see Leterrier, 1985) or granitic intrusions (Gaiduh granite) occurred (Rachidnejad-Omran et al., 2002).

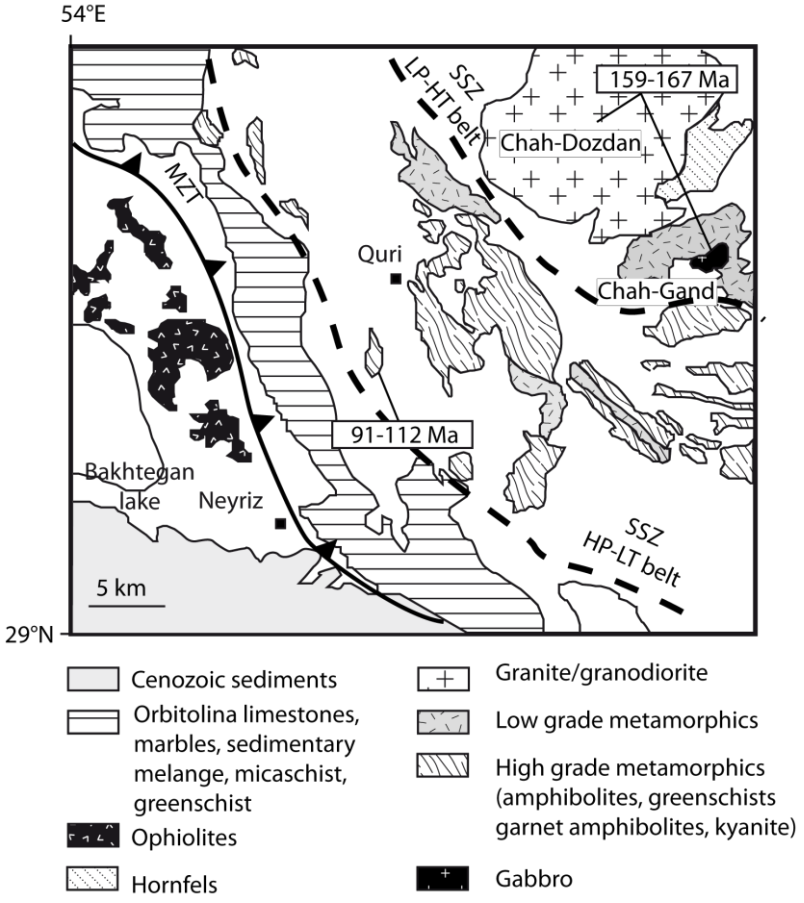

Figure III- 4: Morpho-tectonic evolution of the High Zagros since the Late Cretaceous that may explain the petrographic composition, detrital thermochronometric ages and clay assemblage observed in sandstones of the Miocene foreland of the Zagros (see text for explanations).

II-2-d. The Urumieh-Dokhtar Magmatic Arc (UDMA)

The Urumieh–Dokhtar magmatic assemblage (UDMA; Fig. III- 2) (Alavi, 2004) has been active from the Late Jurassic to the present (Berberian and King, 1981; Berberian et al., 1982). Extrusive volcanism began in the Eocene and continued for the rest of that period with a climax in Middle Eocene (Berberian and King, 1981). The UDMA is composed of voluminous tholeiitic, calc-alkaline, and K-rich alkaline magmatic rocks (with associated pyroclastic and volcanoclastic successions) along the active margin of the Iranian plate (Fig. III- 3). The oldest rocks in the UDMA are calc-alkaline magmatic rocks, which cut across Upper Jurassic formations and are overlain unconformably by Lower Cretaceous fossiliferous limestone. The youngest rocks in the UDMA consist of lava flows and pyroclastics that belong to Pliocene to Quaternary volcanic cones of alkaline and calc-alkaline nature (Berberian and Berberian, 1981). The Plio-Quaternary volcanism was suggested to result from the modification of geothermal gradients due to uplift (Berberian and King, 1981) that was further tentatively related to lithosphere delamination beneath the overthickened Iranian plateau (Hatzfeld and Molnar, 2010) and is supported to some extent by surface waveform tomography data (Maggi and Priestley, 2005).

II-3. Study area: main tectonic, morphologic and stratigraphic features

Our study focuses on well-dated synorogenic sediments outcropping in the northern ZFB in SW of Iran, in the Fars province, 20 km to the NW of Shiraz (Fig. III- 3). The region consists of a series of parallel NW-directed anticlines and synclines which are not associated with emergent reverse faults. The Derak anticline also called Qalat anticline in Mouthereau et al. (2007b) is one of the main structural features (Fig. III- 3) of this area showing a remarkable geomorphic expression with a local mountainous relief larger than 1 km. This particular geomorphological feature outlines the presence of the Eocene Jahrom Formation and Late Oligocene-Miocene Asmari limestones that are more resistant to weathering than surrounding siliciclastic deposits of interest to this study.

More regionally, the dated siliciclastic foreland deposits cropping out in the area of the Derak anticline are located ~100 km to the south of the Main Zagros Thrust and ~100 km to the west of the Neyriz ophiolitic complex (Fig. III- 3). This region is positioned near the NW corner of the Mand river (Rud-e-Mand) catchment (~78000 km^2) that is currently draining the HZ and the ZFB

(Fig. III- 5). In the studied area, the course of rivers is deflected to the southeast parallel to major anticlines indicating that the drainage system has been strongly controlled by fold growth. In the northern ZFB and HZ rivers are characterized by low channel gradients and are connected to intermontane depressions occupied by salt lakes and sabkhas.

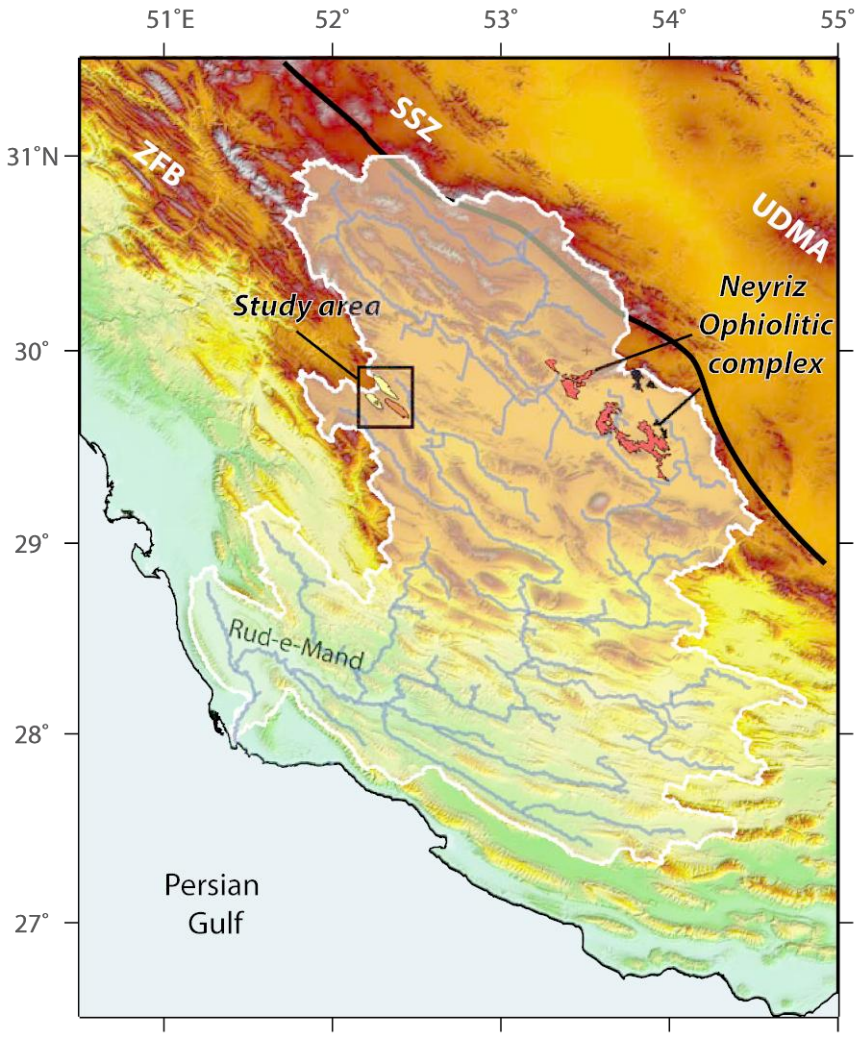

Figure III- 5: Topographic map of the Fars area (SRTM 90 m digital elevation data; http://srtm.csi.cgiar.org/) illustrating the spatial relationships between the boundaries of the Fars drainage basin, Rud-e-Mand river network and the location of the study area (Derak anticline; see Figure III- 6 for location). The current location of the Neyriz Ophiolitic Complex, which is the main outcropping tectono-metamorphic feature of the Fars catchment, is also displayed. It is apparent from the current river network that the ophiolitic units and the studied area are not connected to the same trunk stream. The main tectonic units including the metamorphic belt of the Sanandaj-Sirjan Zone (SSZ), the Urumieh-Dokhtar Magmatic Arc (UDMA), the Zagros Folded Belt and Main Zagros Thrust (MZT) are also shown.

The Derak anticline is flanked by the Chahar-Makan and Qalat synclines (Figs. III- 6, 7 and 8A). The Razak Formation, in the Chahar-Makan syncline, is made up with a 500 m-thick sequence of thin sandstones and yellow calcareous beds alternated with blue to red siltstones and clays and occasional gypsum beds interpreted as coastal sabkha deposits (Figs. III- 7 and 8 B).

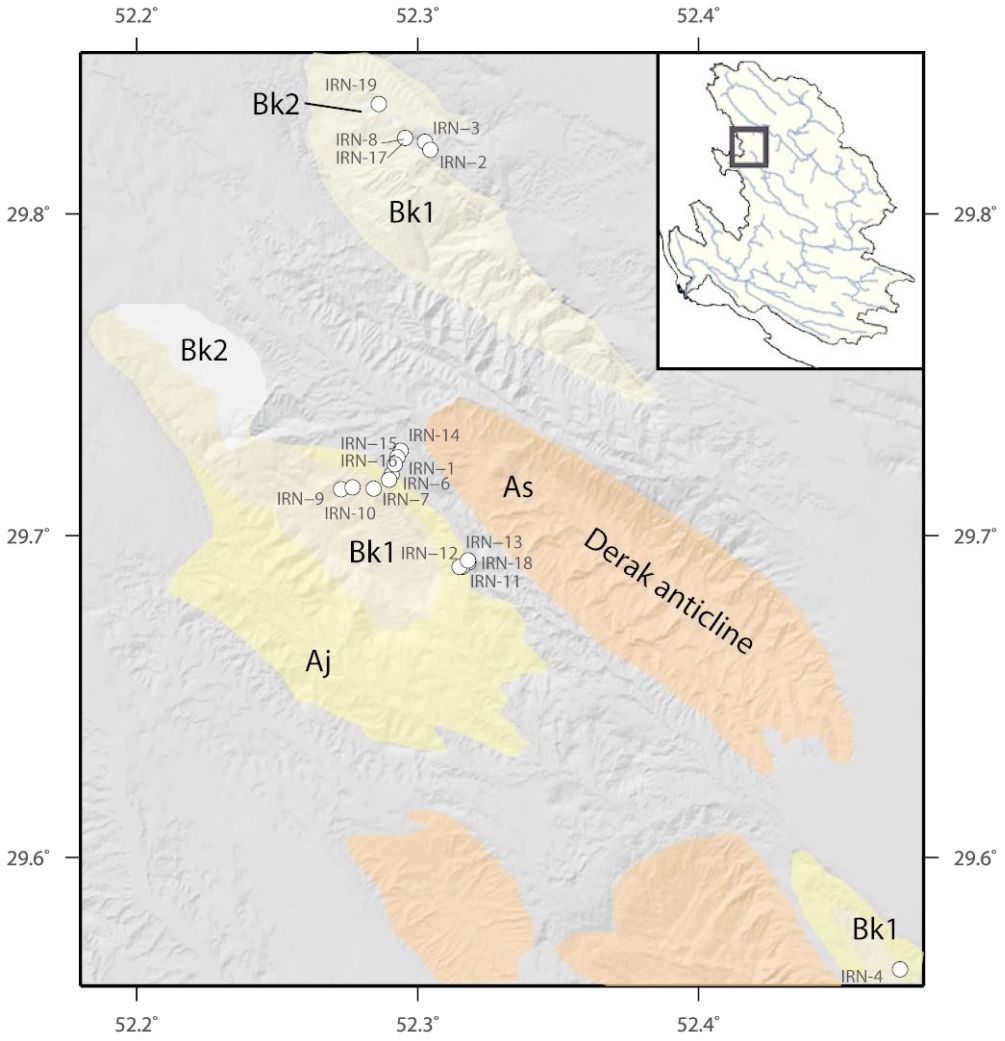

Figure III- 6: Location of sampled sandstones for fission-track dating superimposed on a 30 km digital elevation data digitalized from topographic maps of the northern Fars domain and a simplified geological map of the study area. Abbreviations are Agha Jari Formation (Aj); Bakhtyari 1 Formation (Bk1) and Bakhtyari 2 Formation (Bk2).

The Agha Jari Formation is only ~400 m thick that is remarkably thinner than in the more distal portion of the Zagros foreland where it reaches ~1600 m in the Changuleh and Zarrinabad synclines of the Lorestan area (Homke et al., 2004). In the Chahar-Makan syncline, the Agha Jari Formation is

composed of reddish sandstones and meter-scale conglomeratic sheets interbedded with thick (up to 20 m) intervals of red siltstones. Sandstone beds are often thicker than 2-3 m, and conglomerates include limestone cobbles of Paleogene and Cretaceous formations of up to 10 cm (Khadivi et al., 2010).

The Bakhtyari 1 Formation is represented by clast-supported, poorly-sorted, and well-rounded conglomerates (Fig. III- 8C). They are arranged as thick channel-like conglomeratic beds interbedded with trough cross-bedding in sandstones. Facies association suggests the predominance of subaqueous debris flows and migrating barforms. They likely correspond to an alluvial fan deposited in a fluvial-dominated deltaic environment. Clasts of the Bakhtyari 1 Formation are typically made up of radiolarian cherts (< 10 cm) and well-rounded pebbles of Mesozoic limestones and Nummulitic limestones of the Asmari-Jahrom Formation, with diameters up to 30 cm (Fig. III- 8 C). Currents markers show a more pronounced southward flow, oblique to the main structural patterns.

A magnetostratigraphic section of 1300 m performed in the Chahar-Makan syncline has allowed successful dating of the siliciclastic foreland deposits of the Razak, Agha Jari and Bakhtyari 1 Formations (Khadivi et al., 2010). This study showed that the transition in the Arabian margin from marine carbonaceous platform to prograding siliciclastic deposition of the Razak Fm occurred ca. 19.7 Ma. Erosional efflux from the growing orogen likely increased at 16.6 Ma with the deposition of the Agha Jari sandstones and at 14.8 Ma as evidenced by the age of the oldest conglomerates of the Bakhtyari 1 Formation (Bk1). The age of the youngest Bakhtyari 1 can be deduced by extrapolating the calculated accumulation rate upward to the base of the Bk2 conglomerates that unconformably overlie Bk1 Formation (Fig. III- 8). This yields a minimum age of 12.4 Ma for Bk1 conglomerates. Growth strata within the base of the Bakhtyari 1 Formation (Bk1) allowed dating the initial stage of folding in the ZFB to 14-15 Ma. However, the main phase of folding in the ZFB, which corresponds to the development of regional NW-trending train of folds, occurred later as shown by the post-folding unconformity of the Bakhtyari 2 conglomerates (Fig. III- 8 D).

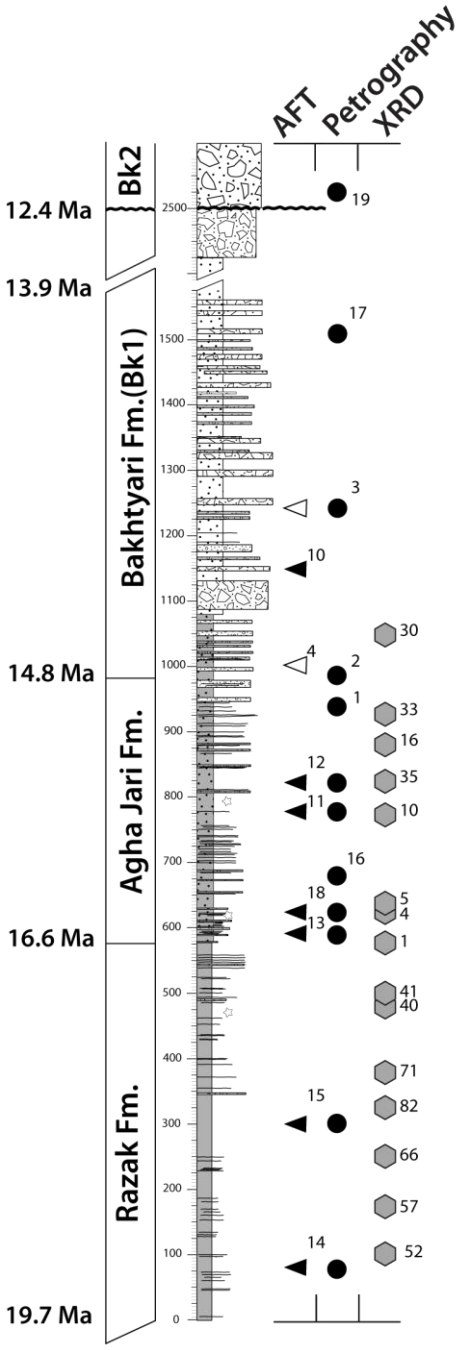

Figure III- 7: Synthetic stratigraphic log of the Chahar-Makan syncline modified from Khadivi et al. (2010). The position of studied samples for petrography and fission-track thermochronology (IRN samples mentioned in the text) and for clay analysis is also shown. Abbreviations are Agha Jari Formation (Aj), Bakhtyari 1 Formation (Bk1), Bakhtyari 2 Formation (Bk2) and Asmari Formation (As).

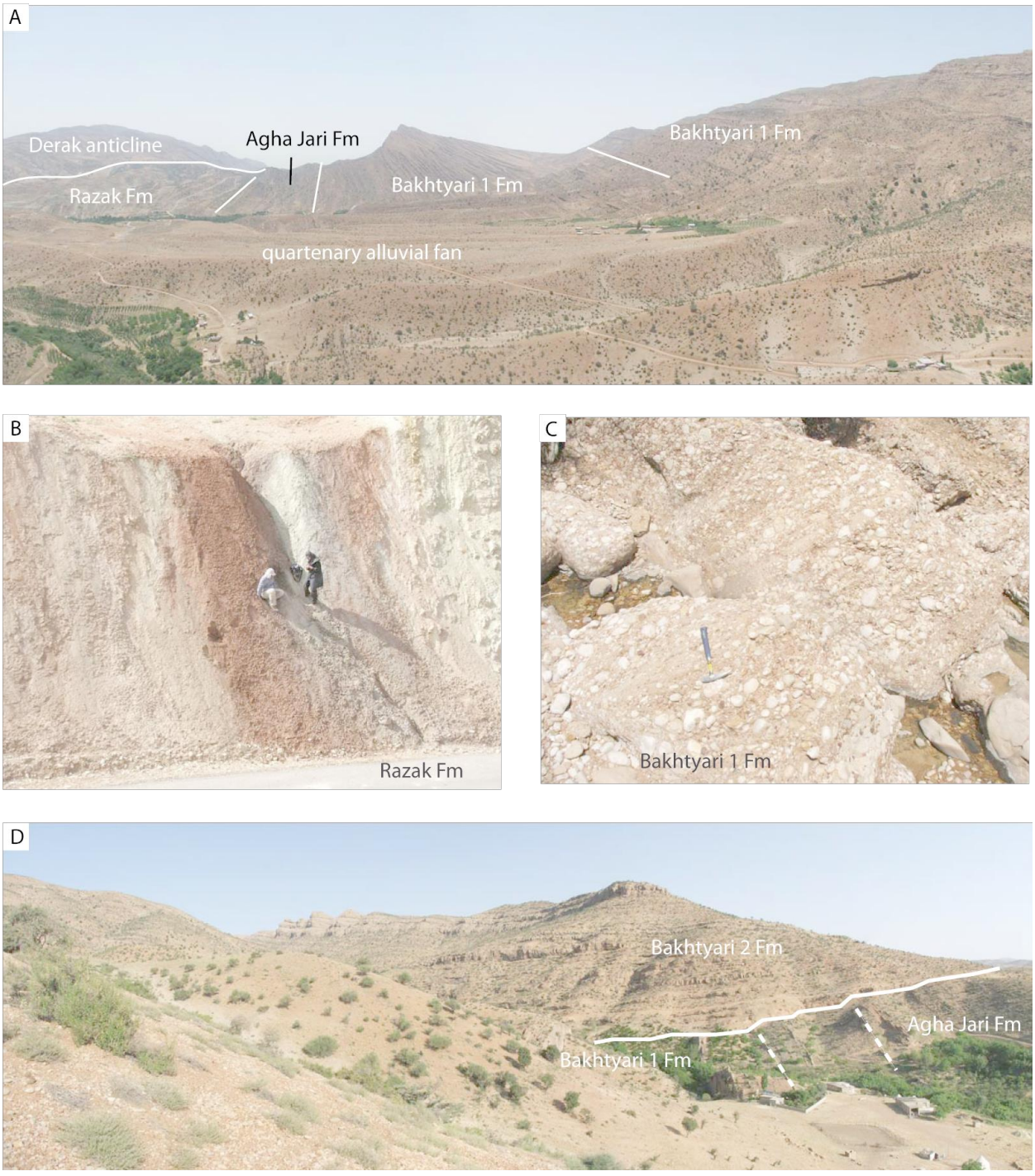

Figure III- 8: A) Field photograph of the Chahar-Makan section above the Derak anticline to the left (North); B) Sandstones and yellow calcareous beds alternated with red siltstones characteristic of sabkhas environment in the Razak Formation; C) Clast-supported, poorly-sorted, and well-rounded conglomerates of the Bakhtyari 1 Formation arranged as thick channel-like conglomeratic beds; D) Alluvial deposits of the Bk2 Formation overlying unconformably above the Bakhtyari 1 and Agha Jari Formations.

II-4. Bulk petrography, provenance and clay mineralogy of Miocene sediments

II-4-a. Sampling, experimental and analytical procedure

With the objective to better constrain the petrological nature and the unroofing history of exhumed source areas we have conducted the analysis of the bulk petrography and heavy minerals signatures of the well-dated Miocene foreland sediments. During field campaigns in 2007 and 2008, 12 sandstone samples (Fig. III- 7 and Table III-1) were collected along the Chahar-Makan sections in fine- to medium-grained sandstones from the Razak (2 samples), Agha Jari (7 samples) and Bakhtyari 1 (2 samples) Formations (Figs. III- 6 and 7) onto which FT dating have been also performed. Above the major unconformity between Bk1 and Bk2 one additional sandstone pebble was collected.

Thin sections were prepared from these 12 sandstones and examined under petrographic microscope. In each sample, a minimum of 300 points were randomly selected and counted following the Gazzi-Dickinson method (e.g. Ingersoll et al., 1984) per thin section. To recover the largest range of detrital grains composition, all samples were also analyzed by X-ray diffraction (XRD) and scanning electron microscopy (SEM). SEM images were obtained on unpolished carbon-coated thin sections analyzed under a SEM-Philips XL 30 (IDES, University Paris-Sud).

Bulk rock and clay mineral assemblages were analyzed by X-ray diffraction (ARL X'TRA Diffractometer) based on procedures described by Kübler (1983) and Adatte et al. (1996). The semi-quantification of whole-rock mineralogy is based on XRD patterns of random powder samples by using external standards with an error margin between 5 and 10% for the phyllosilicates and 5% for grain minerals.

Clay mineral analysis follows the methods developed by Kübler (1987) and Adatte et al. (1996). The intensities of the identified minerals are measured for a semi-quantitative estimate of the proportion of clay minerals, which is therefore given in relative percent without correction factors, because of the small error margin (<5%). When necessary, identification of palygorskite main reflections (8.4–8.9 2Θ) have been obtained by deconvolution using a Pearson type 7 function.

II-4-b. Detrital petrological composition of Miocene sediments

In the attempt to discriminate provenance of sandstones, typical parameters and ternary plots are produced, specifically as lithic grains are concerned, by a spectrum of key indices calculated by the Gazzi-Dickinson method (Fig. III- 7 and Table III-1).

As shown by the Qt-F-L ternary diagram (inset of Fig. III- 9), the petrological composition of the different stratigraphic levels (Razak, Agha Jari and Bakhtyari Fms) appears to be exclusively originated from the recycled lithics of an eroded arc-orogen system. In more details, the Qp-Lv-Ls plot allows to emphasize that, from bottom to top, the petrographic pattern of detrital materials was dominated by volcanic grains and sediment lithics, which proportions varying between 20% and ~70% (Fig. III- 9). Sediment lithics include nearly exclusively cherts and bioclasts (Fig. III- 10). As evidenced by scanning electron microscopy (SEM), volcanics include olivine, pyroxene and plagioclase. The association with accessory heavy minerals such as garnet, kyanite, rutile, chromite, titanite, ilmenite points to ultramafic source rocks (Fig. III- 10).

Sample	*Formation*	*Qt*	*F*	*L*	*Qp*	*Lvm*	*Lsm*	*Lv*	*Lc*	*Lch*	*Lm*
IRN 14	Razak	12.3	0	87.7	10.9	57.1	32.1	55.2	29.2	5.5	1.1
IRN 15	Razak	8.5	2.3	89.2	7.6	70.9	21.5	71.7	4.6	13.3	2.7
IRN 13	Agha Jari	4.6	0.2	95.2	4.6	45.6	49.8	45.6	16.2	32.8	0.8
IRN 18	Agha Jari	12.4	0.5	87.1	10	21.4	68.5	21.4	38.5	26.3	3.7
IRN 16	Agha Jari	5.8	0.5	93.7	5.9	53.3	40.8	53.3	2.7	37.2	1.0
IRN 11	Agha Jari	11.4	0.9	87.7	11.5	64	24.5	64.1	14.5	9	0.9
IRN 12	Agha Jari	5.4	0.2	94.4	5.2	44.2	50.6	44.2	19.6	30.8	0.2
IRN 1	Agha Jari	4.5	0	95.5	3.6	34.1	62.3	34.1	24.9	36.9	0.5
IRN 2	Agha Jari	2	0	98	2	40.5	57.5	40.5	13.4	43.3	0.8
IRN 3	BK1	5	0	95	4.7	60.4	34.9	60.4	17	17	0.8
IRN 17	Bk2	17.9	0	82.1	12.9	13.6	73.5	13.7	58.8	14.5	0.0
IRN 19	Bk2	10.9	0	89.1	9.5	20.1	70.4	31.6	54.3	5.5	0.3

Table III- 1: Detrital modes of the studied samples. Ten primary proportional parameters and secondary ratio parameters, representing an extension of those originally proposed by Dickinson (Dickinson;1970), provide a complete synthesis of framework composition: Q= quartz; F = feldspars; L= total aphanite lithics; Qp = fine- to coarse-grained polycrystalline quartz (excluding chert); Lvm= volcanic and volcanometamorphic lithic; Lsm= sedimentary and metamorphic lithic; Lv = volcanic lithics; Lc = carbonate lithics; Lch = chert lithics; Lm = metamorphic lithics.

Figure III- 9 also documents a change in the compositional characteristics of the detrital materials with time. At the base of the foreland series of the Razak Fm, the volcanic lithics component is dominant but the proportion of sediment lithics is increasing progressively upwards.

The X-ray diffraction bulk rock composition (Fig. III- 11) obtained from 15 shaly and silty intervals (Fig. III- 7) exhibit three main components: calcite (~40 %), phyllosilicate (> 20%) and quartz (including chert) (~20%). Dolomite (10%) and ankerite (Fe-rich dolomite) (10%) are also important components with minor feldspar (plagioclase and K-feldspar). Together with the presence of serpentines as well as dolomite and ankerite, the bulk rock composition points to the alteration of rocks with high Fe-Mg content that support sediments derived from ultramafic rocks. This result is in line with the above petrographic analysis. On the basis of this initial petrological study it appears that the contribution of the SSZ as the original source of sediments was negligible, otherwise metamorphic fragments, plagioclase and K-feldspar as well as quartz would have been much more abundant. By contrast, the noticeably important contribution of recycled sediments (bioclasts and cherts) and volcanics with a remarkable amount of ultramafic grains points to the HZ and the ophiolitic complex of Sahneh-Neyriz as the main potential source rocks.

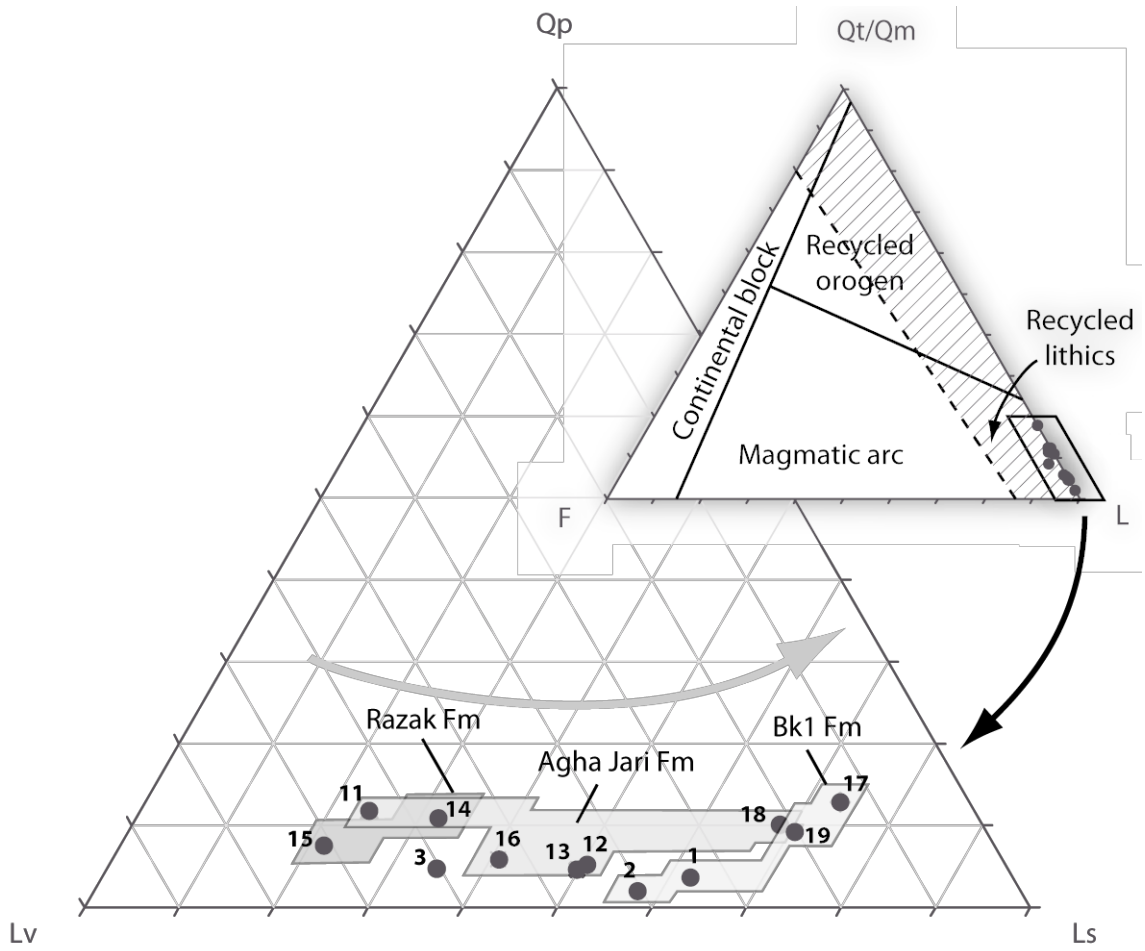

Figure III- 9: Petrographic modes shown in Qt-F-L and Qp-Lv-Ls ternary diagrams for sandstones collected along the Chahar-Makan section (see Figure 6 for stratigraphic location). Qt-F-L diagram shows that all samples belong to recycled lithics from a mixed orogen and magmatic source. Qp-Lv-Ls plot reveals a trend in the type of deposited clasts over time with an increasing amount of sediment lithic fragment upsection.

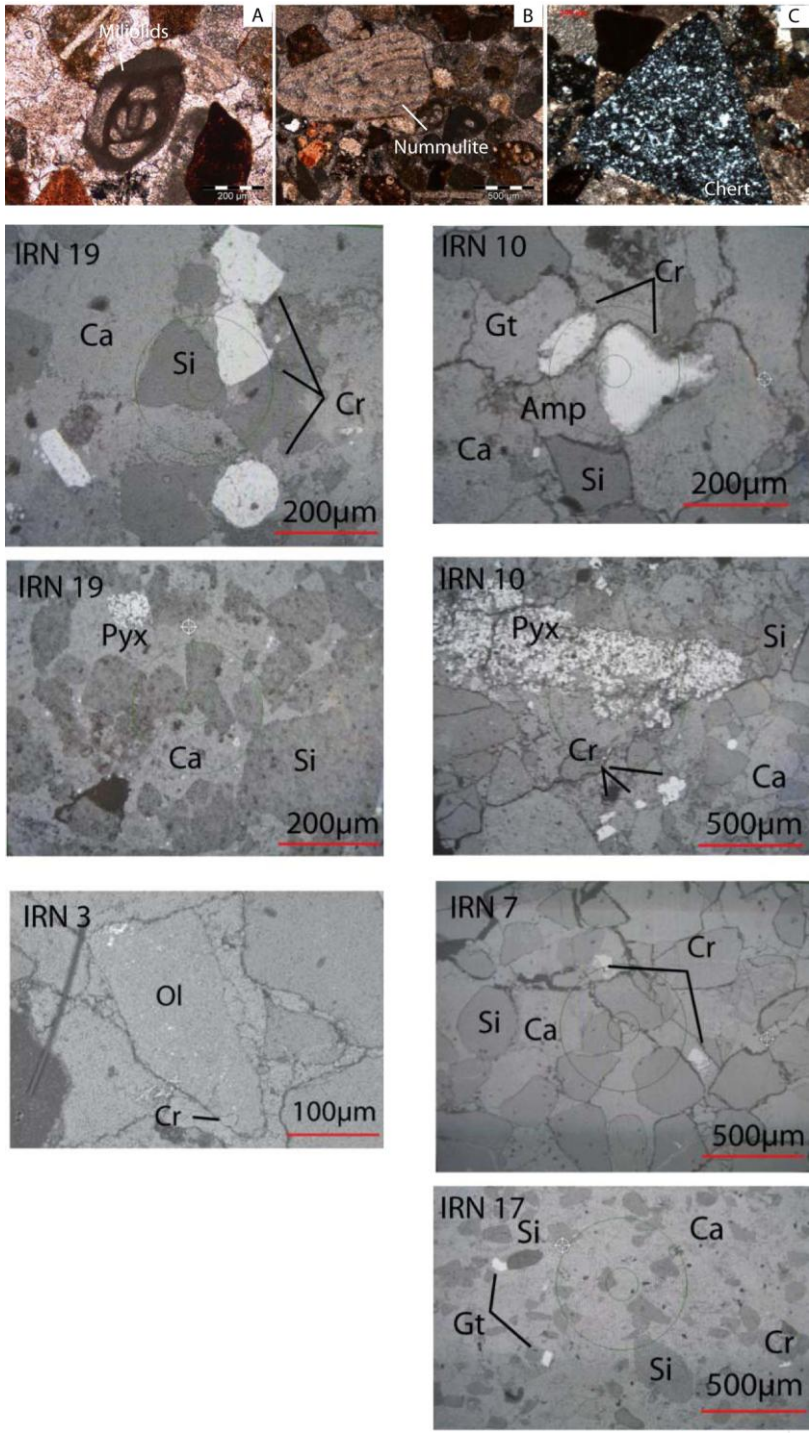

Figure III- 10: Thin-sections and SEM micrograph of sandstone samples. Thin-sections show the main lithic fragments present in our samples. They include miliolids (A), nummulite bioclasts (B) and polycristalline (chert) clast (C). SEM micrographs allowed us to identify Chromite (Cr), Garnet (Gt), Amphibole (Amp), Pyroxene (Pyx), Calcite (Ca) and Chert (Si) in samples IRN10 and IRN19 as well as Olivine (Ol) in sample IRN3.

II-4-c. Bulk rock compositions and clay mineral assemblages

Clay minerals are byproducts resulting from the interplay between climate, continental morphology, tectonic activity and sea-level variations, and therefore can be used as environmental proxies (Chamley, 1989; Weaver, 1989). Among the major clay minerals encountered in sedimentary records are kaolinite, smectite, chlorite and illite. In equatorial zones, kaolinite forms in soil under constant humid conditions as a result of high chemical weathering. Smectite originates either from tropical soil under semi-arid and seasonal climate conditions or as weathering byproduct of basalt (Chamley, 1989; Chamley et al., 1990; Deconinck and Chamley, 1995). Chlorite-Smectite mixed layers (CS) is a weathering product of Mg enriched rocks such as basalt or serpentinites but forms under more temperate and humid conditions than smectite (Chamley, 1989). Illite and chlorite are byproducts of tectonic uplift and physical weathering (Chamley, 1989; Robert and Chamley, 1990).

The clay fraction is composed of palygorskite, smectite, chlorite and irregular to regular (Corrensite type) mixed-layer chlorite-smectite and micas (Fig. III- 12).

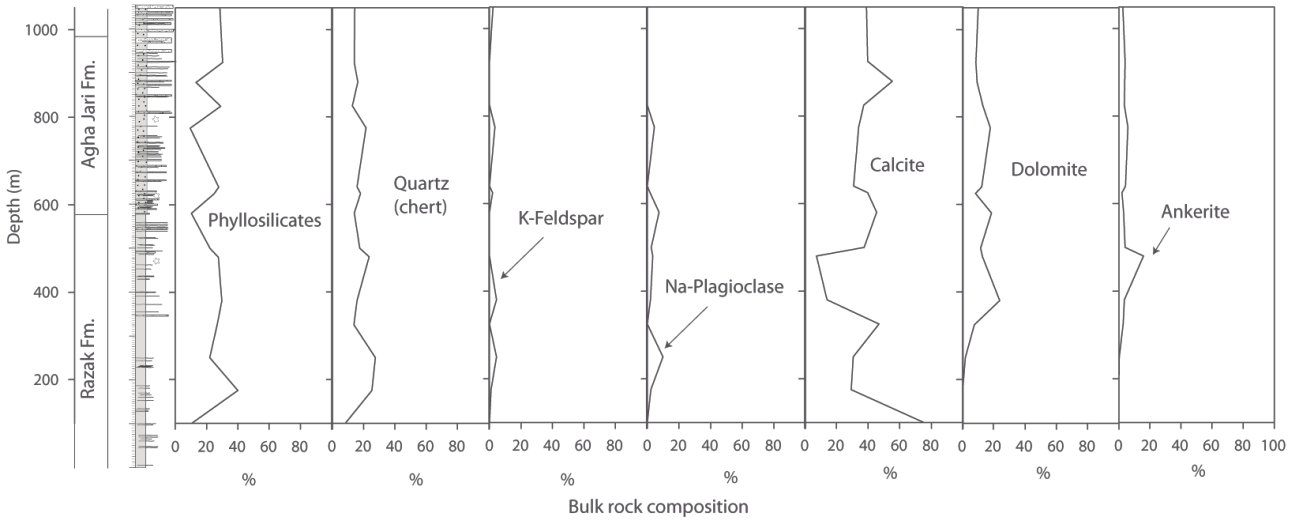

Figure III- 11: X-ray diffraction bulk rock composition along the Chahar-Makan section (see location of sample on Fig. III- 6).

The kaolinite is nearly absent from the clay assemblage. The stratigraphic column can be separated in two parts:

(1) The lower part (0-400 m, upper part of the Razak Fm) is characterized by the lack of palygorskite and the noticeable abundance of smectite, chlorite, mixed-layer chlorite-smectite and especially micas, episodically representing more than 60% of the clay fraction.

(2) The upper levels that that are represented by Agha Jari and Bakhtyari 1 Fm are dominated by palygorskite, mixed-layer chlorite-smectite, chlorite and smectite to the detriment of mica.

This change in clay composition coincides with the appearance of dolomite and ankerite, Mg and Fe (at lesser extent) enriched minerals. The data therefore suggests that from 18.5 Ma onwards, the alteration and erosion involved Fe-Mg rich rock type. Furthermore, the presence of palygorskite and the absence of kaolinite reveal alteration of carbonaceous soils and sabkhas under arid climate condition.

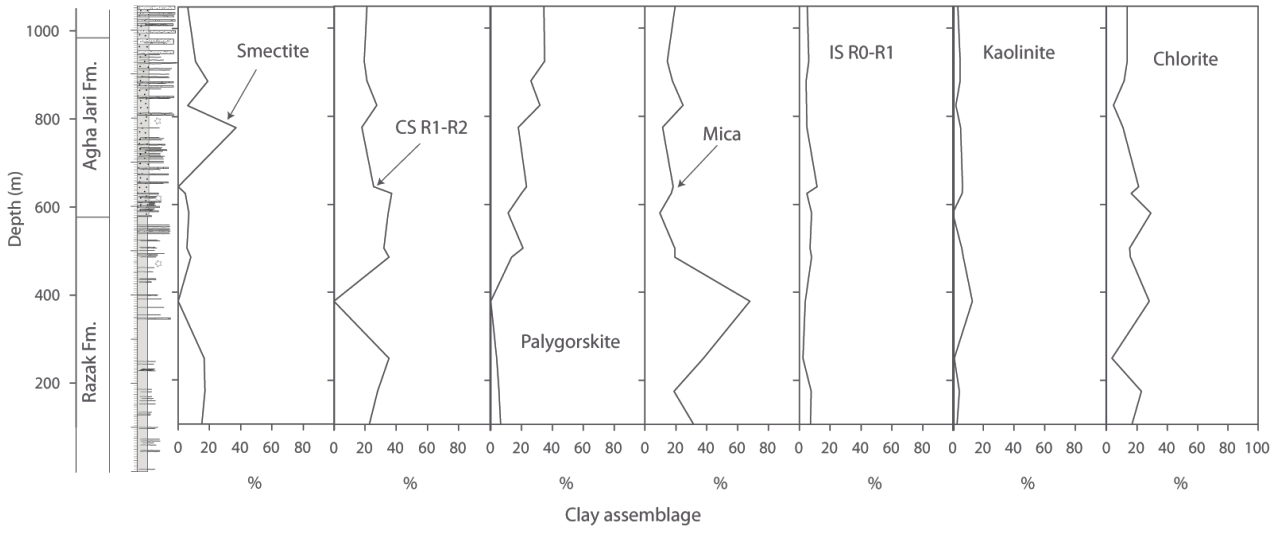

Figure III- 12: X-ray diffraction clay mineral assemblages along the Chahar-Makan section (see location of sample on Fig. III- 6).

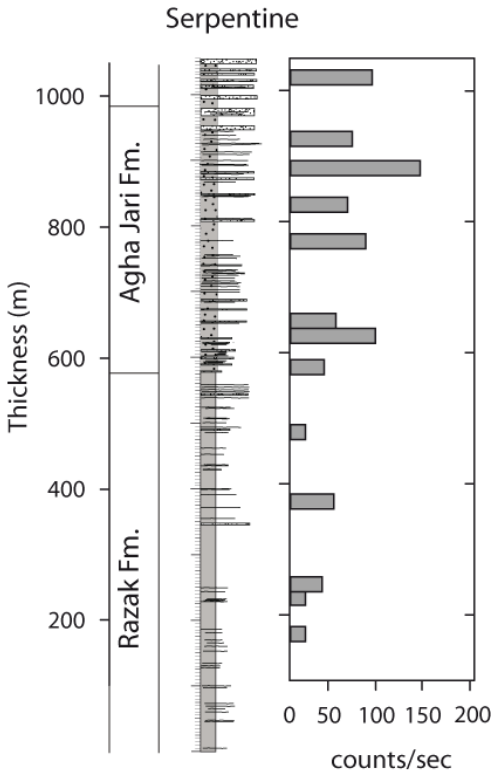

Figure III- 13: X-ray diffraction Serpentine along the Chahar-Makan section indicate erosion from the Neyriz ophiolites (see location of sample on Fig. III- 6).

II-5. Detrital apatite fission-track thermochronology

Nine samples were collected for apatite fission-track analysis along the ~1600 m well-dated section of the Chahar-Makan syncline within the Razak Fm, Agha Jari Fm and Bakhtyari 1 Fm deposited in northern Zagros foreland, NW of Shiraz (Fig. III- 7 and Table III- 2).

Sample	Formation	Approx. Depositional age (Ma)	Depth (m)	Nb. of grains	ρs (Ns) x $10^6 cm^{-2}$	ρi (Ni) x $10^6 cm^{-2}$	ρd (Nd) x $10^5 cm^{-2}$	P (χ^2) (%)	Disp. (%)	Central Age +2σ (Ma)	Nb. of Dpar	Mean Dpar (μm)	SD (μm)
IRN3*	Bk1	14.2	-	8	0.16(71)	0.90(94)	5.141	6.17	47	77±20	39	2.02	0.47
IRN10	Bk1	14.3	1150	7	0.56(127)	0.39(225)	6.238	34.9	23.9	44±11	45	1.59	0.23
IRN4*	Bk1	14	-	3	0.18(9)	0.24(12)	5.141	27.7	-	64±29	13	1.9	0.27
IRN12	Agha Jari	15.5	840	5	0.09(29)	0.25(53)	6.371	65.8	0.3	39±12	-	1.44	0.25
IRN11	Agha Jari	16	790	7	0.22(29)	0.34(46)	6.295	89.5	0.1	66±16	39	1.88	0.86
IRN13	Agha Jari	16.4	620	7	0.55(31)	0.44(70)	6.314	63.9	0.2	46±10	40	1.82	0.36
IRN18	Agha Jari	16.5	600	11	0.48922)	0.68(60)	6.276	6.84	31.7	73±11	54	1.78	0.51
IRN15	Razak	18	300	9	0.24(30)	1.02(126)	6.352	85.7	0.3	25±5	22	1.03	0.15
IRN14	Razak	19.3	80	6	0.54(58)	2.31(156)	6.333	39.9	0.3	25±5	20	1.14	0.19

Table III- 2: Apatite Fission track analytical data. ρs and Ns, density and number of spontaneous fission tracks, respectively. ρi and Ni, density and number of induced fission tracks. ρd and Nd, density and number of measured in fluence dosimeter. ζ calibration factor has been determined by using the following age standards; Durango (31.4 ± 0.8 Ma), Fish Canyon Tuff (27.9 ± 0.7 Ma) and CN5 with 12.19 ppm U. P (χ^2),chi- squared probability that grain ages are concordant. Disp., age dispersion. A sample may contains multiple age populations if P (χ^2) <5 and/or Disp >15 (Galbraith and Green, 1990; Galbraith and Laslett, 1993). SD, standard deviation of mean confined track length and mean D_{par} (μm).

II-5-a. Experimental and analytical procedure

Sample investigation including, mineral separation, counting and analysis were performed in the IDES laboratory (University Paris-Sud). Apatite grains were separated from crushed rocks using classical sieving, density and magnetic separation techniques.

Apatite samples were mounted in epoxy resin and then polished to expose an internal 4π surface. Apatite samples were etched in 5% HNO_3 for 20 seconds at 20±1°C to reveal spontaneous tracks. Apatite samples have been in several irradiations carried out at the Orphée reactor (CEA-Saclay, France) and at the Forschungsneutronenquelle Heinz Maier-Leibnitz (FRM II) research reactor at Garching, (Germany). Thermal neutron fluence was monitored using Corning CN-5 glasses and is equivalent in both irradiation conditions and is 5.1015 neutrons/cm^2. Apatite grains were dated using the external detector method (Gleadow, 1981) with muscovite sheets as external detector. Muscovite detectors were etched after irradiation in a 48% HF solution for 20 minutes at 21±1°C. Spontaneous and induced FTs were counted on an optical Leica DM LM microscope. Central ages (Galbraith and Laslett, 1993) have been calculated with the zeta calibration method (Hurford and Green, 1983) by using the age standards of Durango (31.3±0.3 Ma, Naeser & Fleischer, 1975) and Fish Canyon Tuff (27.8±0.2 Ma, Hurford & Hammerschmidt, 1985).

For each dated apatite crystal, etch-pit length parallel to c-axis (D_{par}) was measured under a 1000X dry objective as they provide good assessment of annealing rate in individual apatite grains (Barbarand et al., 2003). Grain-age distributions were decomposed following the binomial peak-fitting method (Galbraith and Green, 1990) incorporated in the Binomfit software (Brandon, 2002). The best-fit solution is determined by directly comparing the distribution of the grain data to a predicted mixed binomial distribution. Peak-fitting analysis for detrital samples with a low number of dated crystals may provide unreliable results. In order to obtain more information about cooling ages, combined grain-age distributions of several detrital samples from the Razak, Agha Jari and Bakhtyari 1 Formations have been analyzed, assuming that these samples did not record different degrees of partial annealing.

II-5-b. AFT Results

Our samples yielded few apatite crystals. No confined FT lengths could be measured in the nine dated samples. We present, hereafter, the AFT results from the different studied sampled formations as three combined grain-age distributions. Combined probability density plot are only shown (Fig. III- 14).

Razak Formation

As seen in the previous section, sandstones from Razak Fm contain clasts of red radiolarian cherts and ultramafic rocks that were likely derived from the Neyriz ophiolitic complex. Two samples IRN 14 and 15 from Razak Fm sandstone layers located at levels 80 m and 300 m of the Chahar-Makan section (Fig. III- 7) yielded 15 datable apatite grains (Table III- 2, Fig. III- 14). Six and nine apatite fission-track ages in sample IRN 14 and 15, respectively, provided consistent central ages of 25±5 Ma, with similar low dispersion (0.3%) and relatively high χ^2 probability (40% and 85%, respectively) indicating that both samples contain single grain-age populations. A mean low D_{par} value of ~1 μm in both samples argues for a similar chemical composition of apatite crystals. This is consistent with a unique sediment source rock. The decomposition of combined grain-age distribution confirms a single AFT grain-age population of 27±4 Ma for the Razak Formation (Fig. III- 14).

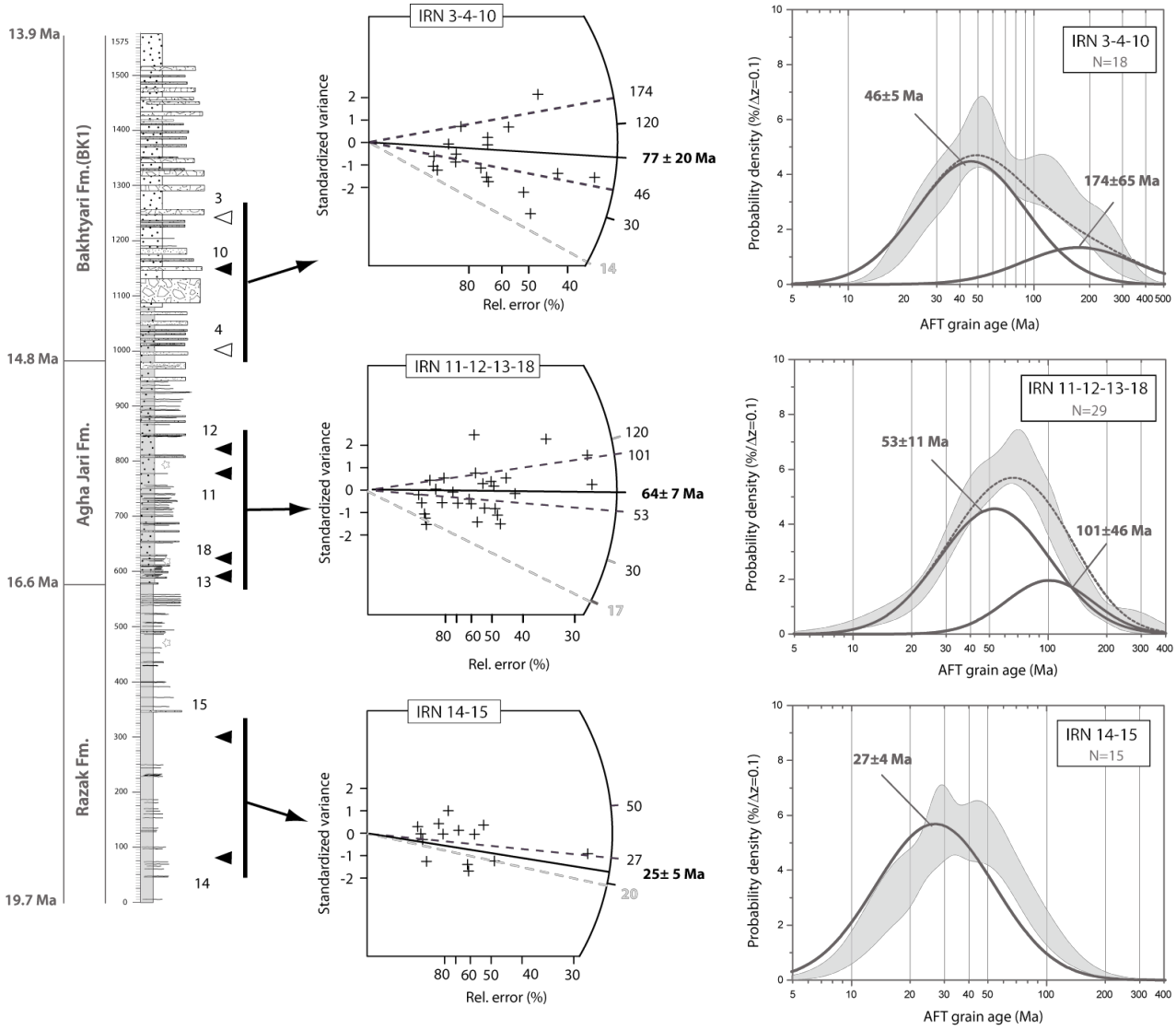

Figure III- 14: Synthetic stratigraphic section studied along the Chahar-Makan syncline. Ages of the formations are based on Khadivi et al. (2010). Collected apatite fission-track samples are located in the section by black triangles. Radial plots with central ages in bold and grain-age probability-density plot with binomial fitted peaks of the three combined apatite populations are shown. The white triangles sample positions are shown the reflected position in studied section.

Agha Jari Formation

Samples IRN 11, 12, 13 and 18 were collected in the Agha Jari Formation between levels 600 and 840 m (Fig. III- 7) and yielded a total of 29 datable grains. From each sample, measured apatite crystals provided unique central ages of 73±11 Ma, 46±10 Ma, 66±16 and 39±12 Ma from bottom to top, with rather low (0.3%, e.g. sample IRN12) dispersion and relatively high χ^2 probability 65%

(IRN 12) that again suggest single-grain age population, expect for sample IRN 18 which has a lower dispersion of 31% and higher χ^2 probability of 6.8. Slightly larger mean D_{par} comprised between 1.4 and 1.8 μm with respect to the underlying Razak Fm may suggest the contribution of different source rocks. Because of the low number of dated apatites (between 5 and 11 grains), these grain-age populations are not well constrained and additional less important grain-age populations may have not been recovered. The decomposition of combined grain-age distribution (29 grains) was therefore performed in order to obtain better resolution on dominant grain-age populations. One dominant population with peak age of 53±11 Ma and another minor population with peak age of 101±46 Ma were obtained. The significance of the older population can be questioned because of the large uncertainty.

Bakhtyari 1 Formation

Samples IRN 4 and IRN 10 were collected near the top of the Chahar-Makan magnetostratigraphic section at ~1150 m (Fig. III- 7) and correspond to sandstones found in the Bakhtyari 1 Fm. Sample IRN 3 was collected in the Qalat syncline. Its position in the Qalat section allows for correlation with the Bakhtyari 1 Fm of the Chahar-Makan section situated ~ 5 km to the south (Fig. III- 6). In each sample low-to-moderate χ^2 probability of 6%, 27% and 35% (IRN 3, 4, 10, respectively) and large age dispersion between 23% and 47% reveal the presence of mixed grain-age populations. However, due to the low number of dated apatites we did not examine the distribution of grain-age populations. Instead, we used the decomposition of combined grain-age distribution (18 grains) in order to identify dominant grain-age populations. One dominant population with peak age of 46±5 Ma and another minor population with peak age of 174±65 Ma were obtained. These results shows strong similarities with the same Eocene and Mesozoic AFT ages obtained in the younger Agha Jari Formation and thus suggest that source rocks shared the same cooling history.

II-6. Constraints on paleogeothermal gradient and Miocene PAZ

The extrapolated total thickness of the Chahar-Makan section below Bk2 erosional surface indicates that the base of the Razak Formation was originally buried to a depth of ~2.5 km

(Fig. III- 7). Taking into account geothermal gradients predicted from recent thermochronometric studies (Gavillot et al., 2010; Homke et al., 2010) and results of tectonic modeling (Mouthereau et al., 2006), a geothermal gradient for the region can be estimated to be in the range 15-24°C/km. Depending on the surface temperature assumed 0°C or 20°C, the maximum averaged temperature recorded by samples IRN 14 and 15 of the Razak Formation is lower than ~59°C. We hence infer that the base of the studied section has not resided in the PAZ for apatites and hence presents the true record of a hinterland exhumation episode at ~27 Ma. The subsequent foreland sedimentation was not sufficiently thick to partially reset these sediments before they were rapidly exhumed by folding and regional uplift sometime after 12.4 Ma. The upper levels comprising the Agha Jari and Bakhtyari 1 Formations were therefore not partially reset during the Miocene and hence AFT grain-age populations can potentially be interpreted as true cooling ages. The distinctive dominant Eocene and Mesozoic AFT ages, above level 400 m, suggests a change in the exhumed source areas. The larger D_{par} values of 1.6-2 μm measured in Agha Jari and Bakhtyari 1 Formations together with the analysis of bulk rock composition and clay mineralogy indicating the occurrence of more Fe-Mg rich clay assemblages effectively advocate such a change in the eroding landscape. On the basis on the good correlation between these independent results we propose that a change in the origin of detrital materials effectively occurred after 18.5 Ma.

II-7. Origin tectonics and detrital AFT ages

The analysis of above AFT results and petrological study must account for the following evidences. Three AFT grain-age populations have been recovered from detrital samples of the Razak, Agha Jari and Bakhtyari Formations: 1) Jurassic to Early Mesozoic (174-101 Ma), 2) Early Eocene (53-46 Ma) and 3) Late Oligocene-Early Miocene (~27 Ma). It must also take into consideration the petrological nature of the Miocene foreland basin which was mainly fed, if not exclusively, by the obducted ophiolitic complex and the Meso-Cenozoic sediments currently exposed in the High Zagros and the SSZ.

II-7-a. Jurassic to Early Mesozoic ages: mixed SSZ and HZ exhumed source areas?

The oldest AFT grain-age populations of 174±65 Ma and 101±46 Ma reported in the Agha Jari and Bakhtyari 1 Formations are not well represented in our samples with less than 20 dated apatite crystals and are thus difficult to interpret. However, these ages are consistent with the regional Mesozoic metamorphism and arc magmatism documented, north of the suture zone, in the SSZ (Figs. III- 3 and 4). This tectonic-thermal event is related to the protracted Neo-Tethyan subduction that started in the Trias in the Zagros region (e.g. Berberian and Berberian, 1981). It has been well documented that regional metamorphism was accompanied by coeval Jurassic-Cretaceous andesitic intrusions and gabbroic/granitic plutons with K/Ar ages on muscovite of 118 Ma (Tc= 300-400°C) and 164 Ma on biotite (Tc~300°C) in the southern SSZ, southwest of Shahr-e-Babak ophiolitic complex (Berberian and Berberian, 1981). This Jurassic metamorphic event is consistent with $^{40}Ar/^{39}Ar$ hornblende age of ~170 Ma obtained from Markran amphibolite in southern SSZ (Haynes and Reynolds, 1980) and $^{40}K/^{40}Ar$ age of ~170 Ma in amphibolitic foliations in the Muteh metamorphic complex of the Golpaygan region to the NW of SSZ (Rachidnejad-Omran et al., 2002) and hence suggests a widespread regional tectonic event in the overriding accretionary wedge in relation with the subduction of the Neo-Tethyan ocean. Closer to the studied area, the emplacement of the Chah-Dozdan granodiorite and Chah-Ghand gabbro of the Sanandaj-Sirjan magmatic arc currently thrusted onto the Neyriz ophiolitic complex can be dated to the middle Jurassic (159 –167 Ma) according to $^{40}K/^{40}Ar$ radiometric dating (Sheikholeslami et al., 2008). Occurrence of metamorphic pebbles within the Late Jurassic clastic sediments south of the Chah-Dozdan granodiorite further indicate erosion of the Jurassic accretionary prism (Sheikholeslami et al., 2008). This orogenic episode is sealed by the deposition of Berriasian-Valanginian Orbitolina limestone (Ricou, 1976; Berberian and King, 1981).

The origin of younger 101 Ma grain-age population is more controversial. As synthesized by Berberian and Berberian (1981) many late Cretaceous intrusive bodies can be found in the NW of the SSZ (e.g Alvand, Borudjerd, Arak and Malayer plutons) (Ghasemi and Talbot, 2006). The Neyriz ophiolitic complex, in the High Zagros, nearby our study area could have also been a major source for apatite grains with Mesozoic cooling ages. For instance, $^{40}Ar/^{39}Ar$ age of 98 Ma from biotite (Tc~300°C) and 96 Ma from muscovite (Tc= 300-400°C) recovered from an olistolithe of

metamorphic rock (upper greenschist facies) in radiolaritic sequence of the Neyriz tectonic mélange suggest that metamorphism and denudation occurred in the Late Cretaceous (Haynes and Reynolds, 1980). The source of the olistolithe is revealed by consistent, although slightly older $^{40}Ar/^{39}Ar$ age of 89 Ma from biotite schist of garnet-bearing amphibolites (HP metamorphism) found in the metamorphosed basic and ultrabasic rocks in the region of Quri city southwest of Chah-Dozdan granodiorite in SSZ (Fig. III- 4), few kilometers northeast of the Neyriz ophiolitic complex (Haynes and Reynolds, 1980). $^{40}Ar/^{39}Ar$ dating on hornblende (Tc ~450°C) in plagiogranite and diabase of the Neyriz Ophiolitic complex yielded a cooling age of 92-93 Ma (Babaie et al., 2006) consistent with $^{40}Ar/^{39}Ar$ ages of ~95 Ma obtained from the amphibolites and ages of tholeiitic sheeted dykes of ~86 Ma (Lanphere and Pamic, 1983). Similar $^{40}K/^{40}Ar$ ages were obtained from the Sahneh ophiolites near Kermanshah (Delaloye and Desmons, 1980). Age constraints on the late stage of obduction of the ophiolitic complex is provided by the depositional age of Tarbur limestones dated to late Campanian-Maastrichtian (~70 Ma) overlying unconformably the ophiolites (James and Wynd, 1965; Ricou, 1976). The obtained Mezosoic AFT ages are basically consistent with cooling ages related to development of a Jurassic-Cretaceous accretionary wedge and arc magmatism in the northern SSZ and Central Iran and with the subsequent Late Cretaceous stage of accretion, exhumation of HP rocks and obduction of ophiolites to the south of the Sanandaj-Sirjan belt.

II-7-b. Early-Middle Eocene cooling/denudational event : magmatic and/or exhumational event ?

A better resolved cooling episode is indicated by grain-age populations of 53 Ma and 46 Ma reported in both the Agha Jari and Bakhtyari 1 formations. Following the obduction in the upper Cretaceous in the High Zagros (e.g. Neyriz area) and magmatism in the Sanandaj-Sirjan belt during the Mesozoic, calc-alkaline arc magmatism resumed in the Eocene and then shifted northwards to the Urumieh-Dokhtar Arc and the Alborz mountains (Berberian and Berberian, 1981; Berberian and King, 1981). The tectonic setting of this Eocene volcanic event is still debated but they are increasing evidence it has been related to post-Cretaceous extensional event associated with possible development of metamorphic-core complexes on the Iranian plate (Verdel et al., 2007). Such an extension is basically consistent with back-arc extension proposed ca. 40 Ma to explain both Eocene

magmatism and rapid subsidence in the Talysh mountains of the South Caspian basin (Vincent et al., 2005).

The age of plutonism is well constrained, for instance, by recent U/Pb age of ~46 Ma recovered from detrital zircons collected in Miocene deposits in southern Alborz and southern Urumieh-Dokhtar belt (Horton et al., 2008). However, it is unlikely that the dated detrital apatites from the Chahar-Makan section (Fig. 14) were derived from the Urumieh-Dokhtar arc since this domain was separated from the Zagros foreland by the remnant of the Neo-Tethyan ocean and a topographic ridge formed by the Sahneh-Neyriz Ophiolitic complex emplaced during the Late Cretaceous.

Other evidence of Eocene heating in the northern SSZ is provided by $^{40}Ar/^{39}Ar$ muscovite ages of 55 and 38 Ma reported from gold mineralization at Muteh in the Golpaygan region (Moritz et al., 2006) and from $^{40}Ar/^{39}Ar$ biotite age of ~58 Ma of Gaiduh granite in the same area (Rachidnejad-Omran et al., 2002). Closer of the region of interest, Eocene mafic intrusions like the Gaveh Rud gabbroic intrusion at approximately 40-38 Ma (e.g. Leterrier, 1985), in the SSZ north of the Sahneh Ophiolitic complex, is consistent with Eocene metamorphism reported from diabasic dykes in the Sahneh ophiolites (Delaloye and Desmons, 1980).

In the Zagros basin, the Paleocene-Eocene ~56 Ma was time of deposition of a thin sequence of non-marine conglomerates (Kashkan Formation) made with radiolarian cherts that recorded the erosion of radiolarite units of the Sahneh ophiolitic complex (James and Wynd, 1965; Homke et al., 2009). In the Fars area, this period is characterized by the deposition of evaporites and dolomites interbedded with red shales and sandstones of the Sachun Formation (Alavi, 2004).

To the NW of the Zagros foreland of the Lorestan area, a subsequent erosional or non-depositional event between the Kashkan conglomerates and the Shahbazan limestones at 45-35 Ma is documented (Homke et al., 2009). In the Fars area, the transition from Sachun Formation (Paleocene-Eocene) to Jahrom dolomites (Late Eocene) at approximately the same time also documents an acceleration of the subsidence but appears more gradational (Motiei, 1993). The renewed subsidence more generally agrees with regional occurrence of Eocene turbiditic basins in the northern Zagros (Hempton, 1987; Beydoun et al., 1992). This Middle-Late Eocene episode fits well with our AFT detrital grain-age populations (Fig. III- 14) and complement former AFT central ages of 39-45 Ma reported from pebble of granites and gneisses of the Dorud area of NW Zagros derived from the Sanandaj-Sirjan belt (Homke et al., 2010). The denudation/cooling event in the inner Zagros coincides well with the timing of emplacement of large magmatic bodies and back-arc

extension on the Iranian plate. This event occurs slightly before the initiation of the collision ca. 35 Ma.

II-7-c. Late Oligocene-Early Miocene exhumational event : the Zagros collision

The Late Oligocene-Early Miocene cooling event at 27 Ma has been reported from the base of the Chahar-Makan section (Razak Fm). This cooling event is coincident with major geological observations indicating that uplift, erosion and contraction in the Zagros was underway, and that final suturing, occurred at the same time, i.e. in the early Miocene (e.g., Agard et al, 2005; Mouthereau et al, 2007b). Initiation of the collision was coincident with the reduction of Africa-Eurasia plate convergence and Red Sea opening at 25 Ma (McQuarrie et al., 2003). More recent AFT ages of 22 Ma (Homke et al., 2010) found in the NW Zagros are consistent with detrital zircon and apatite ages revealing rapid cooling and sedimentation since 19 Ma in the High Zagros (Gavillot et al., 2010). We hence suggest that the AFT age of 27 Ma marks the onset of rapid exhumation of hinterland rocks associated with the acceleration of orogenic processes as deformation started to propagate in the Arabian margin. Evidence of hinterland exhumation (SSZ) is provided by the occurrence of detrital zircons derived from the overriding Iranian microplate and deposited in the late Oligocene conglomerates (Horton et al., 2008). Such an exhumation is also suggested by one AFT grain-age population of 27 Ma reported from a gneiss sample of the Dorud metamorphic complex of the SSZ (Homke et al., 2010) and the age of diabasic dyke of 25 Ma from the Sahneh ophiolitic complex (Delaloye and Desmons, 1980).

II-8. Discussion

II-8-a. Tectonic-morphologic evolution of the High Zagros revealed by AFT dating and petrography

Thermochronological data primarily confirmed that the Arabia/Eurasia plate boundary was the site of a protracted deformation history recorded by successive cooling events in the Jurassic and Late Mesozoic, the Eocene and the Miocene. Petrographic analysis and heavy mineral assemblage in detrital sediments indicate that the Miocene sediment yield were derived from an eroding landscape

in which the radiolaritic and ophiolitic elements of the Neyriz ophiolitic complex. Less abundant garnet, amphibole and kyanite clasts suggest the recycling of rocks originated in the Sandandaj-Sirjan metamorphic belt.

The Jurassic apatite grain-age population recovered from the Zagros Miocene sediments was likely derived from the SSZ in which arc magmatism and metamorphic event of this age is recorded. The Late Mesozoic grain-age population results from a major tectonic episode recorded both in the SSZ and the Neyriz ophiolitic complex and is related to the building of the SSZ accretionary wedge during which amphibolites (Haynes and Reynolds, 1980) and associated HP (garnet-bearing amphibolites, eclogites) continental rocks were exhumed (Sarkarinejad et al., 2009) slightly before exhumation of the ophiolite occurred (Fig. III- 15). The Mesozoic sheared coloured mélange outcropping in the Neyriz area between SSZ and the obducted ophiolites contains lenses of radiolarian cherts, sandstones, metamorphic rocks (including HP rocks) and basalts. These three tectonic units were probably part of a unique accretionary complex exhumed during the Mesozoic (Fig. III- 15). We envisage that during the middle Miocene (Agha Jari and Bakthyari Fms) this area formed an outcropping topographic ridge that was the exhumed source areas for apatite crystals with Mesozoic AFT ages.

After 70 Ma, the slowing of the Africa/Eurasia convergence (Rosenbaum et al., 2002) might have initiated thermal re-equilibration and/or possibly slab retreat (Vincent et al., 2005) at the origin of extension, magmatism and eventually exhumation in the formerly tectonically thickened SSZ (core-complexes are described in SSZ; e.g. Verdel et al, 2007) and the ophiolitic complex. Trench retreat might have also triggered the shift of the centre of magmatic activity northward to the UDMA and the Alborz. Continuing convergence led to the progressive closure of the remnant oceanic domain and the closure of Eocene turbiditic basins such as those observed in the NW Zagros (Agard et al., 2005). The young Eocene cooling ages (46 and 53 Ma) measured in the Miocene foreland sediments are interpreted as resulting from the erosion of Eocene magmatic sills or plutons intruded into older magmatic-metamorphic units of the Sanandaj-Sirjan domain and the exhumed Mesozoic accretionary prism (Fig. III- 15). If the above assumption is correct we must envisage that both corresponding source terrains have not recorded significant post-Eocene burial. Preservation of original Jurassic cooling ages recovered from the Paleocene-Eocene Zagros foreland sediments of the Lorestan area (Homke et al., 2010) together with the absence of thick post-Eocene series in our study area provides support to this hypothesis (Figs. III- 3 and 15).

AFT cooling age of 27 Ma indicates rapid exhumation coeval with change, in the Zagros foreland, from carbonaceous to siliciclastic deposition. Because this cooling episode was recorded in the lower Razak Formation, we can not envisage that exhumation occurred in the same drainage basin along the same eroding stratigraphic section, otherwise the apatite grains in the younger sediments will exhibit a dominant, if not exclusive, cooling age peak with shorter lag times. We hence suggest that these Miocene ages reveal the exhumation in the hangingwall of the High Zagros thrust as it is suggested by recent low temperature thermo-chronometry across the High Zagros thrust (Gavillot et al., 2010). According to this hypothesis, the transition from younger (Oligo-Miocene) to older (Mesozoic-Eocene) AFT ages would reflect a change from local sources of the High Zagros domain dominated by the sediment cover to more regional exhumed source areas including the Zagros suture zone in which old grains are preserved in a fossil PAZ. This peculiar exhumational pattern presumably indicates that older contributing catchments were small enough so the contribution of the ophiolite complex was minor. Such a change is effectively supported by the D_{par} values of 1.6-2 μm measured in apatite crystals of the Agha Jari and Bk1 Formation that might indicate the increasing contribution of mafic rocks with respect to those measured in the Razak Formation. This is also supported by the analysis of bulk rock composition and clay mineralogy showing that Fe-Mg rich clay assemblages become dominant in the eroding landscape above the Razak Formation. Moreover, the petrographic analyses describe a progressive change in the source of materials with more sediment lithics in the upper units. The increase of sediment clasts and mafic units would therefore indicate the expansion of the catchment area to the whole High Zagros and the suture zone.

Growth strata in the Bakhtyari 1 Formation and the minimum age for the unconformity between Bk1 and Bk2 reveal that deformation and uplift of the northern part of the Zagros Folded Belt was initiated ca. 14-15 Ma and became more important after 12.4 Ma, which is in agreement with recent AHe ages of 12-8 Ma in the southeastern High Zagros from the High Zagros Fault (Gavillot et al., 2010).

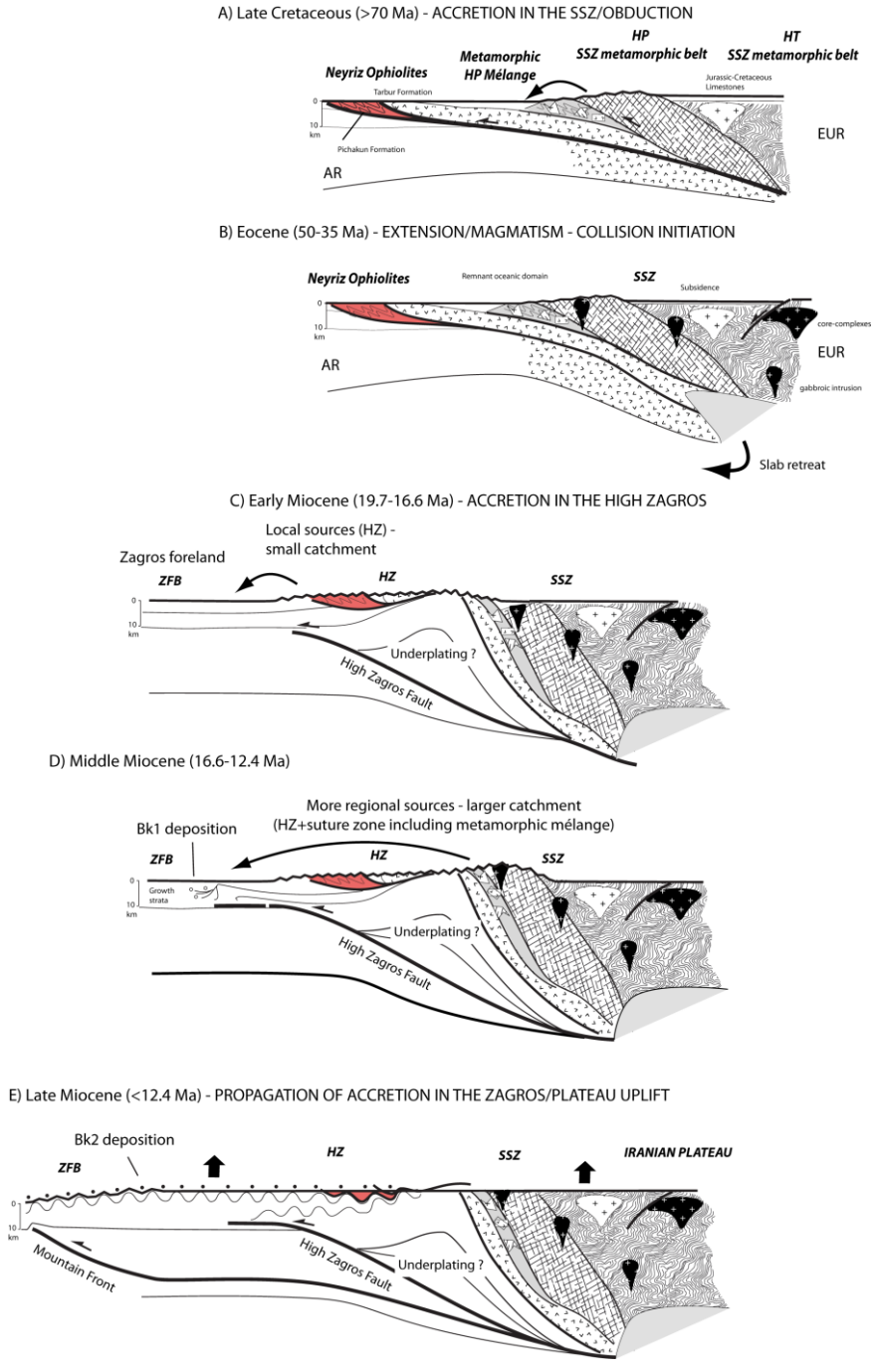

Figure 15: Morpho-tectonic evolution of the High Zagros since the Late Cretaceous that may explain the petrographic composition, detrital thermochronometric ages and clay assemblage observed in sandstones of the Miocene foreland of the Zagros (see text for explanations).

II-8-b. Constraints on climate and paleogeography of the Zagros region

Clay mineralogy analysis and sedimentological analysis of the synorogenic deposits both emphasize that the climate in the Zagros basin was essentially warm and dry since 19.7 Ma. Moderate average denudation rates of 0.6-0.9 km/Ma in the lower Miocene deduced from detrital AFT age of 27 Ma recovered in the Razak Formation indicate limited feedback between river erosion and mountain uplift that is compatible with an arid climate.

The geological evidence of early Miocene aridification in the Zagros supports previous works that established the possible initiation of aridity in Central Asia (e.g. Kazakhstan) ca. 24 Ma (Sun et al., 2010). This major climate event resulted from the Para-Tethys retreat and the Tibetan plateau uplift as suggested by modeling of the Asian climate (Ramstein et al., 1997; Zhang et al., 2007).

Despite the development of an initial mountain range in the northern Zagros (HZ, ophiolitic domain and SSZ) and the start of southward propagating deformation in the ZFB (growth strata), marine sedimentation dominated until ca. 15 Ma in the Zagros basin as indicated by the occurrence of marine nannoplanktons (Khadivi et al., 2010). The persistence of such marine gateway connecting the Mediterranean Sea and the Indo-Pacific Ocean can be more precisely dated by taking into account 1) the minimum age of the Bk1/Bk2 unconformity that outlined a major, regional event, like the Zagros/Iranian plateau uplift and 2) the age of the outermost folds and the time needed to build the ZFB. The characteristic Zagros folding started presumably after 12.4 Ma (Fig. 7) coeval with deformation in the Alborz (Guest et al., 2007) and Kopet Dagh (Hollingsworth et al., 2010). Recent modeling (Yamato et al., submitted) and age constraints on folding at the belt front (Homke et al., 2004) both argued that regional cover folding occurred in ~5 Myr and reached the front before the Messinian.

The sea retreat between the Mediterranean Sea and the Indo-Pacific Ocean was thus likely terminated by 5 Ma, which was also the time of exhumation acceleration in the Alborz (Axen et al., 2001), major plate reorganization (Allen et al., 2004) and Zagros/Iranian plateau uplift.

II-9. Conclusions

The coupled analysis of petrographic study, clay mineralogy and low-temperature fission-track dating carried out on well-dated Miocene detrital sediments (19.7-14.8 Ma) of the Zagros foreland

successfully provided new insights on the temporal evolution of uplift and exhumation patterns associated with the building of the Zagros.

We identify from the analysis of FT data on detrital apatites three main tectonic-magmatic episodes including the Jurassic-early Mesozoic accretion, metamorphism and magmatism in the SSZ, the obduction of the Neyriz ophiolitic complex and the associated tectonic mélange, the Eocene magmatic period and finally the initiation of rapid exhumation related to the ongoing Zagros collision. The preservation of such a protracted history in the detrital AFT record of the northern Zagros foreland limits to 2.5 km the burial of the Miocene series for an assumed cold geothermal gradient of 15-24°C/km.

Petrographic analysis reveals that the Miocene eroding catchment was essentially eroding ophiolitic and mélange derived rocks and the overlying carbonaceous sediment cover. Second order metamorphic clasts of the HP metamorphic belt were probably recycled from the SSZ and likely originated from clasts of the mélange series outcropping in the suture zone.

A remarkable change in the detrital record occurred after 16.6 Ma when the eroding landscape originally made with local and small-scale catchments in which younger (Oligo-Miocene) AFT ages originated from the exhumation of the High Zagros fault hangingwall changed to older (Mesozoic-Eocene) AFT ages indicating the contribution of more regional exhumed source areas including the Zagros suture zone. With this change, more sediment cover and deeper, more mafic, structural level of the ophiolitic sheets were eroded. This modification of the type of exhumed source areas was coincident with the initiation of folding in the Zagros Folded Belt.

However, the remarkable regional train of folds did not develop before 12.4 Ma. Since this time onwards both the Zagros Folded Belt and the Iranian plateau were uplifted as argued by the stratigraphy of the oldest marine sediments. This very fast accretion in the Zagros occurred probably in less than 5 Myrs and in association with weak erosion feedbacks as revealed by the arid climatic conditions that prevailed during the Miocene.

Acknowledgements

The authors acknowledge the Geological Survey of Iran for visa and the logistic-administrative supports provided during sampling and especially S. Kargar for his kind help during previous field surveys. This work has been funded by the INSU-Relief program funded to F. Mouthereau.

Conclusions

Conclusion

One of the main objectives of the thesis was to provide new constraints on the timing of deformation in the Zagros and exhumation associated with mountain building. The distribution and precise timing of Cenozoic shortening in the Zagros as well as the degree of uplift and exhumation in the Zagros collision zone in Iran are effectively keys to better understanding how the Arabia (AR) plate motion was accommodated during the collision with the overriding Eurasia (EUR) plate. This is particularly important if plate reconstructions are used to infer the connectivity between the Indo-Pacific Ocean, the Mediterranean Sea and the Para-Tethyan (sea e.g. Kocsis et al., 2009; Reuter et al., 2009), to interpret the impact of the Arabia/Eurasia convergence on the regional aridification of Central Asia (Ramstein et al., 1997) and on the Cenozoic global climate changes (Allen and Armstrong, 2008) or to deduce the mechanisms of Iranian plateau uplift (Hatzfeld and Molnar, 2010).

To resolve the temporal evolution of uplift and exhumation patterns associated with the building of the Zagros in the Fars area during the Cenozoic, I have first carried out accurate dating of the foreland sediments deposited in the northern Fars region. In particular, I seek to provide new constraints on the nature of exhumed source areas and weathering/climatic conditions in the eroding landscape of the northern Zagros, which is key location to unravel the initial collision stage and late regional uplift. To this aim, we present a provenance study of middle Miocene (19.7-14.8 Ma) detrital sediments in the northern Zagros based on the analysis of petrological assemblages and clay mineralogy combined with new detrital apatite fission-track ages. The implications of the results have been discussed in terms of plate geodynamics, landscape evolution and regional paleogeography.

Magnetostratigraphy dating in the northern flank of the Chahar-Makan syncline provided the first time constraints on the onset of foreland sedimentation and the initiation of folding in the northern part of the Zagros folded belt. The correlation of magnetic polarity sequences to the GPTS indicates that deposition of the synorogenic siliciclastic succession started as early as the Early Miocene at least 19.7 Ma ago, and corresponds to the Razak Formation in the Chahar-Makan syncline. The overlying Agha Jari Formation was deposited between 16.6 Ma and 14.8 Ma. The deposition of the Bakhtyari 1 conglomerates started after 14.8 Ma. The sediment accumulation rates increase from 0.18 mm/yr in the Razak Formation to 0.52 mm/yr in the Bakhtyari Formation (Bk1) at the top of the studied section.

The onset of deformation in the northern Zagros likely started around 14-15 Ma and was associated with growth strata at the base of the Bk1 succession found in the northern limb of the Qalat syncline. We suggest that the onset of folding might be related to the rapid (nearly

instantaneous) propagation associated with the buckling of the sedimentary cover as previously proposed. A second stage of folding reveals increasing contraction marked by the change towards more continental environmental conditions. This phase is found in association with the growth of the Derak anticline and produced tilting of the Bk1 conglomerates. The Bk1 conglomerates are truncated by an erosional surface on top of which Bk2 conglomerates are deposited unconformably. Though new dating campaigns are necessary to unravel the age of the Bk1/Bk2 unconformity, this study reveals that tectonic deformation was already ongoing in the Middle-Upper Miocene in the northern part of the Zagros folded belt.

Following the accurate dating of foreland sediments, I carried out a coupled analysis of petrographic study, clay mineralogy and low-temperature fission-track dating carried out on these well-dated Miocene detrital sediments (19.7-14.8 Ma) of the Zagros foreland successfully provided new insights on the temporal evolution of uplift and exhumation patterns associated with the building of the Zagros.

We identify from the analysis of FT data on detrital apatites three main tectonic-magmatic episodes including the Jurassic-early Mesozoic accretion, metamorphism and magmatism in the SSZ, the obduction of the Neyriz ophiolitic complex and the associated tectonic mélange, the Eocene magmatic period and finally the initiation of rapid exhumation related to the ongoing Zagros collision. The preservation of such a protracted history in the detrital AFT record of the northern Zagros foreland limits to 2.5 km the burial of the Miocene series for an assumed cold geothermal gradient of 15-24°C/km.

Petrographic analysis reveals that the Miocene eroding catchment was essentially eroding ophiolitic and mélange derived rocks and the overlying carbonaceous sediment cover. Second order metamorphic clasts (e.g. garnet, amphibolite, kyanite) of the HP metamorphic belt were probably recycled from the SSZ and likely originated from clasts of the mélange series outcropping in the suture zone.

A remarkable change in the detrital record occurred after 16.6 Ma when the eroding landscape originally made with local and small-scale catchments in which younger (Oligo-Miocene) AFT ages originated from the exhumation of the High Zagros fault hangingwall changed to older (Mesozoic-Eocene) AFT ages. This change reveals the contribution of more regional exhumed source areas including the Zagros suture zone and the Sanandaj-Sirjan belt. With this change, more sediment cover and deeper, more mafic, structural level of the ophiolitic sheets were eroded. This modification of the

type of exhumed source areas was coincident with the initiation of folding in the Zagros Folded Belt. However, the remarkable regional train of folds did not develop before 12.4 Ma as indicated the minimum age of the Bk2 unconformity. Since this time onwards both the Zagros Folded Belt and the Iranian plateau were uplifted as argued by the stratigraphy of the oldest marine sediments. This very fast accretion in the Zagros occurred probably in less than 5 Myrs and in association with weak erosion feedbacks as revealed by the arid climatic conditions that prevailed throughout the Miocene revealed by clay mineral assemblage.

Significant efforts in dating the youngest sediments and especially Bk2 unconfirmity are still necessary if we want to understand both the mechanism of folding and the growth of the Zagros topography and Iranian Plateau development. These studies must be associated with more analysis of climate proxies and paleo-altitude constraints (e.g. stable oxygen isotope) to tackle with changes of topography and climate throughout the Miocene and Pliocene.

References

References

Adatte, T., Stinnesbeck, W., and Keller, G., 1996, Lithostratigraphic and mineralogic correlations of near K/T boundary sediments in northeastern Mexico: implications for origin and nature of deposition, The Cretaceous-Tertiary Event and other Catastrophes in Earth History, v. 307: Boulder, Colorado, Geological Society of America, p. 211-226.

Agard, P., Monié, P., Gerber, W., Omrani, J., Molinaro, M., Meyer, B., Labrousse, L., Vrielynck, B., Jolivet, L., and Yamato, P., 2006, Transient, synobduction exhumation of Zagros blueschists inferred from P-T, deformation, time, and kinematic constraints: Implications for Neotethyan wedge dynamics: Journal of Geophysical Research, v. 111, no. B11401.

Agard, P., Omrani, J., Jolivet, L., and Mouthereau, F., 2005, Convergence history across Zagros (Iran): constraints from collisional and earlier deformation: International Journal of Earth Sciences, v. 94, p. 401-419. doi: 10.1007/s00531-005-0481-4.

Aghanabati, a., 2004, Geology of Iran, Geological Survay of Iran, 583 p.

Ahmadhadi, F., Daniel, J.-M., Azzizadeh, M., and Lacombe, O., 2008, Evidence for pre-folding vein development in the Oligo-Miocene Asmari Formation in the Central Zagros Fold Belt, Iran: Tectonics, v. 27, no. 1, p. TC1016. doi:10.1029/2006TC001978.

Ahmadhadi, F., Lacombe, O. and Daniel, J.-M., 2007, Early Reactivation of Basement Faults in Central Zagros (Sw Iran): Evidence from Pre-Folding Fracture Populations in Asmari Formation and LowerTertiary Paleogeography. In: Thrust Belts and Foreland Basins: From Fold Kinematics to Hydrocarbon Systems (Ed. by O. Lacombe, J. Lave., J.Verges & F. Roure) Front. Earth Sci., p. 205-228. Springer-Verlag, Berlin.

Alavi, M., 1980, Tectonostratigraphy evolution of the Zagrosides of Iran: Geology, v. 8, p. 144-149.

-, 1991, Sedimentary and structural characteristics of the Paleo-Tethys remnant in NE Iran: Gological Society of America Bulletin, no. 103, p. 983-992. doi: 10.1130/0016-7606(1991)103<0983:SASCOT>2.3.CO;2.

-, 1994, Tectonics of the zagros orogenic belt of iran: new data and interpretations: Tectonophysics, v. 229, no. 3-4, p. 211-238. doi:10.1016/0040-1951(94)90030-2.

-, 2004, Regional stratigraphy of the Zagros fold-thrust belt of Iran and its proforeland evolution 10.2475/ajs.304.1.1: American Journal of Science, v. 304, no. 1, p. 1-20. doi:10.2475/ajs.304.1.1.

References

Allen, M. B., and Armstrong, H. A., 2008, Arabia-Eurasia collision and the forcing of mid-Cenozoic global cooling: Palaeogeography, Palaeoclimatology, Palaeoecology, v. 265, no. 1-2, p. 52-58. doi:10.1016/j.palaeo.2008.04.021.

Allen, M. B., Jackson, J., and Walker, R., 2004, Late Cenozoic reorganization of the Arabia-Eurasia collision and the comparison of short-term and long term deformation rates: Tectonics, v. 32, p. 659-672. doi:10.1029/2003TC001530.

Alsharhan, A. S., Nairn, A. E. M., and Nairn, A. E. M., 1997, The End of the Paleozoic and the Early Mesozoic of the Middle East: The Absaroka Cycle Sedimentary Basins and Petroleum Geology of the Middle East: Amsterdam, Elsevier Science B.V., p. 161-233.

Ambraseys, N.N. & Melville, C.P., 1982, A History of Persian Earthquakes: CambridgeUniversity Press, Cambridge,UK.

ArRajehi, A., McClusky, S., Reilinger, R., Daoud, M., Alchalbi, A., Ergintav, S., Gomez, F., Sholan, J., Bou-Rabee, F., Ogubazghi, G., Haileab, B., Fisseha, S., Asfaw, L., Mahmoud, S., Rayan, A., Bendik, R., and Kogan, L., 2010, Geodetic constraints on present-day motion of the Arabian Plate: Implications for Red Sea and Gulf of Aden rifting: Tectonics, v. 29, no. TC3011.

Arvin, M., 1982, Petrology and geochemistry of ophiolites and associated rocks from the Zagros suture, Neyriz, Iran; PhD: London University.

Aubourg, C., Smith, B., Bakhtari, H.R., Guya, N. & Eshraghi, A.,2008, Tertiary block rotations in the Fars Arc (Zagros, Iran): Geophys. J. Int., v.173, p. 659-673.

Authemayou, C., Bellier, O., Chardon, D., Malekzade, Z., and Abassi, M., 2005, Role of the Kazerun fault system in active deformation of the Zagros fold-and-thrust belt (Iran): Comptes Rendus Geosciences, v. 337, no. 5, p. 539-545. doi:10.1016/j.crte.2004.12.007.

Authemayou, C., Chardon, D., Bellier, O., Malekzadeh, Z., Shabanian, E., and Abbassi, M. R., 2006, Late Cenozoic partitioning of oblique plate convergence in the Zagros fold-and-thrust belt (Iran): Tectonics, v. 25, no. doi:10.1029/2005TC001860.

Axen, G. J., Lam, P. S., Grove, M., Stockli, D. F., and Hassanzadeh, J., 2001, Exhumation of the west-central Alborz Mountains, Iran, Caspian subsidence, and collision-related tectonics: Geology, v. 29, no. 6, p. 559-562. doi:10.1130/0091-7613(2001)029<0559:EOTWCA>2.0.CO;2.

References

Babaie, H. A., Babaei, A., Ghazi, M. A., and Arvin, M., 2006, Geochemical, 40Ar/39Ar age, and isotopic data for crustal rocks of the Neyriz ophiolite, Iran: Canadian Journal of Earth Sciences, v. 43, p. 57-70.

Babaie, H. A., Ghazi, A. M., Babaei, A., La Tour, T. E., and Hassanipak, A. A., 2001, Geochemistry of arc volcanic rocks of the Zagros Crush Zone, Neyriz, Iran: Journal of Asian Earth Sciences, v. 19, p. 61-76. doi:10.1016/S1367-9120(00)00012-2.

Bahroudi, A., and Koyi, H. A., 2004, Tectono-sedimentary framework of the Gachsaran Formation in the Zagros foreland basin: Marine and Petroleum Geology, v. 21, no. 10, p. 1295-1310.

Bahroudi, A., and Talbot, C. J., 2003, The configuration of the basement beneath the Zagros basin: Journal of Petroleum Geology, v. 26, no. 3, p. 257-282.

Ballato, P., Uba, C., Landgraf, A., Strecker, M., Sudo, M., Stockli, D., Friedrich, A., and Tabatabaei, S., 2010, Arabia-Eurasia continental collision: insights from late Tertiary foreland-basin evolution in the Alborz mountains, northern Iran, in EGU General Assembly 2010, Vienna.

Barbarand, J., Carter, A., Wood, I., and Hurford, T., 2003, Compositional and structural control of fission-track annealing in apatite: Chemical Geology, v. 198, no. 1-2, p. 107-137. doi:10.1016/S0009-2541(02)00424-2.

Barrier, E., and Vrielynck, B., 2008a, Early Burdigalian: CGMW, scale 1:18,500,000.

-, 2008b, Early Campanian: CGMW, scale 1:18,500,000.

-, 2008c, Middle Toarcian: CGMW, scale 1:18,500,000.

Berberian, F., and Berberian, M., 1981, Tectono-Plutonic episodes in Iran, in Gupta, H. K., and Delany, F.M., ed., Zagroz-Hindu Kush-Himalaya Geodynamic Evolution: Washington, American Geophysical Union & Geological Society of America, p. 5-32.

Berberian, F., Muir, I. D., Pankhurst, R. J., and Berberian, M., 1982, Late Cretaceous and early Miocene Andean-type plotunic activity in northern Makran and Central Iran: Journal of Geological Society of London, v. 139, p. 605-614.

Berberian, M., 1986, Seismotectonics and earthquake-fault hazard study of the Karkheh river project: Jahad-e-Sazandegi.

-, 1995, Master "blind" thrust faults hidden under the Zagros folds: active basement tectonics and surface morphotectonics: Tectonophysics, v. 241, no. 3-4, p. 193-195. doi:10.1016/0040-1951(94)00185-C.

References

Berberian, M., and King, G. C. P., 1981, Towards a paleogeography and tectonic evolution of Iran: Canadian Journal of Earth Sciences, v. 18, p. 210-265.

Berberian, M., and Tchalenko, J., 1976, Earthquake of southern Zagros (Iran): Bushehr region, in Contribution to the Seismotectonics of Iran: Geological survay of Iran.

Berbserian, M., and Yeats, R. S., 2001, Contribution of archaeological data to studies of earthquake history in the Iranian Plateau: Journal of Structural Geology, v. 23, no. 2-3, p. 563-584. doi:10.1016/S0191-8141(00)00115-2.

Besse, J., Torcq, F., Gallet, Y., Ricou, L. E., Krystyn, L., and Saidi, A., 1998, Late Permian to Late Triassic palaeomagnetic data from Iran: constraints on the migration of the Iranian block through the Tethyan Ocean and initial destruction of Pangaea: Geophysical Journal International, v. 135, p. 77-92.

Beydoun, Z. R., 1991, Arabian plate hydrocarbon geology and potential- a plate tectonic approach, American Association of Petroleum Geologists, 77 p.

Beydoun, Z. R., Clarke, M. W. H., and Stoneley, R., 1992, Petroleum in the Zagros Basin: A late Tertiary foreland basin overprinted onto the outer edge of a vast hydrocarbon-rich Paleozoic-Mesozoic passive margin shelf: Foreland Basins and Fold Belts, AAPG Mem, v. 55, p. 309-339.

Bordenave, M. L., 2003, Gas prospective area in the Zagros domain of Iran and in the Gulf Iranian waters, in AAPG, Houston-Texas, USA.

Bradley, R. S., 1985, Quaternary Paleoclimatology: Methods of Paleoclimatic Reconstruction: London, Chapman and Hall, 472 p.

Braun, J., van der Beek, P., and Batt, G., 2006, Quantitative Thermochronology: Numerical Methods for the Interpretation of Thermochronological Data, Cambridge University press, 270 p.

Burbank, D.W., Puigdefabregas, C. and Munoz, J.A., 1992, The chronology of eocene tectonic and stratigraphic development of the Eastern Pyrenean Foreland Basin, Northeast Spain: Geol. Soc. Am. Bull., v. 104, p. 1101-1120.

Burbank, D.W. & Reynolds, R.G.H., 1988, Stratigraphic keys to the timing of thrusting inTerrestrialForelandBasins: applications of the Northwestern Himilaya. In: New Perspectives in Basin Analysis (Ed. by K.L. Kleinspehn & C. Paola), p. 331-351. Springer-Verlag, NewYork.

References

Callen, R. A., 1981, Palygorskite in sediments: Detrital, diagenetic or neoformed- A critical review - Discussion: South Australian Department of Mines and Energy.

Chamley, H., 1989, Clay sedimentology, Springer Verlag, Berlin, 623 p.

Chamley, H., Deconinck, J. F., and Millot, G., 1990, Sur l'abondance des minéraux smectitiques dans les sédiments marins communs déposés lors des périodes de haut niveau marin du Jurassique au Paleogene: Comptes Rendus de l'Académie des Sciences, v. 311, p. 1529-1536.

Colman-Sadd, S. P., 1978, Fold Development in Zagros Simply Folded Belt, Southwest, Iran: American Association of Petroleum Geologists Bulletin, v. 62, p. 984-1003.

Cotton, J. T., and Koyi, H. A., 2000, Modeling of thrust fronts above ductile and frictional detachments: Application to structures in the Salt Range and Potwar Plateau, Pakistan: Geological Society of America Bulletin, v. 112, no. 3, p. 351-363.

Covey, M.,1986, The evolution of Foreland Basins to Steady State: evidence from theWesternTaiwan Foreland Basin: Spec.Publ. Int. Assoc. Sedimentol., v. 8, p. 77-90.

Davoudzadeh, M., Lensch, G., and Weber-Dierenbach, K., 1986, Contribution to the paleogeography, stratigraphy and tectonics of the Infracambrian and Lower Paleozoic of Iran: Neues Jahrbuch für Geologie und Paläontologie Abhandlungen, v. 172, p. 245 – 269.

Davoudzadeh, M., and Schmidt, K., 1984, A review of the Mesozoic Paleogeography and Paleotectonic evolution of Iran: N. Jb. Geol. Palaont. Abh., v. 168, no. 2/3, p. 182-207.

Davoudzadeh, M., and Weber-Dierenbach, K., 1987, Contribution to the paleogeography, stratigraphy and tectonics of the Upper Paleozoic of Iran: Neues Jahrbuch für Geologie und Paläontologie Abhandlungen, v. 175, p. 121 – 146.

Deconinck, J. F., and Chamley, H., 1995, Diversity of smectite origins in Late Cretaceous sediments: example of chalks from northern France: Clay Minerals, v. 30, p. 365-379.

Delaloye, M., and Desmons, J., 1980, Ophiolites and melange terranes in Iran: a geochronological study and its paleotectonic implications: Tectonophysics, v. 68, p. 83-111.

Dercourt, J., Zonenshain, L. P., Ricou, L.-E., Kazmin, V. G., Le Pichon, X., Knipper, A. L., Grandjacquet, C., Sbortshikov, I. M., Geyssant, J., Lepvrier, C., Pechersky, D. H., Boulin, J., Sibuet, J.-C., Savostin, L. A., Sorokhtin, O., Westphal, M., Bazhenov, M. L., Lauer, J. P., and Biju-Duval, B., 1986, Geological evolution of the tethys belt from the atlantic to the pamirs since the LIAS: Tectonophysics, v. 123, no. 1-4, p. 241-315.

References

Dettman, D. L., Kohn, M. J., Quade, J., Ryerson, F. J., Ojha, T. P., and Hamidullah, S., 2001, Seasonal stable isotope evidence for a strong Asian monsoon throughout the past 10.7 m.y.: Geology, v. 29, p. 31-34.

Dickinson, W. R., 1985, Interpreting provenance relations from detrital modes of sandstones, in Zuffa, G. G., ed., Provenance of Arenites: NATO Advanced Science Series: Dordrecht, D. Reidel Publishing Company, p. 333-361.

Dickinson, W. R., Beard, S. L., Brakenridge, G. R., Erjavec, J. L., Fergusson, R. C., Inman, K. F., Knepp, R. A., Lindberg, F. A., and Ryberg, P. T., 1983, Provenance of North American Phanerozoic sandstones in relation to tectonic setting: Geological Society of America Bulletin, v. 94, p. 222-235.

Dickinson, W. R., and Suczek, C. A., 1979, Plate tectonics and sandstone compositions: AAPG Bulletin, v. 63, no. 12, p. 2164-2182.

Ehrenberg, S.N., Pickard, N.A.H., Laursen, G.V., Monibi, S., Mossadegh, Z.K., Svana, T.A., Aqrawi, A.A.M., McArthur, J.M. & Thirlwall, M.F., 2007, Strontium isotope stratigraphy of the Asmari Formation (Oligocene-Lower Miocene), Sw Iran : J. Petrol. Geol., v.30, p.107-128.

Emami, H., 2008, Foreland propagation folding structure of the mountain front flexure in the Pusht-e-Kuh arc (NW Zagros, Iran): University of Barcelona, 199 p.

Fakhari, M. D., Axen, G. J., Horton, B. K., Hassanzadeh, J., and Amini, A., 2008, Revised age of proximal deposits in the Zagros foreland basin and implications for Cenozoic evolution of the High Zagros: Tectonophysics ,Asia out of Tethys: Geochronologic, Tectonic and Sedimentary Records, v. 451, no. 1-4, p. 170-185. doi:10.1016/j.tecto.2007.11.064.

Falcon, N. L., 1961, Major earth-flexuring in the Zagros Mountains of south-west Iran: Quarterly Journal of the Geological Society of London,, v. 117, p. 367-376.

-, 1974, Southern Iran: Zagros Mountains, in Spencer, A. M., ed., Mesozoic-Cenozoic orogenic belts-Data for orogenic studies: London, Special Publication of Geological Society of London, p. 199-211.

Fleischer, R. L., Price, P. B., and Walker, R. M., 1975, Nuclear tracks in solids: principles and applications: Berkeley, California, University of California Press, 626 p.

Fluteau, F., Ramstien, G., and Besse, J., 1999, Simulating the evolution of the Asian and African monsoons during the past 30 Myr using an atmospheric general circulation model: J. Geophys. Res., v. 104, p. 11995-12018.

References

Fuentes, F., DeCelles, P. G., and Gehrels, G. E., 1990, The radial plot: graphical assessment of spread in ages: Nucl. Tracks Radiat. Meas, v. 17, p. 207-214.

-, 1994, Genetic algorithms: A powerful new method for modelling fission-track data and thermal histories. In: Lanphere, M.A., Dalrymple, G.B., Turrin, B.D. (eds.), in International Conference of Geochronology, Cosmochronology and Isotope Geology, US Geological Survey.

-, 2005, Statistics for Fission Track Analysis, Chapman and Hall/CRC, Interdisciplinary Statistics Series, 224 p.

Galbraith, R. F., 1988, Graphical Display of Estimates Having Differing Standard Errors: Technometrics, v. 30, p. 271-281.

- 1990, The radial plot: graphical assessment of spread in ages: Nucl. Tracks Radiat. Meas, v. 17, p. 207-214.

- 1994, Genetic algorithms: A powerful new method for modelling fission-track data and thermal histories. In: Lanphere, M.A., Dalrymple, G.B., Turrin, B.D. (eds.): International Conference of Geochronology, Cosmochronology and Isotope Geology.

Galbraith, R. F., and Laslett, G. M., 1993, Statistical models for mixed fission track ages: International Journal of Radiation Applications and Instrumentation. Part D. Nuclear Tracks and Radiation Measurements, v. 21, no. 4, p. 459-470.

Gansser, A., 1992, The enigma of the Persian dome inclusions: Eclogae Geologica Helveticae, v. 85, p. 825-846.

Gavillot, Y., Axen, G. J., Stockli, D. F., Horton, B. K., and Fakhari, M. D., 2010, Timing of thrust activity in the High Zagros fold-thrust belt, Iran, from (U-Th)/He thermochronometry: Tectonics, v. 29, no. TC4025. doi:10.1029/2009TC002484.

Ghasemi, A., and Talbot, C. J., 2006, A new tectonic scenario for the Sanandaj-Sirjan Zone (Iran): Journal of Asian Earth Sciences, v. 26, no. 6, p. 683-693.

Ghasemi, A., and Talbot, C. J., 2006, A new tectonic scenario for the Sanandaj-Sirjan Zone (Iran): Journal of Asian Earth Sciences, v. 26, no. 6, p. 683-693.

Gleadow, A. J. W., 1981, Fission-track dating methods: What are the real alternatives?: Nuclear Tracks, v. 5, no. 1-2, p. 3-14.

Glennie, K., 1995, The geology of the Oman Mountains. An outline of their origin: Beaconsfield, Bucks, Scientific Press Ltd, 110 p.

References

Golonka, J., 2000, Cambrian-Neogen Plate Tectonic Maps: Wydawnictwo Uniwersytetu Jagiellonskiego.

-, 2004, Plate tectonic evolution of the southern margin of Eurasia in the Mesozoic and Cenozoic: Tectonophysics. doi:10.1016/j.tecto.2002.06.004.

Golonka, J., and Ford, D., 2000, Pangean (Late Carboniferous-Middle Jurassic) paleoenvironment and lithofacies: Palaeogeography, Palaeoclimatology, Palaeoecology, v. 161, no. 1-2, p. 1-34. doi:10.1016/S0031-0182(00)00115-2.

Green, P. F., 1981, A new look at statistics in fission track dating: Nucl. Tracks Radiat. Meas., v. 5, p. 77–86.

Guest, B., Horton, B. K., Axen, G. J., Hassanzadeh, J., and McIntosh, W. C., 2007, Middle to late Cenozoic basin evolution in the western Alborz Mountains: Implications for the onset of collisional deformation in northern Iran: Tectonics, v. 26, no. TC6011.

Haghipour, A., 2009, International Geological Map of Middle East: CGMW, scale 1:5,000,000.

Hailwood, E. A., 1989, Magnetostratigraphy: Geological society London special report 19, Blackwell.

Hallam, A., 1976, Geology and plate tectonics interpretation of the sediments of the Mesozoic radiolarite-ophiolite complex in the Neyriz region, southern Iran: Geological Society of America Bulletin, v. 87, p. 47-52.

Harzhauser, M., Kroh, A., Mandic, O., Piller, W. E., Göhlich, U., Reuter, M., and Berning, B., 2007, Biogeographic responses to geodynamics: A key study all around the Oligo-Miocene Tethyan Seaway: Zoologischer Anzeiger - A Journal of Comparative Zoology, Special Issue: Phylogenetic Symposium, 48th Phylogenetic Symposium on Historical Biogeography, v. 246, no. 4, p. 241-256. doi:10.1016/j.jcz.2007.05.001.

Hatzfeld, D., and Molnar, P., 2010, Comparisons of the kinematics and deep structures of the Zagros and Himalaya and of the Iranian and Tibetan plateaus and geodynamic implications: Review of Geophysics, v. 48, 48 p. doi:10.1029/2009RG000304.

Hatzfeld, D., Tatar, M., Priestley, K., and Ghafory-Ashtiany, M., 2003, Seismological constraints on the crustal structure beneath the Zagros Mountain belt (Iran): Geophysical Journal International, v. 155, no. 2, p. 403-410. doi:10.1046/j.1365-246X.2003.02045.x

Haynes, S. J., and McQuillan, H., 1974, Evolution of the Zagros suture zone, southern Iran: Geological Society of America Bulletin, v. 85, p. 739-744.

Hempton, M. R., 1987, Constraints on Arabian Plate motion and extensional history of the Red Sea: Tectonics, v. 6, p. 687– 705.

Heermance, R.V.,Chen, J., Burbank, D.W. and Wang, C., 2007, Chronology and tectonic controls of LateTertiary Deposition in the SouthwesternTian Shan Foreland, NwChina: BasinRes., v.19, doi:10.1111/j.1365-2117.2007.00339.x.

Hessami, K., Koyi, H. A., Talbot, C. J., Tabasi, H., and Shabanian, E., 2001, Progressive unconformities within an evolving foreland fold-thrust belt, Zagros Mountains: Journal of the Geological Society of London, v. 158, p. 969-981.

Hilley, G. E., and Strecker, M. R., 2004, Steady state erosion of critical Coulomb wedges with applications to Taiwan and the Himalaya: Journal of Geophysical Research, v. 109, no. B01411.

Hollingsworth, J., Fattahi, M., Walker, R., Talebian, M., Bahroudi, A., Bolourchi, M. J., Jackson, J., and Copley, A., 2010, Oroclinal bending, distributed thrust and strike-slip faulting, and the accommodation of Arabia–Eurasia convergence in NE Iran since the Oligocene: Geophysical Journal International, v. 181, no. 3, p. 1214-1246.

Homke, S., Vergés, J., Garcés, M., Emami, H., and Karpuz, R., 2004, Magnetostratigraphy of Miocene–Pliocene Zagros foreland deposits in the front of the Push-e Kush Arc (Lurestan Province, Iran): Earth and Planetary Science Letters, v. 225, p. 397-410. doi:10.1016/j.epsl.2004.07.002.

Homke, S., Verges, J., Serra-Kiel, J., Bernaola, G., Sharp, I., Garces, M., Montero-Verdu, I., Karpuz, R., and Goodarzi, M. H., 2009, Late Cretaceous-Paleocene formation of the proto-Zagros foreland basin, Lurestan Province, SW Iran: Geological Society of America Bulletin, v. 121, no. 7-8, p. 963-978. doi: 10.1130/B26035.1.

Homke, S., Vergès, J., Van der Beek, P. A., Fernandez, M., Saura, E., Barbero, L., Badics, B., and Labrin, E., 2010, Insights in the exhumation history of the NW Zagros from bedrock and detrital apatite fission-track analysis: evidence for a long-lived orogeny: Basin Research, v. 22, no. 5, p. 659–680. doi:10.1111/j.1365-2117.2009.00431.x

Horton, B. K., Hassanzadeh, J., Stockli, D. F., Axen, G. J., Gillis, R. J., Guest, B., Amini, A., Fakhari, M., Zamanzadeh, S. M., and Grove, M., 2008, Detrital zircon provenance of Neoproterozoic to Cenozoic deposits in Iran: Implications for chronostratigraphy and

collisional tectonics: Tectonophysics, v. 451, no. 1-4, p. 97-122. doi:10.1016/ j.tecto. 2007. 11.063.

Hosseini, S. Z., and M. Mohebbi, 1996, Geological Map of Shurab: Geological Survey of Iran.

Houshmand Zadeh, A., Ohanian, A. T., Sahandi, N., Taraz, B. H., Aghanabati, A., Soheili, C. M., Azarm, F., and Hamdi, B., 1990, Geological Map of Eqlid: Geological Survey of Iran, Quadrangle G10, scale 1:250,000.

Hudson, A., and Anthony, C. R., 1998, Depleted Uranium, in Harley, N. H., Foulkes, E. C., Hilborne, L. H., Hudson, A., and Anthony, C. R., eds., A Review of the Scientific Literature as It

Hurford, A. J., and Green, P. F., 1982, A users' guide to fission track dating calibration: Earth and Planetary Science Letters, v. 59, no. 2, p. 343-354.

Hurford, A.J., and Hammerschmidt, K., 1985. $^{40}Ar/^{39}Ar$ dating of the Bischop and Fish Canyon Tufs: calibration ages for fssion-track dating standards: Chem.Geol., v. 58, p. 23-32.

Husseini, M. I., 1989, Tectonic and deposition model of Late Precambrian-Cambrian Arabian and adjoining plates: The American Association of Petroleum Geologists Bulletin, v. 73, no. 9, p. 1117-1131.

-, 2000, Origin of the Arabian plate structures: Amar collision and Najd rift: GeoArabia, v. 5, no. 4, p. 527-542.

Ingersoll, R. V., Bullard, T. F., Ford, R. L., Grimm, J. P., Pickle, J. D., and Sares, S. W., 1984, The effect of grain size on detrital modes: a test of the Gazzi–Dickinson point-counting method: Journal of Sedimentary Petrology, v. 54, no. 1, p. 103-116.

Jackson, J., 1980, Reactivation of basement faults and crustal shortening in orogenic belts: Nature, v. 283, p. 343-346.

-, 1992, Partitioning of strike-slip and convergent motion between Eurasia and Arabia in Eastern Turkey and the Caucasus: J. Geophys. Res., v. 97, p. 12471-12479.

Jackson, J., Hains, J., and Holt, W., 1995, The accomodation of Arabia-Eurasia plate: Journal of Geophysical Research, v. 100, no. B8, p. 15,205-15,219.

Jahani, S., J.-P. Callot, J. Letouzey, and D. Frizon de Lamotte, 2009, The eastern termination of the Zagros Fold-and-Thrust Belt, Iran: Structures, evolution, and relationships between salt plugs, folding, and faulting: Tectonics, v. 28, p. TC6004, doi:10.1029/ 2008TC002418.

James, G. A., and Wynd, J. G., 1965, Stratigraphic nomenclature of Iranian Oil Consortium Agreement Area: AAPG Bulletin, v. 49, no. 12, p. 2182-2245.

References

Jordan, T.E. & Alonso, R.N., 1987, Cenozoic stratigraphy and BasinTectonics of the AndesMountains, 20-28° South Latitude: Am. Assoc. Petrol. Geol. Bull., v.71, p. 49-64.

Kadinsky-Cade, K., and Barzangi, M., 1982, Seismotectonics of Southern Iran: The Oman line: Tectonics, v. 1, p. 389-412.

Kazmin, V., Ricou, L.-E., and Sbortshikov, I. M., 1986, Structure and evolution of the passive margin of the eastern tethys: Tectonophysics, v. 123, no. 1-4, p. 153-179.

Kent, P. E., 1979, The emergent Hormuz salt plugs of southern Iran: Journal of Petroleum Geology, v. 2, no. 2, p. 117-144.

Ketcham, R. A., Donelick, R. A., and Donelick, M. B., 2000, Aftsolve: A program for multi-kinetic modeling of Apatite Fission-Track Data.: Geol.Mater. Res., v. 2, p. 1-32.

Khadivi, S., Mouthereau, F., Larrasoaña, J.-C., Vergés, J., Lacombe, O., Khademi, E., Beamud, E., Melinte-Dobrinescu, M., and Suc, J.-P., 2010, Magnetochronology of synorogenic Miocene foreland sediments in the Fars arc of the Zagros Folded Belt (SW Iran): Basin Res. doi: 10.1111/j.1365-2117.2009.00446.x.

Kirschvink, J.L., 1980, The least- squares line and plane and the analysis of Paleomagnetic data: Geophys. J. R. Astronom. Soc., v. 62, p. 699-718.

Kocsis, L., Vennemann, T. W., Hegner, E., Fontignie, D., and Tütken, T., 2009, Constraints on Miocene oceanography and climate in the Western and Central Paratethys: O-, Sr-, and Nd-isotope compositions of marine fish and mammal remains: Palaeogeography, Palaeoclimatology, Palaeoecology, v. 271, p. 117–129.

Koop, W., and Stoneley, R., 1982, Subsidence history of the Middle East Zagros basin, Permian to recent: Philosophical Transactions of the Royal Society of London, v. 305, p. 149-168.

Lacombe, O., Amrouch, K., Mouthereau, F., and Dissez, L., 2007, Calcite twinning constraints on late Neogene stress patterns and deformation mechanisms in the active Zagros collision belt: Geology, v. 35, no. 3, p. 263-266.

Lacombe, O., Mouthereau, F., Kargar, S., and Meyer, B., 2006, Late Cenozoic and modern stress fields in the western Fars (Iran): Implications for the tectonic and kinematic evolution of central Zagros: Tectonics, v. 25, no. TC1003, p. doi:10.1029/2005TC001831.

Lanphere, M. A., and Pamic, T., 1983, 40Ar/39Ar ages and tectonic setting of ophiolites from Neyriz area, south-east Zagros range, Iran: Tectonophysics, v. 96, p. 245-256.

References

Lanza, R., and Meloni, A., 2006, The Earth's Magnetism, An Introduction for Geologists, Springer-Verlag Berlin Heidelberg, 278 p.

Larrasoaña, J.C., Murelaga, X. and Garcés, M., 2006, Magnetobiochronology of Lower Miocene (Ramblian) Continental Sediments from theTudela Formation (Western Ebro Basin, Spain): Earth Planet. Sci. Lett., v. 243, p. 409-423.

Lensch, G., Schmidt, K., and Davoudzadeh, M., 1984, Introduction to the Geology of Iran: N. Jb. Geol. Palaont. Abh., no. 168, p. 155-164.

Leterrier, J., 1985, Mineralogical geochemical and isotopic evolution of two Miocene mafic intrusions from the Zagros (Iran): Lithos, v. 18, p. 311–329.

Lourens, L. J., F.J. Hilgen, J. Laskar, Shackleton, N. J., and Wilson, D., 2004, The Neogene Period.in, A Geologic Time Scale 2004, A Geologic Time Scale 2004, (Ed. by F.M.Gradstein, J.G. Ogg & A.G. Smith), Cambridge University Press, 409-440 p.

Lowrie, W., 2007, Fundamentals of geophysics, Cambridge, Cambridge University Press, 381 p.

Maggi, A., and Priestley, K., 2005, Surface waveform tomography of the Turkish-Iranian Plateau: Geophysical Journal International, v. 160, p. 1068-1080.

Masson, F., Anvari, M., Djamour, Y., Walsperdorf, A., Tavakoli, F., Daignières, M., Nankali, H., and Van Gorp, S., 2007, Large-scale velocity field and strain tensor in Iran inferred from GPS measurements: new insight for the present-day deformation pattern within NE Iran: Geophysical Journal International, v. 170, p. 436-440.

McClusky, S., Reilinger, R., Mahmoud, S., Ben Sari, D., and Tealeb, A., 2003, GPS constraints on Africa (Nubia) and Arabia plate motions: Geophysical Journal International, v. 155, p. 126-138.

McFadden, P.L. and McElhinny, M.W., 1990, Classification of the reversal test in palaeomagnetism: Geophys. J. Int., v.103, p.725-729.

McQuarrie, N., 2004, Crustal scale geometry of the Zagros fold-thrust belt, Iran: Journal of Structural Geology, v. 26, no. 3, p. 519-535. doi:10.1016/j.jsg.2003.08.009.

McQuarrie, N., Stock, J. M., Verdel, C., and Wernicke, B. P., 2003, Cenozoic evolution of Neotethys and implications for the causes of plate motions: Geophysical Resarch Letters, v. 30, p. doi:10.1029/2003GL017992.

Meyer, B., Mouthereau, F., Lacombe, O., and Agard, P., 2005, Evidence of Quaternary activity along the Deshir Fault: implication for the Tertiary tectonics of Central Iran: Geophysical Journal International, v. 164, p. 192-201.

Mohajjel, M., and Fergusson, C. L., 2000, Dextral transpression in Late Cretaceous continental collision, Sanandaj-Sirjan Zone, western Iran: Journal of Structural Geology, v. 22, no. 8, p. 1125-1139.

Mohajjel, M., Fergusson, C. L., and Sahandi, M. R., 2003, Cretaceous-Tertiary convergence and continental collision, Sanandaj-Sirjan Zone, western Iran: Journal of Asian Earth Sciences, v. 21, no. 4, p. 397-412.

Molinaro, M., Guezou, J.C., Leturmy, P., Eshraghi, S.A. and Frizon de Lamotte, D., 2004, The origin of changes in structural style across the Bandar Abbas Syntaxis, Se Zagros (Iran): Mar. Petrol. Geol., v. 21, p. 735-752.

Molinaro, M., Leturmy, P., Guezou, J. C., Frizon de Lamotte, D., and Eshraghi, S. A., 2005, The structure and kinematics of the southeastern Zagros fold-thrust belt, Iran: from thin-skinned to thick-skinned tectonics: Tectonics, v. 24, p. doi:10.1029/2004TC001633.

Molnar, P., and England, P., 1990, Late Cenozoic Uplift of Mountain-Ranges and Global Climate Change - Chicken or Egg: Nature, v. 346 (6279), p. 29-34.

Moritz, R., Ghazban, F., and Singer, B., 2006, Eocene Gold Ore Formation at Muteh, Sanandaj-Sirjan Tectonic Zone, Western Iran: A Result of Late-Stage Extension and Exhumation of Metamorphic Basement Rocks within the Zagros Orogen: Economic geology, v. 101, p. 1497-1524.

Motiei, H., 1993, Stratigraphy of Zagros: Tehran, Geological Survey of Iran, 536 p.

-, 1995, Petroleum Geology of Zagros: Tehran, Geological Survey of Iran, 589 p.

Mouthereau, F., Lacombe, O., and Meyer, B., 2006, The Zagros folded belt (Fars, Iran): constraints from topography and critical wedge modelling: Geophysical Journal International, v. 165, no. 1, p. 336-356.

Mouthereau, F., Lacombe, O., Tensi, J., Bellahsen, N., Kargar, S., and Amrouch, K., 2007a, Mechanical Constraints on the Development of The Zagros Folded Belt (Fars), in Thrust belts and foreland basins: form fold kinematics to hydrocarbon systems, Frontiers in Earth Sciences, edited by O. Lacombe, J. Lavé, F. Roure and J. Verges, Springer-Verlag, pp. 245-264, Springer-Verlag. doi:10.1007/978-3-540-69426-7_13.

References

Mouthereau, F., Tensi, J., Bellahsen, N., Lacombe, O., De Boisgrollier, T., and Kargar, S., 2007b, Tertiary sequence of deformation in a thin-skinned/thick-skinned collision belt: The Zagros Folded Belt (Fars, Iran): Tectonics, v. 26, no. doi: 10.1029/2007TC002098.

NASA, 1992, Earth Observatory, p. http://earthobservatory.nasa.gov/.

Naeser, C.W., and Fleischer, R.L., 1975. Age of the apatite at Cerro de Mercado, Mexico: a problem for fission-track annealing corrections: Geophys. Res. Lett., v. 2, p. 67-70.

Ni, J., and Barzangi, M., 1986, Seismotectonics of the Zagros Continental Collision Zone and a Comparison with the Himalayas: J. Geophys. Res., v. 91, p. 8205-8218.

Nilfroushan, F., Masson, F., Vernant, P., Vigny, C., Martinod, J., Abbasi, M., Nankali, H., Hatzfeld, D., Bayer, R., Tavakoli, F., Ashtiani, A., Doerflinger, E., Daigniéres, M., Collard, P., and Chéry, J., 2003, GPS network monitors the Arabia-Eurasia collision deformation in Iran: Journal of Geodesy, v. 77, p. 411-422.

NIOC, 1979, Geological Map of Shiraz: National Iranian Oil Company, Quadrangle G11, scale 1:250,000.

Omrani, J., Agard, P., Whitechurch, H., Benoit, M., Prouteau, G., and Jolivet, L., 2008, Arc-magmatism and subduction history beneath the Zagros Mountains, Iran: A new report of adakites and geodynamic consequences: Lithos, v. 106, no. 3-4, p. 380-398. doi: 10.1016/ j.lithos.2008.09.008

Opdyke, M., and Channell, J., 1996, Magnetic Stratigraphy, San Diego, CA: Academic Press, 346 p.

Oveisi, B., 2005, Geological Map of Kalestan (1:100,000): Geological Survey of Iran.

Price, P. N., and Walker, R. M., 1963, Fossil tracks of charged particles in mica and the age of mineral: J. Geophys. Res., v. 68, p. 4847.

Rachidnejad-Omran, N., Emami, M. H., Sabzehei, M., Rastad, E., Bellon, H., and Piqué, A., 2002, Lithostratigraphie et histoire paléozoïque à paléocène des complexes métamorphiques de la région de Muteh, zone de Sanandaj–Sirjan (Iran méridional): Comptes Rendus de l'Académie des Sciences, v. 334, p. 1185–1191.

Raffi, I., Backman, J., Fornaciari, E., Pälike, H., Rio, D., Lourens, L., and Hilgen, F., 2006, A review of calcareous nannofossil astrobiochronology encompassing the past 25 million years: Quaternary Science Reviews Critical Quaternary Stratigraphy, v. 25, no. 23-24, p. 3113-3137. doi:10.1016/j.quascirev.2006.07.007.

Ramstein, G., Fluteau, F., Besse, J., and Joussaume, S., 1997, Effect of orogeny, plate motion and land-sea distribution on Eurasian climate change over the past 30 million years: Nature, v. 439, p. 788-795.

Ramezani, J., and Tucker, R. D., 2003, Convergence history across Zagros (Iran): constraints from collisional and earlier deformation: International Journal of Earth Sciences, v. 94, p. 401-419.

Raymo, M. E., and Ruddiman, W. F., 1992, Tectonic forcing of late Cenozoic climate: Nature, v. 359, p. 117-122.

Reuter, M., Piller, W. E., Harzhauser, M., Mandic, O., Berning, B., Rogl, F., Kroh, A., Aubry, M.-P., Wielandt-Schuster, U., and Hamedani, A., 2009, The Oligo-/Miocene Qom Formation (Iran): evidence for an early Burdigalian restriction of the Tethyan Seaway and closure of its Iranian gateways: International Journal of Earth Sciences, v. 98, p. 627–650.

Reynolds, J.H., Jordan, T.E., Johnson, N.M., Damanti, J.F. and Tabbutt, K.D., 1990, Neogene deformation of the Flat- Subduction Segment of the Argentine-Chilean Andes: magnetostratigraphic constraints from Las Juntas, La Rioja Province, Argentina: Geol. Soc. Am. Bull., v. 102, p. 1607-1622.

Ricou, L. E., 1971, Le croissant ophiolitique péri-arabe, une ceinture de nappes mise en place au crétacé supérieur: Revue de géographie physique et de géologie dynamique, v. 13, p. 327-350.

-, 1994, Tethys reconstructed: plates, continental fragments and their boundaris since 260 Ma from Central America to South-eastern Asia: Geodinamica Acta, v. 7, p. 169-218.

-, 1976, Evolution structurale de Zagrides. La region clef de Neyriz (Zagros iranien): Memoire Société Géologique de France, v. 126, no. 11, p. 1-140.

Robert, C., and Chamley, H., 1990, Paleoenvironmental significance of clay mineral association at the Cretaceous-Tertiary boundary: Palaeogeography, Palaeoclimatology, Palaeoecology, v. 79, p. 205-219.

Robin, C., Gorican, S., Guillocheau, F., Razin, P., Dromart, G., and Mosaffa, H., 2010, Mesozoic deep-water carbonate deposits from the southern Tethyan passive margin in Iran (Pichakun nappes, Neyriz area): biostratigraphy, facies sedimentology and sequence stratigraphy, in Leturmy, P., and Robin, C., eds., Tectonic and Stratigraphic Evolution of Zagros and Makran during the Mesozoic-Cenozoic Volume 330: London, Geological Society of London, p. 179-210.

Rosenbaum, G., Lister, G. S., and Duboz, C., 2002, Relative motions of Africa, Iberia and Europe during Alpine orogeny: Tectonophysics, v. 359, p. 117-129.

Roustaei, M., Nissen, E., Abassi, M., Gholamzadeh, A., Ghorashi, M., Tatar, M., Yamini-Fard, F., Bergman, E., Jackson, J., and Parsons, B., 2010, The 2006 March 25 Fin earthquakes (Iran)-insights into the vertical extents of faulting in the Zagros Simply Folded Belt: Geophysical Journal International, v. 181, no. 3, p. 1275-1291.

Rowley, D. B., and Currie, B. S., 2006, Palaeo-altimetry of the late Eocene to Miocene Lunpola basin, central Tibet: Nature, v. 439, p. p. 677-681.

Sarkarinejad, K., and Alizadeh, A., 2009, Dynamic model for the exhumation of the Tutak gneiss dome within a bivergent wedge in the Zagros Thrust System of Iran: Journal of Geodynamics, v. 47, p. 201-209. doi:10.1016/j.jog.2008.09.003.

Sarkarinejad, K., and Azizi, A., 2008, Slip partitioning and inclined dextral transpression along the Zagros Thrust System, Iran: Journal of Structural Geology, v. 30, no. 1, p. 116-136. doi: DOI: 10.1016/j.jsg.2007.10.001.

Sarkarinejad, K., Godin, L., and Faghih, A., 2009, Kinematic vorticity flow analysis and 40Ar/39Ar geochronology related to inclined extrusion of the HP–LT metamorphic rocks along the Zagros accretionary prism, Iran: Journal of Structural Geology, v. 1, no. 7, p. 691-706. doi: 10.1016/j.jsg.2009.04.003.

Schlunegger, F., Matter, A., Burbank, D.W. and Klaper, E.M., 1997, Magnetostratigraphic constraints on relationships between evolution of the Central Swiss Molasse Basin and Alpine Orogenic events: Geol. Soc. Am. Bull., v. 109, p. 225-241.

Schlunegger, F., and Willett, S. D., 1999, Spatial and temporal variations in exhumation of the central Swiss Alps and implications for exhumation mechanisms.mechanisms, in Ring, U., Brandon, M. T., Lister, G. S., and Willett, S. D., eds., Exhumation Processes: Normal Faulting, Ductile Flow, and Erosion: Special Publications: london, Geological Society, p. 157-179.

Schmalholz, S. M., Podladchikov, Y., and Burg, J. P., 2002, Control of folding by gravity and matrix thickness: implications for large-scale folding: Journal of Geophysical Research, v. 107, no. B1, p. 10.1029/2001JB000355.

Schuster, F., and Wielandt, U., 1999, Oligocene and Early Miocene coral faunas from Iran: palaeoecology and palaeobiogeography: International Journal of Earth Sciences, v. 88, p. 571-581.

Segalen, L., Lee-Thorp, J. A., and Cerling, T. E., 2007, Timing of C4 grass expansion across sub-Saharan Africa: Journal of Human Evolution, v. 53, p. 549-559.

Sella, G. F., Dixon, T. H., and Mao, A., 2002, Revel: A model for Recent plate velocities from space geodesy: J. Geophys. Res., v. 107. doi:10.1029/2000JB000033.

Sepehr, M., Cosgrove, J., and Moieni, M., 2006, The impact of cover rock rheology on the style of folding in the Zagros fold-thrust belt: Tectonophysics, v. 427, no. 1-4, p. 265-281. doi:10.1016/j.tecto.2006.05.021.

Sepehr, M., and Cosgrove, J. W., 2004, Structural framework of the Zagros Fold-Thrust Belt, Iran: Marine and Petroleum Geology ,Oil and Gas in Compressional Belts, v. 21, no. 7, p. 829-843. doi:10.1016/j.marpetgeo.2003.07.006.

Setudehnia, A., 1978, The Mesozoic sequence in south-west Iran and adjacent areas: Journal of Petroleum Geology, v. 1, no. 1, p. 3-42.

Shafaii Moghadam, H., Stern, R. J., and Rahgoshay, M., 2010, The Deshir ophiolite (central Iran): Geochemical constraints on the origin and evolution of the Inner Zagros ophiolitic belt: Geological Society of America Bulletin, v. 122, no. 9/10, p. 1516-1547. doi: 10.1130/B30066. 1.

Sharland, P. R., Archer, R., Casey, D. M., Davies, R. B., Hall, S. H., Heward, A. P., Horbury, A. D., and Simmon, M. D., 2001, Arabian Plate sequence stratigraphy, GeoArabia Special Publication: Manama Bahrain, Oriental Press, 371 p.

Sheikholeslami, M. R., Pique, A., Mobayen, P., Sabzehei, M., Bellon, H., and Hashem Emami, M., 2008, Tectono-metamorphic evolution of the Neyriz metamorphic complex, Quri-Kor-e-Sefid area (Sanandaj-Sirjan Zone, SW Iran): Journal of Asian Earth Sciences, v. 31, p. 504-521. doi:10.1016/j.jseaes.2007.07.004.

Sherkati, S., and Letouzey, J., 2004, Variation of structural style and basin evolution in the central Zagros (Izeh zone and Dezful Embayment), Iran: Marine and Petroleum Geology, v. 21, no. 5, p. 535-554. doi:10.1016/j.marpetgeo.2004.01.007.

Sherkati, S., Letouzey, J., and Frizone de Lamotte, D., 2006, Central Zagros fold-thrust belt (Iran): New insights from seismic data, field observation and sandbox modeling: Tectonics, v. 25, p. 1-27.

Sherkati, S., Molinaro, M., Frizon de Lamotte, D., and Letouzey, J., 2005, Detachment folding in the Central and Eastern Zagros fold-belt (Iran): salt mobility, multiple detachments and late

basement control: Journal of Structural Geology, v. 27, no. 9, p. 1680-1696. doi:10.1016/j.jsg. 2005.05.010.

Sinclair, H.D., 1997, Tectonostratigraphic model for under- filled peripheral Basins: an Alpine perspective: Geol. Soc. Am. Bull., v. 109, p. 324-346.

Smith, B.,Aubourg, C.,Guezou, J.C.,Nazari, H.,Molinaro, M., Braud, X. and Guya, N. , 2005, Kinematics of a Sigmoidal fold and vertical axis rotation in the East of the Zagros-Makran Syntaxis (Southern Iran): paleomagnetic, magnetic fabric and microtectonic approaches: Tectonophysics, v. 411, p. 89-109.

Soleimany, B., and Sabat, F., 2010, Style and age of deformation in the NW Persian Gulf,: Petroleum Geoscience, v. 16, no. 1, p. 31-39. doi: 10.1144/1354-079309-837.

Stampfli, G., Marcoux, J., and Baud, A., 1991, Tethyan margins in space and time: Palaeogeography, Palaeoclimatology, Palaeoecology Palaeogeography and Paleoceanography of Tethys, v. 87, no. 1-4, p. 373-409.

Stampfli, G. M., and Borel, G. D., 2002, A plate tectonic model for the Paleozoic and Mesozoic constrained by dynamic plate boundaries and restored synthetic oceanic isochrons: Earth and Planetary Science Letters, v. 196, no. 1-2, p. 17-33.

Sten, R. J., 1985, The Najd fault system, Saudi Arabia and Egypt: a Late Precambrian rift-related transform system: Tectonics, v. 4, p. 497-511.

Stocklin, J., 1968, Structural history and tectonics of Iran; a review: American Association of Petroleum Geologists Bulletin, v. 52, no. 7, p. 1229-1258.

-, 1974, Possible ancient continental margins in Iran, in Burk, C., and Drake, C., eds., Geology of continental margins: New York, p. 873-877.

Stoneley, R., 1981, The geology of the Kuh-e Dalneshin area of southern Iran, and its bearing on the evolution of southern Tethys: Journal of the Geological Society of London, v. 138, p. 509-526.

-, 1990, The Arabian Continental Margin in Iran During the Late Cretaceous. In:The Geology and Tectonics of the Oman Region (Ed. by A.H.F. Robertson, M.P. Searle & A.C. Ries), Geological Society of London, London, p. 787-795.

Sun, J., Ye, J., Wu, W., Ni, X., Bi, S., Zhang, Z., Liu, W., and Meng, J., 2010, Late Oligocene-Miocene mid-latitude aridification and wind patterns in the Asian interior: Geology, v. 38, no. 6, p. 515-518. doi:10.1016/j.tecto.2008.09.008.

Synder, D. B., and Barzangi, M., 1986, Deep crustal structure and flexure of the Arabian plate beneath the Zagros collisional mountain belt as inferred from gravity observations: Tectonics, v. 5, no. 3, p. 361-373.

Talbot, C. J., and Alavi, M., 1996, The past of a future syntaxis across the Zagros, in Alsop, G. I., Blundell, D. J., and Davison, I., eds., Salt Tectonics, Geological Society Special Publication, p. 89-109.

Talebian, M., and Jackson, J., 2002, Offset on the Main Recent Fault of NW Iran and implications for the late Cenozoic tectonics of the Arabia-Eurasia collision zone: Geophysical Journal International, v. 150, p. 422-439.

-, 2004, Reappraisal of earthquake focal mechanisms and active shortening in the Zagros mountains of Iran: Geophysical Journal International, v. 156, p. 506-526.

Tatar, M., Hatzfeld, D., and Ghafori-Ashtiany, M., 2004, Tectonics of the Central Zagros (Iran) deduced from microearthquake seismicity: Geophysical Journal International, v. 156, p. 255-266.

Tatar, M., Hatzfeld, D., Martinod, J., Walpersdorf, A., Ghafori-Ashtiany, M., and Chéry, J., 2002, The presend-day deformation of the cnetral Zagros from GPS measurements: Tectonics, v. 29.

Tchalenko, J. S., and Baraud, J., 1974, Seismicity and structure of the Zagros (Iran)- the main recent fault between 33 and 35_N: Royal Sosiety of Londen, v. 277, p. 1-25.

Van der Beek, P., X. Robert, J.-L. Mugnier, M. Bernet, P. Huyghe, and E. Labrin, 2006, LateMiocene-recent exhumation of the central himalaya and recycling in the Foreland Basin assessed by Apatite Fission-Track Thermochronology of Siwalik Sediments,Nepal.: Basin Res., v. 18.

Verdel, C., B. P. Wernicke, J. Ramezani, J. Hassanzadeh, P. R. Renne, and T. L. Spell, 2007, Geology and thermochronology of Tertiary Cordilleran-style metamorphic core complexes in the Saghand region of central Iran: Geological Society of America Bulletin, v. 119, p. 961-977.

Vernant, P., and Chéry, J., 2006, Low fault friction in Iran implies localized deformation for the Arabia-Eurasia collision zone: Earth and Planetary Science Letters, v. 246, no. 3-4, p. 197-206. doi:10.1016/j.epsl.2006.04.021.

Vernant, P., Nilforoushan, F., Chéry, J., Bayer, R., Djamour, Y., Masson, F., Nankali, H., Ritz, J.-F., Sedighi, M., and Tavakoli, F., 2004, Deciphering oblique shortening of central Alborz in Iran

using geodetic data: Earth and Planetary Science Letters, v. 223, no. 1-2, p. 177-185. doi:10.1016/j.epsl.2004.04.017

Vincent, S. J., Allen, M. B., Ismail-Zadeh, A. D., Flecker, R., Foland, K. A., and Simmons, M. D., 2005, Insights from the Talysh of Azerbaijan into the Paleogene evolution of the South Caspian region: Geological Society of America Bulletin, v. 117, no. 11/12, p. 1513–1533. doi: 10.1130/B25690.1.

Walter, R. C., 1989, Application and limitation of fission-track geochronology to Quaternary tephras: Quat. Int., v. 1, p. 35-46.

Weaver, C. E., 1989, Clays, muds and shales, Amsterm; New York, Elsevier, 819 p.

Weidlich, O., and Bernecker, M., 2003, Supersequence and composite sequence carbonate platform growth: Permian and Triassic outcrop data of the Arabian platform and Neo-Tethys: Sedimentary Geology, v. 158, no. 1-2, p. 87-116. doi: 10.1016/S0037-0738(02)00262-2.

Whipple, K. X., and Meade, B. J., 2004, Controls on the strength of coupling among climate, erosion, and deformation in two-sided, rictional orogenic wedges at steady state: Journal of Geophysical Research, v. 109, F01011. doi:10.1029/2003JF000019.

Willett, S. D., 1999, Orogeny and orography: The effects of erosion on the structure of mountain belts: Journal of geophysical research, v. 104, p. 28957-28981.

Yamato, P., Kaus, B. J. P., Mouthereau, F., and Castelltort, S., submitted, Dynamic constraints on crustal-scale rheology from the Zagros Mountains: Geology.

Zhang, Z., Wang, H., Guo, Z., and Jiang, D., 2007, What triggers the transition of palaeoenvironmental patterns in China, the Tibetan Plateau uplift or the Paratethys Sea retreat?: Palaeogeography, Palaeoclimatology, Palaeoecology, v. 245, no. 3-4, p. 317-331. doi: 10.1007/s00376-006-0258-0.

Ziegler, M. A., 2001, Late Permian to Holocene paleofacies evolution of the Arabian Plate and its hydrocarbon occurrences: GeoArabia, v. 6, p. 445 – 504.

Zijderveld, J. D. A., 1967, A.C. demagnetization of rocks: Analysis of results. In Methods in Paleomagnetism (eds D.W. Collinson, K.M. Creer & S.K. Runcorn): Elsevier, A mesterdam, p. 254-286.

Annexes

I. Concepts and methodology of Magnetostratigraphy

I-1. Nature and Origin of Earth's magnetic field

Earth's magnetic field is a magnetic dipole, with the magnetic field N pole near the Earth's geographic north pole and the other magnetic field S pole near the Earth's geographic south pole. The cause of the field can be explained by dynamo theory. The geomagnetic field is generated by convection currents in the liquid outer core of the Earth which is composed of iron, nickel and some unknown lighter component(s). The source of energy for this convection is not known for certain, but is thought to be partly from cooling of the core and partly from the buoyancy of the iron/nickel liquid outer core caused by freezing out of the pure iron inner core (Tauxe et al., 2010). The geomagnetic field is not perfectly modeled by a geocentric axial dipole, but is somewhat more complicated.

Vectors are specified by three parameters and in many paleomagnetic applications these are two the angles (D and I) and the strength (B) as shown in Anx I- 1b and c. The angle from the horizontal plane is the inclination I and it is taken positive downward and ranges from +90° for straight down to -90° for straight up. If the geomagnetic field were that of a perfect geocentric axial dipole (GAD) field, the horizontal component of the magnetic field BH (equation I- B) would point directly toward geographic north. In most places on Earth there is a deflection away from geographic north and the angle between geographic and magnetic north is the declination D (equation I- C). D is measured positive clockwise from North and ranges from 0 → 360°. The vertical component BV (equation I- A) of the surface geomagnetic field, is given by

$$B_V = B \sin I \qquad \text{(I- A)}$$

and the horizontal component BH by

$$B_H = B \cos I \qquad \text{(I- B)}$$

BH can be further resolved into north and east components (BN and BE in Fig. II- 1 c) by

$$B_N = B \cos I \cos D \quad \text{and} \quad B_E = B \cos I \sin D \qquad \text{(I- C)}$$

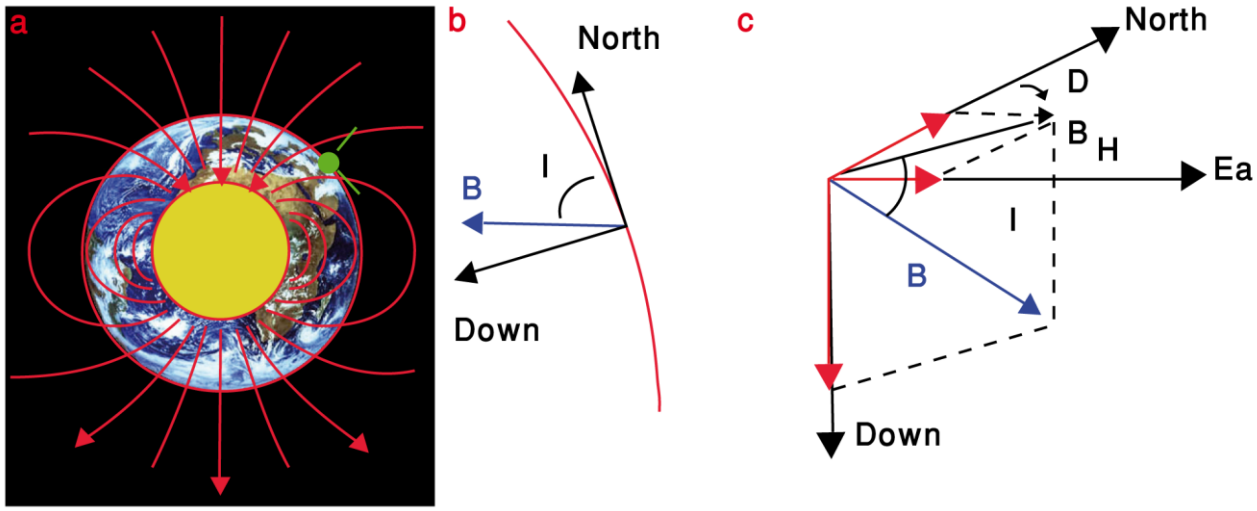

Annex I- 1: The Earth's magnetic field and its elements. a) Magnetic field lines as predicted by a simple model of geocentric axial dipole; magnetic field lines predicted from the international geomagnetic reference field from 1980 in the Earth's mantle (green) (Courtesy of R.L. Parker). The core is the source of the field and is shown in yellow; b) the specific location on the Earth's surface (I ¼ inclination angle); c) three elements of the geomagnetic field's vector: inclination angle (I), declination angle (D) and intensity, represented by the length of line B ; after (Butler, 2004; Lanza and Meloni, 2006; Merrill et al., 1996)

Paleomagnetism

Paleomagnetism is the record study of the Earth's magnetic field which preserved in various magnetic minerals through the time. The study of paleomagnetism has demonstrated that the Earth's magnetic field varies substantially in both orientation and intensity through time. Study the ancient magnetic field by measuring the magnetic direction recorded in minerals in rocks and sediments, acquired at the time of their formation (remanent magnetisation), help to determine what configuration of the Earth's magnetic field may have resulted in the observed orientation.

Normal and Reversal polarity

When the past magnetic field is oriented similar to present-day field (North Magnetic Pole near the North Rotational Pole) the strata retain a Normal Polarity. Inversely, when the data indicate that the North Magnetic Pole was near the South Rotational Pole, the strata show Reversed Polarity. Inclination (I) angle with respect to vertical is between 90° and -90° and the declination (D) angle with respect to horizontal is near to 0° in case of normal polarity and 180° in case of reverse polarity (Anx I - 2).

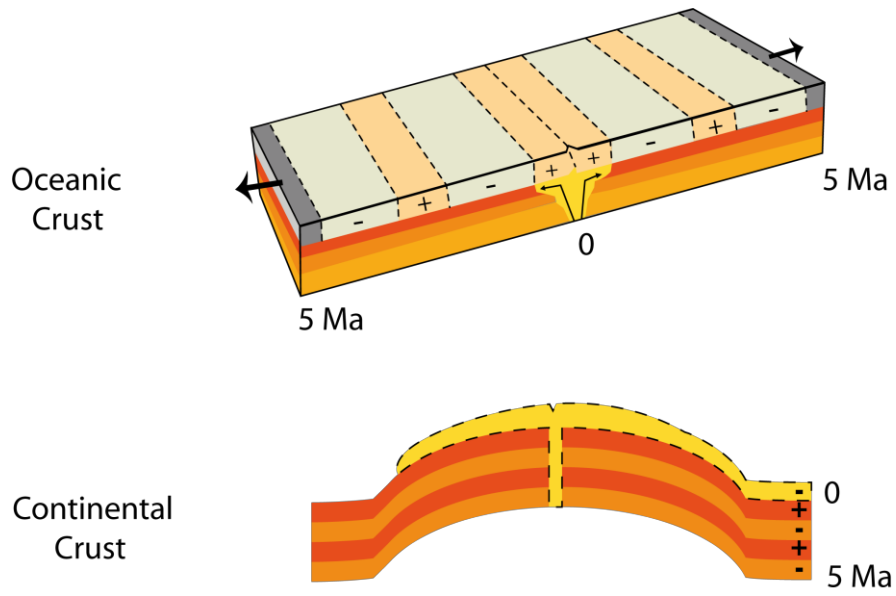

Annex I- 2: Reversals of Earth's magnetic field as it is revealed by magnetic chronological studies in oceanic and continental crusts. The Earths magnetic field has been shown to have reversed its polarity in the past: that is the magnetic field has "flipped" to flow from the North Pole to the South Pole.

I-2. Principles of remanent magnetisation

The study of paleomagnetism is possible because iron-bearing minerals such as magnetite may record past directions of the Earth's magnetic field. Paleomagnetic signatures in rocks can be recorded by four different mechanisms.

Thermal remanent magnetisation (TRM): The iron-titanium oxide minerals in basalt and other igneous rocks may preserve the direction of the Earth's magnetic field when the rocks cool through the Curie temperatures of those minerals. The Curie temperature of magnetite, a spinel-group iron oxide, is about 580°C, whereas most basalt and gabbro are completely crystallized at temperatures above 900°C. Hence, the mineral grains are not rotated physically to align with the Earth's field, but rather they may record the orientation of that field. The record so preserved is called a thermal remanent magnetisation (TRM). Because complex oxidation reactions may occur as igneous rocks cool after crystallization, the orientations of the Earth's magnetic field are not always accurately recorded, nor are the record necessarily maintained. Nonetheless, the record has been preserved well enough in basalts of the ocean crust to have been critical in the development of theories of sea floor spreading related to plate tectonics. TRM can also be recorded in pottery kilns, hearths, and burned adobe

buildings. The discipline based on the study of thermoremanent magnetisation in archaeological materials is called archaeomagnetic dating.

Chemical remanent magnetisation (CRM): In a third process, magnetic grains may be deposited from a circulating solution, or be formed during chemical reactions, and may record the direction of the magnetic field at the time of mineral formation. The field is said to be recorded by chemical remanent magnetisation. The mineral recording the field commonly is hematite, another iron oxide. Redbeds, clastic sedimentary rocks (such as sandstones) that are red primarily because of hematite formation during or after sedimentary diagenesis, may have useful CRM signatures, and magnetostratigraphy can be based on such signatures.

Natural Remanent Magnetisation (NRM); is the permanent magnetism of a rock. The most important paleomagnetic laboratory work is the isolating the characteristic component of NRM by selective removal of secondary NRM. The NRM is stripped away in a stepwise manner using thermal or alternating field demagnetisation techniques to reveal the stable magnetic component.

NRM analysis is the method which measures the intensity and direction of residual magnetism in rocks to determine their age and history. Detrital Remanent Magnetisation (DRM) show the polarity of Earth's magnetic field at the time a stratum was deposited (Anx. I - 3).

Detrital remanent magnetisation (DRM): is acquired during deposition and lithification of sedimentary rocks. In most sedimentary environments, the dominant detrital ferromagnetic mineral is magnetite. In a completely different process, magnetic grains in sediments may align with the magnetic field during or soon after deposition; this is known as detrital remnant magnetisation (DRM) (Anx. I - 3). If the magnetisation is acquired as the grains are deposited, the result is a depositional detrital remanent magnetisation (dDRM); if it is acquired soon after deposition, it is a post-depositional detrital remanent magnetisation (pDRM). pDRM processes can operate in the upper 10-20 cm of the accumulating sediment, where water contents are high.

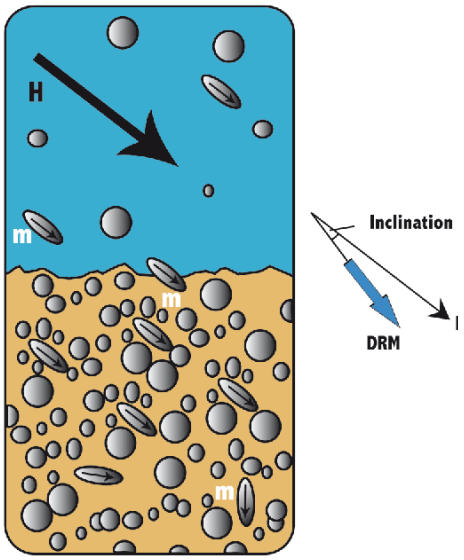

Annex I- 3: Acquisition of the Detrital Remanent Magnetism (DRM) by sediments due to the physical orientation of ferromagnetic grains with magnetic moments m, setting along the ambient geomagnetic field (H) during the sediment deposition and compaction, after (Butler, 2004; Lowrie, 2007).

The Brownian motion theory of pDRM has been quite successful in describing many properties of postdepositional detrital remanent magnetism. But success of the theory does not mean that all DRM is actually pDRM. In natural sediments, a portion of DRM may be deposit and forming by action of aligning and gravitational torques at the time of deposition. The remainder is the result of post-depositional alignment. Depositional DRM can lead to inclination error, whereas pDRM realignment tends to remove inclination error. The portion of total DRM resulting from depositional alignment as opposed to pDRM processes is thus of major concern. The ratio of depositional to postdepositional alignment depends upon a number of factors that are imperfectly understood. Some of the most important are the following:

- *Grain size*. Small grain size enhances Brownian motion of ferromagnetic particles. Fine-grained sediments have high water contents when initially deposited and slowly decrease in water content during initial compaction and consolidation. Accordingly, there is ample time (perhaps 10^2-10^3 yr) for pDRM alignment to operate. Conversely, coarse-grained sediments may have a larger portion of total DRM formed by depositional processes;

- *Rate of deposition*. Residence time for a ferromagnetic particle within the zone of high water content depends on rate of deposition. Slow rates probably enhance post-depositional alignment;
- *Bioturbation*. Sediments stirred by bioturbation acquire all detrital remanence by post-depositional processes. Bioturbation ensures high water content in the top of the accumulating sediment column, and high water content is known to enhance pDRM alignment.

It appears that inclination error of about 10° can be documented for some sediment, whereas absence of inclination error can be demonstrated for other sedimentary rocks. We cannot yet predict which rock types contain inclination error. Nevertheless, we can make some generalizations about sources of inclination error and sedimentary rocks that are most likely to contain inclination error.

- *Depositional inclination error.* Shallowed inclinations during acquisition of depositional DRM are most likely to occur in larger grain-size sediments. High deposition rate may enhance this effect. For most fine sands and smaller grain-size sediments and any bioturbated sediment, postdepositional alignment dominates and has the effect of erasing depositional inclination error.
- *Compaction.* Shallowing of inclination can be induced by compaction and is probably a larger effect for fine-grained sediments. Lithologies that undergo substantial compaction (e.g., claystone, mudstone, or sediments with muddy matrix) are probably most susceptible to inclination shallowing through compaction. Lithologies showing minimal compaction such as grain-supported sandstones might not experience compaction shallowing of inclination.
- *Deformation*. It is likely that deformation can affect inclination. Folding of sedimentary strata involves strain, and high degrees of strain might realign magnetic grains producing magnetic anisotropy.
- *Cementation*. While there are many unknowns regarding inclination error, it is clear that early cementation prevents compaction-induced inclination error because cementation essentially halts compaction. Sedimentary rocks that have been cemented soon after deposition are probably immune to shallowing of DRM by compaction.

I-3. Sampling strategy

The samples are cored with a portable gasoline-powered driller (Anx. I- 4 b) or electric-powered driller. Samples are located using hand-held GPS, and spatial orientations of samples (azimuth and dip) were measured by using a magnetic compass and a dipmeter mounted on the core axis drill (Anx. I - 4 d). The accuracy of orientation by such methods is about ±2°.

Spacing between adjacent sites usually express considerable variation determined by the availability of fine-grained strata (Reynolds, 2002). Spacing of the sample sites within a stratigraphic section depends on:

- *The type of depositional environment.* The farther away from the orogenic front, the closer the sample spacing due to generally lower rates of deposition. For instance, in Argentine Andean foreland basins, the common distance between the samples are of 15-40 meters, whereas in the Himalayan foreland of Pakistan intervals of 5-10 meters are more typical;
- *The suitability of the rocks for paleomagnetic analysis.* Mudstones, siltstones, and very fine-grained sandstones are the preferred lithologies because the magnetic grains are finer and more likely to orient with the ambient field during deposition. It is more likely that these samples will deliver a reliable paleomagnetic signal (Reynolds, 2002) but due to the scarcity of suitable lithologies the carbonates and coarse-grained sandstones also would be study.

Orientations of samples are one of the most important processes of sampling in the field and design to provide an unambiguous in situ geographic orientation of each sample (Anx. I - 5).

Annex I- 4: a,c) Delving for fresh sample point drill; b) portable gasoline-powered drill; d) compass for determining azimuth (Zagros-Iran field; 2008).

Type of samples materials

Marine sediments are a rich potential source of paleomagnetic data because biostratigraphic data can provide accurate age information and thick sections can encompass large time intervals. In addition, numerous sub-aerially exposed sections of marine sediments (especially shallow-water carbonates) are available. Although intensities of remanent magnetisation (RM) are low (typically 10^{-6} to 10^{-8} G, 10^{-3} to 10^{-5} A/m) (Zijderveld, 1967), modern magnetometers can measure these weak magnetisations quite accurately (Zijderveld, 1967). Some deep-sea cores and sub-aerial sections of marine sediments yield high-quality paleomagnetic data, while others do not. Destruction of original detrital ferromagnetic minerals and late diagenetic production of ferromagnetic minerals are basic reasons for failure to obtain useful paleomagnetic data. But oxidizing or reducing conditions vary

widely from the nominally oxidizing conditions of seawater to highly reducing conditions within sediments containing abundant organic matter.

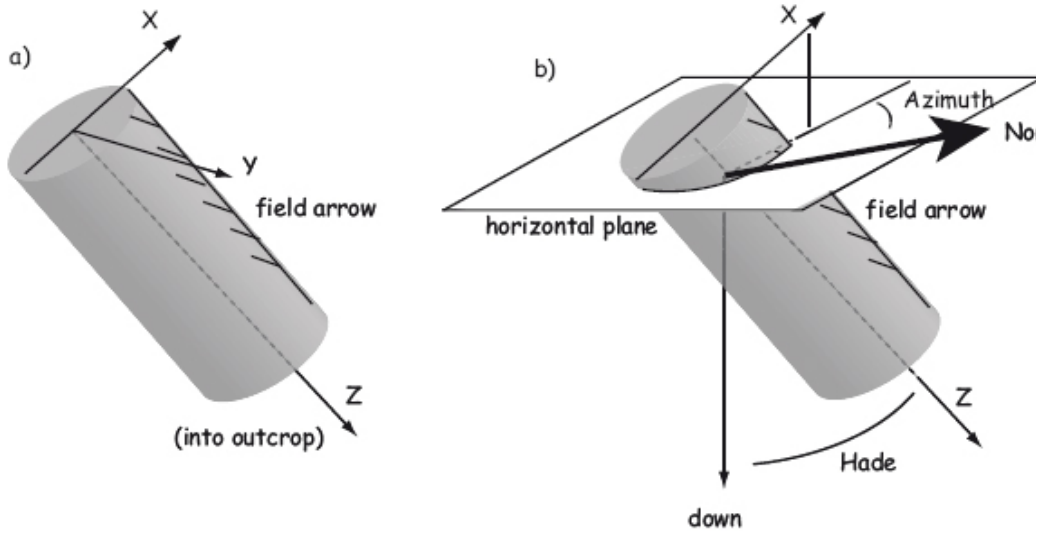

Annex I- 5: Orientation system for sample collected by portable core drill. a) Schematic representation of core sample in situ. The z axis is the core axis (positive z into the outcrop), the X axis is in the vertical plane (orthogonal to z); the Y axis is horizontal; b) Orientation angles for core samples. In the field, the angles measured are the hade of the Z axis (angle of Z from vertical) and geographic azimuth of the horizontal projection of the +X axis measured clockwise from geographic north. Laboratory measurements are made with respect to these specimen coordinate axes, after (Butler, 2004; Tauxe et al., 2009; Tauxe et al., 2010).

Hemipelagic sediments have at least 25% of coarse fraction composed of terrigenous, volcanogenic, and/or neritic detritus. These sediments are usually deposited on the continental margin and adjacent abyssal plain. Rates of sediment accumulation are typically 1 m/ kyr. The dominant detrital ferromagnetic mineral is magnetite with typical concentration 0.05% by volume. Grain size of magnetite is dominantly ≤1 mm. This magnetite is an efficient recorder of primary DRM. However, diagenetic alteration of detrital ferromagnetic minerals can take place in the upper few meters of hemipelagic sediments. If a high sedimentation rate prevents complete oxidation of organic matter prior to burial, a two-layer system develops with an oxidizing upper layer less than 1 m thick overlying anoxic sediment below. Indeed, the magnetite content of organic-rich hemipelagic muds has been observed to decrease by at least a factor of 10 in the upper meter. This decrease in magnetite content and attendant NRM are caused by dissolution of detrital magnetite with accompanying

precipitation of pyrite. If this sulfurization completely dissolves the detrital magnetite, the original DRM is destroyed.

Pelagic sediments cover about the half the oceanic area and they are primarily calcareous, diatomaceous, or radiolarian in nature. Gradual lithification and cementation take place by dissolution and recrystallization of foraminifera and coccoliths. Rates of sediment accumulation for pelagic sediments are only a few mm/ kyr, and conditions are more uniformly oxidizing than for hemipelagic sediments. Detrital magnetite and titano-magnetite constitute about 0.01% by volume. Fossil-bearing pelagic sediments are commonly reliable paleomagnetic recorders, whereas pelagic sediments without recognizable fossils tend to yield paleomagnetic records that progressively deteriorate in quality down the core (Butler, 2004). Two diagenetic processes are thought to be responsible:

- Progressive low-temperature oxidation of detrital magnetite often yields maghemite (Fe_2O_3, γ-Fe_2O_3).This process might be particularly important for pelagic red clays which common in the North Pacific. Organic matter in fossil-bearing pelagic sediments might prevent oxidation and account for the superior quality of paleomagnetic records from fossil-bearing sediments.
- Authigenic precipitation of ferromagnetic ferromanganese oxides produces a slowly acquired characteristic remanent magnetization (ChRM) that overprints the original DRM.

I-4. Demagnetisation

Alternating Field Demagnetisation (AF). In the absence of external direct magnetic fields and significant distortion in the applied AF, the sample will be "cleaned" of any remanent magnetisation of coercivity less than the peak intensity of the applied AF. This cleaning is the result of randomizing the mobile magnetic domains along the axis of the applied field. Because it is decaying, the amplitude of each half-cycle of the applied AF is smaller than its predecessor. With each half-cycle, the domains whose coercivities are less than the applied field align themselves with the field. During each half-cycle of the AF, a small percentage of these mobile domains will have coercivity greater than the following half-cycle and will therefore become fixed in direction. In this way, equal numbers of

domains will be magnetized in the positive and negative directions oriented along the axis of demagnetisation, resulting in a net zero remanent field on the sample.

AF demagnetisation is often effective in removing secondary NRM and isolating ChRM in rocks with titano-magnetite as the dominant ferromagnetic mineral. In such rocks, secondary NRM is dominantly carried by multi-domain (MD) grains, whereas ChRM is retained by single-domain (SD) grains. MD grains have coercivity force (hc) dominantly <20 mT (200 O_e), whereas SD grains have higher hc. AF demagnetisation thus can remove a secondary NRM carried by the low-hc grains and leave the ChRM unaffected. AF demagnetisation is a convenient technique because of speed and ease of operation and is thus preferred over other techniques when it can be shown to be effective (Anx. I- 6).

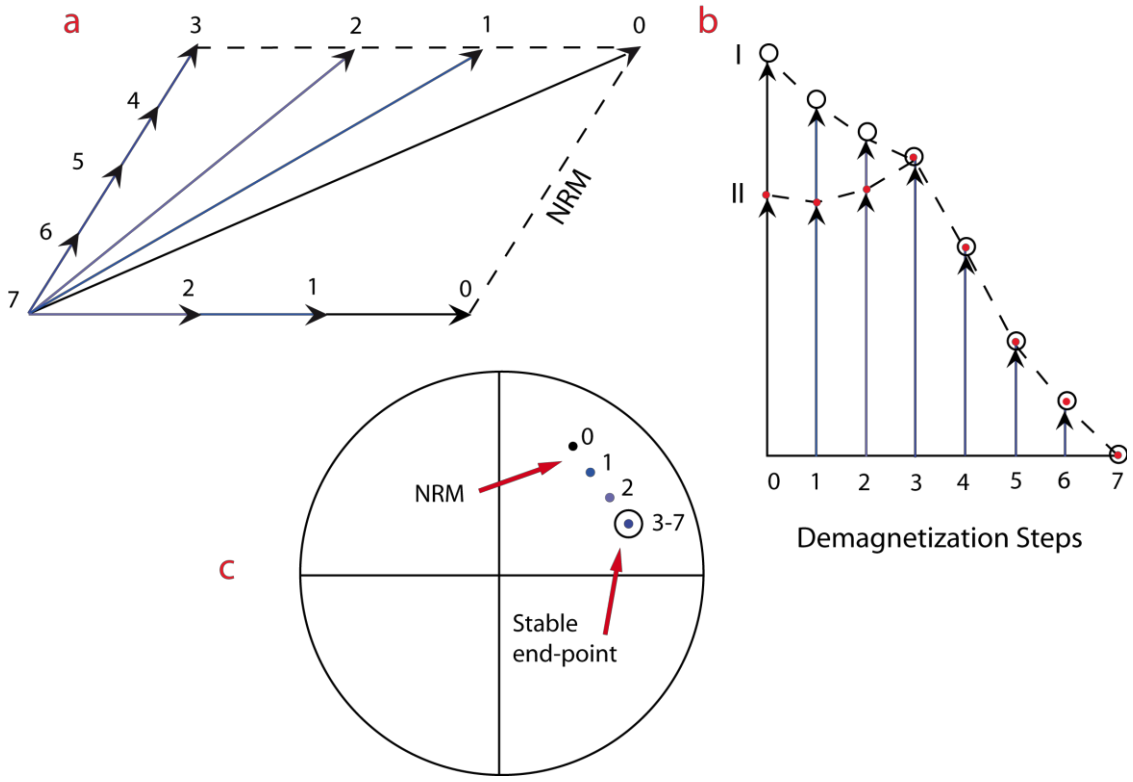

Annex I- 6: a) Stepwise demagnetisation of a NRM (Natural Remanent Magnetisation) consisting of two components with different blocking temperature or coactivity spectra; b) variation of intensity between I and II; c) directional changes of NRM on a stereogram. Numbers on points indicate successive demagnetisation temperatures in C, after (Lanza and Meloni, 2006; Lowrie, 2007).

Thermal Demagnetisation (Relaxation Time and Blocking Temperature). In order to discuss the theory behind thermal demagnetisation of a specimen, it is necessary to understand the principles of relaxation time and blocking temperature for a SD grain. Relaxation time, the time over which remanent magnetisation of an assemblage of SD grains decays, may vary over many orders of magnitude. Relaxation time for SD grains of a given material at a constant temperature depends on grain volume (v) and microscopic coercive force (hc). Grains with low product (v·hc) have short relaxation time, whereas grains with high product (v·hc) have long relaxation time. Ultimately, these properties help to define the range over which an SD grain will remain stable.

Relaxation time, however, has strong temperature dependence. For instance, relaxation time for an elongate SD magnetite grain with a length of 0.1 the age of Earth at 510°C. With decreasing temperature, this grain changes behavior from super paramagnetic (unstable; it will decay to zero very soon after removal of the magnetizing field) to stable SD at 550°C. The temperature at which this transition occurs is the blocking temperature. Between the Curie temperature (TC; temperature at which saturation magnetisation becomes zero; 580°C for magnetite) and the blocking temperature (TB), the grain is super paramagnetic. Below TB, relaxation time increases rapidly during continued cooling. SD grains with short relaxation time also have low TB. Rocks have distributions of ferromagnetic grain sizes and shapes yielding distributions of TB between TC and surface temperatures. The strong dependence of relaxation time on temperature and the transition in behavior from super paramagnetic above TB to stable below TB are critical to understanding acquisition of thermoremanent magnetism.

I-4-a. Theory of thermal demagnetisation

The procedure for thermal demagnetisation involves heating a specimen to an elevated temperature (T demag) below the Curie temperature of the constituent ferromagnetic minerals and then cooling to room temperature in zero magnetic field. This causes all grains with blocking temperature (TB) < T demag to acquire a "thermoremanent magnetisation" in H = 0, thereby erasing the NRM carried by these grains. In other words, the magnetisation of all grains for which TB < T demag is randomized, as with low hc grains during AF demagnetisation.

SD grains with short relaxation time also have low TB and can more easily acquire secondary NRM, whereas SD grains with long relaxation time are stable against acquisition of secondary NRM. Thus, thermal demagnetizers are effective in selectively erasing secondary NRM when Tdemag > TB of grains carrying secondary NRM, leaving unaffected the ChRM carried by grains with longer relaxation time (= higher TB).

Schonstedt TSD-1 Thermal Demagnetizer

The TSD-1 (Anx. I - 7) is used to provide progressive thermal demagnetisation of rock specimens by heating them to any specified temperature up to 850°C and then cooling them in a low magnetic field environment (<10 nT). External fields are attenuated by the shield assembly so that the instrument can be operated in a laboratory environment.

Annex I- 7: Thermal demagnetizer (Institute of Earth Sciences Jaume Almera, CSIC).

I-4-b. Principal topics

The part of the remanence that remains after a demagnetisation treatment has been "magnetically cleaned." The direction and intensity of the remanent magnetisation are affected. The demagnetisation procedure is repeated using successively higher values of the peak alternating field, remeasuring the remaining magnetisation after each step, until the magnetisation is reduced to zero. Suppose that the NRM of a sample consists of two components 0-7 and 3-7 (Anx. I - 6 a) with different directions and different coercivity spectra (Anx. I - 6 a). In the early stages of progressive demagnetisation (steps 0–3) the "soft" component I-II (Anx. I - 6 b) is first reduced to zero. The vector measured after each step in the progressive demagnetisation is the sum of the "hard" component, which has not yet been affected by the field used, and the residual part of the soft component. After removal of the soft component in step 3, higher alternating fields (steps 4–7) progressively reduce the hard component AB. During this stage the intensity decreases constantly but the direction remains consistent with little scatter, defining the "stable end-point" direction of the magnetisation (Anx. I - 6 c) (Lowrie, 2007).

Viscous remanent magnetism (VRM) is a remanent magnetisation that is gradually acquired during exposure to weak magnetic fields. Natural VRM is a secondary magnetisation resulting from action of the geomagnetic field long after formation of the rock. From the paleomagnetic viewpoint, this VRM usually is undesirable noise (Butler, 2004). There is some difference between VRM and DRM techniques that both of them effectively randomize the VRM component allowing the stable DRM to dominate:

- VRM may change polarity during magnetic reversals; the DRM does not;
- VRM may or may not be stronger than the DRM, so it is essential to removed it to determine the true orientation of the DRM;
- VRM removal is usually accomplished by either Thermal Demagnetisation or Alternating Field Demagnetisation.

In most cases, the purpose of the demagnetisation is to isolate the more stable magnetisation component, which is called Characteristic Remanent Magnetisation (ChRM). Hence the expression of magnetic cleaning is often used to indicate the demagnetisation process (Anx. I - 8, 9). Components with lesser stability are of interest in many applications, whilst those cancelled in the very first few steps often correspond to VRM. The direction of declination and inclination (D and I) (Anx. I - 8) of

each component is calculated by interpolating the points of the curve that correspond to its stability interval.

In the analysis of magnetisation components, the directional stability of a remanent magnetisation is demonstrated by plotting the remaining intensity after each step against the corresponding temperature or AF (Alternating field) during stepwise demagnetisation. The method was introduced by Zijderveld, (1967) (Anx. I - 8).

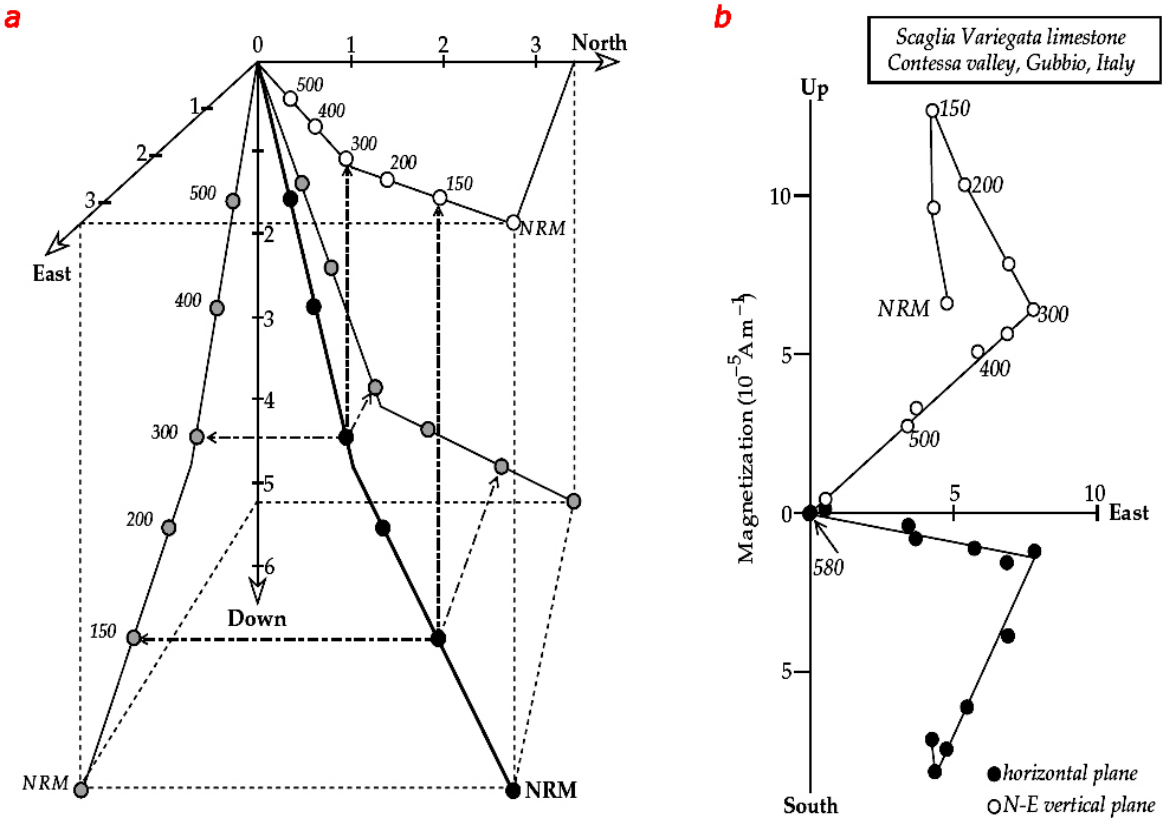

Annex I- 8: Construction of Zijderveld (1967) diagram for analyzing progressive AF (Alternating field) or thermal demagnetisation. a) Schematic diagram showing how the components of the vector remaining at each stage of demagnetisation are projected as points on three orthogonal planes (horizontal, vertical N–S and vertical E–W); b) Vector diagram for the thermal demagnetisation of a limestone sample. Magnetisation components with non-overlapping spectra of thermal blocking temperatures show as linear segments (Lowrie, 2007).

The magnetisation at each stage of demagnetisation is resolved into north (N), east (E) and vertical (V) components. Zijderveld diagram are then made by plotting the north component against the east component, and the horizontal component (north or east) against the vertical component (Anx. I - 8a). In Figure II- 8b shows three distinct linear segments on the horizontal and vertical

projections. The slopes of the straight lines represent NRM components with different directions. During demagnetisation of the overlapping components the vector diagram exhibits a curved trajectory. If the spectra overlap completely, no straight segment can be determined. In this case the sample does not have a single stable magnetisation component (Lowrie, 2007).

The ChRM direction for each sample was used to compute the virtual geomagnetic pole (VGP) latitude for each stratigraphic horizon. Because VGP latitude is computed from both inclination and declination of ChRM, it is a convenient parameter for displaying results of a magnetostratigraphy investigation. Positive VGP latitude indicates normal polarity of the geomagnetic field at the time of ChRM acquisition, while negative VGP latitude indicates reversed polarity (Butler, 2004). Paleomagnetic data (ChRM inclination, declination, VGP latitude, or some combination thereof) are plotted against stratigraphic position. These data are then used to define a magnetic polarity zonation for the stratigraphic section (Anx. I - 9) (Butler, 2004).

Confident magnetic cleaning is the greatest obstacle to magnetostratigraphic analysis. Demagnetized sample orientations from each site are averaged and field test for statistical significance. Sites that pass the test are designated Class I. Class II sites have only two surviving samples, but both exhibit the same polarity. These are used only to support adjacent sites of the same polarity (Butler, 2004).

Laboratory experiments suggest that interactions between fine-grained magnetite and clay particles may be important during compaction. During compaction, the long axes of magnetite grains are passively rotated toward the bedding plane along with the clay particles (Butler, 2004).

Another piece of valuable information comes from anisotropy of magnetic susceptibility (AMS). From AMS measurements, one can calculate the degree of anisotropy as well as the shape parameter (Jelinek, 1981).

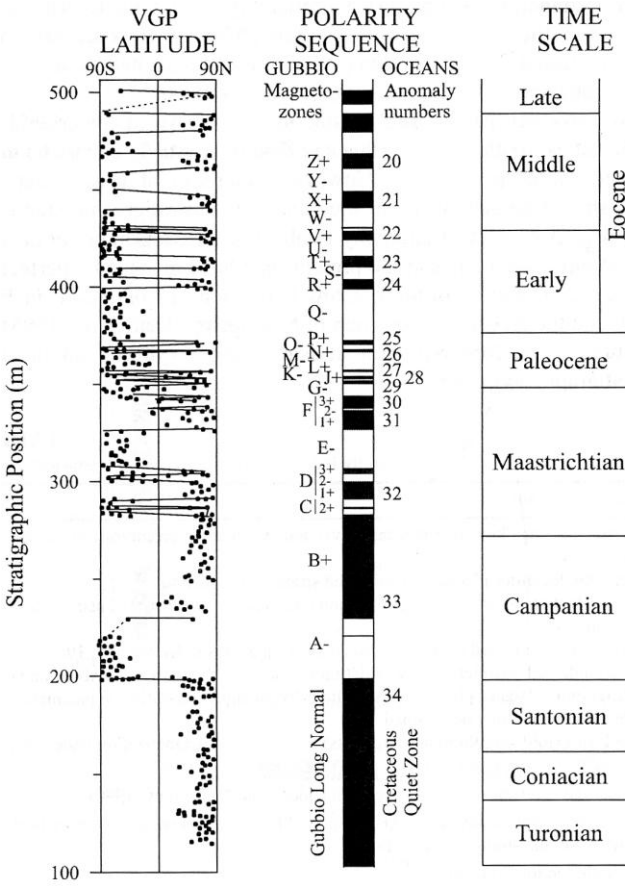

Annex I- 9: The Late Cretaceous to Eocene reversal sequence recorded at Gubbi-Italy. Normal polarity is in black (McElhinny and McFadden, 2000).

I-5. Anisotropy of magnetic susceptibility

Identification of the mineralogical sources of AMS and AMR is of fundamental importance in the interpretation of these anisotropies, and considerable effort has been expended in elucidating the relationships between mineralogy and magnetic anisotropy (Jackson, 1991). In this definition we can explain about Low-field susceptibility and Remanence susceptibility.

Low-field Susceptibility. Every mineral species present in a rock or sediment has a nonzero magnetic susceptibility. Most of the important rock-forming minerals, such as quartz, calcite, and many types of feldspar are diamagnetic, i.e., they have very low, negative susceptibilities. Many important auxiliary minerals such as hornblende, biotite, and chlorite are paramagnetic, with moderate

positive susceptibilities. Ferromagnetic minerals such as magnetite, pyrrhotite, and hematite, with very large susceptibilities, are rarely present in more than trace amounts. Because of this general inverse relationship between relative abundance and susceptibility of different mineral families, the major sources of magnetic susceptibility in rocks are quite variable, and there may be significant contributions from a number of different minerals in a single sample. The overall low-field susceptibility of a rock or sediment thus represents a summation of the contributions from all mineral species present, weighted according to their relative abundances and specific susceptibilities (Jackson, 1991).

Remanence susceptibility in contrast, magnetic remanence resides exclusively in hysteretic trace minerals, principally ferrimagnetic (titano-magnetite), maghemite, pyrrhotite, antiferromagnetic hematite and geothite. Because these are geochemically stable under different conditions, it is uncommon for more than two or three of these to occur in significant amounts in the same rock; in many rocks the magnetic remanence is carried by a single mineral. The sources of AMR are therefore relatively simple to characterize, and the degree of AMR is in principle much less sensitive to mineralogical variations than AMS. However, as noted below, grain size and grain shape effects are quite important in determining the degree of AMR, so the lithological controls cannot be completely eliminated. Remanence susceptibilities vary both with mineralogy (being generally much higher for ferrimagnets than for antiferromagnets) and with grain size. The same is true of strong-field RMs.

In the other hand we faced by Particle Anisotropy that describe the individual mineral grains in a rock or sediment are magnetically anisotropic by virtue of their shape, crystallography, and/or stress state. In the absence of an applied field, the internal magnetic structure of a particle tends to arrange itself in a way that minimizes the total of magnetostatic, exchange, and magnetostrictive energies (Jackson, 1991).

Shape Anisotropy. The internal demagnetizing field and magnetostatic energy are used to introduce shape anisotropy. A highly elongate ferromagnetic grain has much lower magnetostatic energy if magnetized along its length rather than perpendicular to its length. This is because the percentage of surface covered by magnetic charges is small when js points along the long dimension of the grain (Butler, 2004). So, for ferrimagnetic spinels, with their intense spontaneous magnetisation, grain shape is most often the major factor controlling anisotropy. In order to minimize

the total magnetostatic energy of a grain, the magnetisation orients itself in such a way as to minimize the area where magnetisation is perpendicular to the surface. This state of minimum magnetostatic energy occurs for an elongate SD grain when the magnetisation is parallel to the long axis (Anx. I - 10). For elongate MD grains, magnetostatic energy is minimized when the magnetisations of the major domains are oriented parallel to the long axis, and smaller "closure" domains have their magnetisation parallel to the surface at the grain ends. It is important to point out that susceptibility and remanence behave in very different ways in SD ferrimagnetic particles with prolate shape anisotropy (or any uniaxial prolate anisotropy).

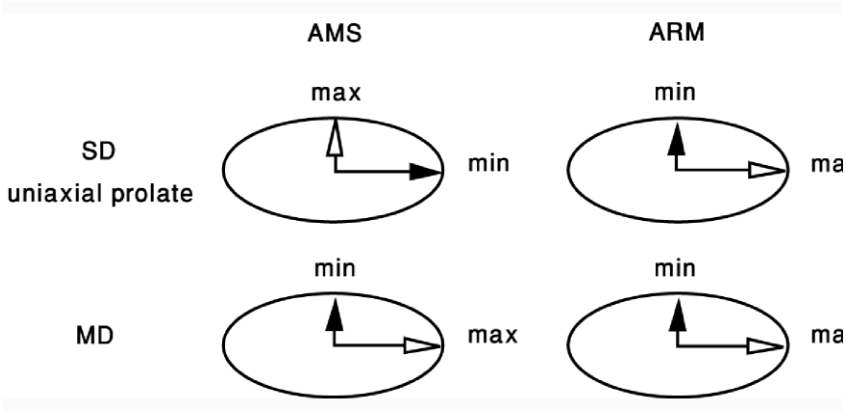

Annex I- 10 : Inverse AMS in prolate SD particles, with minimum k parallel to the long axis. In contrast, AMR in the same particles is Normal, with maximum k R along the greatest dimension (Jackson,M ; 1991).

In the absence of a magnetic field, the particle magnetisation (i.e., remanence) always orients itself parallel to the long axis of such a particle, in order to minimize magnetostatic energy. Thus these particles are only able to acquire a remanence parallel to their long axes. The remanence susceptibility is zero perpendicular to this axis and at a maximum parallel to it. In contrast, maximum low-field susceptibility of such particles is normal to their long axis; this is referred to as an "inverse" magnetic anisotropy. This arises because the applied field does not increase the net magnetisation (SD particles are magnetically saturated), but only changes its orientation.

Magnetocrystalline Anisotropy. In nearly equidimensional ferrimagnetic particles (length/width < 1.3), in ferrimagnetic pyrrhotite, and in antiferromagnetic particles (where the weak spontaneous magnetisation makes magnetostatic energies much smaller), shape anisotropy is less important than

magnetocrystalline anisotropy. Due to the geometric arrangement of atoms within the crystal lattice, and interaction between the magnetic moments of those atoms, there are particular crystallographic orientations for the magnetisation that minimize exchange energy. For many minerals, crystallography also tends to control the shape of individual particles. For example, minerals such as hematite, pyrrhotite, chlorite and biotite have a platy habit, tending to form flakes normal to the magnetically-hard crystallographic c-axis. Others tend to form elongate crystals along the magnetically-easy axis. Similarly, plastic deformation mechanisms are often crystallographically controlled. Several minerals, however, possess an "inverse" magnetocrystalline susceptibility anisotropy, related to their or deformation mechanism. Magnetocrystalline easy directions of magnetisation are crystallographic directions along which magnetocrystalline energy is minimized. An example of magnetisation along different crystallographic directions in a single crystal of magnetite is shown in Anx. I -11. Magnetisation is more easily achieved along the magnetocrystalline easy direction. The origin of magnetocrystalline anisotropy is the dependence of exchange energy on crystallographic direction of magnetisation (Butler, 2004).

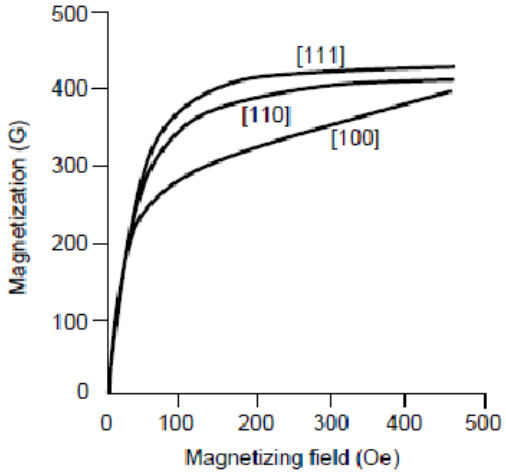

Annex I- 11: Magnetisation of a single crystal of magnetite as a function of the magnetizing field. Magnetisation curves are labelled indicating the crystallographic direction of the magnetizing field; [111] is the magnetocrystalline easy direction; [100] is the magnetocrystalline hard direction (Butler, 2004).

Stress Anisotropy. Magnetisation actually causes an unconfined material to become slightly elongated (when the magnetostriction coefficient 2> 0) or shortened (when) <0) in the direction of the magnetisation. This phenomenon is known as magnetostriction. Under differential stress, magnetostrictive energy is minimized when the magnetisation is oriented in the direction of least

compression for materials with positive magnetostriction, or when the magnetisation is oriented parallel to the maximum compressive stress for materials with negative magnetostriction. Thus both "normal" and "inverse" anisotropies may be induced by this phenomenon. However, magnetostriction is generally important only for titano-magnetites, which have positive average magnetostriction coefficients for all compositions.

I-6. Petrofabric and Remanence Anisotropy of Rocks and Sediments

The anisotropy of a rock is determined by the distribution and preferred orientations of the magnetic particles, as well as their anisotropies. An assemblage of anisotropic particles may be isotropic (if the particles are randomly oriented) or anisotropic (if the particles have a preferred orientation). Anisotropy increases with the degree of particle alignment, i.e., with petrofabric intensity. Petrofabric may be developed by sedimentary, igneous, or structural-tectonic processes.

For an assemblage of particles, the maximum anisotropy is attained when they are all identically oriented; in this state the anisotropy of the assemblage is determined by that of the individual particles. Quantitative models relating the measured anisotropy of a rock sample ($P= (K_{max}/K_{min})$ rock) to the degree of anisotropy of the constituent source particles ($\alpha = (K_{max} /K_{min})$ particle) and to the orientation distribution function (ODF) for their long axes. All of these can be applied to either AMR or AMS, but it is important to remember that (Jackson, 1991):

- AMR and AMS may have different mineralogical sources, and thus different α and ODF,
- Even when a single ferrimagnetic mineral controls both AMS and AMR, α will generally be different (larger for AMR).

I-7. Identification of magnetic minerals

To find the relation between ChRM and secondary magnetisations, it is necessary to know which minerals carry them and which are their main magnetic properties.

Magnetisation of ferromagnetic solids to saturation is most easily achieved along certain crystallographic directions, called magnetocrystalline easy directions, and the crystallographic dependence of ferromagnetism is called magnetocrystalline anisotopy. This crystallographic directional dependence arises because electron orbitals must rotate as the atomic magnetic moments

are forced to rotate. Magnetocrystalline anisotropy is a major source of stability for paleomagnetism in rocks (Anx. I- 12) (Butler, 2004).

Classic mineralogical techniques, such as X-ray diffraction, reflected light microscopy, micro-probe analysis are made difficult by the very low content of ferromagnetic minerals and by their very small dimensions, even <1 μm. They can be helpful in the case of igneous rocks, but they are seldom useful for sedimentary rocks (Lowrie, 2007).

Temperature analyses are performed from the Curie point down to a few degrees Kelvin. Temperature acts both directly on the exchange forces and on the characteristics of the crystal, modifying the lattice and thus causing a change in the magnetic properties (Lanza and Meloni, 2006).

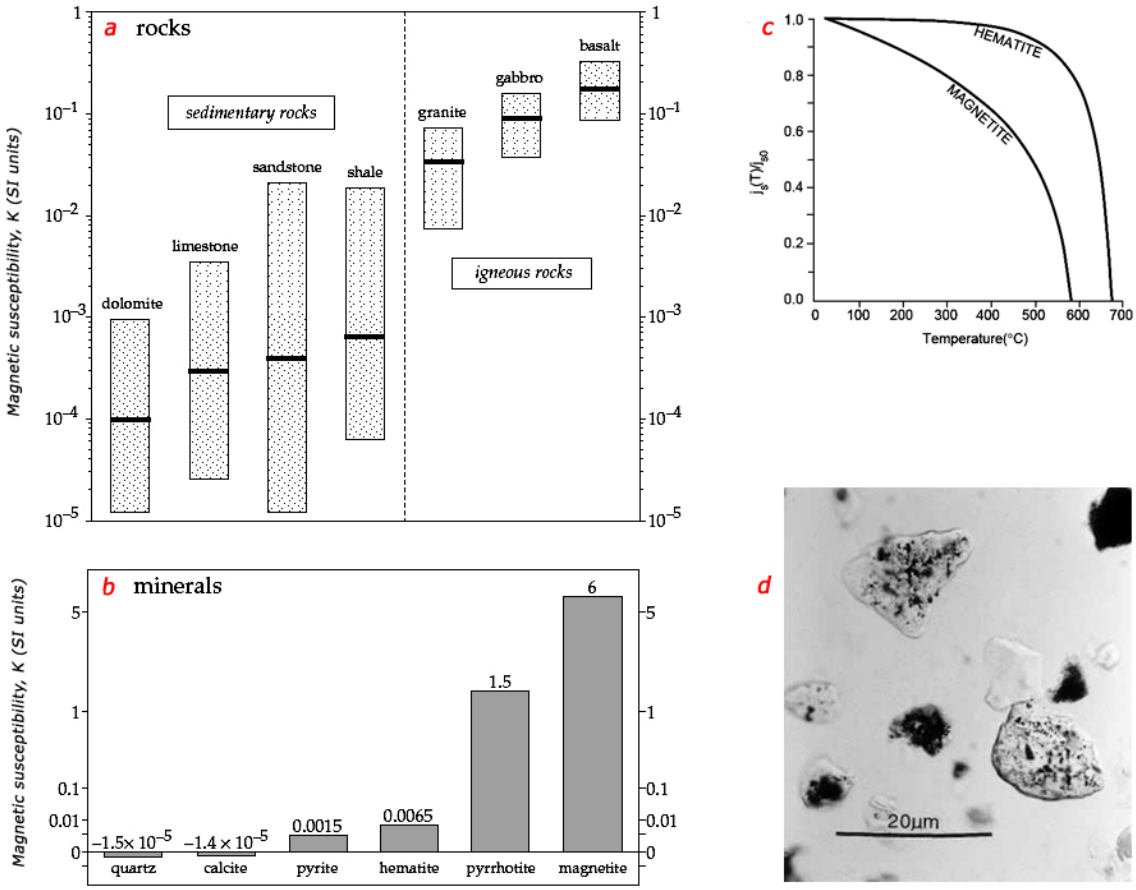

Annex I- 12: a) Median values and ranges of the bulk magnetic susceptibility of some common rock types; b) the susceptibilities of some important minerals (Lowrie, 2007); c) Normalized saturation magnetization (js) versus temperature for magnetite and hematite in CGS unit of Gauss (G). js 0 = saturation magnetisation at room temperature; for hematite, js 0 » 2 G; for magnetite, js 0 = 480 G (Butler, 2004); d) Optical micrograph of Fe-Oxide particles included within host quartz grains. Note the variable size and inclusion density within the different grains; from Quaternery pelagic ooze (Maher and Thompson, 1999).

I-8. Field test

Once the site mean direction of ChRM is determined, the paleomagnetist has to give it a geological meaning. The process is typically deductive and has to consider both the magnetic and the geological data. The field tests are similar criteria to those typical of stratigraphy and can provide indications on the primary nature of the ChRM.

Consisting and reversal test: If a single geological unit or formation can be sampled over a wide area and through a considerable thickness, in which are represented a variety of rock types with different mineralogy, and if consistent directions of magnetisation are observed, then there is good reason to believe that the magnetisation has been stable since the time of formation. This is generally referred to as the consistency test (McElhinny and McFadden, 2000). In case of sedimentary rocks or superposed lava flows, the time elapsed during the deposition of the layers or the emplacement of the flows may cover one or more polarity reversals. If the specimens collected at various levels have opposite polarity, the ChRM can reasonably be considered primary. In this case it is important to perform demagnetisation in the best possible way, since the presence of a secondary component not fully removed may introduce a systematic error. If the time interval covered by the outcrop is long enough to apply the GAD hypothesis which is the principle on which paleogeographic reconstructions rely to constrain paleolatitude (Tauxe, 2005), the normal and reverse mean directions should be antipodal (Anx. I- 13).

Fold test: The fold test is one of the most important paleomagnetic field tests. It is applied to samples taken from beds that were originally horizontal and have been tilted by later tectonic effects. In the classic fold test, the samples are taken from separate limbs of a fold. If the in-situ directions of magnetisation on the separate limbs differ, but agree after unfolding the limbs to the horizontal, then the magnetisation must predate the folding and must have been stable since that time (McElhinny and McFadden, 2000). If the directions of ChRM are grouped, the magnetisation was acquired by the rock after it was folded, it will have a uniform direction at all points of the fold; in this situation the ChRM is post-tectonic and hence secondary. If the directions are dispersed before and grouped after unfolding, it means the paleomagnetic direction in the rock is stable, it will experience the same rigid-body rotation as the tilted strata; its direction will vary around the fold. In this case, the ChRM is pre-

tectonic and hence is likely primary. Lastly, the ChRM can be syn-tectonic and it is common when the magnetisation is acquired during the tectonic event; in this case the direction of magnetisation changes around the fold but by a smaller amount than the folding so the maximum clustering of the directions occurs after partial unfolding (Anx. I- 14 A). If samples with a stable magnetisation are taken from all parts of the fold, their uncorrected directions should be smeared out. After correction for bedding tilt, the dispersion of directions should be reduced, and the directions should group around a common direction, which is the pre-folding direction of the formation. This is called a positive fold test. If the magnetisation is unstable or is due to post-folding remagnetisation, the tilt corrections will increase the scatter of the distribution of directions; this is a negative fold test (Anx. I- 14B) (Lowrie, 2007).

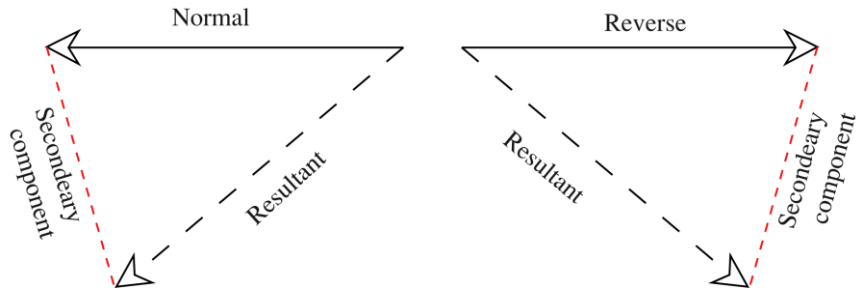

Annex I- 13: Normal and Reverse magnetisation originally 180° apart acquire a secondary component causing the result directions of magnetisation to deviate from being antiparallel (McElhinny and McFadden, 2000).

Baked contact test: If the ChRM directions in the dike and the heated country rock are similar and different from that of unbaked country rock, then the ChRM of the dike is stable and likely primary, and that of the unbaked country rock is older. When both baked and unbaked country rock have the same direction, their ChRM is secondary and acquired later than the emplacement of the dike. If even the dike shares the same direction, all lithologies were remagnetized during a major regional event. This test is particularly useful for dikes intruding a crystalline basement.

Conglomerate test: The spatial arrangement of the clasts of a conglomerate is random. If their ChRM directions are randomly dispersed, the magnetisation of individual clasts was acquired before the deposition of the conglomerate and has since remained stable. If they are similar, the magnetisation was acquired after the deposition.

Unconformity test: The unconformity test can be applied in the special case when successive zones of normal and reverse magnetisation are truncated by an unconformity in the sequence. Sedimentation ceased and erosion took place to produce the unconformity prior to deposition of the upper part of the sequence. If the polarity zones in the upper younger sequence do not match those in the lower older sequence, then the magnetisation in the lower beds is older than the episode of erosion that created the unconformity. On the other hand, if the polarity zones show continuity across the unconformity, then the sediments must carry a ChRM that postdates the younger sedimentation) (McElhinny and McFadden, 2000)

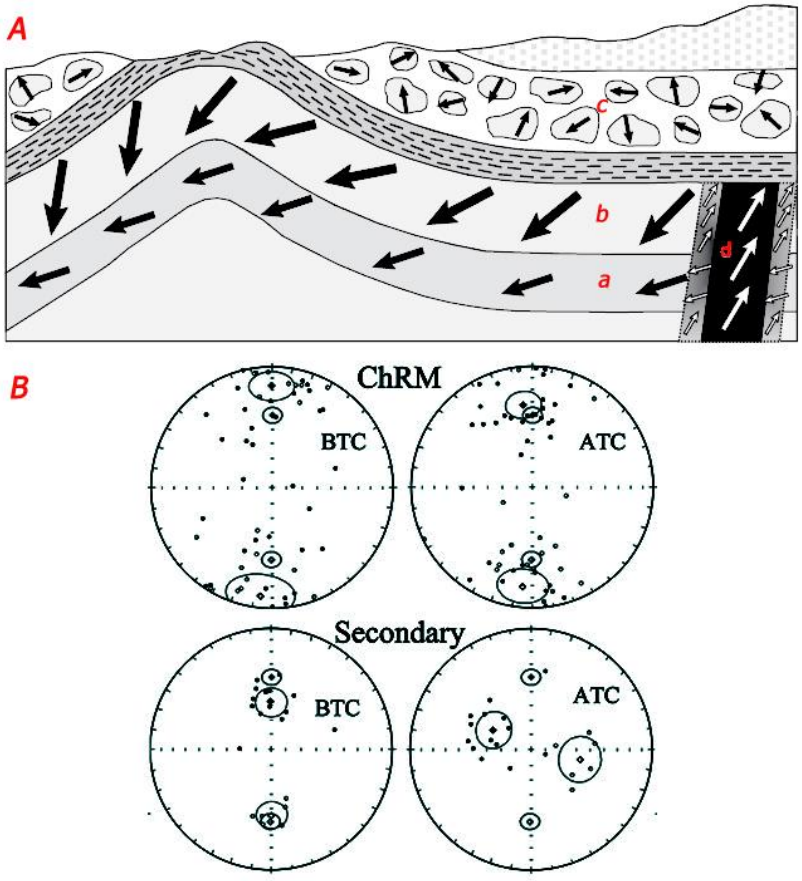

Annex I- 14: A),Paleomagnetic field tests for stability. (1) Fold test. Remanence direction varies along layer (b), and is uniform along layer a. Unfolding makes uniform the directions in b; remanence predates folding and may be primary in origin. Remanence in (a) is secondary, acquired after folding. (2) Conglomerate test. The dispersion of the remanence direction of pebbels in layer (c) which originated from rocks of layer b, strenghtens the hypothesis of primary remanence in layer (b). (3) Baked contact test. The dike (d) intruded during a reverse polarity interval and remagnetized the country rock close to its walls. Rocks of layer (b) still have the same direction of the dike, whose remanence can be inferred to be primary. Rocks of layer (a) have the same direction they have far from the dike; the remagnetisation of layer a occurred during a normal polarity interval later than the dike intrusion (Lanza and Meloni, 2006); B) Equal-area stereographic projections of the ChRM (upper panel) and component P (lower panel) directions before (BTC) and after (ATC) tectonic correction (Khadivi et al., 2010).

I-9. Magnetostratigraphy

Magnetostratigraphy is a chronostratigraphic technique which is classically used to date sedimentary and volcanic sequences. The method works by collecting oriented samples at measured intervals throughout the section. The most important geomagnetic property for stratigraphy purposes is a periodic polarity reversal of the geomagnetic field. The direction of the magnetisation of a rock is by definition its north, so magnetisation can be designated either normal or reverse polarity (Opdyke and Channell, 1996). Such reversals of the polarity have taken place many times during geologic history. They are recorded in the rocks because the rocks may record the direction of the Earth's magnetic field at or near the time of rock formation. Understanding where and when the deformation occurred is essential to build tectonic or geodynamic models. These reversals are not periodic and episodes of constant polarity vary greatly in length. The history of reversals of the Earths magnetic field is very well known for the past 200 Myr. Magnetostratigraphy involves measuring the pattern of reversals in a sequence of rocks. This yields a unique fingerprint, or "barcode", of reversals that can be matched to known reversal records elsewhere. This fingerprint can be used to date rocks and in correlating different rock sequences.

The direction of the remnant magnetic polarity (ChRM direction for each sample after corrected for tectonic effects) is used to compute the virtual geomagnetic pole (VGP) latitude for each stratigraphic horizon. Because VGP latitude is computed from both inclination and declination of ChRM, it is a convenient parameter for displaying results of a magnetostratigraphy investigation. A positive VGP latitude indicates normal polarity of the geomagnetic field at the time of ChRM acquisition, while a negative VGP latitude indicates reversed polarity.

The VGP latitudes allow determination of magnetic polarity zones in the stratigraphic succession, the term “zone” being used to refer to a particular rock stratigraphic interval. This is now common (and well-advised) practice in magnetostratigraphy. The observed paleomagnetic data (ChRM inclination, declination, VGP latitude, or some combination thereof) are plotted against stratigraphic position. These data are then used to define a magnetic polarity zonation for the stratigraphic section. By determination the biostratigraphic zonations of stratigraphic sections, the stratigraphic position of various geologic time boundaries are well known. The placement of geologic time boundaries within the pattern of polarity intervals thus can be determined.

I-9-a. The geomagnetic polarity time scale (GPTS)

Detailed accounts of the development of the Pliocene–Pleistocene GPTS are given by (Cox, 1973) and (McDougall, 1979). An excellent and detailed review of the development of the polarity time scale is given by Hailwood in 1989. Modern development of the geomagnetic polarity time scale was initiated in the 1960s following advances allowing accurate potassium-argon (K-Ar) dating of Pliocene–Pleistocene igneous rocks. In general, igneous rocks with the same age but from widely separated collecting localities were found to have the same polarity. Age and magnetic polarity determinations of increasing numbers of igneous rocks were compiled and led to the development of the first geomagnetic polarity time scales in the 0- to 5-Ma time interval.

A completely new approach to the calibration of the geomagnetic polarity timescale, which was based on planetary mechanics (Johnson, 1982). Polar magnetic reversals have been correlated with the astronomical polarity time scale and independently from the radiometric time scale. These have been used to construct an astronomical time scale for Cretaceous period to late Cenozoic time. Sedimentary cycles reflect climatic oscillations that are ultimately controlled by the Earth's orbital cycles. Gravitational interactions of Earth with the Sun, the Moon, and the other planets cause perturbations in the Earth's orbit and rotation axis. These interactions give rise to cyclic changes in the eccentricity of the Earth's orbit.

I-9-b. Biostratigraphic calibrations

When the GPTS was developed, ages of polarity chrons were predicted, testing the predicted ages of polarity chrons was a major objective of the Magnetostratigraphist. So magnetostratigraphic investigations of marine sedimentary sequences have provided detailed biostratigraphic calibrations.

The result of the magnetostratigraphic investigations can allow by biostratigraphic calibration of the geomagnetic polarity time scale. Development of geologic time scales involves association of isotopically dated horizons with the biostratigraphic zones. There are numerous geologic time scales because evaluating these absolute age calibrations is complex. The process of developing a geomagnetic polarity time scale invariably requires the choice of a geologic time scale.

I-9-c. Sediment accumulation rates

Perhaps the most powerful application of Magnetostratigraphy data is to determine the rate at which the sediment accumulated. This is accomplished by plotting the age of each reversal (in millions of years ago) vs. the stratigraphic level at which the reversal is found (in meters). This provides the rate in meters per million years which is usually rewritten in terms of millimeters per year.

Another application of these results derives from the fact that they illustrate when sediment accumulation rates changed. Such changes require explanation. The answer is often related to either climatic factors or to tectonic developments in nearby or distant mountain ranges. Evidence to strengthen this interpretation can often be found by looking for subtle changes in the composition of the rocks in the section. Changes in sandstone composition are often used for this type of interpretation.

These data are also used to model basin subsidence rates. Knowing the depth of a hydrocarbon source rock beneath the basin-filling strata allows calculation of the age at which the source rock passed through the generation window and hydrocarbon migration began (Reynolds, 2002). Because the ages of cross-cutting trapping structures can usually be determined from magnetostratigraphic data, a comparison of these ages will assist reservoir geologists in their determination of whether or not a play is likely in a given trap.

I-9-d. Regional tectonics and VGPs

Use of paleomagnetism in regional tectonics depends on the scale of the problem. In the case of a crustal block or a terrane, we have a tectonic domain which separated from a major plate and for a certain period of time moved independently on the Earth's surface (Anx. I- 15). This movement has to be fitted in the global frame of the plate motion and the paleomagnetic directions or the VGPs are compared with expected directions or VGPs, where "expected" means that they are calculated starting from an apparent polar wander (APW) curve used as a reference on the grounds of a certain geodynamic hypothesis. Limiting ourselves to the directions, we see that an inclination I different from the expected one indicates a latitudinal movement, while a discordance of the declination D indicates a rotation about a vertical axis. If both D and I are different from the expected ones, the

movement of the block can be interpreted as a rotation around a point of the Earth's surface external to the block, called Euler pole. At the local scale, i.e. within a same tectonic domain, the differences between the paleomagnetic directions are interpreted in terms of rotations, whose axes can be vertical, horizontal or variously inclined. In this case, it is important to keep in mind that local rotations do not involve the entire crust: the moving tectonic unit is freed at a certain depth by decollement levels.

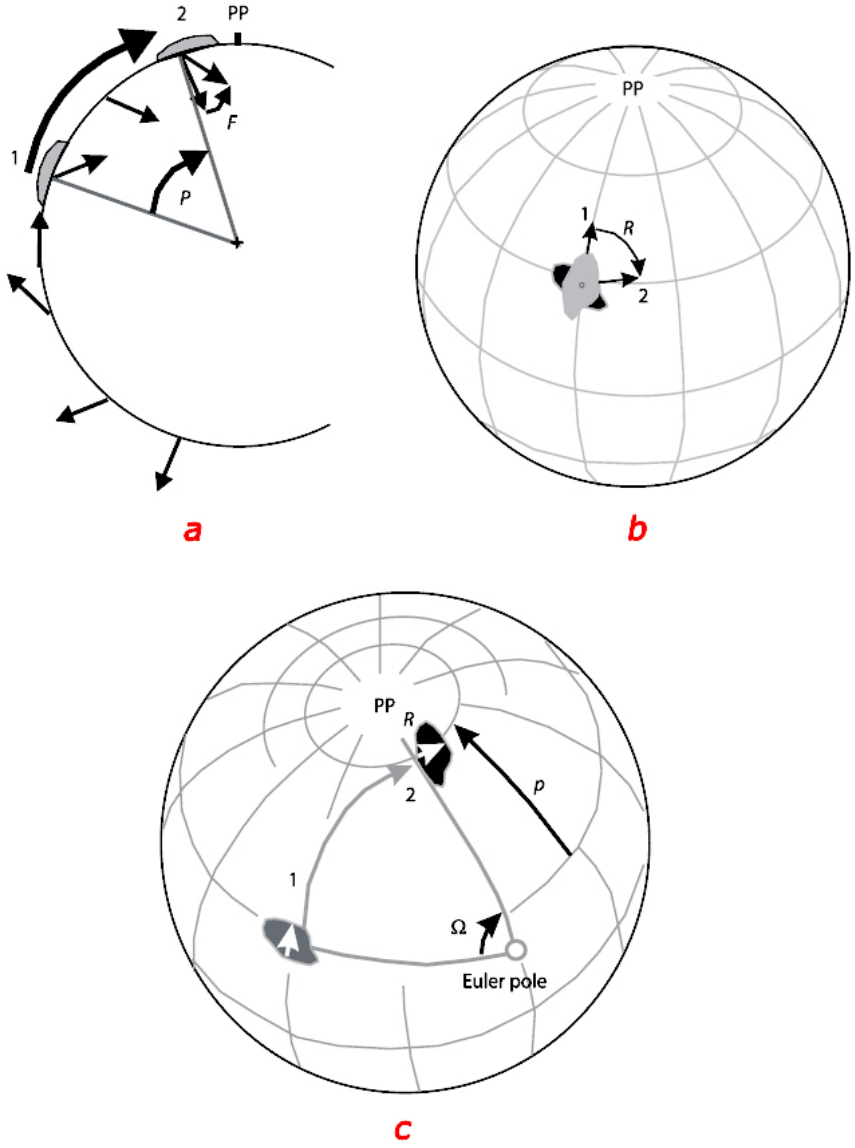

Annex I- 15: Effect of large movements on paleomagnetic directions of a crustal block. Symbols: 1=original position; 2 = present-day position; PP = paleomagnetic pole. a) Latitudinal movement. Symbols: black arrow = direction of a dipolar field with magnetic pole at PP; gray arrow= paleomagnetic direction. The block was magnetized along the direction of the field (the black and gray arrows do coincide). Poleward translation of the block by an angle P toward PP results in a paleomagnetic direction shallower than expected by an angle F; b) Rotation around a vertical axis. The block was magnetized along the paleomeridian (Arrow 1, pointing toward the pole); rotation has caused the paleomagnetic declination to rotate clockwise by the angle R (Arrow 2); c) Rotation around an Euler pole. Rotation by an angle Ω results in a poleward translation p and a rotation R *(Butler, 1992).*

I-9-e. Cenozoic terrestrial magnetic stratigraphy

One of the long-standing problems of stratigraphy has been the correlation of nonmarine sediments to marine sediments. Among the various dating methods, magnetostratigraphy is the most suitable tool for studying the age of thick Cenozoic sedimentary sequences in both marine and terrestrial paleo-environment (Sun and Zhang, 2009).

As geomagnetic polarity reversals are globally synchronous magnetic polarity stratigraphy offers the opportunity to correlate between these two contrasting sedimentary environments (Opdyke and Channell, 1996). The Plio-Pleistocene geomagnetic polarity time scale (GPTS) developed from early studies in 1963 by Cox which coupled K-Ar age determinations and geomagnetic remanence data in volcanic rocks from California.

The remanent magnetism of a rock shows the direction of the Earth's magnetic field at the time the rock formed. At irregular intervals during the Cenozoic era every half-million years in average, the north and south poles of the Earth's magnetic field swapped position. The periods of normal and reversed magnetism vary in length, so that they form a distinctive enough pattern to correlate sequences of rocks around the world, from land and sea. This is called the magnetostratigraphic scale (Hecht, 1995)

Two points should be made about the Late Cretaceous and Cenozoic polarity time scale:

- Although different approaches have been used in developing polarity time scales, the differences between recent time scales are minor. At least for the Cenozoic, we can conclude that absolute ages of magnetic polarity chrons are known to a precision of ±2 Myr. It is also important to realize that relative age determinations within a particular polarity time scale are known to much better precision than are the absolute ages. The precision of relative age determinations can approach 10^4 yr.
- A major feature of the geomagnetic polarity time scale in the Cretaceous is the Cretaceous normal polarity superchron, during which the geomagnetic field was of constant normal polarity. On the Cox (1982) time scale, this interval has absolute age limits of 118 and 83 Ma; the geomagnetic field did not reverse polarity for ~35 Myr. McFadden and Merrill (1986) present an interesting discussion of polarity superchrons, changes in reversal frequency, and possible links to mantle convection.

I-9-f. Neogene GPTS scale

Gradual closing of Tethys and formation of more distinctive latitudinal biota belts under influence of climatic cooling phases are shown in new Neogene GPTS scale. In contrast to Paleozoic and Mesozoic fauna (e.g. trilobites, graptolites, brachiopods, ammonites), invertebrate macrofossils are of no importance for constructing standard biozonal schemes in the Neogene. However, they do play an important role for correlations on a regional scale especially when other microfossil groups are rare or absent, such as in shallow-marine. A good example is the Para-Tethys where mollusc zonations have been erected for different basins to cope with endemic species evolution and distributions, which result from intermittently interrupted connections. For the eastern Para-Tethys, ecozonal schemes have been developed, which employ multiple invertebrate groups at the same time as a kind of assemblage of zones to avoid the problem of endemism and strong environmental control (Anx. I-16) (Lourens et al., 2004).

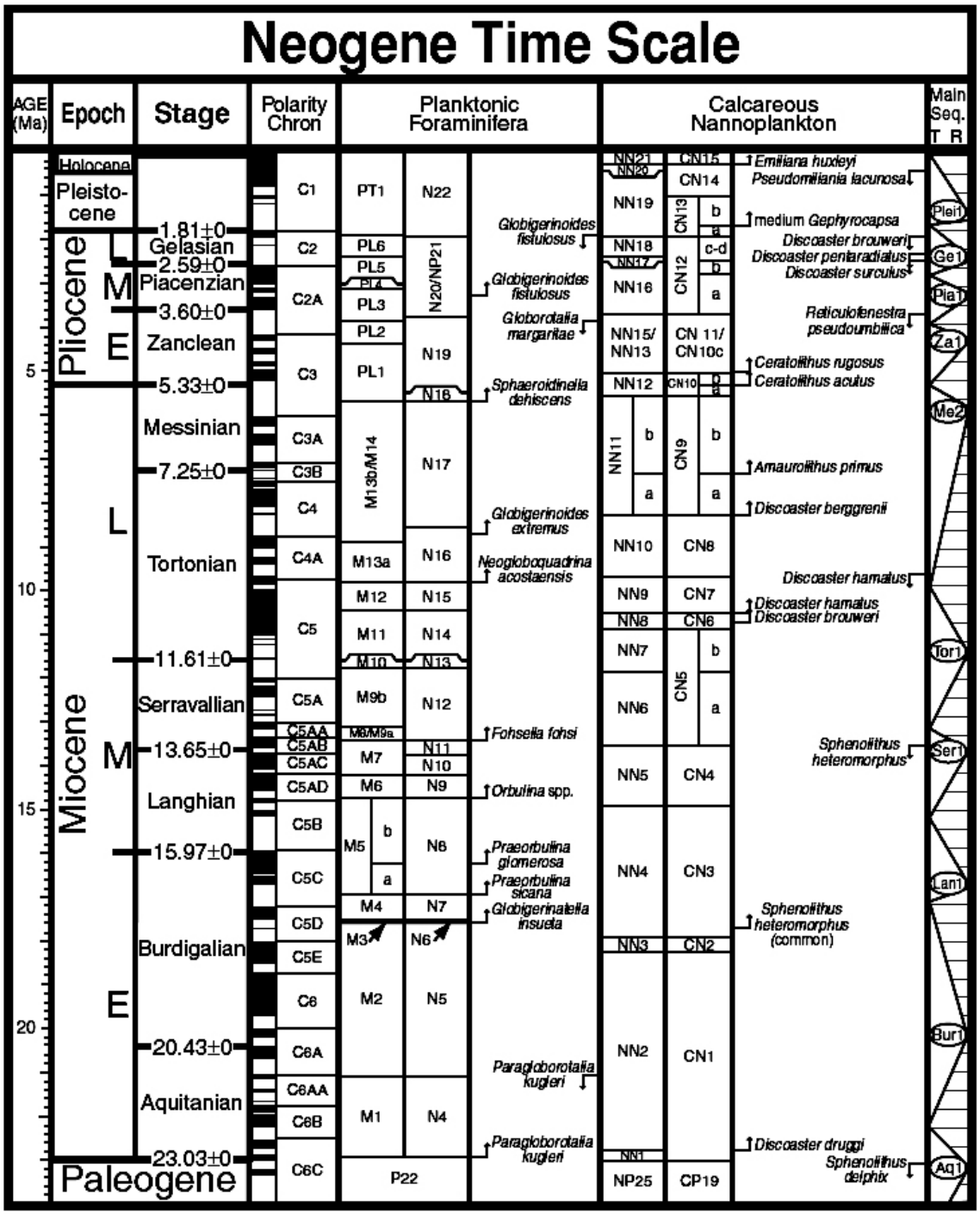

Annex I- 16: Neogene stratigraphic subdivisions, geomagnetic polarity scale, pelagic zonations, and selected datums of planktonic foraminifera and calcareous nannoplankton (Lourens et al., 2004).

I-10. Field and laboratory problems

- Eroded surface and humiliation of planet coverage is one of the problems in drilling. Base of these problems, one has to delve more than 50 cm for each sample point.
- Due to the logistic problems such as regions close to the Border of some countries, sampling intervals were up to 30 m.
- Intervals of Gypsum layer, coarse grains beds, Conglomerate and Breccia beds have conditioned the presence of some sampling gaps up to 30 m.
- Difficulty to carry the portable gasoline-powered drill or electric-powered drill, portable electric engine, water for drilling and other relative equipments incase of difficult accessible place.
- Breaking the samples, during the transport or slicing to suitable size for magnetometer. The gum that use for connecting the piece will be affected to calculate the NRM.
- Cracking or broking the mud samples in thermal demagnetizer in high temperature steps.
- The compaction and possibly deformation can often shallow the inclination of magnetisation. Thus, it appears that inclination error of about 10° can be documented for some sediment, whereas absence of inclination error can be demonstrated for other sedimentary rocks. We cannot yet predict which rock types contain inclination error (Anx. I- 3)

II.Compliment Biostratigraphic calibrations

The samples for nanoplankton dating which presented in article have been collected from marine sediments that located around the transition from the Razak to the Agha Jari formations in order to provide independent age constraints.

These nannoplanktons can be ascribed to biozone NN4, which range from Burdigalian to Langhian in age (Chapter II, Fig.- 11) i.e. 18-14.9 Ma (e.g. (Khadivi et al., 2009). This constrains the characteristic triplet formed by N4 to N6 (Anx. II-1).

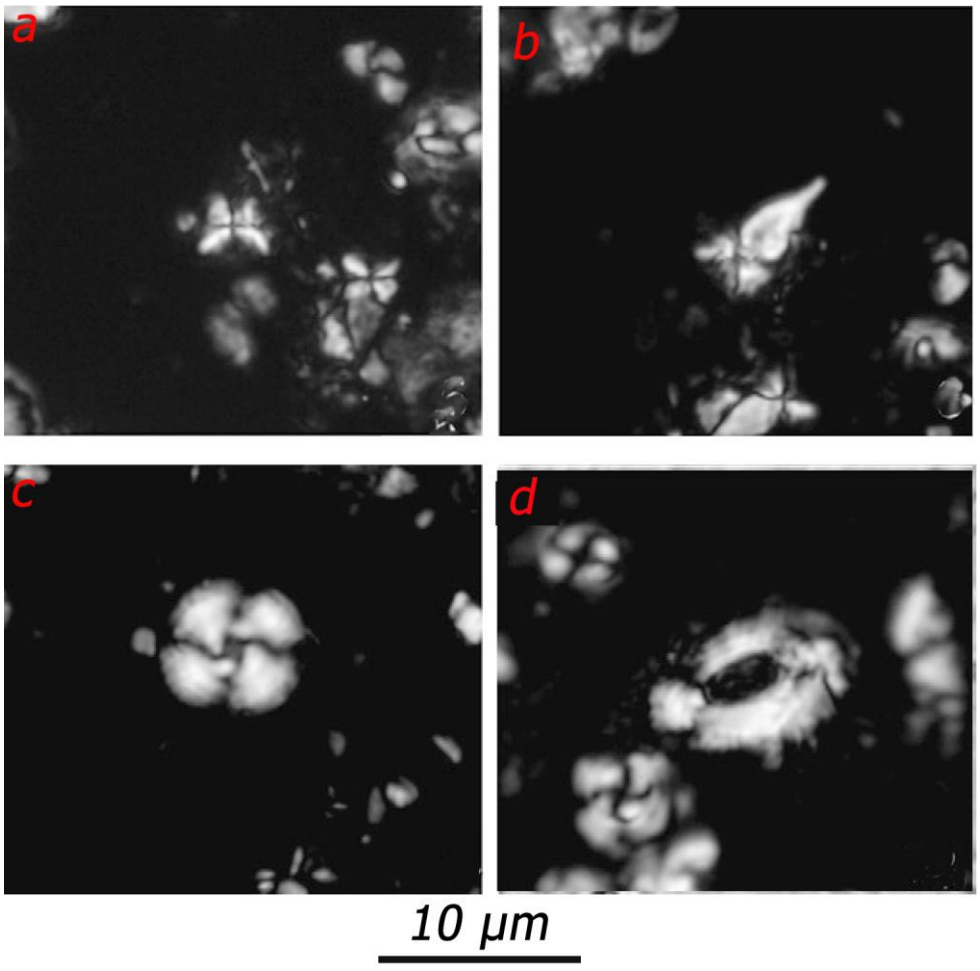

Annex II- 1: Taxa relative to the biohorizons considered in the upper and middle Miocene (all specimens _1500.X). a, b) Sphenolithus heteromorphus ; c) Cyclicargolithus floridanus; d) Helicosphaera ampliaperta (Raffi et al., 2006).

III. Concepts and methodology of Provenance study and Low-temperature thermochronology

III-1. Basic of thermochronology theory

Radiometric techniques were developed after the discovery of radioactivity in 1896. The regular rates of decay for unstable, radioactive elements were found to constitute virtual "clocks" within the earth's rocks.

Radioactive elements such as uranium (U) and thorium (Th) decay naturally to form different elements or isotopes of the same element (Isotopes are atoms of any elements that differ in mass from that element, but possess the same general chemical and optical properties). This decay is accompanied by the emission of radiation or particles (alpha α, beta β, or gamma γ rays) from the nucleus, by nuclear capture, or by ejection of orbital electrons. Alpha decay was seen only in heavier elements with atomic number 52 and greater but beta and gamma were seen in all of the elements. The product which remains after an original isotope has undergone radioactive decay. The original isotope is termed the Parent and a decay product, also known as a Daughter product, daughter isotope or daughter nuclide. Radioactive decay often involves a sequence of steps (decay chain).

The processes underlying thermochronology are the accumulation of the daughter products of radioactive decay and their subsequent diffusion through and out of the host mineral (Braun et al., 2006). The accumulation of daughter products (which determines the thermochronolgical age of a sample) results from the interplay between these two process, there exists a highly non-liner relationship between the thermal history a sample has experienced and its thermochronological age (Braun et al., 2006). Multistep radioactive decay series include, as same as the ^{235}uranium, 232thorium families. If a daughter isotope is stable, it accumulates until the parent isotope has completely decayed. If a daughter isotope is also radioactive, however, equilibrium is reached when the daughter decays as fast as it is formed. For example, ^{238}U decays to ^{234}Th which decays to ^{234}Pa which decays, and so on, to ^{206}Pb, which is stable (Anx. III- 1).

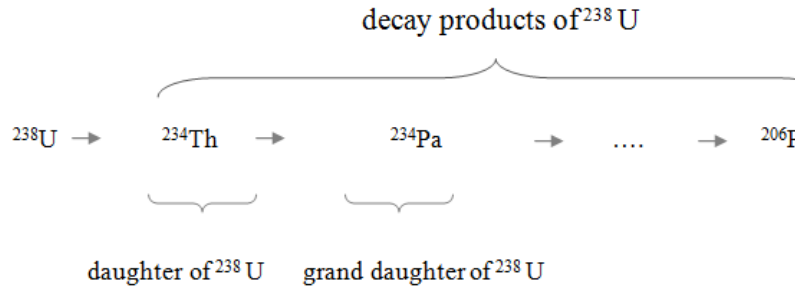

Annex III- 1: In this example, the ^{234} Th, ^{234}Pa till ^{206}Pb are the decay products of ^{238}U (Hudson and Anthony, 1998).

Radioactive decay rates

The decay rate, or activity, of a radioactive substance is characterized by constant quantities and time-variable quantities factors. Constant quantities are used for definition the time of activity:

- Half life (t1/2) the time taken for the activity of a given amount of a radioactive substance to decay to half of its initial value;
- Mean lifetime (τ) the average lifetime of a radioactive particle;
- Decay constant (λ) the inverse of the mean lifetime (equation III- A).

Although these are constants, they are associated with statistically random behavior of populations of atoms. In consequence predictions using these constants are less accurate for small number of atoms. In time-variable quantities, the mean definitions are based on activity:

- Total activity number of decays an object undergoes per second (equation III- B);
- Number of particles (N) the total number of particles in the sample;
- Specific activity (S_A) number of decays per second per amount of substance. The amount of substance can be the unit of either mass or volume (equation III- C).

These are related as follows:

$$t\,½ = \ln(2)/\lambda = \tau \ln(2) \qquad \text{(III- A)}$$

$$A = -dN/dt = \lambda N \qquad \text{(III- B)}$$

$$SA\, a_0 = -\, dN/dt \Big/_{t=\upsilon} = \lambda\, N_0 \qquad \text{(III- C)}$$

Where a_0 is the initial amount of active substance-substance that has the same percentage of unstable particles as when the substance was formed.

III-2. Apatite fission track analysis (low-temperature thermochronology)

The fission-track method, also known as spontaneous fission-track dating, is a radioisotope dating method that depends on the tendency of ^{238}Uranium to undergo spontaneous fission in parallel the usual decay process.

The high relative abundance of ^{238}U and the longer half-life with respect to fission of other naturally fission isotopes (such as ^{235}U and ^{232}Th) infer that all natural tracks in terrestrial minerals are the products of fission of ^{238}U atoms, located within the mineral itself (Fleischer et al., 1975).

The large amount of energy released in the fission process ejects the two nuclear fragments into the surrounding material, causing damage paths called fission tracks (Anx. III- 2).

In apatite, tracks are formed continuously with an approximately uniform length of ca. 16.3 mm. Upon heating, tracks are annealed or shortened to a length that is determined by the maximum temperature and the time experienced. For example, at a temperature of 110°-120°C for a period of 10^5-10^6 years, tracks are completely annealed. This characteristic allows construction of time-temperature paths of many different rock types by inverse modelling of observed FT age and confined track length data (Galbraith, 1994; Ketcham et al., 2000).

The major difference between fission track dating and other conventional isotopic dating methods is that the daughter product causes physical damage to the crystal lattice, rather than the production of another isotope (Braun et al., 2006).

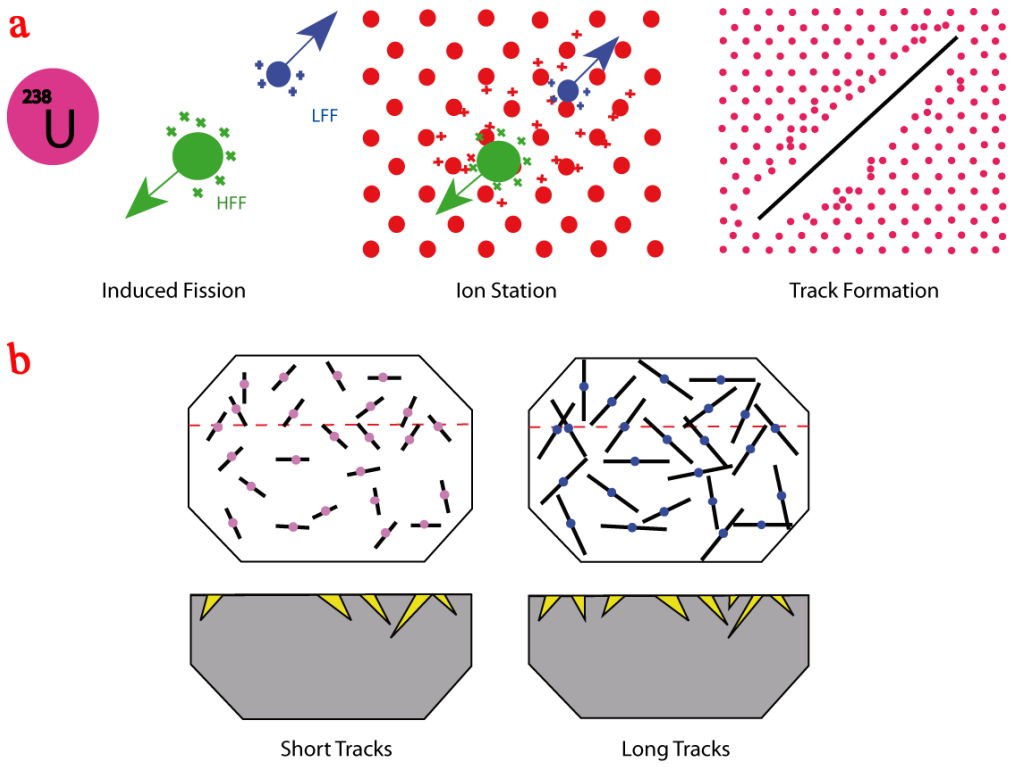

Annex III- 2: a) the three stages of track formation, natural fission of the U nucleus is an explosive event during which two highly charged particles fly in opposite direction from each other at high velocity (Fleischer et al., 1975) producing a single damage trail in the crystal that is identified as a spontaneous fission track; b) different fission track lengths.

Fission track analysis was proposed as a geological dating tool by Price and Walker (1963). They also demonstrated that a simple chemical etching procedure served to enlarge these fission tracks to optical dimensions so that they could be observed and measured under an ordinary optical microscope. This simple procedure quickly opened the way for a wide range of nuclear particle track studies in natural minerals and glasses. Spontaneous, or fossil, fission tracks provided explanations for various anomalous etch pits in apatite. The essence of a fission track age determination involves measuring the number of tracks that have accumulated over the lifetime of the mineral along with an estimate of the amount of uranium that is present. Knowing the rate of spontaneous fission decay, a geological age can be calculated (Anx. III- 3) (Gleadow et al., 2002). Age in years is calculated by determining the ratio of spontaneous fission-track density to that of induced fission tracks. Uranium content is determined by irradiating samples under a neutron flux to induce the fission of ^{235}U.

Low-temperature thermochronometric dating techniques provide a direct constraint in cooling of exhumed rocks by tectonic processes. This method is widely used to unravel thermal history of

sedimentary successions and evolution of the source region (provenance analysis, metamorphic terranes...). In fact, it is even possible to calculate different burial depths and post-depositional uplifts; so this method is ideally suited to record the cooling effects of exhumation processes that operate in the upper crust.

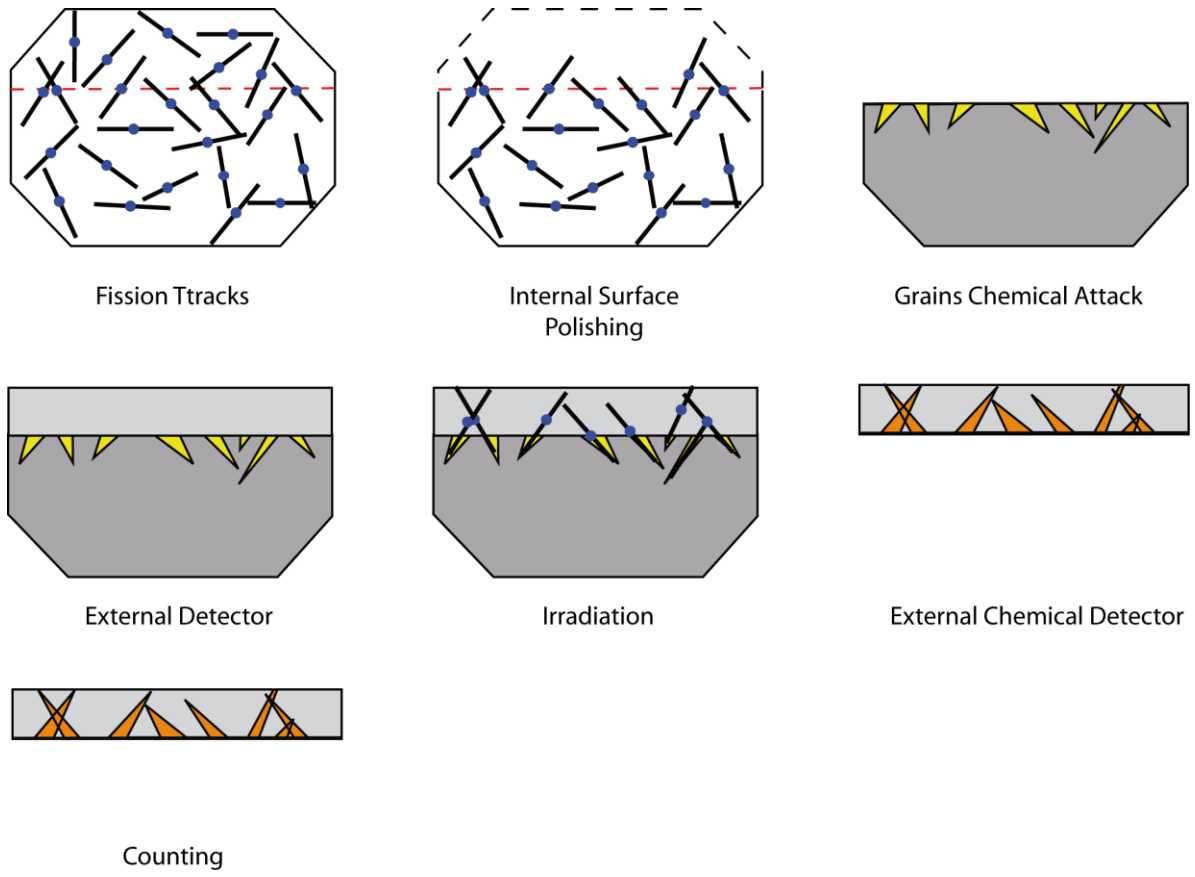

Annex III- 3: The submicroscopic tracks accumulate over time and are revealed by chemical etching of polished internal surfaces of the crystal (Price and Walker, 1963). This figure show the experimental processes for Fission track analysis (external detector method).

Several phosphate minerals have been investigated for their usefulness in geochronology and thermochronology by the fission track method. Apatite [$Ca_5(PO_4)3(F,Cl,OH)$], is one of the first minerals, among many others, to be investigated for fission track dating by Fleischer and Price (1964) which has subsequently become by far the most important of all the minerals used for dating by this method because of: (Anx. III- 4) (Gleadow et al., 2002; Wagner and Van Den Haute, 1992)

- Low temperature sensitivity;
- widespread occurrence in all of the major rock groups.

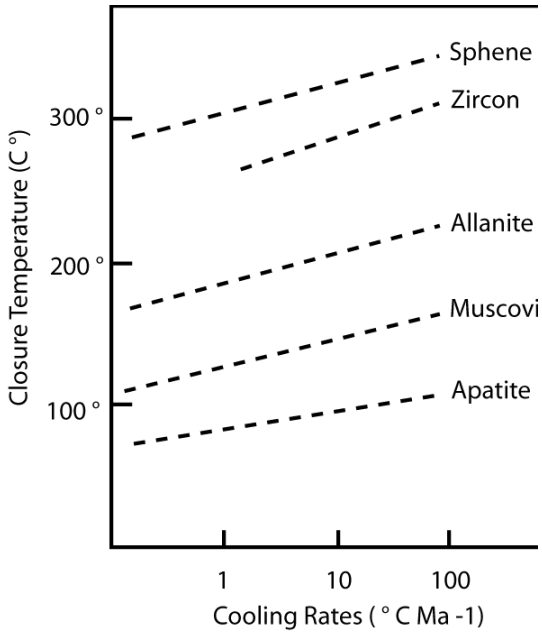

Annex III- 4: Apparent closure (annealing) temperatures of fission tracks as a function of cooling rate for a variety of minerals (White, 2003).

The sensitivity of track annealing in apatite from 60° to 120°C has resulted in the development of AFTA, which is widely used in geomorphology to constrain the cooling history of rock masses in the shallow crust. AFTA in synorogenic sediments has turned out to be a powerful tool for the reconstruction of long-term thermal and denudation histories of mountain belts (Köppen and Carter, 2000; Seward et al., 2002); as well as the rate of exhumation relateded to thermal evolution of upper crust during the mountain building process, show off the source of them sedimentary proveance (Hurford and Carter, 1991) and discrimination the source area are revealed through the reserved history in minerals. The other usage of AFTA performs by oil industry because its Partial Annealing Zone (PAZ) coincides with the oil generation window. Moreover, fission-track analysis is used for provenance studies since it is possible to date single crystal and therefore discriminate the possible presence of different source areas. In fact, suitable algorithms establish the range of temperature-time paths that are consistent with an input set of fission-track data given some essential geological constraints. Practically, the observed fission-track data (single-grain ages, track-length data) are input

together with all the known geologic information (stratigraphic age, present temperature, recognized thermal events ...), which constrain the calculation procedure. A higher resolution can be obtained by comparing thermal-history data from both the source and the depositional site. AFTA is unique in this ability to produce direct timing information.

The use of detrital apatite is limited by the degree of post-depositional heating, because minor burial and subsequent heating may cause track annealing, which can modify the original source thermal record (Garver et al., 1999). A problem with fission-track dating is that the rates of spontaneous fission are very slow and requires the presence of a significant amount of uranium in a sample to produce useful numbers of tracks over time. Additionally, variations in uranium content within a sample can lead to large variations in fission track counts in different sample sections (Bradley, 1985). Most forms of fission track dating use a calibration or comparison of spontaneous and induced fission track density against a standard of known age for reducing the error in estimations. Zeta constants have been determined for system calibration in fission track dating (Tagami, 1987). In the zeta calibration approach, the use of highly reliable age standards is essential. Several criteria should be taken into account for the selection of age standards (Hurford and Green, 1983).

I-3. Closure temperatures (CT) and fission track partial annealing zone (PAZ)

Apatite in sediments which have been heated to a maximum paleotemperature less than ~110°C, at some time in the past and subsequently cooled will contain two populations of tracks; A shorter component formed prior to the thermal maximum and a longer component representing tracks formed after cooling. In the other side, the annealing rate increases with temperature. At sufficiently low temperatures, in the so-called Total Retention Zone (TRZ), annealing is so slow that all tracks are fully preserved. Above a critical temperature, the annealing rate becomes so important that, at geological time scale, no track is preserved. The temperature range between the TRZ and the Total Annealing Zone (TAZ) is known as the Partial Annealing Zone (PAZ). Although the position of the PAZ varies slightly according to the time-temperature history of minerals, an idealized PAZ can be defined between ~60°C and ~110°C for apatite. The length of the shorter component indicates the maximum paleotemperature while the proportion of short to long tracks indicates the timing of cooling in relation to the total duration over which tracks have been retained. More complex thermal

histories result in more complex distributions of track length. If the maximum paleotemperature exceeds ~110°C, all tracks are totally annealed, and tracks are only retained once the sample cools below this temperature. The result of this effect is that in a detrital sample containing individual apatite grains may show a spread in the degree of annealing, manifested by a range of fission track ages and lengths between apatite grains. Also, apatites are more or less resistant to annealing according to their chemical composition, Cl-rich apatites being more resistant than F-rich ones. The resistance to annealing can be efficiently monitored measuring the etch-pit length parallel to the c-crystallographic axis (D_{par}) (Barbarand et al., 2003). AFT age and the track length distribution can thus be inverted, using the D_{par} annealing kinetic parameter, to model the thermal history experienced by a studied sample (Ketcham et al., 1999).

Once fission track age of a sample has been determined, it is important to define what does record the measured age. To regard of rapid cooling or more protracted cooling associated with exhumation, the concept of closure temperature has been widely adopted. The closure temperature is dependent on the activation energy for diffusion, the geometry and size of the diffusion domain and the cooling rate (McDougall and Harrison, 1988). The basic equation used to quantify the closure temperature (T_c) concept of Dodson (1973,1986), is expressed by III- D equation:

$$Tc= R/[E(\ln A\tau D/a^2)] \qquad \text{(III- D)}$$

Where: R= gas constant; E= activation energy; A= numerical constant related to the geometry and decay constant; τ = time constant with which the diffusion coefficient; D= dimension related to the cooling rate; a = characteristic diffusion size.

The basic equation III- D shows that the closure temperature is mostly dependent on the activation energy, because it is a linear function of the activation energy for diffusion relative to a dependence on the logarithm of the cooling rate and geometry of diffusion.

The concept of closure temperature is not universally applicable to all geochronological methods and there are problems with the concept. The key issues include that:

- It does not allow for variable rates of isotope exchange in the other minerals;
- It is applicable only if the cooling interval is short with respect to the half-life of the decay system;

- The diffusion rates are affected by lattice damage (radiation/defects) and compositional variation;
- It is vulnerable to the effects of non-uniform cooling rates inherited isotopes, and mineral recrystallization.

III-4. Laboratory techniques and methodology

The samples extraction process, counting and analysis have been done in the Group of Crustal Movement Quantification in the department of Interactions and Dynamics of Surface Environments (IDES) at the Institute of Earth Sciences in Paris-Sud University (France) by myself under the supervision of Jocelyn Barbarand. The laboratory of IDES is well equipped for all the procedures of sample processing and analysis.

The aim of mineral separation is to isolate individual apatite crystals from rock samples. The different steps of mineral separation processing are described in below. To avoid any artificial partial annealing of the apatites, working temperatures were never allowed to exceed 50°C during preparation.

- *Cleaning* all parts of instruments by alcohols and forced air for wiping from other samples effects.
- *Crushing* the rocks in the aim to obtain rock powder. This step could be done in several steps by using a jaw crusher in purpose to reach the more amounts of the samples to the target size. It is possible by gradually reducing the spacing of the jaw.
- *Sieving* the sample powder and retain the grains 0.4 mm. Grains from within this size interval were used for dating.
- *Washing* with water, to produce a preliminary separation, removing fine dust particles.
- *Separate* heavy minerals from light minerals, using bromoform liquid characterized by density < 2.82. This procedure produces a heavy fraction with a density greater than 2.82 correspond by quartz, feldspar… This separation has been done in a suction hood for safety reasons.
- *Magnetic* separating for removing metallic minerals. Pass through the separator at increasingly higher field strengths until about 1 Amp. The final obtained grains were just few grams and contain apatite crystals concentrated in the nonmetallic grains.

- *Handpicks* the apatite grains by using a binocular microscope. The geometry of grain is one of the important factors for selection the apatite through the other final sorted grains such as zircon and gypsum (Anx. III- 5).

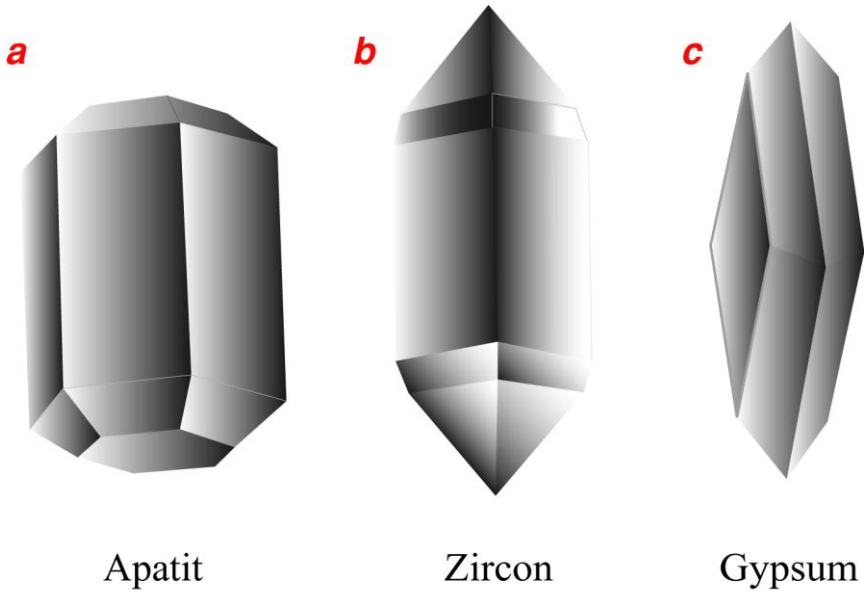

Annex III- 5: The geometry of some nonmetallic-heavy grains which could be useful in apatite handpicks step. a) the Crystallography of apatite is shown a hexagonal dipyramidal Class in all composition type of it (F, Cl, Sr, OH apatite); b) the Crystallography of zircon is shown a tetragonal-ditetragonal dipyramidal Class which this prismatic-crystal is shaped like a slender; c) the Crystallography of gypsum is shown a monoclinic-prismatic and from dimensions are thin in one direction; modified after (Mineralogy Database, 2010).

-*Etching* the grains has been done by 5% HNO_3 for 20 seconds at 21°C and the muscovites, which were used as solid state track detectors, were etched by 48% HF for 20 min at 24°C. All etchings were stopped by running water.

- *Resin* coverage of the selected grains.

- *Polish* the sample using the adhesive-backed paper (Anx. III- 6).

- *Irradiation* with muscovite (mica) external detectors standard. The samples were irradiated in radiation center of Orphée reactor at CEA-Saclay (French) and Garching researching reactor in Munich (Germany). Thermal neutron fluence was monitored using Corning CN-5 glasses and is equivalent in both irradiation conditions and is 5.1015 neutrons/cm^2.

- *Counting the tracks and measuring the* D_{par} were carried out with a Leica DM LM optical microscope which fitted with a digitizing tablet and mobile stage and the AFT Solve software.

Annex III- 6: Process and laboratory equipments of apatite fission track analyses in Paris-Sud University.

III-4-a. Principles and dating methods

In terms of analytical procedure for age determination, two techniques have been developed: the population and external detector methods.

External detector method (EDM) has the distinct advantage that data are recorded on an individual crystal basis such that sum of measured spontaneous (N_s) and sum of induced tracks (N_i) are derived from the same concentration of uranium. A major advantage of the external detector method is that grains or crystal can be dated individually.

Muscovite is a very suitable reference material because of the ease with which the tracks can be etched and recognized in the plane and because this plane exhibits an etching efficiency close to unity due to its extremely low Vs (Anx. III- 7) (Wagner and Van Den Haute, 1992). By counting the number of induced tracks in the mica, the uranium (or parent) concentration of the mineral is estimated, whereas by counting the number of spontaneous tracks in the mineral, the concentration of the daughter product is estimated.

In this technique a single aliquot of sample is used to obtain ρ_s, by counting n crystals in an area Aj of the j^{th} crystal to give number of trace (N_{sj}). The induced track density (ρ_i) is obtained from an external detector which gives a mirror imprint of the uranium variation within each crystal enabling the derivation of N_{ij} from exactly the same area as N_{sj} (equation III- E) (Anx. III-8) (Hurford and Green, 1983).

This enables any variation within a data-set to be detected and attributed to specific grains. Thus, for the EDM method ρ_s and ρ_i are given by;

$$\rho_s = \frac{\sum N_{sj}}{\sum A_j};\ \rho_i = \frac{\sum N_{ij}}{\sum A_j} \qquad \text{(III- E)}$$

ρ_s = measured spontaneous fission-track density (number of tracks cm^2)

ρ_i = measured induced fission-track density (number of tracks cm^2)

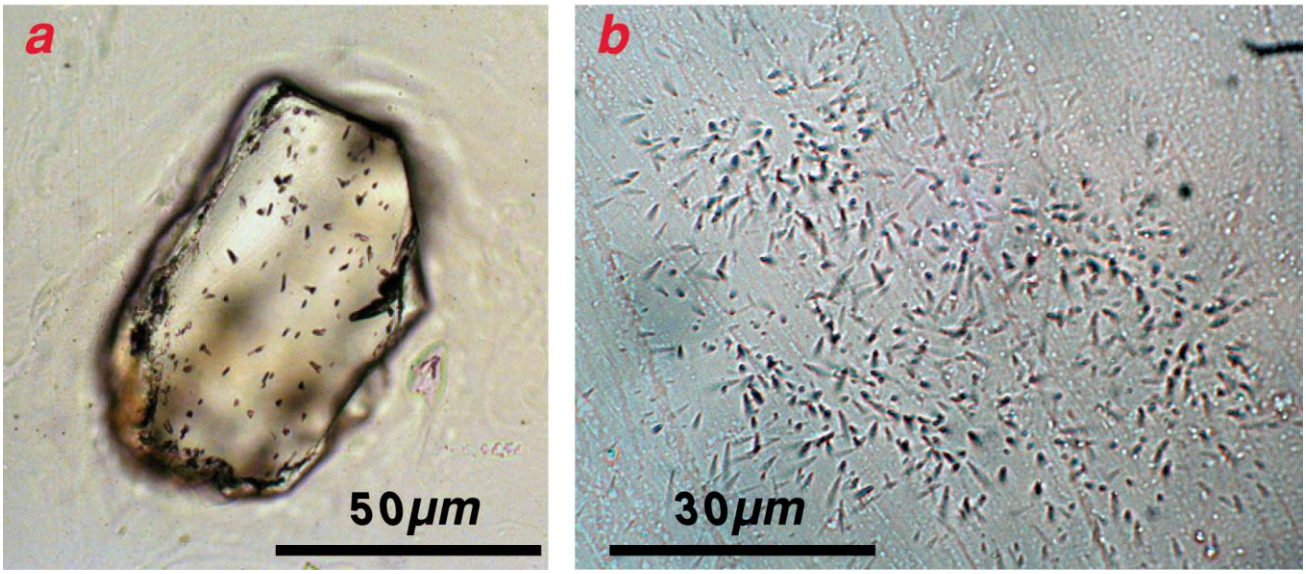

Annex III- 7: Photomicrograph; a) an apatite crystal after polishing and etched (sample IRN 3); b) an external detector (mica) after etched. The induced tracks are visible (sample IRN 15).

An advantage of the external detector method of fission track counting is the ability to determine a separate age from each grain. This capability is useful if a heterogeneous age population is suspected in the sample, as in the case of sedimentary rocks with mixed provenance (Hurford and Carter, 1991).

The spontaneous fission decay constant (λ_f) was a major problem for the age equation. Several factors such as decay constant, etched efficiency and thermal flux have been delicate to determine accurately. In 1982, Hurford and Green proposed an alternative calibration system based on independently characterised age standards. The resultant Zeta(ζ) calibration method has become the standard approach to fission track age determination (Hurford, 1990) and replaces λ_f, σ and I (equation III- F).

$$\zeta = \frac{\left[e^{\lambda d\, t^{std}} - 1\right]}{\lambda_d \left[\frac{\rho_s}{\rho_i} g\right]_{std} \rho} \qquad \text{(III- F)}$$

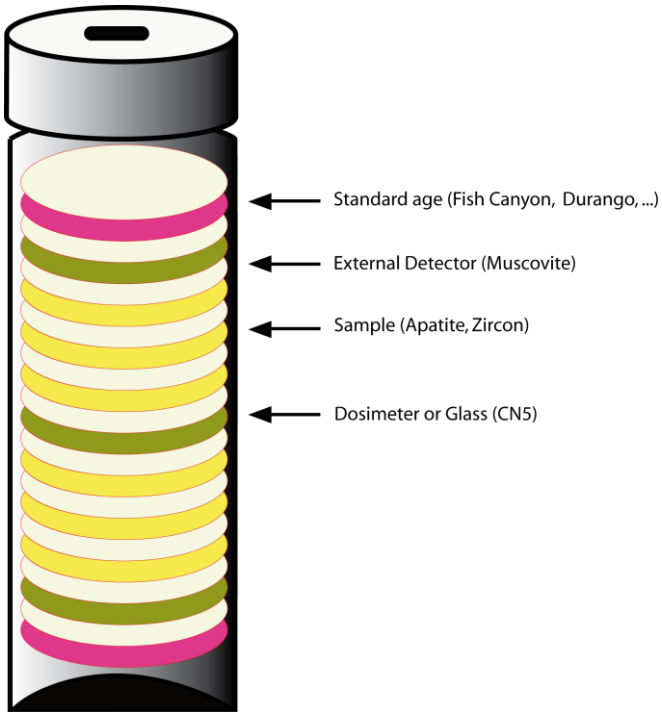

Annex III- 8: Schematic samples position in irradiation cylinder, a piece of dosimeter is put on top, middle and bottom to define the fluence cross the tube during irradiation. Dosimeters, samples and standard are cover with external detector (muscovite). The most important is to compress them well with the external detector to obtain a good contact.

The neutron fluence [(1)](Φ) is represented by the induced track density of a standard uranium glass mica detector (ρ_d). Thus, the age equation becomes (equation III- G);

$$t = \frac{1}{\lambda_d} \ln\left[1 + \lambda_d \, \zeta \frac{\rho_s}{\rho_i} g \, \rho_{\iota} \right] \qquad \text{(III-G)}$$

As well as removing ambiguity concerning the true value of the spontaneous fission decay constant for ^{238}U and determination of the neutron fluence (Φ), Zeta also subsumes, and corrects for, elements of method-based bias that relates to an individual experimenters sample preparation, observation conditions and counting efficiency.

(1) *Neutron flux* is a term referring to the number of neutrons passing through 1 square centimeter of a given target in 1 second. It is most commonly measured in neutrons/ ($cm^2 \cdot s$). The *neutron fluence* is defined as the neutron flux integrated over a certain time period and represents the number of neutrons per unit area that passed during this time (U.S.N.R.C., 2010).

An analyst has first to derive its own zeta calibration value, against a specific standard uranium glass, before fission track analysis begins.

III-4-b. Fission track dating approach

Zeta calibration factor has been determined by using the following age standards; Durango (DUR) from the Cerro de Mercado (iron mountain) Mexico (31.4 ± 0.8 Ma), Fish Canyon Tuff (FCT) from Colorado (27.9 ± 0.7 Ma). Zeta value is expressed relative to the CN5 glass with a U of 12.19 ppm.

Ages (±1σ) were calibrated by the zeta method (Hurford and Green, 1983), my zeta factor is 333.48 ± 17.21 which have been determined by multiple analyses of apatite age standards (Table III.1) (Hurford, 1990).

	N_s	N_i	N_g	ρ_s	ρ_i	ρ_s / ρ_i	ρ_d	N_d	Central Zeta	χ^2	$\rho(\chi^2)$
Dur2	*369*	*1339*	*2800*	*0.132*	*0.478*	*0.275*	*$6112*10^5$*	*6112*	*394.76*	*7.65*	*99.99*
	72	*259*	*460*	*0.157*	*0.563*	*0.278*	*$5.525*10^5$*	*5525*	*409.88*	*5.43*	*96.44*
	223	*726*	*1600*	*0.139*	*0.454*	*0.3072*	*$7.2845*10^5$*	*4368*	*281.36*	*13.27*	*58.12*
FCT	*90*	*342*	*599*	*0,150*	*0,571*	*0,2632*	*$6.683*10^5$*	*6683*	*318.19*	*4.48*	*99.89*
	109	*347*	*510*	*0.214*	*0.68*	*0.3141*	*$5.525*10^5$*	*5525*	*322.21*	*7.58*	*97.47*
	147	*526*	*567*	*0.259*	*0.928*	*0.2795*	*$6.406*10^5$*	*6405*	*314.41*	*7.65*	*99.65*
	180	*525*	*578*	*0.311*	*0.908*	*0.3429*	*$5.528*10^5$*	*5528*	*296.11*	*7.77*	*99.33*
	292	*80*	*78*	*3.744*	*1.026*	*3.65*	*$5.141*10^5$*	*5141*	*29.8*	*6.77*	*81.7*

Table III.1: Zeta calibration for this study on base of Hurford (1990).

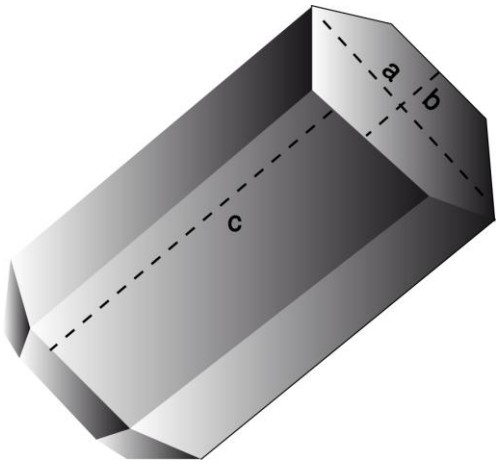

Annex III- 9: Schematic of apatite grain; Axis conventionally used for fission track measurement. To obtain a good reproducibility of the FT ages only tracks in c-axis have been counted.

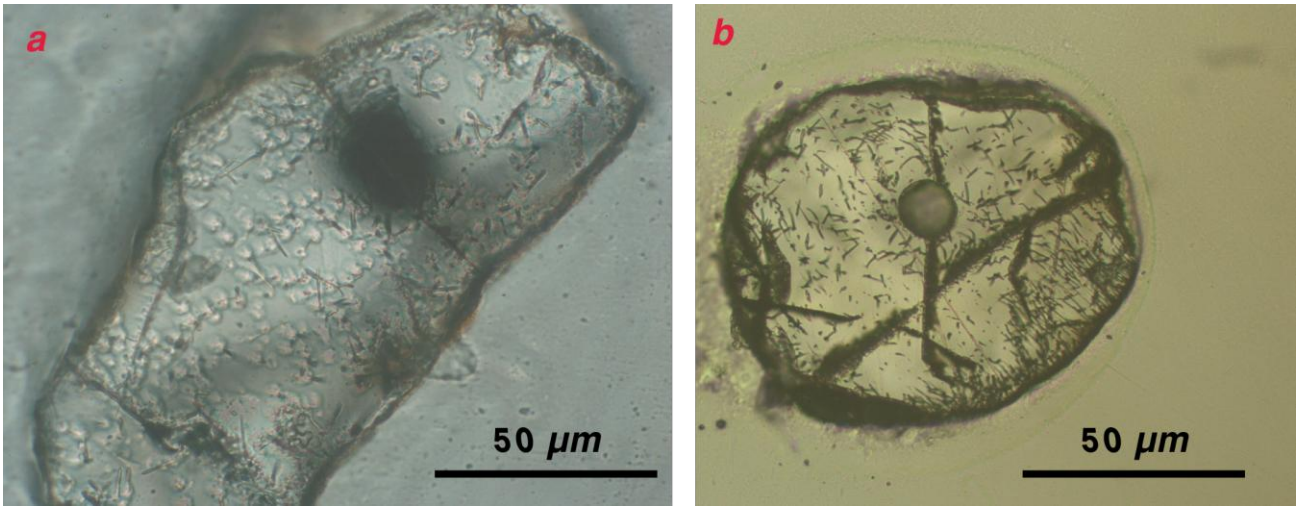

Annex III- 10: Photomicrograph of studied samples a) a-crystallographic-axis with characteristic fission track shape (sample IRN 3); b) Sometimes crystal defects can be confused with fission tracks (sample IRN 10); the repartition of the defects is a good indicator to distinguish them from FT because their repartition is random.

There are three common mean age estimation for single grain age method; the mean, pooled, and central ages. The pooled age is simply the sum of the spontaneous counts divided by the sum of the induced counts, while the mean age is the arithmetic mean of the individual ratios of spontaneous to induced tracks. The central age is a more recent development (Galbraith and Laslett, 1993) and is essentially the weighted mean of the log normal distribution of single grain ages. When the variation in the count population is consistent with a Poisson distribution, then all three age estimates are

essentially the same. When there is extra-poissonian variation, due to variable grain composition, provenance (in sedimentary samples) or simply bad experimentation, the central age offers the best measure of the spread in single grain ages.

III-4-c. Detrital populaton

Fission track results for individual detrital grains may be presented in histogram form. However, a more quantitative age estimate is possible if errors are assigned to each individual grain determination, so that the data can be presented as a probability density function (Anx. III- 11) (Hurford et al., 1984).

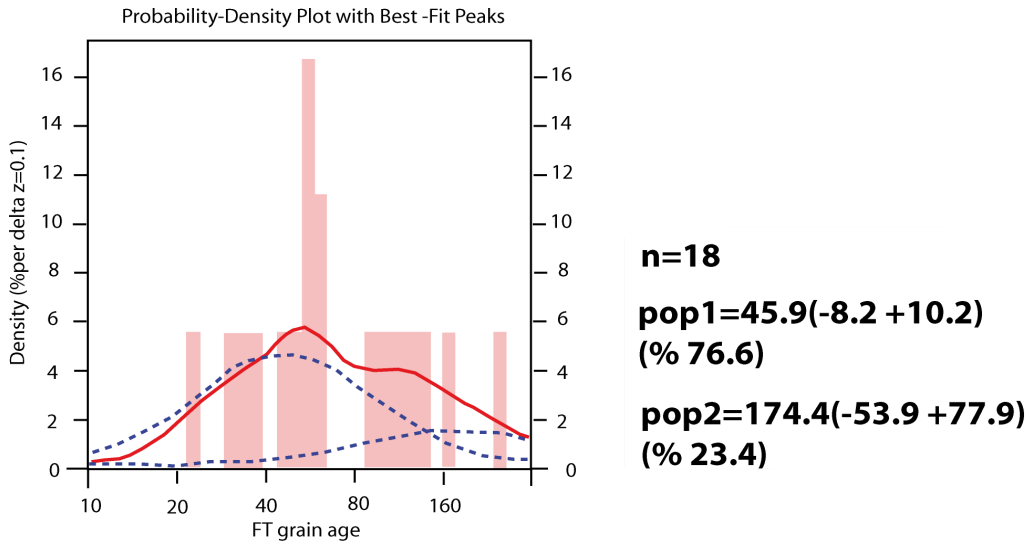

Annex III- 11: Fission track age probability-density plot of detrital apatite from study area in the Zagros-Iran. Vertical columns are shown the histogram; red color curve is the density plot of the peaks and blue color curves are the best-fit peaks.

A problem with the probability density plot is that individual data points cannot be distinguished, so that some important but small components in the data distribution can be buried under the other data. To avoid these problem, Galbraith (1988) introduced a kind of isochron diagram for the presentation of fission track data measured on individual grains of a heterogeneous sample (Galbraith, 1988). Radial plots (Galbraith, 1990) were used to graphically display single crystal ages of each sample(Anx. III- 12).

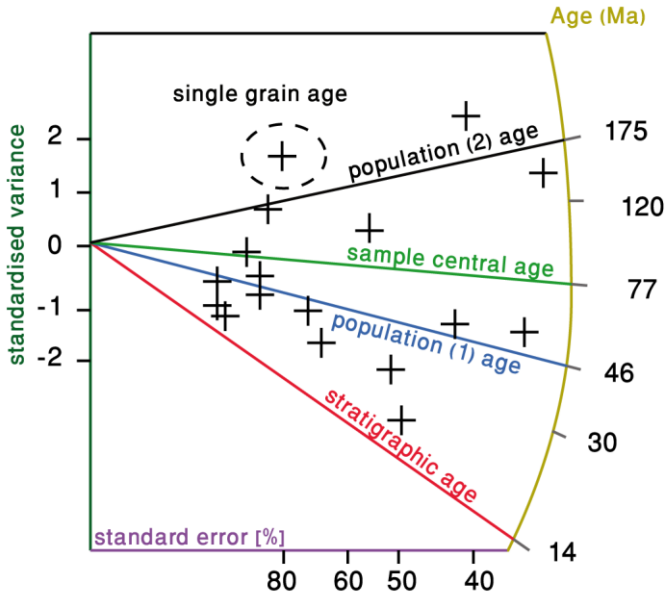

Annex III- 12: Radial plot to distinguish the burial data for each separate detrital apatite vs the stratigraphic age. The more precise data plot further from the X origin and each point has the same ±2σ error, given on the Y axis.

This diagram differs from other isochron plots used in geology because the two variables plotted are the apparent fission track age of each grain, and the standard error of each grain age. On each radial plot, the dots represent the age of an individual apatite grain (function of the number of spontaneous and induced tracks). The dots are placed on an "age line" joining the "0" on y-axis, to the age on the log-scaled graduated arc-circle to the right, which represents individual grain ages. The position of each dot along the "age-line" is defined by the x-axis value, which corresponds to the standard error of the single grain age, defined by the total number of tracks (spontaneous plus induced tracks) counted for the grain (Galbraith, 2005). Dots located closest to the arc-circle therefore have the highest reliability, because their age is defined by more counted tracks. The y-axis on the left represents the width of the single grain age-distribution, the values 1 and -1 corresponding to 1 and -1 bracketing the mean grain age. Thus, the smaller the scale on y-axis, the less dispersed the single-grain ages are. In practice, Galbraith argued that it is more convenient to normalise the average slope to the horizontal, and plot the y-axis on a log scale from +2 to –2. The age of any individual point is then determined by projecting from the zero point on the y-axis, through the data point, to the calibrated arc of ages (on a log scale).

The method of mix grain age distributions is proposed by Brandon in 1996. In this method probability density is estimated as a function of FT age τ.

The results are discriminate the populations of cooling ages (Bernet and Garver, 2005). The youngest age referre to depositional age of the sample or detecting partial resetting during low-temperature thermal events. The calculating the mean age is interesting to determine average exhumation rates.

III-4-d. Lag-time

The other usage of fission tracks data in geology context is the estimation of the lag-time. The lag-time is the time consisting of the cooling age and the time of formation of the sediment or sedimentary rock. In orogenic settings, closure of low-temperature chronometers is commonly related to exhumation-related cooling caused by erosion or normal faulting. The lag time of a dated detrital mineral, defined as the amount of time between closure and deposition, provides a measure of the rate of exhumation (Bernet et al., 2001). Suggesting no thermal event after the deposition biasing the measurement the determined intervals can be referred as the time of exhumation and the time of transportation (Bernet and Garver, 2005). According to geological periods the latter interval is negligible. So lag-time is regarded as the time passed between crossing the closure isotherm and reaching the surface. The lag-time is a function of exhumation rate in the source terrain except the active volcanic basin. If the measured age of a grain is younger than the stratigraphic position a thermal overprint had occurred and reset the thermochronological clock. The values of some concepts are available; t_c= time of closure, or time at which the apatite crosses the closure isotherm surface (~110°C) and the fission-track clock starts (applying the simplified closure temperature concept), t_e= time when the apatite arrives at the surface because of exhumation and is eroded, at this point the sedimentary cycle starts, t_d= time of deposition in the sedimentary basin. Thus the following value data will be estimated:

$t_u = t_c - t_e$= time between closure at depth and exposure at the surface

$t_t = t_e - t_d$= transport time in the fluvial system, between erosion at the surface an deposition in a sedimentary basin

$t_s = t_d - t_{present\text{-}day}$= lag time between deposition in the basin and today, that is to say, the stratigraphic age of the sediment

$l_t = t_c - t_d$= lag time, is the time required for the sample to cool, get exhumed to the surface, and then get deposited in a nearby basin (Bernet and Garver, 2005).

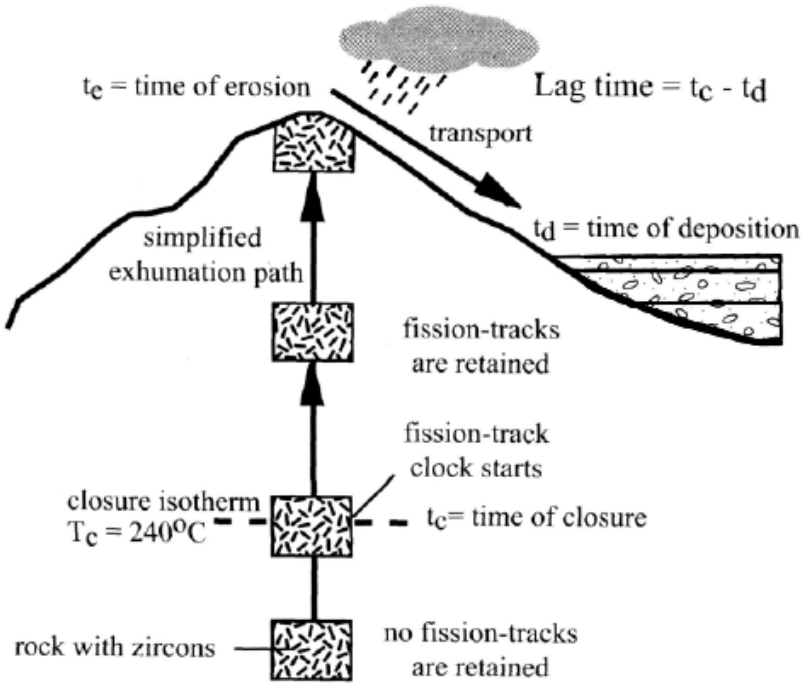

Annex III- 13: This schematic figure shows the cycle system of one detrital apatite grain in process of exhumation-erosion-deposition. The lag-time of is the time required to cool, get exhumed to the surface, become eroded and then get deposited in a nearby basin. As a rock is exhumed to the surface, the rock cools below the closure temperatures of the different thermochronometers. The time for erosion and sediment transport is generally regarded as geologically instantaneous, but this is not always the case. Lag time integrates the time between closure and the time of deposition, and mainly represents the time needed to exhume the rock to the surface (Bernet and Garver, 2005).

For determining rates of exhumation from detrital apatite fission rack ages it is necessary to know the t_t and t_s. The stratigraphic age (ts) can be obtained by techniques such as magnetostratigraphy, palinology or biostratigraphy. The fission track dating method can provide a stratigraphic age for volcanic ash layers (Crowley et al. 1989; Bernet and Garver, 2005). The other important parameter in estimation of exhumation rate is the

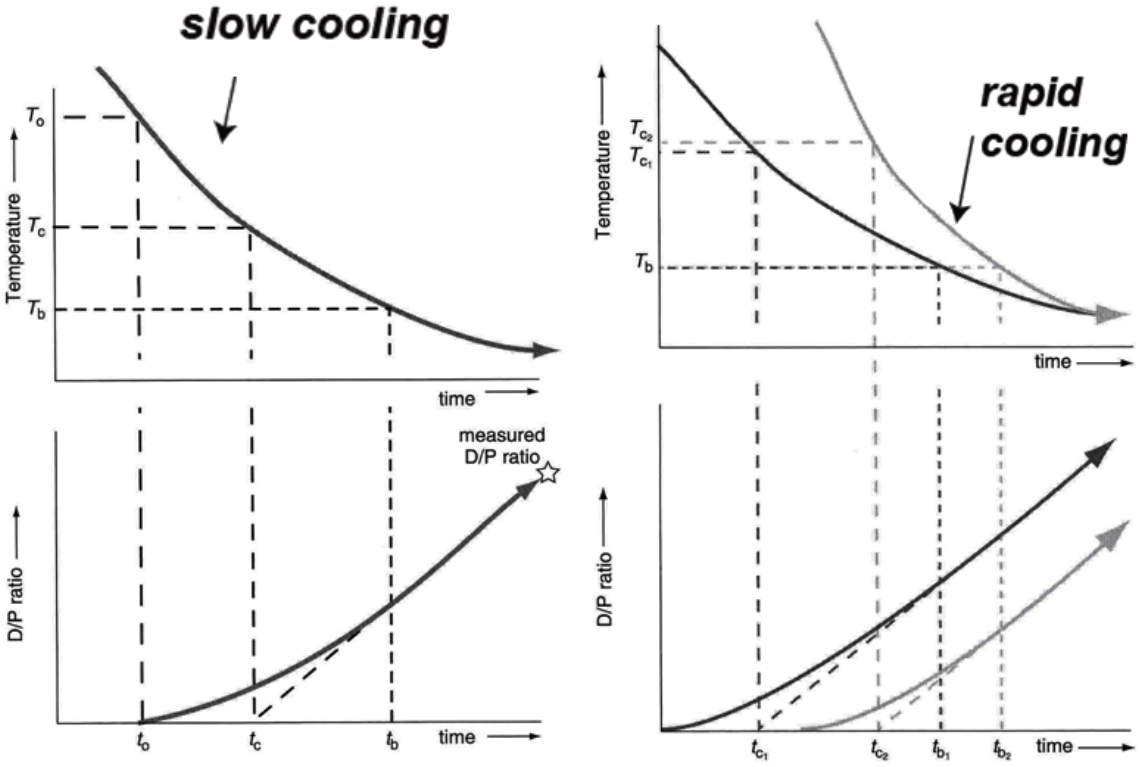

Annex III- 14: A comparison of the slowly and rapid cooling. The abbreviation which used: T_o - temperature of "open system"high diffusivity; T_c - closure temperature; T_b - blocking temperature; t_o - time of initial retention; t_c - apparent thermochronological age; t_b - time of blocking (Braun et al., 2006).

III-5. Sediment Provenance study

The sediment provenance study on base of Gazzi-Dickinson method is a point-counting technique used in geology to statistically measure the components of a sedimentary rock, chiefly sandstone. This method was developed by Dickinson and Suczek (1979) and later modified by Dickinson (1985); Dickinson et al (1983) is potentially a powerful tool for reconstructing palaeo-plate tectonic settings on the basis of the detrital composition. The main focus and most controversial part of the technique is the counting of all sand-sized components as separate grains, regardless of what they are connected to. Gazzi-Dickinson point counting is used in the creation of ternary diagrams, such as Quartz-Feldspar-Lithic diagram (Q-F-L) (Table III- 2) (e.g. McBride, 1963). Results from such analyses help in the interpretation of uplift and sediment input from surrounding source terrains.

In addition, by integrating petrographic and geochemical techniques from the sediment sorting, recycling and terrain weathering study, we can constrain temporal distribution of distinct sources. This is important for understanding the controls on the depositional systems.

Abbreviation	Explanation
Qm	monocrystalline quartz
Qp	polycrystalline quartz, including chert
Q	total quartz (Q= Qm+Qp)
Fk	potassic feldspar
Fp	plagioclase feldspar
F	total feldspar (F= Fk+ Fp)
Lv	volcanic lithic components
Ls	sedimentary lithic components
Lm	metasedimentary lithic components
Lt	lithic components (Lt=Qp+Ls)
L	total lithic components (L= Lv+ Lm+ Lt+ Chert)

Table III- 2: Framework grains (Gazzi–Dickinson point-counting method) and recalculated data.

III-5-a. Technique

To perform a point count using the Gazzi-Dickinson method, a minimum 300 points are selected from a thin section of sedimentary rock through a petrographic microscope. On each selected point, it needs to choose it as a mineral grain that is sand sized (larger than 62.5 μ) or a finer-grained fragment of another rock type, called a lithic fragment (e.g. a sand-sized piece of shale). These are then converted to percentages and used for compositional comparisons in provenance studies. Typically, only framework (non-matrix) grains are counted, or non-framework are counted and then excluded from percentages when using quartz, feldspar and lithics (Q-F-L) triangles (Anx. III- 15).

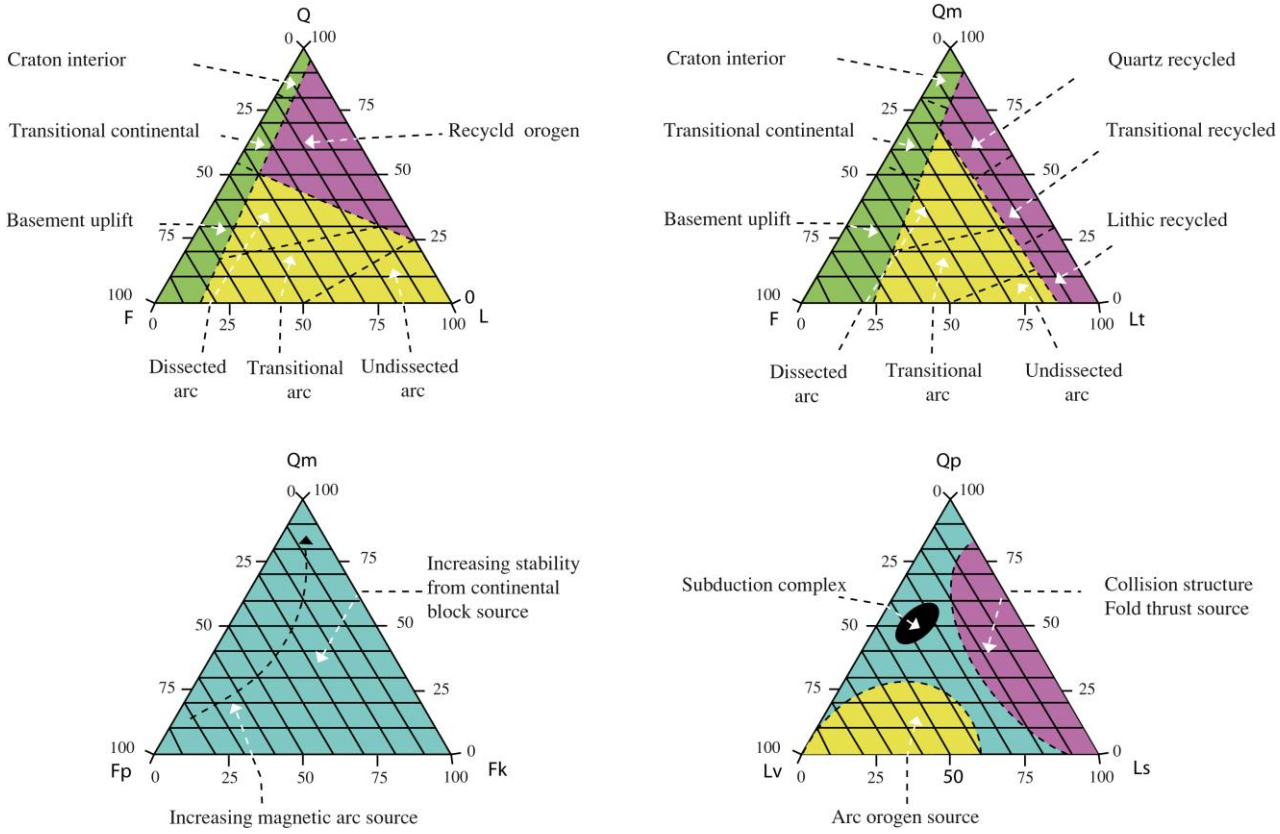

Annex III- 15: Provenance diagrams; modified after (Dickinson, 1985; Dickinson et al., 1983; Dickinson and Suczek, 1979; Fuentes et al., 2009).

III-5-b. Rock fragments

Provenance study is the most effective when using a combination of several ternary diagrams rather than relying on a single diagram, because combinations of specific end members discriminate between different grain properties, a standard combination, after Dickinson and Suczek (1979), includes Q-F-L, Qm-F-Lt, Qp-Lv-Ls, and Qm-Fk-Fp diagrams (Table III- 2).

In Anx. III- 15, the Q-F-L plot describes relative grain stability and weathering processes of the three end members, this diagram indicate transport mechanisms and source rocks. The Qm-F-Lt plot includes the polycrystalline quartz and chert fragments (Qp) in the total lithic fragment (Lt) end member. This diagram takes in account the source rock grain size. The Qm-Fk-Fp plot excludes the total lithic fragments (Lt) and proportionate feldspars in potassium feldspar (Fk) and plagioclase (Fp). This plot may differentiate between continent-derived, Fk-rich source rocks versus Fp-rich sources of

a magmatic arc. The Qp-Lv-Ls plot differentiates the principal lithic fragments by separating them in sedimentary and metasedimentary lithic fragment (Ls), volcanic lithic fragment (Lv) and polycrystalline quartz and chert fragments (Qp). It therefore distinguishes effectively between subduction-related source rocks, collision suture and fold-thrust-belt sources, and arc orogen sources. The cherts and bioclasts are added to percentage of Lithics fragments

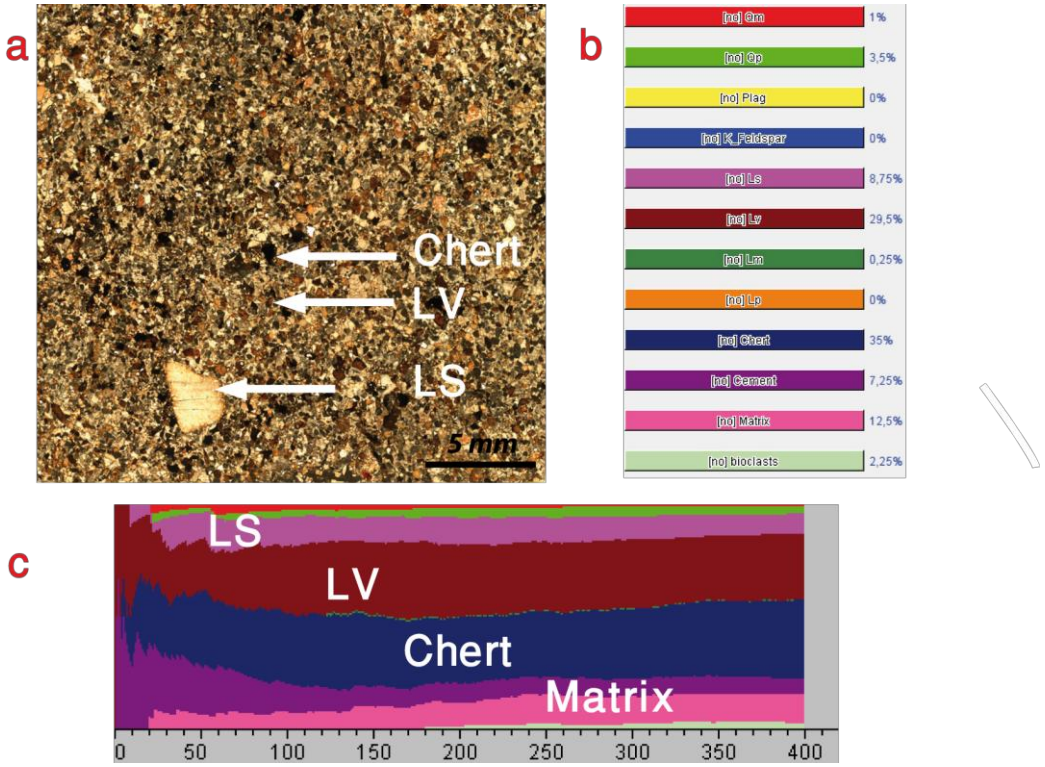

Annex III- 16: point counting process; the scanned images of thin sections were studied through the software JMicro Vision (V. 1/2) (sample IRN 1). To recognize the mono-crystalline and poly-crystalline Quartz, the numerous images of each thin section were studied at resolution of 1mm or 500µm.

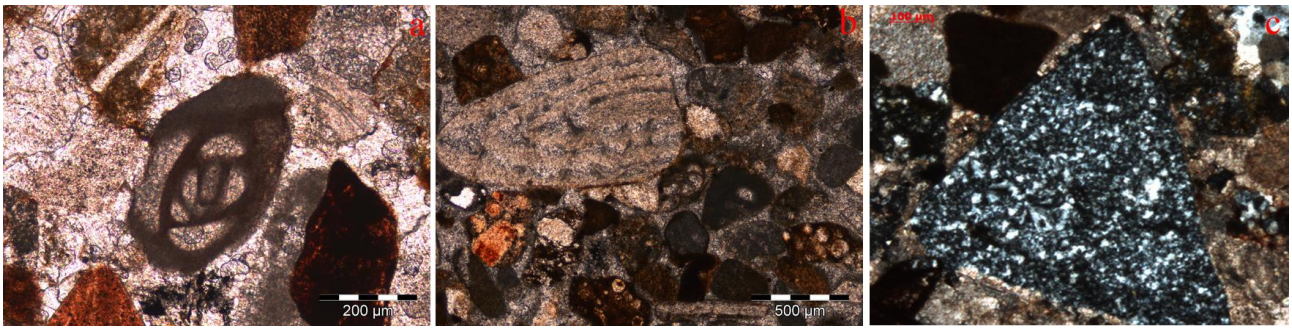

Annex III- 17: Microphotograph of a,b) clast of Nummulites and c) radiolarite grains (cherts) from detrital Agha Jari Formation in NW of Shiraz (sample IRN 3).

III-6. Cathodoluminescence

Cathodoluminescence (CL) is the visible light emitted by minerals when they are bombarded with a beam of high-energy electrons in a vacuum. The earliest geological use of CL was made by Long and Agrell (1965) and Sipple (1968). Since that time, commercial luminoscopes and luminescence detectors have become available and CL is now a standard techniques in the petrographic description of rock sample (Emery and Robinson, 1993). The resulting luminescence in minerals allows us to see textures and compositional variations that are not otherwise evident using light microscopy.

Two types of cathodoluminescence microscopes are in use. One is working with a cold cathode generating an electron beam by a corona discharge tube, the other one produces a beam using a hot cathode.

Cold cathodoluminescence is a commonly used termed for optical-CL system. It is an attachment to a microscope that allows the sample to be examined optically with the microscope and with CL in the same area. An electron gun attached to the side of the chamber fires electros at a low angle of incidence on to the samples surface, activating luminescence which can then be viewed through an ordinary optical microscope. The cold luminoscope is operating with a lower voltage (15-20 keV) in compared with hot luminoscope. The minerals with low energy of activation can be study by CL (carbonates and less commonly quartz).

Hot cathodoluminescence is an instrument that generates the electrons by a heated filament and the electrons are directed at lower voltage toward the anode. This stage has a more stable beam and has greater CL intensity. The hot luminoscope is operating with several tens of thousands of kilovolts.

These instruments have higher sensitivity and the ability detect short-lived luminescence in minerals. This CL is most suitable for examination of sandstone samples because quartz luminescence is lower than this of carbonates.

Cathodoluminescence usage in provenance study

The more important usage of Cathodoluminescence study in the geological context is the fundamental insights image that gives information about processes of crystal growth, mineral replacing, deformation and same provenance minerals. These applications include:

- investigations of cementation and diagenesis processes in sedimentary rocks;
- provenance of clastic material in sedimentary and metasedimentary rocks;
- details of internal structures of fossils;
- growth/dissolution features in igneous and metamorphic minerals;
- deformation mechanisms in metamorphic rocks (Anx. III- 18) (Flugel, 2004).

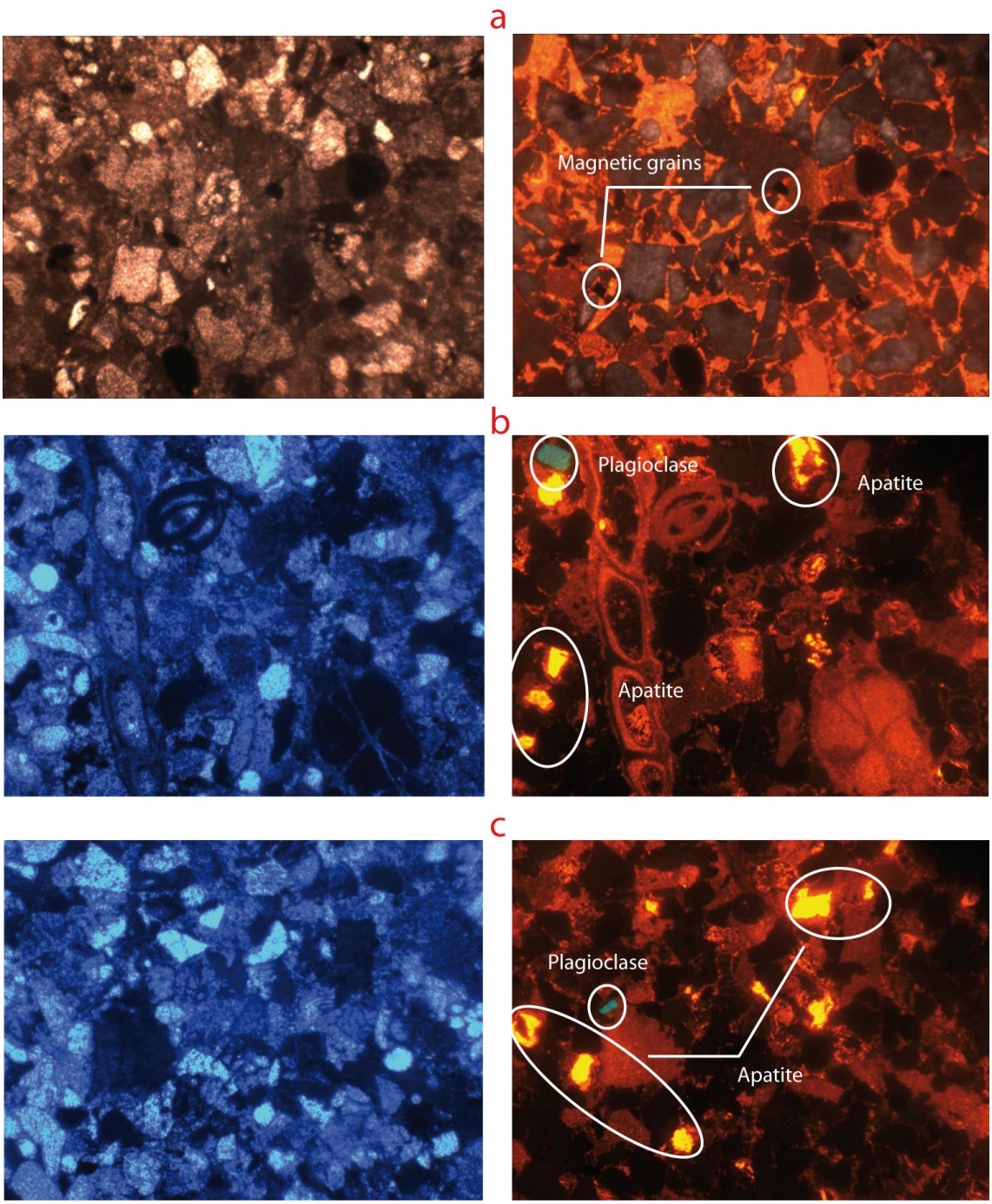

Annex III- 18: Cathodoluminescence micrograph of thin sections of Agha-Jari F. in NW Shiraz, images related to samples IRN6 (a), IRN 19 (b) and IRN 10 (c) (zoom 10x). These samples are contain, silicate fragments and carbonate cement. Light yellow grains show the abundance of apatite, the blue grins in b and c are Plagioclase grains and the black ones are magnetic grains.

III-7. Scanning electron microscopy (SEM)

The scanning electron microscope (SEM) is a type of electron microscope that images the sample surface by scanning it with a high-energy beam of electrons in a raster scan pattern. The electrons interact with the atoms that make up the sample producing signals that contain information about the sample's surface topography, composition and other properties such as electrical conductivity.

The signals produced by an SEM include secondary electrons, back-scattered electrons (BSE), characteristic X-rays, light (cathodoluminescence), specimen current and transmitted electrons (Goldstein et al., 2003). Secondary electron detectors are common in all SEM, but it is rare that a single machine would have detectors for all possible signals. Due to the very narrow electron beam, SEM micrographs have a large depth of field yielding a characteristic three-dimensional appearance useful for understanding the surface structure of a sample (Reed, 2005). A wide range of magnifications is possible, from about 10 times (about equivalent to that of a powerful hand-lens) to more than 500,000 times, about 250 times the magnification limit of the best light microscopes. Back-scattered electrons (BSE) are beam electrons that are reflected from the sample by elastic scattering. BSE are often used in analytical SEM along with the spectra made from the characteristic X-rays. Because the intensity of the BSE signal is strongly related to the atomic number (Z) of the specimen, BSE images can provide information about the distribution of different elements in the sample. Characteristic X-rays are emitted when the electron beam removes an inner shell electron from the sample, causing a higher energy electron to fill the shell and release energy. These characteristic X-rays are used to identify the composition and measure the abundance of elements in the sample (Reed, 2005). So the general advantages of SEM study are:

-High spatial resolution;
-High depth of field;
-Large range of magnification (from 10-100,000x);
-Simple sample preparation.

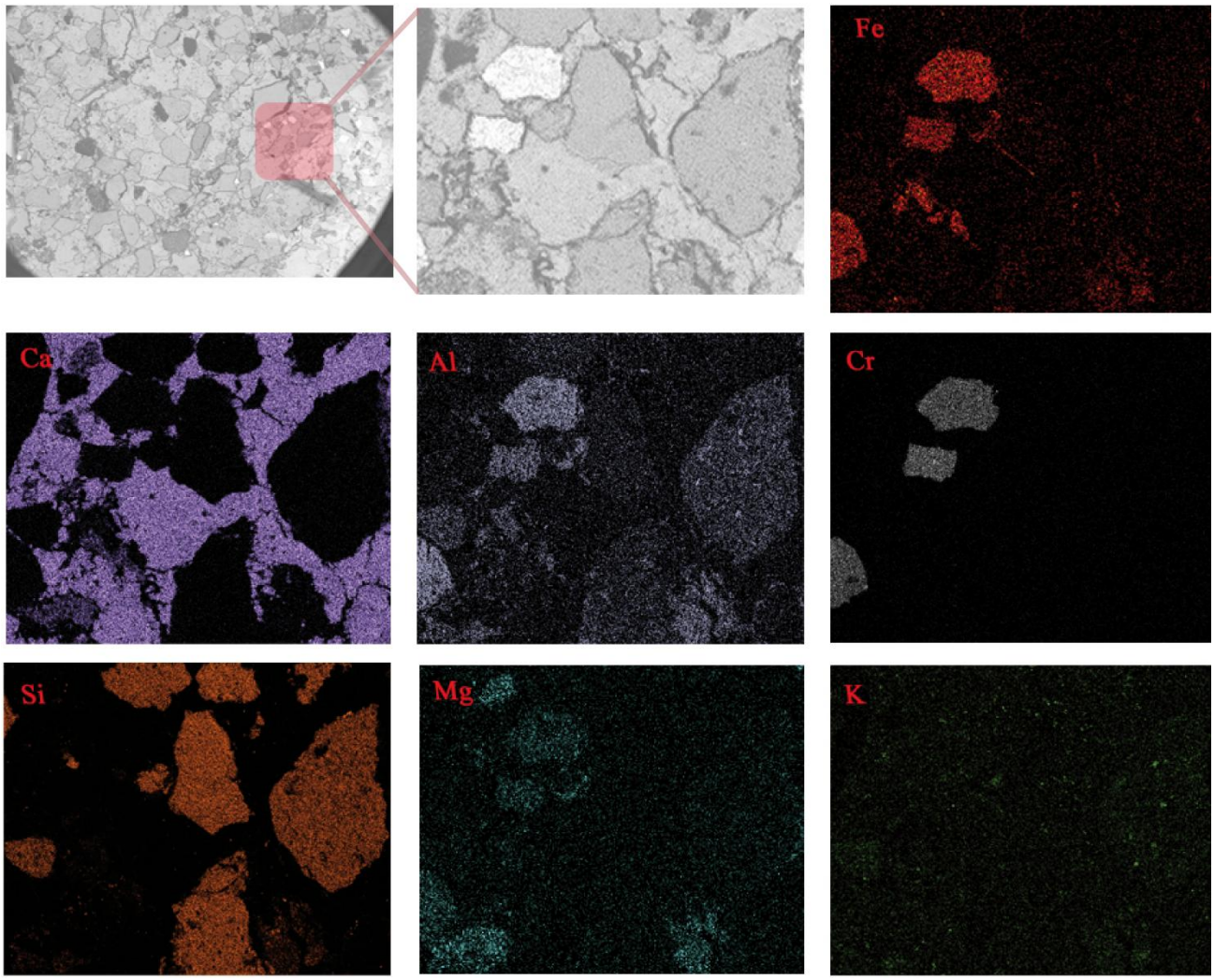

Annex III- 19: Geochemistry map (sample IRN3). On base of mineral database, SEM is analyzing the trace elements. Through this method the abundance of elements and the host minerals are recognized.

III-8. Field and laboratory Problems

- Bulk sample about 4-8 Kg (φ > 30 cm) has to be collecting from outcrops for extract the good quality and enough quantity grains of apatite. Carrying such volume of several samples from high altitudes is a problem.
- Transferring the samples in international research.
- Cleaning the instruments in laboratory process especially in crushing and sieving steps from any possibility of remaining previous samples effect as size 0.4 mm.

- Attention to room temperature and time in etching process to avoid increasing the etch-pit widths.
- Wasted time between transferring the samples for irradiation and returning back to laboratory, some times it takes more than one year.
- Sensibility of apatite grains to erosion and lag time.

III-9. Provenance study of some accessory minerals in detrital sedimentary samples

Ophiolitic detritus and mafic minerals mainly occur in detrital deposits in the study area. Identification of accessory minerals in thin section and bulk rock composition have been done through SEM and CL study or X-ray diffraction analysis. Due to the characteristic of these minerals, the source of detrital material, paleoenvironment and paleogeography or region could be constrainted.

The source rocks which provide the heavy mineral sands determine the composition of the economic minerals. The sources of zircon, monazite, rutile and some ilmenite are usually granites. The sources of ilmenite and garnet are ultramafic and mafic rocks, such as kimberlites or basalts. Garnet is also sourced commonly from metamorphic rocks, such as amphibolite schists. Precious metals are sourced from ore deposits hosted within metamorphic rocks.

Association	Source
apatite, biotite, rutile, titanite, zircon, tourmaline, monazite	acid igneous rocks
garnet, xenotime, monazite, tourmaline	granite pegmatites
chromite, ilmenite, olivine, magnetite, augite	basic igneous rocks
garnet, staurolite, topaz,	contact metamorphic rocks
garnet, kyanite, staurolite, titanite, epidote, sillimanite	dynamothermal metamorphic rocks
barite, rutile, zircon (rounded grain), tourmaline (rounded grain)	reworked sediments

Table III- 3: Heavy minerals suites characteristic of principal kinds of source rocks (Boggs, 2009).

Surface weathering	Burial diagenesis
olivine	olivine, pyroxene
apatite	andalusite, sillimanite
pyroxene	amphibole
garnet	epidote
amphibole	sphen
kyanite	kyanite
staurolite	staurolite
monazite	garnet
tourmaline	apatite, chloritoid, spinel
rutile	rutile, tourmaline, zircon
zircon	

Table III- 4: Relative stabilities of heavy minerals under conditions of weathering and intractable solution during diagenesis; stability increases downward (Boggs, 2009).

Metamorphic minerals are those that form only at high temperatures and/or pressures condition. These minerals, known as index minerals, include sillimanite, kyanite, staurolite, andalusite, and some garnets.

Other minerals, such as olivines, pyroxenes, amphiboles, micas, feldspars, and quartz, may be found in metamorphic rocks, but are not necessarily the result of the process of metamorphism. These minerals formed during the crystallization of igneous rocks. They are stable at high temperatures and pressures and may remain chemically unchanged during the metamorphic process. However, all minerals are stable only within certain limits, and the presence of some minerals in metamorphic rocks indicates the approximate temperatures and pressures at which they formed.

- *Chert* is a fine-grained silica-rich microcrystalline, cryptocrystalline or microfibrous sedimentary rock.In petrology the term of chert is used to refer generally to all rocks composed primarily of microcrystalline, cryptocrystalline and microfibrous quartz. There are numerous varieties of chert, classified based on their visible, microscopic and physical characteristics. In our studied samples, the Radiolarite type is found. This type of chert formed as primary deposits and containing radiolarian microfossils. Radiolarite indicates deep water deposition below the lysocline where siliceous sediments are stable and carbonates are dissolved.

- *Garnet* $X_3Y_2(SiO_4)_3$ consists of isolated silica groups (SiO_4) that have various metal atoms arranged around them. There are two groups of garnet: the aluminum-silicate garnets and the calcium-silicate garnets. The Garnet group is a key mineral in interpreting the genesis of many igneous and metamorphic rocks via geothermobarometry. For instance, eclogite can be defined as a rock of basalt composition, but mainly consisting of garnet and omphacite. Pyrope-rich garnet is restricted to relatively high-pressure metamorphic rocks, such as those in the lower crust and in the Earth's mantle. Peridotite may contain plagioclase, or aluminium-rich spinel, or pyrope-rich garnet, and the presence of each of the three minerals defines a pressure-temperature range in which the mineral could equilibrate with olivine plus pyroxene: the three are listed in order of increasing pressure for stability of the peridotite mineral assemblage. Hence, garnet peridotite must have been formed at great depth in the earth. Garnet is also relatively resistant to alteration. Iron-rich almandine, the most common garnet, is widespread in metamorphic rocks such as schists and gneisses and in granitic igneous rocks. The magnesium garnet, favored by high pressures of formation, is found in magnesium rich metamorphic rocks formed at great depth and may be an important mineral in the mantle of the Earth. Spessartine is found in manganese-rich gneisses and in coarse grained, igneous rocks (pegmatites). Grossular, containing calcium and aluminum, is found in clay-rich limestones that have been metamorphosed in to marbles and in contact metamorphic deposits (skarns), formed when an igneous rock intrudes and reacts with limestones.

- *Chromite* ($FeCr_2O_4$) is an oxide mineral belonging to the spinel group. It is found in peridotite from the Earth's mantle. It also occurs in layered ultramafic intrusive rocks. In addition, it is found in metamorphic rocks such as some serpentinites. It is commonly associated with olivine, magnetite, serpentine, and corundum.

- *Pyroxene* $(Mg,Fe,Ca)_2(SiO_3)_2$ are abundant primary minerals in basalt, peridotite and other mafic igneous rocks. Some also are metamorphic mineralin high-grade rocks. The upper mantle of Earth is composed mainly of olivine and pyroxene and is dominated by olivine, typical for common peridotite. Pyroxene and feldspar are the major minerals in basalt and gabbro. Pyroxenes are found in many rocks, often those crystallized from a melt (sometimes in metamorphic rocks).

- *Amphibole* has an atomic structure made of double chains of silica (SiO_4) tetrahedra, surrounded by metal and hydroxyl ions. They form at high temperatures in igneous and metamorphic rocks that contain water. Amphiboles are minerals of either igneous or metamorphic origin; in the former case occurring as constituents (hornblende) of igneous rocks, such as granite, diorite, andesite and others. Those of metamorphic origin include examples such as those developed in limestones by contact metamorphism (tremolite) and those formed by the alteration of other ferromagnesian minerals (hornblende). Pseudomorphs of amphibole after pyroxene are known as uralite. It occurs frequently as a constituent of greenschists found in ultramafic rocks.

- *Olivine* $(Mg,Fe)_2SiO_4$ is a major rock-forming mineral in the oceanic crust and basaltic rocks and the most common mineral in the Earth's mantle.

Olivine occurs in a range of compositions between pure magnesium silicate (forsterite) and pure iron silicate (fayalite). Olivine prefers to live deep in the upper mantle, where it makes up about 60 percent of the rock. It does not occur in the same rock with quartz (except in the rare fayalite granite). The olivine grains were swept to the surface in a volcanic eruption. In olivine-bearing rocks of the deep oceanic crust, olivine readily takes up water and metamorphoses into serpentine.

- *Kyanite* (heavy mineral) is one of three versions, or polymorphs, of Al_2SiO_5. Andalusite and sillimanite are the others. Which one is present in a given rock depends on the pressure and temperature that the rock was subjected to during metamorphism. Kyanite signifies medium temperatures and high pressures, whereas andalusite is made under high temperatures and lower pressures and sillimanite at high temperatures. Kyanite is typical in schists of pelitic (clay-rich) origin.

- *Rutile* (heavy mineral) is the natural mineral form of titanium dioxide, TiO_2, in plutonic and metamorphic rocks. Rutile is a common accessory mineral in high-temperature and high-pressure metamorphic rocks and in extrusive igneous rocks, particularly those which have deep mantle sources. Also the rutile is found as an accessory mineral in some altered igneous rocks, and in certain gneisses and schists.

- *Titanite* ($CaTiSO_5$) is typically found in calcium-rich metamorphic rocks and scattered in some granites. It occurs as a common accessory mineral in intermediate and felsic igneous rocks and associated pegmatites. It also occurs in metamorphic rocks such as gneiss and schists and skarns. Titanite has been known as sphene too.

- *Ilmenite* ($FeTiO_3$) (heavy mineral) is commonly recognised in altered igneous rocks by the presence of a white alteration product, the pseudo-mineral leucoxene. Often ilmenites are rimmed with leucoxene, which allows ilmenite to be distinguished from magnetite and other iron-titanium oxides.

Ilmenite is a common accessory mineral found in metamorphic and igneous rocks. It is found in large concentrations in layered intrusions where it forms as part of a cumulate layer within the silicate stratigraphy of the intrusion. Ilmenite generally occurs within the pyroxenitic portion of such intrusions.

- *Siderite* ($FeCO_3$) is commonly found in hydrothermal veins, and is associated with barite, fluorite, galena, and others. It is also a common diagenetic mineral in shales and sandstones, where it sometimes forms concretions. In sedimentary rocks, siderite commonly forms at shallow burial depths and its elemental composition is often related to the depositional environment of the enclosing sediments. Primarily bedded, biosedimentary deposits, also in metamorphic and igneous rocks. Siderite is easily altered to iron oxides.

- *Xenotime* (YPO_4) (heavy mineral) is occurring as a minor accessory mineral. Xenotime is found in pegmatites and other igneous rocks, as well as gneisses rich in mica and quartz. Associated minerals include biotite and other micas, chlorite group minerals, quartz, zircon, certain feldspars, analcime, anatase, brookite, rutile, siderite, and apatite. It may form as minute grains or as extremely thin (less than 10 μ) coatings on detrital zircon grains in siliciclastic sedimentary rocks.

- *Baryte* ($BaSO_4$) (heavy mineral) is a mineral that commonly occurs as concretions in sedimentary rocks. Baryte occurs in a large number of depositional environments, and is deposited through a large number of processes including biogenic, hydrothermal, and evaporation, among others.

- *Palygorskite* $(Mg,Al)_2Si_4O_{10}(OH)•4(H_2O)$ is a fibrous mineral which often classified as a clay mineral because it is present in some soils and behaves like many other clay minerals. Unlike most other clay minerals, palygorskite can form large crystals. Two possibilities for palygorskite genesis have been suggested: direct crystallization and alteration of smectite (Cagatay, 1990). Its commercial deposits form under alkaline conditions or closed marginal marine with normal salinity basins (Callen, 1981). Small deposits are associated with hydrothermal alteration of magnesium-rich rocks or the small deposits of pedogenic palygorskite are associated with weathered dolomitic sediments. Magnesium concentrations in presence of dolomite was sufficient for Palygorskite precipitation; the necessary Si and Al were derived by dissolution of silicates under alkaline conditions.

- *Kaolinite* $Al_2Si_2O_3(OH)_4$ produced by the chemical weathering of aluminium silicate minerals like feldspar and mineral found in sediments, soils, hydrothermal deposits, and sedimentary rocks. Kaolin-type clays undergo a series of phase transformations upon thermal treatment in air at atmospheric pressure. Endothermic dehydroxylation (or alternatively, dehydration) begins at 550-600° C to produce disordered metakaolin, $Al_2Si_2O_7$.

Kaolinite clay occurs in abundance in soils that have formed from the chemical weathering of rocks in hot, moist climates. Comparing soils along a gradient towards progressively cooler or drier climates, the proportion of kaolonite decreases, while the proportion of other clay minerals such as illite (in cooler climates) or smectite (in drier climates) increases.

- *Ankerite* Ca (Fe, Mg, Mn)$(CO_3)_2$ in composition it is closely related to dolomite, but differs from it in having magnesium replaced by varying amounts of iron(II) and manganese. The crystallographic and physical characters resemble those of dolomite and siderite.

Ankerite occurs with siderite in deposits of iron-ore. It is one of the minerals of the dolomite-siderite series. Ankerite can result from hydrothermal or direct groundwater precipitation. It can also be the result of metamorphic recrystallization of iron-rich sedimentary rocks.

References

References

Barbarand, J., Carter, A., Wood, I., and Hurford, T., 2003, Compositional and structural control of fission-track annealing in apatite: Chemical Geology, v. 198, no. 1-2, p. 107-137.

Bernet, M., and Garver, J. I., 2005, Fission-track Analysis of Detrital Zircon: Reviews in Mineralogy and Geochemistry, v. 58, no. 1, p. 205-237.

Bernet, M., Zattin, M., Garver, J. I., Brandon, M. T., and Vance, J. A., 2001, Steady-state exhumation of the European Alps,10.1130/0091-7613(2001)029<0035:SSEOTE>2.0.CO;2: Geology, v. 29, no. 1, p. 35-a-38.

Boggs, S., Jr., 2009, Petrology of Sedimentary Rocks(second edition), Cambridge University Press, 600 p.

Bradley, R. S., 1985, Quaternary Paleoclimatology: Methods of Paleoclimatic Reconstruction: London, Chapman and Hall, 472 p.

Brandon, M. T., 1996, Probability density plot for fission-track grain-age samples: Radiation Measurements, v. 26, p. 663-676.

Braun, J., van der Beek, P., and Batt, G., 2006, Quantitative Thermochronology: Numerical Methods for the Interpretation of Thermochronological Data, Cambridge University press, 270 p.

Butler, R. F., 1992, Paleomagnetism: Magnetic domains to geological terranes: Oxford, UK, Blackwell Scientific Publications, 319 p.

-, 2004, PALEOMAGNETISM: Magnetic Domains to Geologic Terranes, Rock and Paleomagnetism: Portland, Oregon, Electronic Edition, 238 p.

Cagatay, M. N., 1990, Palygorskite in the Eocene rocks of the Dammam Dome, Saudi Arabia: Clays and Clay Minerals, v. 38, no. 3, p. 299-307.

Callen, R. A., 1981, Palygorskite in sediments: Detrital, diagenetic or neoformed- A critical review - Discussion: South Australian Department of Mines and Energy.

Cox, A., 1973, Plate tectonics and geomagnetic reversal, Tectonophysics: San Francisco, California: W. H. Freeman, p. 138–145, 222–228.

Crowley, K. D., Naeser, C. W., and Naeser, N. D., 1989, Fission track analysis: Theory and applications, in Geological Society of America Annual Meeting, St. Louis, Missouri. USA.

Dickinson, W. R., 1985, Interpreting provenance relations from detrital modes of sandstones, in Zuffa, G. G., ed., Provenance of Arenites: NATO Advanced Science Series: Dordrecht, D. Reidel Publishing Company, p. 333-361.

References

Dickinson, W. R., Beard, S. L., Brakenridge, G. R., Erjavec, J. L., Fergusson, R. C., Inman, K. F., Knepp, R. A., Lindberg, F. A., and Ryberg, P. T., 1983, Provenance of North American Phanerozoic sandstones in relation to tectonic setting.: Geolobical Society of America Bulletin, v. 94, p. 222-235.

Dickinson, W. R., and Suczek, C. A., 1979, Plate tectonics and sandstone compositions.: American Association of Petroleum Geologist Bulletin, v. 63, p. 2164-2182.

Dodson, M. H., 1973, Closure temperature in cooling geochronological and petrological systems: Contrib. Miner. Petrol, v. 40, p. 259–274.

-, 1986, Closure profiles in cooling systems: Mater. Sci. Forum, v. 7, p. 145–154.

Emery, D., and Robinson, R., 1993, Inorganic geochemistry: applications to petroleum geology, Wiley-Black Well Scientific Publications, 264 p.

Fleischer, R. L., and Price, P. B., 1964, Techniques for geological dating of minerals by chemical etching of fission fragment tracks: Geochimica et Cosmochimica Acta, v. 28, no. 10-11, p. 1705-1712, IN3-IN21, 1713-1714.

Fleischer, R. L., Price, P. B., and Walker, R. M., 1975, Nuclear tracks in solids: principles and applications: Berkeley, California, University of California Press, 626 p.

Flugel, E., 2004, Microfacies of Carbonate Rocks. Analysis, Interpretation and Application, Geological Magazine: New York, Springer, 976 p.

Fuentes, F., DeCelles, P. G., and Gehrels, G. E., 2009, Jurassic onset of foreland basin deposition in northwestern Montana, USA: Implications for along-strike synchroneity of Cordilleran orogenic activity,10.1130/G25557A.1: Geology, v. 37, no. 4, p. 379-382.

Galbraith, R. F., 1988, Graphical Display of Estimates Having Differing Standard Errors: Technometrics, v. 30, no. 3, p. 271-281.

-, 1990, The radial plot: graphical assessment of spread in ages: Nucl. Tracks Radiat. Meas, v. 17, p. 207-214.

-, 1994, Genetic algorithms: A powerful new method for modelling fission-track data and thermal histories. In: Lanphere, M.A., Dalrymple, G.B., Turrin, B.D. (eds.), in International Conference of Geochronology, Cosmochronology and Isotope Geology, US Geological Survey.

-, 2005, Statistics for Fission Track Analysis, Chapman and Hall/CRC, Interdisciplinary Statistics Series, 224 p.

Galbraith, R. F., and Laslett, G. M., 1993, Statistical models for mixed fission track ages: International Journal of Radiation Applications and Instrumentation. Part D. Nuclear Tracks and Radiation Measurements, v. 21, no. 4, p. 459-470.

Garver, J. I., Brandon, M. T., Roden-Tice, M., and Kamp, P. J. J., 1999, Exhumation history of orogenic highlands determined by detrital fission-track thermochronology, in Ring, U., Brandon, M. T., Lister, G. S., and Willett, S. D., eds., Exhumation Processes: Normal Faulting, Ductile Flow and Erosion, Geological Society of London, p. 238-304.

Gleadow, A. J. W., Belton, D. X., Kohn, B. P., and Bronw, R., 2002, Fission Track Dating of Phosphate Minerals and the Thermochronology of Apatite: Mineralogy and Geochemistry, v. 48, no. 1, p. 579-630.

Goldstein, J., Newbury, D. E., Joy, D. C., Lyman, C. E., Echlin, P., Lifshin, E., Sawyer, L., and Michael, J., 2003, Scanning electron microscopy and x-ray microanalysis: New York, Kluwer academic/Plenum, 689 p.

Hecht, J., 1995, The geological timescale: New Scientist magazine, p. 1.

Hudson, A., and Anthony, C. R., 1998, Depleted Uranium, in Harley, N. H., Foulkes, E. C., Hilborne, L. H., Hudson, A., and Anthony, C. R., eds., A Review of the Scientific Literature as It Pertains to Gulf War Illnesses, National Defense Research Institute-Rand, p. 120.

Hurford, A. J., 1990, Standardization of fission track dating calibration: Recommendation by the Fission Track Working Group of the I.U.G.S. Subcommission on Geochronology: Chemical Geology: Isotope Geoscience section, v. 80, no. 2, p. 171-178.

Hurford, A. J., and Carter, A., 1991, The role of fission track dating in discrimination of provenance, in Morton, A., and Todd, S., eds., Developments in Sedimentary Provenance Studies, Special Publication, Geological Society London, p. 67-78.

Hurford, A. J., Fitch, F. J., and Clarke, A., 1984, Resolution of the age structure of the detrital zircon population of two Lower Cretaceous sandstones from the Weald of England by fission tarck dating: Geological Magazine, v. 121, p. 269-277.

Hurford, A. J., and Green, P. F., 1983, The zeta age calibration of fission-track dating: Chemical Geology, v. 41, p. 285-317.

Jackson, M., 1991, Anisotropy of magnetic remanence: a brief review of mineralogical sources, physical origins, and geological applications, and comparison with susceptibility anisotropy: Pageophys, v. 136, no. 1, p. 1-28.

References

Jelinek, V., 1981, Characterization of the magnetic fabric of rocks: Tectonophysics, v. 79, no. 3-4, p. T63-T67.

JMicroVision(1/2), 2002-2007, http://www.jmicrovision.com/.

Johnson, R., G.,, 1982, Brunhes-Matuyama magnetic reversal dated at 790,000 yr B.P. by marine-astronomical correlations: Quat.Res, v. 17, p. 135-147.

Ketcham, R. A., Donelick, R. A., and Carlson, W. D., 1999, Variability of apatite fission track annealing kinetics III: Extrapolation to geological time scales: American Mineralogist, v. 84, p. 1235-1255.

Ketcham, R. A., Donelick, R. A., and Donelick, M. B., 2000, Aftsolve: A program for multi-kinetic modeling of Apatite Fission-Track Data.: Geol.Mater. Res., v. 2, p. 1-32.

Khadivi, S., Mouthereau, F., Larrasoaña, J.-C., Vergés, J., Lacombe, O., Khademi, E., Beamud, E., Melinte-Dobrinescu, M., and Suc, J.-P., 2009, Magnetochronology of synorogenic Miocene foreland sediments in the Fars arc of the Zagros Folded Belt (SW Iran): Basin Research, v. 9999, no. 9999.

-, 2010, Magnetochronology of synorogenic Miocene foreland sediments in the Fars arc of the Zagros Folded Belt (SW Iran): Basin Research, v. 9999, no. 9999.

Köppen, A., and Carter, A., 2000, Constraints on provenance of the central European Triassic using detrital zircon fission track data: Palaeogeography, Palaeoclimatology, Palaeoecology, v. 161, no. 1-2, p. 193-204.

Lanza, R., and Meloni, A., 2006, The Earth's Magnetism, An Introduction for Geologists, Springer-Verlag Berlin Heidelberg, 278 p.

Long, J. V. P., and Agrell, S. O., 1965, The cathodoluminescence of minerals in thin section: Mineralogical Magazine, v. 34, p. 318–326.

Lourens, L. J., F.J. Hilgen, J. Laskar, Shackleton, N. J., and Wilson, D., 2004, The Neogene Period.in, A Geologic Time Scale 2004, A Geologic Time Scale 2004, Cambridge University Press, 409-440 p.

Lowrie, W., 2007, Fundamentals of geophysics, Cambridge, 381 p.

Maher, B. A., and Thompson, R., 1999, Quaternary climates, environments and magnetism, Cambridge University Press, 47 p.

McBride, J. H., 1963, A classification of common sandstones: Sedimentery Petrology, v. 33, p. 664-669.

References

McDougall, I., and Harrison, T. M., 1988, Geochronology and Thermochronology by the 40Ar/39Ar method, Oxford University Press, 212 p.

McDougall, L., 1979, Thep resenstt satus of the geomagnetic polarity time scale,in The earth:Its origin,structurea ande evolution, in McElhinny , M. W., ed.: Newyork, Academic Press, p. 543-566.

McElhinny, M. W., and McFadden, P. L., 2000, Paleomagnetism: continents and oceans, International Geophysics Series v. 73: California, Academic Press.

McFadden, P. L., and Merrill, R. T., 1986, Geodynamo energy source constrains from paleomagnetic data: Phys.Earth and Planet, v. 43, p. 22-33.

Merrill, R. T., McElhinny, M. W., and McFadden, P. L., 1996, The magnetic field of the earth: paleomagnetism, the core, and the deep mantle, International geophysics series ; v. 63: California, Academic Press, 531 p.

Opdyke, M., and Channell, J., 1996, Magnetic Stratigraphy, ACADEMIC PRESS, 346 p.

Price, P. N., and Walker, R. M., 1963, Fossil tracks of charged particles in mica and the age of mineral: J. Geophys. Res., v. 68, p. 4847.

Raffi, I., Backman, J., Fornaciari, E., Pälike, H., Rio, D., Lourens, L., and Hilgen, F., 2006, A review of calcareous nannofossil astrobiochronology encompassing the past 25 million years: Quaternary Science Reviews Critical Quaternary Stratigraphy, v. 25, no. 23-24, p. 3113-3137.

Mineralogy Database, M., 2010, p. http://webmineral.com/.

Reed, S. J. B., 2005, Electron microprobe analysis and scanning electron microscopy in geology: New York, Cambridge, 163 p.

Reynolds, J. H., 2002, Magnetostratigraphy Adds a Temporal Dimension to Basin Analysis: Search and Discovery Article-online article.

Seward, D., Brown, D., Hetzel, R., Friberg, M., Gerdes, A., Petrov, G. A., and Perez-Estaun, A., 2002, The syn- and post-Orogenic low temperature events of the southern and middle Uralides: evidence from fission-track analysis, in Brown, D., Juhlin, C., and Puchkov, V., eds., Orogenic processes in the Uralides, AGU Geophys. Mon.

Sipple, R. F., 1968, Sandstone petrology, evidence from luminescence petrograpy: Sedimentery Petrology, v. 38, p. 530-554.

Sun, J., and Zhang, Z., 2009, Syntectonic growth strata and implications for late Cenozoic tectonic uplift in the northern Tian Shan, China: Tectonophysics, v. 463, no. 1-4, p. 60-68.

References

Tagami, T., 1987, Determination of zeta calibration constant for fission track dating: International Journal of Radiation Applications and Instrumentation. Part D. Nuclear Tracks and Radiation Measurements, v. 13, no. 2-3, p. 127-130.

Tauxe, L., 2005, Inclination flattening and the geocentric axial dipole hypothesis: Earth and Planetary Science Letters, v. 233, no. 3-4, p. 247-261.

Tauxe, L., from, w. c., Butler, R., Banerjee, S., and van der Voo, R., 2009, Essentials of Paleomagnetism, University of California Press (in press).

Tauxe, L., from:, w. c., Butler, R., Banerjee, S., and van der Voo, R., 2010, Essentials of Paleomagnetism, University of California Press, 351 p.

U.S.N.R.C., 2010, Basic References, p. http://www.nrc.gov/.

Wagner, G. A., and Van Den Haute, P., 1992, Fission-track dating, The Netherlands, Kluwer Academic Publishers, 285 p.

White, W. M., 2003, Geochronology: Fission track dating, Isotope Geochemistry: New York, Cornell University, p. 90-96.

Zijderveld, J. D. A., 1967, A.C. demagnetization of rocks: Analysis of results. In Methods in Paleomagnetism (eds D.W. Collinson, K.M. Creer & S.K. Runcorn): Elsevier, A mesterdam, p. 254-286.